Leishmania mexicana induced perturbations of macrophage metabolism

Kevin Michael Rattigan

BAmod (Hons), MRes

Thesis submitted in fulfilment of the requirements for the degree of Doctor of Philosophy

Institute of Infection, Immunity and Inflammation
School of Life Sciences
College of Medical, Veterinary and Life Sciences

University of Glasgow

November 2016

Abstract

The interaction between the *Leishmania* parasite and the macrophage is a bidirectional one of which the outcome of is important for determining if disease progresses or regresses. The parasite is able to modulate the host cell at epigenetic, transcript and metabolic levels. In the context of the latter, immune metabolism is a rapidly growing area of research, and its importance in the context of normal immune function and pathology is increasingly being recognised.

In this thesis a robust, untargeted metabolomics protocol has been developed in order to profile a classical *in vitro* model of immune metabolism, the inflammatory M1 macrophage. While previous studies use single or multiple M1 stimuli without dissecting their importance, a combinatorial approach is used here to dissect the contribution and interaction of two key M1 stimuli, interferon γ (IFNγ) and LPS. An obvious stimulus-specific response is obvious in our data.

We next used this untargeted metabolomics protocol in parallel with RNAseq to examine the cost of hosting a parasite to the macrophages metabolic and transcriptional profile. By using a heat-killed control it was possible to differentiate between general immune responses and response specific to the live parasite. Additionally, a FACS protocol coupled to untargeted metabolomics was used in order to focus on the infected cell. Furthermore, the inclusion of the above mentioned M1 control revealed that either live or heat-killed *Leishmania* failed to elicit as strong a response. Finally, stable isotope labelled metabolomics was used to validate key findings.

In summary, our untargeted metabolomics protocol has revealed immune-metabolic perturbations that are induced by IFNγ and LPS or their interaction. This information should be considered if targeting these pathways in a therapeutic context. Furthermore, by using an integrated metabolic-transcriptomics profiling approach, perturbations in glycerol-phospholipid metabolism, central carbon metabolism and arginine metabolism were found. Using stable isotope labelled metabolomics ($U^{13}C$-Arginine) the current study has given unprecedented insight into how the parasite utilises this crucial amino acid, as well as confirm novel pathways.

Table of Contents

List of Tables

List of Figures

Acknowledgement

I would first like to thank my supervisors Michael Barrett and Carl Goodyear for their help and support throughout my PhD. You introduced me to an exciting area of research and made this project possible. Additionally, I've had great advice during my project from my assessors, Iain McInnes, Jeremy Mottram and Ruaidhri Carmody. Additionally, Fiona Achcar has been a great mentor, not only advising and working together on projects, but also, alongside Emily Armitage in giving help and advice on the next career step.

I've had a great experience working between two groups and gotten endless help and advice. Thanks to Clement Regnault and Andrew (LM) Pountain for helping producing samples for metabolomics, Isabel Vincent for assistance and advice on data processing (and putting up with my constant badgering to get it off the server!). Barrett members (and friends!!) including Pete, Fede, Julie, Katharina, Rai, Gordon, Lesley, Jane, Susan and Ann, you have been a huge help and it's been a pleasure working with you.

In the Goodyear group, thanks to James, Lewis, Hussain, Felicity, Cecilia, and Aysin for helping me with my immunology over the last 3 years, especially the FACs which Diane, Shafqat and Rebecca also were a massive help. I've learned more than I ever thought I would about protein purification from Dan Walker and his group members. Thanks Cameron, Kesha, and Rhy in this regard as well for some quality football with the Level 2 ankle breakers such as Nicky, Michael and Khuram. Thanks to squash buddies, Dan, Fernando, and Sam for letting me win occasionally, the beers and help with my project.

Thanks to Wellcome Trust buddies Hussain, Catrina, Nina, Marlene and Johannes for a fun 4 years as well as Directors Darren and Olwyn for running an amazing programme. I'm sure Andrew, Joanne, Sile, Andrei, Hannah and Alejandro will sign off in style.

In Glasgow Polyomics I'd like to thank Gavin Blackburn and Suzanne McGill, for making sure the data I got was top quality, Amy Cattanach for dealing with my endless requests and questions, Stefan, Justin and Karl for lending me their expertise. In my final year I underestimated the challenges of last minute

RNAseq, and Nick, John, Graham, Julie and Julian helps me surmount these difficulties.

To my mother, brothers (Patrick and Brendan), sister (Sinéad), aunts uncles and first cousins, thank you for the support, visits and presents! I'm sure my father, Martin, would have been proud and relieved that I am better scientist that a farmer.

Finally, I'd like to thank my wonderful fiancé Steph, for her love and support that helped me through the past three years. Payment of Prosecco will be made in full.

Author’s Declaration

I declare that, unless otherwise stated, all results presented here in this dissertation is my own work

Kevin Michael Rattigan

Abbreviations

aa	amino acid
ADI	arginine deiminase
ADMA	asymmetric dimethylarginine
Arg	arginase
ASL	arginosuccinate lysase
BMDM	bone marrow derived macrophages
bp	base pair
BSA	bovine serum albumin
CCL	chemokine ligand
CCR	chemokine receptor
cDNA	complementary DNA
CL	cutaneous leishmaniasis
CMW	chloroform/methanol/water
CR	complement receptors
DC	dendritic cells
DCL	diffuse cutaneous leishmaniasis
DDAH	dimethylarginase
dDCs	dermal dendritic cells
DE	differentially expressed
dLN	draining lymph node
DMSO	dimethyl sulfoxide
DNA	deoxyribonucleic acid
DNDi	Drugs for Neglected Disease initiative
dPBS	Dulbecco's phosphate-buffered saline
DTH	delayed-type hypersensitivity
ELISA	enzyme-linked immunosorbent assay
ESI	electrospray ionisation
FACS	fluorescence activated cell sorting
FAO	fatty acid oxidation
FC	fold change
FCS	fetal calf serum
FDR	false discovery rate
FLO-1	Fluorescent-1

g	gram
GC-MS	gas chromatography-mass spectrometry
GLM	General Linear mode
GM-CSF	granulocyte-macrophage colony stimulating factor
gp63	GPI-anchored metalloprotease
GSH-GSSH	glutathione disulphide glutathione disulphide
HILIC	hydrophilic interaction chromatography
HK	macrophages infected with heat-killed parasites
HMDB	Human Metabolome Database
HPLC	high-performance liquid chromatography
HRP	horseradish peroxidase
iC3b	Inactive complement component C3b
IFAT	immunofluorescence antibody test
IL	Interleukin
INF	Macrophages infected with live parasites
iNOS	inducible nitric oxide synthase
Kb	kilo base
kDa	kilo Dalton
KEGG	Kyoto Encyclopedia of Genes and Genomes
LB	Lysogeny broth
LC-MS	liquid chromatography-mass spectrometry
LCL	localized cutaneous leishmaniasis
LFC	log fold change
LPG	lipophosphoglycan
LPS	Lipopolysaccharides
LRT	likelihood ratio model
m	milli/meter
M	Molar
M-CSF	macrophage colony stimulating factor
M0	naïve macrophage
M1	pro-inflammatory macrophage
mABs	monoclonal antibodys
M2	anti-inflammatory macrophage
MAC	membrane attack complex
MBL	mannose-binding lectin

MCL	mucocutaneous cutaneous leishmaniasis
MHC II	major histocompatibility complex class II
Mo-DCs	monocyte derived DCs
mRNA	messenger ribonucleic acid
MS	mass spectrometry
MSI	Metabolomics Standards Initiative
n	nano
NETs	neutrophil extracellular traps
NHS	non-immune human serum
NK	natural killer cells
NMR	nuclear magnetic resonance
NOŸ	nitric oxide
NTDs	neglected tropical diseases
NTDs	Neglected tropical Diseases
ODC	ornithine decarboxylase
ONO_2^-	peroxynitrite
opn	osteopontin
OPPF	Oxford Protein Production Facility
OTC	ornithine transcarbamoylase
PCR	polymerase chain reaction
PKDL	post-kalazar dermal
PM	peritrophic matrix
PNA	peanut agglutinin
PPG	phosphoglycan
PPP	pentose phosphate pathway
PSG	promastigote secretory gel
PV	parasitophorous vacuole
qPCR	quantitative PCR
RNA	ribonucleic acid
RNS	reactive nitrogen species
ROS	reactive oxygen species
RSD	relative standard deviation
SDS-PAGE	sodium dodecyl sulphate polyacrylamide gel electrophoresis
SODs	superoxide dismutase
sPPG	secreted PPG

TCA cycle	tricarboxylic acid
Th1	T helper
TLR	toll like receptor
U	Unit
Uv	ultra violet
V	volts
v/v	volume to volume
VL	visceral leishmaniasis
w/v	weight to volume
WH	World Heath Organisation
µ	micro

1. General Introduction

1.1. Leishmania species

1.1.1. Leishmaniasis: pathology and prevalence

The Leishmaniases are a spectrum of diseases caused by protozoan parasites belonging to the genus *Leishmania,* and is transmitted by sandfly vectors of the genus *Phlebotomus*. While there are over 40 different species of *Leishmania,* 20 of these are known to be infectious to man. Depending on the infecting species, the parasite causes visceral (VL) or cutaneous (CL) forms of leishmaniasis.

CL is the most prevalent form of this disease. It is characterized by chronic progression, which affects the skin and cartilaginous structures. The main clinical forms of diseases associated with CL are localized cutaneous leishmaniasis (LCL), mucocutaneous cutaneous leishmaniasis (MCL), and diffuse cutaneous leishmaniasis (DCL). CL characterised by skin ulcers that, in a majority of cases, are self-resolving. VL begins with skin ulcers and progresses to infection of the liver and spleen while MCL is characterised by ulcers throughout the skin, mouth and nose. According to the second World Heath Organisation (WHO) report on neglected tropical diseases (NTDs), 1.2 million people are currently infected with 20 to 30 thousand of these cases resulting in deaths each year (Alvar *et al*. 2012). The WHO also estimated that a total of about 556 million people are at risk of VL in VL high-burden countries, and almost 399 million people are at risk of CL in CL high-burden countries.

Over 90% of VL cases occur in six countries: Bangladesh, Brazil, Ethiopia, India, South Sudan and Sudan. For CL, the majority of cases occur in Afghanistan, Algeria, Brazil, Colombia, the Islamic Republic of Iran, Pakistan, Peru, Saudi Arabia and the Syrian Arab Republic. In the instance of mucocutaneous leishmaniasis, 90% of cases occur in Bolivia, Brazil and Peru. CL can arise from anthroponotic transmission mainly in urban areas (*Leishmania tropica*) or zoonotic transmission in more rural areas (*Leishmania major*).

Poverty is a major factor in the prevalence of Leishmaniasis according to the WHO (WHO 2010). For example, surveillance programs can be inadequate or

destroyed during war, medicines are relatively expensive and therefore often unaffordable in the countries where they are most needed, or treatment protocols may not be optimal or adhered to. The malnutrition of people in poor epidemic regions increases the likelihood that infection of VL causing parasites will result in a clinical disease. The recent civil war in Syria has led to a breakdown in medical services and increased prevalence of (Hayani *et al*. 2015). 22,365 cases were reported in 2013 in Aleppo alone. One of the causes of this is the fact that since 2002 the government has control over only one part of the city. This in combination with the influx of hundreds of thousands of refugees has led to an increase in the presence and dissemination CL.

Human behaviour is important with regards to epidemiology. In areas with zoonotic transmission of Leishmaniasis, animals that attract sandflies are kept in or in near proximity to human settlements and therefore favour transmission to humans. Human migration, often forced in the case of poverty, famine and war can increase disease prevalence. This mainly effects anthroponotic transmission and is characterised by large outbreaks in densely populated cities, as seen in Kabul in the 1990s and early 2000s (Bern *et al*. 2008). Economically driven migration may result in non-immune individuals entering epidemic areas. Reasons for migration can include the lack of agricultural land due to increased population or drought or lack of jobs (Ramdas 2012). Expansion into tropical areas for agricultural land or jobs such as mining not only increases exposure to disease but also moves individuals away from established primary health care centres.

Several initiatives have been established with the overall goal of tackling the global health burden caused by neglected tropical diseases (NTDs), including leishmaniasis. A sustained advocacy campaign culminated in the London Declaration, which was launched in January 2012, and supported by a coalition of international and philanthropic organizations, together with 14 pharmaceutical companies (WHO 2012). One of the commitments of the London Declaration was control of VL among other NTDs by 2020; the others included the elimination or eradication of other NTDs. To meet this aim it was agreed that drug access programmes would be sustained and expanded to ensure a sufficient supply of drugs and other interventions. Furthermore, it was agreed

that funding would be provided for research and development to discover the next generation of anti-leishmanial treatments. The publishing of the fourth progress report of the London Declaration in 2016 has recorded a 75% reduction in the number of cases of VL (UtcNTDs, 2016). In Bangladesh, India and Nepal, 10,209 cases were reported, the lowest recorded number since the target of elimination as a public health problem was launched (UtcNTDs 2016). In Africa, a marked decrease in numbers of cases was reported, with no major outbreaks occurring (UtcNTDs 2016).

Despite progress towards disease control there is a dearth of treatments available. Of the 850 new therapeutic products approved between 2000 and 2011, only 4% were indicated for NTDs, despite these diseases accounting for 11% of the global disease burden (Pedrique *et al*. 2013). As NTDs are epidemic in developing nations there is little or no financial incentive for pharmaceutical companies to develop new treatment. To address this, in 2003 the Drugs for Neglected Disease initiative (DNDi) was established as a collaborative effort between global partners including academic researchers, the public sector and the pharmaceutical industry. As of 2015, DNDi has raised €350 million and delivered six treatments and by 2023 DNDi aims to deliver 16 to 18 new treatments with an estimated total budget of €650 million. Delivered treatments include combinations of existing therapies, of which two were developed for VL. There are currently seven *Leishmania*-specific compounds in the DNDi portfolio that are at development stages ranging from hit-to lead up to Phase IIa/Proof of concept. Two are these are targeted against CL. Such business models are critical to ensure the availability and development of safe, cheap and potent medicines with a simple administration route.

1.1.2. Leishmaniasis an ancient disease

Accounts of Leishmaniasis have been dated as far back as 700 BC where lesions similar to CL were inscribed on tablets from King Ashurbanipal whose empire covered large swathes of the Middle East and North Africa (Cox 2002). Some of these accounts may have originated from even earlier texts from 1500 to 2500 BC. In regards to New World CL, anthropomorphic pottery discovered on the Peruvian coast from the Mochica and Chimu periods (200 AD to 1100 AD) show facial lesions that depict ‘espundia’ (MCL) (Gade 1979).

Credit for discovery of the parasites responsible for the Old World CL is debatable (Cox 2002). In 1895, David Douglas Cunningham, Surgeon Major of the British Indian army, reported observing parasitic organisms in the tissue of a specimen of “Delhi boil” without knowing what they were. Peter Borovsky, a Russian military surgeon based in Tashkent, examined the aetiology of the "oriental sore and in 1898 published the first accurate description of the causative agent, and correctly referred it to the protozoa. However, this work was not widely disseminated. In 1903, James Wright reported observing round bodies, 2-4 μM in diameter from ‘tropical ulcers’ biopsies and proposed them to be the causative agent (Wright 1903). These parasites later classified as *Leishmania tropica*.

The discovery of the parasite (amastigote stage) that causes VL, *Leishmania donovani*, is widely accredited to the Scottish pathologist and army doctor, William Leishman (Leishman 1903), and the Irish medical officer Charles Donovan (Donovan 1903). Leishman stained infected spleen samples with ‘Leishman’s stain’, a methylene blue and eosin mixture while, in parallel and independently, Donovan discovered the parasite in the spleens of patients with kala-azar (VL). Leishman proposed that the parasites were trypanosomes, found for the first time in India. Later the same year Ronald Ross proposed that Leishman-Donovan bodies were the intracellular stages of a new parasite, which he named *Leishmania donovani* (Ross 1903).

In regards to New World CL, in 1911 Brazilian pathologist Gaspar Vianna reported that the causative parasites in South America were different to those in Africa (*L. tropica*) and India (*L. donovani*) leading to the assignment new species, *L. braziliensis* (Lainson 2010). Subsequently, a number of other species unique to the New World were described. Sequencing the genomes of *Leishmania species* in combination with phylogenetic techniques have helped aid in categorising the various species (Harkins *et al*. 2016). By carrying out a phylogenomic reconstruction using both 200,000 informative sites across the genomes of multiple species, and 48 annotated genes, Harkins *et al* proposed a southern super-continental origin and ancient dispersal of the genus.

The two main sub genera are *Leishmania* (Old world): *L. tropica, L. aethiopica*, and *L. major* that predominantly cause LCL and *Vianna* (New World). However,

in the case of New World LCL there are some species that are exceptions. New world LCL is mainly caused by species that fit into the *Leishmania* subgenera (*L. amazonensis*, *L. infantum*, *L. mexicana, and L. venezuelensis*) or the *Viannia* subgenera (*Leishmania braziliensis*, *L. guyanensis*, *L. panamensis*, and *L. peruviana*). Interestingly, *L. chagasi* is not distinct from *L. infantum* and likely represents its New World equivalent. A summary of this diversity is represented in **Figure 1-1**.

A further compounding factor with attempts to classify *Leishmania* is that the different species can exchange genetic material creating hybrids. Romano *et al* co-infected *Lutzomyia longipalpis* sandflies with *L. major* (CL) and *L. infantum* (VL) and obtained eleven full genomic hybrids that displayed differences in their ability cause CL or VL in mice (Romano *et al*. 2014). As these important pathological traits seem to be polymorphic within the parental species its may be possible to identify them using classical linkage analysis.

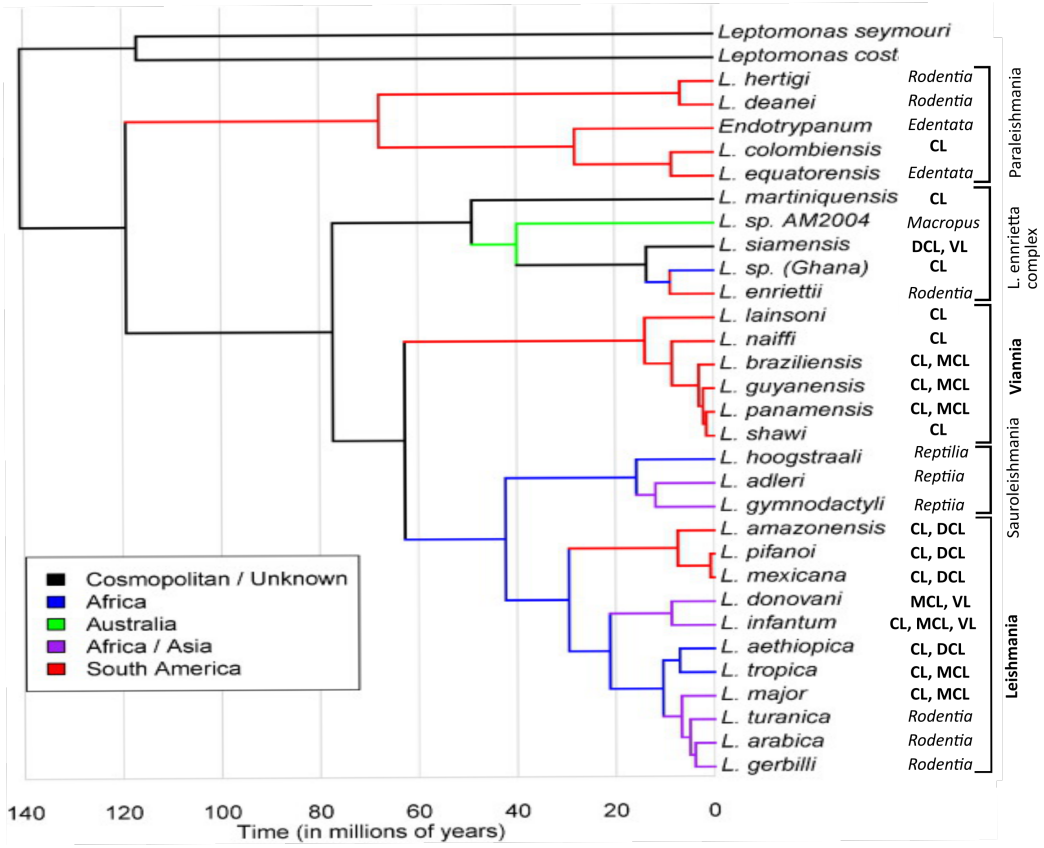

Figure 1-1: Phylogeny of *Leishmania* species, including the mainly human-infective *Leishmania* and *Vianna*. The clinical forms and geographical location are noted. CL: cutaneous leishmaniasis, VL: visceral leishmaniasis, DCL: diffuse cutaneous leishmaniasis, MCL: mucocutaneous leishmaniasis. Adapted from **Harkin *et al* (2016)**.

1.1.3. Current diagnosis and treatments: Limitations and future

To date, there is no vaccine nor is there a single effective treatment for all *Leishmania* species and syndromes. However considerable advances have been made in our understanding of both protective and pathological immune responses to *Leishmania* infection. For centuries, live parasites have been used for protection in a procedure called leishmanization (Khamesipour *et al*. 2005). Although usually effective, leishmanization was limited by loss of parasite virulence, difficulty in standardization and, most importantly, the development of non-healing lesions. Additionally, as total parasite clearance does not occur, recurrent infections are likely if a patient were to become immune-compromised. While crude and not without adverse outcomes, its success indicated that a vaccine should be possible. While attenuated or killed parasites and DNA vaccines have had limited success, it was recently discovered that a parasite protein; glycosomal phosphoenolpyruvate carboxykinase provokes an

immune-dominant response from $CD4^+$ T cells (Mou *et al*. 2015). Importantly, it is conserved across many different *Leishmania* parasite. Promisingly, immunization with this protein provided significant protection in mice models against both CL and VL.

For VL, diagnosis can include clinical, parasitological, and serological diagnosis and these methods have various limitations (WHO 2010). Chronic malaria, schistosomiasis or other systemic infections can have similar clinical symptoms. In regards to parasitological diagnosis, microscopy has high specificity but low sensitivity, and while polymerase chain reaction (PCR) is sensitive, it is currently restricted to referral hospitals and research centres. Serological tests based on immunofluorescence antibody test (IFAT), enzyme-linked immunosorbent assay (ELISA) or western blotting all demonstrate good diagnostic accuracy in most studies but require equipment that is ill suited to field settings. Additionally, parasite-specific antibodies remain detectable up to several years after cure. For CL, the preferred method is parasitological diagnosis; with microscopy (Giemsa stained slides) often the only available method at primary, secondary or tertiary health care level. In endemic areas and multiplex-PCR is used to improve the diagnostic sensitivity as well as to identify the responsible *Leishmania* species. The latter is useful for New World CL where several *Leishmania* species coexist, some with differing clinical outcomes and responses to treatment.

While there is as yet no vaccine, several treatments exist. In 1912, Gaspar Vianna described the use of tartar emetic in the treatment of CL though this drug was later found to be highly toxic (Nagle *et al*. 2014). In 1925, Sir Upendranath Brahmachari synthesized the less toxic pentavalent antimony compound, urea stibamine which was instrumental in saving the lives of millions of Indians infected with VL during the 1922 epidemic. Further progress in reducing toxicity of antimony therapy of VL followed with the synthesis of antimony gluconate (Solustibosan) in 1937 and sodium stibogluconate (Pentostam) in 1945. Currently, there are two formulations of pentavalent antimonials in use: sodium stibogluconate (100 mg antimony/100 mL) and meglumine antimoniate (85 mg antimony/100 mL) (Nagle *et al*. 2014) (**Table 1-1)**.These drugs are limited by their cardiotoxicity, relative expense, need for a

long, paternally administered treatment and widespread resistance leading to a high failure rate. In the Bihar state (where ~90% of VL cases in India occur) more than 60% of VL cases were found to be refractory to pentavalent antimonials (Bhandari *et al*. 2012).

Increased investment in identifying anti-*Leishmania* compounds has led to alternative treatments such as Amphotericin B, Paromomycin, Miltefosine, and Pentamidine. There are on-going collaborations between the Drugs for Neglected Disease initiative (DNDi), pharmaceutical companies and academia aiming to add to the anti-leishmanial repertoire. The access to pharmaceutical compound libraries will allow for similar or improved analogues of seed compounds and this will aid greatly with lead optimization.

In 1955, Amphotericin B, an antifungal polyene antibiotic was discovered and subsequently it was found that it was effective against VL. Amphotericin B increases membrane permeability by binding to ergosterol present in the parasite cell membrane. While highly efficacious, Amphotericin B caused adverse side affects such as nephrotoxicity and this led to the development of the lipid formulation, AmBisome®. In 2011 the WHO negotiated a partnership deal with the suppliers Gilead to donate 445,000 vials of AmBisome® over five years, which was essential in allowing developing countries access to an otherwise unaffordable drug. Currently the WHO recommends a single AmBisome® infusion as the first line therapy in epidemic countries.

Other anti-fungal medicines have also been used such as Ketoconazole, which inhibits ergosterol biosynthesis at the lanosterol demethylase step. Additional anti-fungal medicines have been found to be anti-leishmanial and these are reviewed elsewhere (Nagle *et al*. 2014).

Paromomycin is an aminoglycoside broad-spectrum antibiotic that inhibits protein synthesis by binding to 16S rRNA in bacteria. It was shown to be efficacious for the treatment of VL and CL. Paromomycin is also used in ointment form for the local treatment of CL by application to the lesion twice daily for 20 days. Other locally applied treatments include intra-lesional stibogluconate, “Flash” cryo-therapy or heat-therapy.

Miltefosine was originally developed as an anticancer drug but in the 1990s, several laboratories discovered that Miltefosine has antileishmanial activity (Nagle *et al*. 2014). It is currently the only orally available treatment for VL and CL, which is invaluable as patients can use it in remote areas that lack either the resources or facilities for paternal administration. It is limited by the fact that treatment times are long (28 days or up to 12 weeks for post-kalazar dermal (PKDL)) and common adverse side effects include gastrointestinal side effects and nephrotoxicity. Additionally, its teratogenicity and long half-life (1 week) means that women of child-bearing age must use contraceptives during treatment and for 3 weeks after (Nagle *et al*. 2014).

Pentamidine, which has been in use since the 1940s for treatment of sleeping sickness, is used both to treat CL via an intra-lesional injection as well as VL (Ramdas 2012). Its injection is extremely painful and relatively unaffordable ($90 for 3 rounds of injections). This, in combination with limited access to treatments, has led to some cultures avoiding CL treatment. Instead, they turn to self-'treatment' with harsh chemicals such as battery acid and pesticide (Ramdas 2012). Increased use of topical Paromomycin should help reduce the occurrence of these actions.

A single AmBisome infusion is the preferred first line therapy for VL. For CL locally applied treatments such as Paromomycin in conjunction with systematic stibogluconate are commonly used. Nevertheless there are still different treatments\combination of treatments currently used depending on the parasite species, the disease form, and the country in question. This is reviewed elsewhere (WHO 2010; McGwire & Satoskar 2014).

The use of immunomodulatory inhibitors and agonists that are already used in cancer treatment has been investigated. Drugs that have shown promise are the inhibitor of TNF-α; pentoxyphylline, and the anti-viral TLR7 agonist; imiquimod (Nagle *et al*. 2014; Lessa *et al*. 2001; Miranda-Verastegui *et al*. 2009). These have been used as adjunct therapies to antimonials resulting in shorter treatment times. These approaches have great promise and the DNDi's funding of the latter study shows its commitment to this area of research. A summary of current treatments and their limitations is presented in **Table 1-1.**

Table 1-1: Current treatments for Leishmaniasis. The available treatments and their limitations are listed. These are used to treat cutaneous (CL), visceral (VL), mucocutaneous (MCL) and post-kalazar dermal (PKDL) leishmaniasis. Adapted from (Croft & Olliaro 2011).

Treatment	Property and route of administration	Disease Treated	Limitations
Pentavalent antimonials: (sodium stibogluconate [SSG]) **And meglumine antimoniate**	Organo-metal complexes; intravenous and intramuscular	VL, CL, PKDL & MCL	Acquired resistance. Serious cardiotoxicity leading to death In monotherapy, they require a 30-day parenteral treatment
Amphotericin B deoxycholate:	Polyene antibiotic; intravenous	VL, CL, PKDL & MCL	Need for hospitalization, constant renal monitoring of patients, 28-day duration of treatment, infusion-related adverse events, and dose-limiting toxicity.
AmBisome®	Unilamellar liposome; intravenous (WHO recommends single application)	VL, CL, PKDL and MCL	High cost and the need for a cold chain
Miltefosine:	Hexadecylphosphocholine; oral	VL, CL (3 species), PKDL and MCL	Is expensive and requires 28-day treatment. Suffers from low compliance, risk of resistance, and its contraindication in pregnancy and mandatory contraception for women of childbearing age for the duration of therapy and three months beyond limits its use. Is not registered in many endemic countries and consequently not available
Paromomycin	Aminoglycoside, intramuscular (VL) or topical (CL)	VL & CL	Requires three weeks of painful intramuscular administration. Is highly efficacious in Asia but is associated with some degree of renal and ototoxicity, with limited efficacy as monotherapy in East Africa
Pentamidine	Diamidine, intramuscular	CL and VL (variable)	Requires intramuscular injection, side effects include diabetes mellitus, severe hypoglycaemia, shock, myocarditis and renal toxicity

1.1.4. Sandflies: life cycle in the vector

In 1921 the Sergent brothers, Edouard and Etienne demonstrated the transmission of CL to humans by sandflies of the genus *Phlebotomus*, and in 1941 the requirement of the bite was shown (Cox 2002). It was subsequently shown the genus *Lutzomyia* is the vector of CL causing parasites in the New World. Comparison studies of *L. mexicana* and *L. braziliensis*-infected sandflies led to the original classification of *Leishmania* into two distinct subgenus: *Viannia* and *Leishmania*. The former was defined by the presence of a hindgut stage and the latter by its absence (Lainson 2010). This introduction will focus on *Leishmania*, to which *L. mexicana* belongs. *Leishmania* parasites undergo an obligate intracellular stage (amastigote) when inside its mammalian host. This begins when an infected female sandfly takes a blood meal; infective metacyclic parasites are injected into the host **(Figure 1-2)**.

Here the parasites are taken up directly by professional phagocytes such as macrophages, or by neutrophils, which are in turn phagocytised by macrophages. Ultimately the increased temperature and decreased pH of the host cell, causes differentiation into the amastigote. The parasites' complex and dimorphic life cycle is completed when an uninfected sandfly feeds. Within the fly, the infected host cell lysis, at this lower temperature, the amastigotes differentiate into sluggish extracellular, procyclic promastigotes that replicate within the blood meal. The following section describes metacyclogenesis, which is the transformation of procyclic promastigotes to infective metacyclic promastigotes.

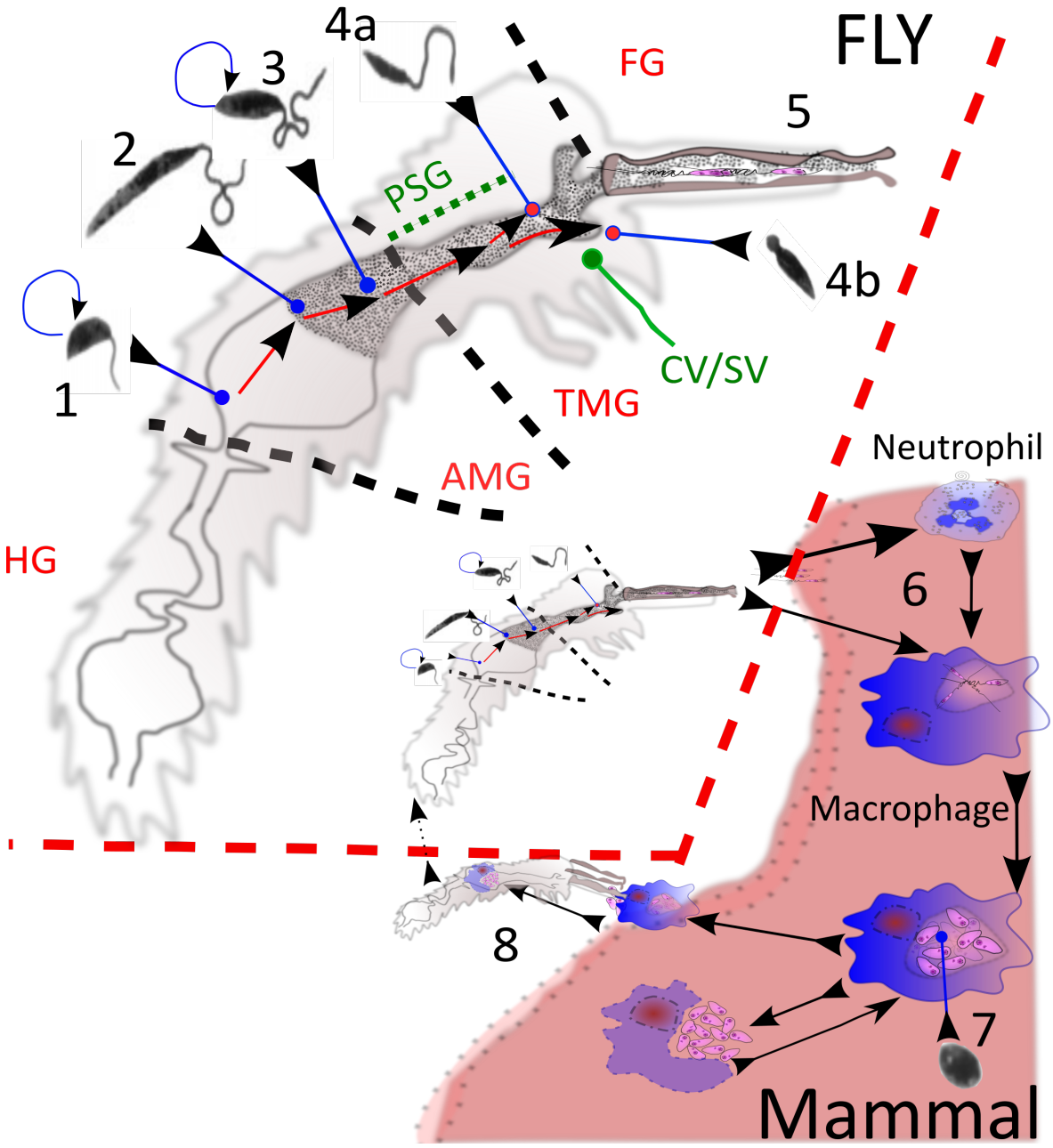

Figure 1-2: Life cycle of Leishmania parasite in the fly. 1 & 8: Lifecycle begins when non-infected female sandfly takes up infected mammalian host cells during blood meal. Lysis in the anterior midgut (AMG) releases the amastigote, which differentiate into the replicating procyclic promastigote. 2: Differentiation into non-replicating nectomonads migration to and traversal of the peritrophic matrix (not shown, located near 1) into the thoracic midgut (TMG). 3: Parasites differentiate into replicating leptomonads. 4a: These can differentiate into infectious, non-replicating metacyclic promastigotes 4b: Either nectomonads or leptomonads (not known which) differentiate into haptomonads, which attach to cardiac or stomodeal valve, possible preventing its opening (CV/SV). 5: metacyclics can infiltrate the foregut (FG) or are injected into the mammalian host. Heavy infection causes the accumulation of promastigote salivary gel (PSG) in the TMG. 6: Parasites are taken up either directly via professional phagocytes or first by neutrophils, which are in turn phagocytised by macrophages. 7: Metacyclics differentiate into the intracellular stage: the amastiogote. Adapted from (Rogers 2012).

In order to survive the lytic environment of the fly gut, promastigotes must upregulate expression of glycoconjugates. These are a group of phosphoglycans either attached to the cell surface via glycosylphospatidylinositol lipid anchors (lipophosphoglycans (LPG), and phosphoglycans (PPG) or secreted PPG (sPPG) (Secundino *et al*. 2010). In *Phlebotomus papatasi*, the LPG of *L. major* attaches to a midgut epithelial galectin. Expression of the galectin, and specific binding to it by LPG is essential in determining species-specific vector competence in sandfly species (Kamhawi *et al*. 2004). LPG binding to galectin also prevents parasite clearance by fluid flow in the gut.

Near the end of blood meal digestion (72-94 hours) procyclics transform into the more motile, larger and slender nectomonads (Kamhawi 2006). Nectomonads migrate towards the anterior part of the peritrophic matrix (PM). By secreting a chitinase, nectomonads can disrupt PM integrity, transverse it, and establish an infection at the stomodeal valve and transform into the replicative leptomonads (Schlein *et al*. 1991). **(Figure 1-2)**. Over the next 4-7 days, leptomonads produce promastigote secretory gel (PSG), a gel-like matrix that plays a key role in transmission by forming a 'plug'. This prevents parasite clearance and results in the enrichment of the subsequent, infective stage metacyclic promastigotes (Rogers *et al*. 2002; Rogers *et al*. 2004). Metacyclics, which are highly motile, express a modified non-attaching LPG that allows anterior migration in response to a chemotactic cue, and subsequent transmission (Rogers *et al*. 2002; Kamhawi 2006). In the host, this modified LPG aids in resisting and/or avoiding host immune responses

To replicate some of the life stages mentioned above *in vitro*, parasites are seeded at low cell density (1-5x10^5/mL). This results in rapidly dividing procyclic promastigotes that proliferate to a high density, where they undergo growth arrest and differentiation into the virulent, stationary metacyclic stage. For species such as *L. major* and *L. infantum* it was shown that their metacyclic forms can be enriched using agglutination by the lectin peanut agglutinin (PNA) which negatively selects metacyclics (R. da Silva & Sacks 1987). This study by da Silva and Sacks also showed there is a loss of virulence caused by serial passage, an important consideration for *in vivo* studies.

There is another subpopulation derived from either nectomonads or leptomonads that are named haptomonads. These attach to the cuticle-lined surface of the stomodeal valve (SV) via the expansion of the flagellar tip into hemi-desmosome-like structures, preventing its opening (Kamhawi 2006). In heavily infected sandflies, the SV degenerates and a few metacyclics migrate into the foregut. The 'blocked' fly attempts to feed multiple times, eventually regurgitating the metacyclic-rich 'plug', and this altered feeding pattern may enhance transmission **(Figure 1-2)** (Stierhof *et al*. 1999).

1.2. Host-pathogen interactions: a multifaceted relationship

The interaction between *Leishmania* parasites and the immune system involves both the innate and adaptive arms. The fly delivers approximately 600 metacyclic parasites during feeding (Kimblin *et al*. 2008). These parasites are first subjected to the host complement system, as well as professional phagocytes such as dendritic cells (DC) or macrophages. In addition, in the fly, metacyclics secrete PSG, which is regurgitated by the biting fly. This has been shown to recruit macrophages to the site of the bite (Rogers *et al*. 2009). During metacyclogenesis, the parasites upregulate expression of the GPI-anchored metalloprotease (gp63) and lipophosphoglycan (LPG). While procyclic promastigotes have a high abundance of LPG to permit binding to the sandfly midgut, in metacyclic promastigotes it is elongated by the addition of phosphorylated disaccharide repeat unit. This modification gives protection to complement mediated lysis (Puentes *et al*. 1990).

Once phagocytosed by the macrophage the parasite must differentiate into its obligate intracellular form: the amastigote. The differentiation to this form is driven by both the higher temperature of the host and the lysosome-driven acidification of the parasitophorous vacuole (Alexander *et al*. 1999). The subsequent replication of amastigotes can lead to lesion development and in the case of visceral leishmaniasis, dissemination to internal organs such as the liver and spleen. In mouse models, the immune response of the host is critical to if and to what extent these latter events occur, and thus determine how the disease progresses.

1.2.1. Animal models of Leishmaniasis: a brief history

Using *in vitro* or *in vivo* models of the immune response to *Leishmania* species has revealed a great deal about the roles of different immune cells but it is important to note that the results of these studies can, and are impacted on by the species/strain of parasite, and/or the species/strain of animal used. For a review of the different mice models currently used to study leishmaniasis see (Loeuillet *et al*. 2016). Despite these limitations, the detailed insight these models give into the complex immune responses in disease resolution and disease progression is invaluable. By identifying appropriate and inappropriate responses it will be possible to target pathological immune responses with chemotherapy.

Animal models have a long history in Leishmaniasis research dating back to the early 1900s when Charles Nicolle obtained cultures in Novy and McNeal's medium (NNN medium) medium of *L. tropica*, which is the parasitic agent of cutaneous leishmaniasis and went on to transmit the dermatosis to monkeys and dogs (Pelis 2006). A key milestone in modelling host pathogen immunity was discovery of *L major*-resistant and -susceptible mouse strains (Kellina 1973). This allowed the investigation and modelling of immune responses that drive disease progression or resolution. Further work revealed the requirement of suppressor T cells in regulating susceptibility in BALB/c mice (Howard 1980).

1.2.2. Discovery of the Th1/Th2 paradigm: pioneered by Leishmania research

Experimental leishmaniasis was the first model that directly demonstrated the relevance of the T helper 1/T helper 2 (Th1/ Th2) dichotomy for the outcome of an infectious disease *in vivo* (Heinzel *et al*. 1989). Here it was found that IFNγ and IL-4 were produced reciprocally in resolving or progressive infection in murine leishmaniasis. Furthermore, by administering a neutralising IL-4 antibody, the requirement of this cytokine for disease progression became apparent. IL-12 was shown to be essential for the development of protective CD4+ Th1 cells, as determined by antibody treatments (Heinzel *et al*. 1993). Timing of the response seems to be important in the context of IL-12 (Sacks & Noben-Trauth 2002). In studies where anti-IL-12 antibody treatment was used to

exacerbate the Th2 mediated disease in susceptible BALB/c mice, the greatest effect was observed when administration was delayed until seven days after infection. This was in agreement with studies of IL-12-deficient C57BL/6 mice subjected to a low-dose challenge, where parasite growth was identical to that in wild-type mice during the first 4-5 weeks (Belkaid *et al*. 2000).

C57BL/6, C3H or CBA have been used as a model of the self-resolving type of disease while Balb/c mice have been used as a model to study the progressive form. There are exceptions in that C57BL/6 mice are susceptible to *L. mexicana* and *L. amazonensis* (Sousa *et al*. 2014; Hurrell *et al*. 2015). Thus resistance and susceptibility here is not strictly associated with the Th1 vs. Th2 immune response paradigm. Nevertheless, C57BL/6 mice, which are resistant to *L. major* infection, become susceptible when they are deficient in draining lymph nodes (Ehrchen *et al*. 2008). The net result here demonstrated that the inability to develop a Th1 response is important for disease progression.

1.3. The immune Response: the components

1.3.1. Site of the bite; the early immune response

Transmission is initiated when an infected female sandfly takes a blood meal. The bite wounds the local microvasculature, creating a hemorrhagic pool from which to feed. The epidermis is mainly composed up of keratinocytes. The dermis, which is connected to epidermis via the basal membrane, is primarily formed by fibroblasts and extracellular tissue and is vascularized with both blood and lymphatic vessels. The damage response of keratinocytes at the local microenvironment of the bite has been found to be important in the context of the resistance of C57BL/6 mice to *L. major* (Ehrchen *et al*. 2010). Here the authors analysed gene expression at infected epidermis and found that IL-1ß, IL-12, osteopontin (opn), IL-4 and IL-6 were more strongly produced in the skin of resistant mice. Keratinocytes also produced CXCL2, which leads to the recruitment of neutrophils as well as opn, CCL2, and CCL5, which drive macrophage recruitment **(Figure 1-3)**. Expression of these genes was temporally restricted to the crucial time of Th1/2 differentiation (Ehrchen *et al*. 2010). Furthermore, either using mice with keratinocytes deficient in IL-6 or the early,

local neutralisation of IL-4, both led to a Th2 switch, and worse disease outcome, demonstrating the importance of epidermal cells to disease control (Ehrchen *et al*. 2010).

The contribution of fly specific factors to disease outcome is of interest, specifically, their immunogenicity. It has been found that rhesus macaques exposed to non-infected *Phlebotomus duboscqi* sandfly bites or immunized with salivary protein PdSP15 were protected against cutaneous leishmaniasis (*L. major*) initiated by the bite of infected flies (Oliveira *et al*. 2015). This protection resulted in reduced parasite and disease burden and correlated with the early appearance of *Leishmania*-specific $CD4^+$ $IFN\gamma^+$ lymphocytes. In a separate study, a correlation was found between the presence of antibodies against the salivary protein PpSP32 from *Phlebotomus papatasi* and reduced disease severity (Mondragon-Shem *et al*. 2015).

In addition to vector specific factors, it has emerged that parasite-synthesised factors formed in the fly and injected alongside the parasite, can impede immune cell function (Rogers *et al*. 2009). The use of models of fly transmission of *Leishmania* has shown that the flies regurgitate a proteophosphoglycan gel synthesized by the parasites. This substance termed promastigote secretory gel (PSG), occludes the anterior midgut of the sandfly preventing parasite clearance (Rogers *et al*. 2004). It has been found to be present in all *Leishmania*-sandfly combinations studied to date. Rogers *et al* showed that this gel enhances infection in the context of *L. mexicana* (Rogers *et al*. 2009). The authors showed that PSG caused the early recruitment of macrophages to the site of infection **(Figure 1-3)**. Additionally, PSG drove the macrophages to an alternative activation state by increasing host cell arginase activity.

In the case of *L. major* infected C57BL/6 mice, it as found that, within 30 minutes for infection there is a massive neutrophil extravasation from vasculature. This occurred in a directed manner to the inoculation site (Peters *et al*. 2008a). Here the authors used two-photon intravital microscopy (2P-IVM) to study the events that occur during infection. They also reported that the influx of neutrophils was independent of the infection state of the fly. This seems to preclude the involvement of a parasite specific factor in the context of neutrophil recruitment. However, it has been shown that the combination of

saliva from *Lutzomyia longipalpis* and *Leishmania chagas*i parasites enhances the CCL2-dependent recruitment of macrophages and neutrophils in susceptible BALB/c mice, but not in resistant C57BL/6 mice (Teixeira *et al*. 2005). This could be due to differences in engaging adaptive immune responses or different recruitment of innate immune cells (Sousa *et al*. 2014).

1.3.2. The complement system: an instant response

Once the parasites come in contact with host blood, they immediately encounter the complement system **(Figure 1-3)**. The three main complement-activating pathways are the Classical, Lectin and Alternative pathways. The net result of these pathways is the formation of the C3 convertases, which cleave C3 into C3b and C3a. These products combine to form the C5 convertase that cleaves C5, generating the C5a chemotactic factor and C5b. Subsequently C5b, C6, C7, C8 and C9 combine, resulting in the formation of the C5b-C9 membrane attack complex (MAC) (Peitsch & Tschopp 1991). This results in a pore like structure that causes lysis of the target cell. The lectin pathway is activated when mannose-binding lectin (MBL) binds to mannose on the pathogen surface and in the alternative pathway; C3 in the plasma interacts with the pathogens surface. Additional functions include inducing inflammation due to the generation of the potent pro-inflammatory anaphylatoxins C3a, C4a, and C5a that interact with macrophages and DCs. Finally, the opsonisation and clearance of opsonized pathogens is mediated by C4b, C3b, and C3bi that bind to complement receptors (CR1 and CR3) on phagocytic cells. In studies that used non-immune human serum (NHS) and depleting classical pathway activators is was reported that majority of *Leishmania* species such as *L. major* and *L. mexicana* activate the alternative complement pathway while in contrast, *L. donovani* appears to activate the classical pathway (Mosser *et al*. 1986). Studies using whole human blood or containing physiological concentrations of serum have revealed however, that opsonisation occurs rapidly against *L. major*, *L. amazonensis*, *L. donovani* and *L. infantum* (Domínguez *et al*. 2003). Thus it seems that there are multiple complement pathways that are engaged by *Leishmania* species, and the extent of which, depends on parasites life-phase and additional host factors.

Leishmania parasites have developed numerous strategies to evade the complement system, including the zinc-dependent metalloproteinase gp63 and

lipophosphoglycan (LPG), which are among the most abundant surface molecules. When compared to promastigotes. *L. major* metacyclics are more resistant to MAC mediated lysis and this resistance has been attributed to an elongation modification of LPG **(Figure 1-3)** (Puentes *et al*. 1990). It has also been shown that gp63 hinders MAC formation by accelerating the conversion of C3b to iC3b **(Figure 1-3)** (Brittingham *et al*. 1995). Here the authors used a gp63-deficient clone of *L. amazonensis* that were transfected with constructs encoding either proteolytically active or inactive gp63 from *L. major*. Cells expressing the wild type gp63 rapidly converted C3b to iC3b and these iC3b-coated parasites were found to interact strongly with CR3. This led to authors to propose that the parasites exploit the opsonic properties of complement while avoiding its lytic effects.

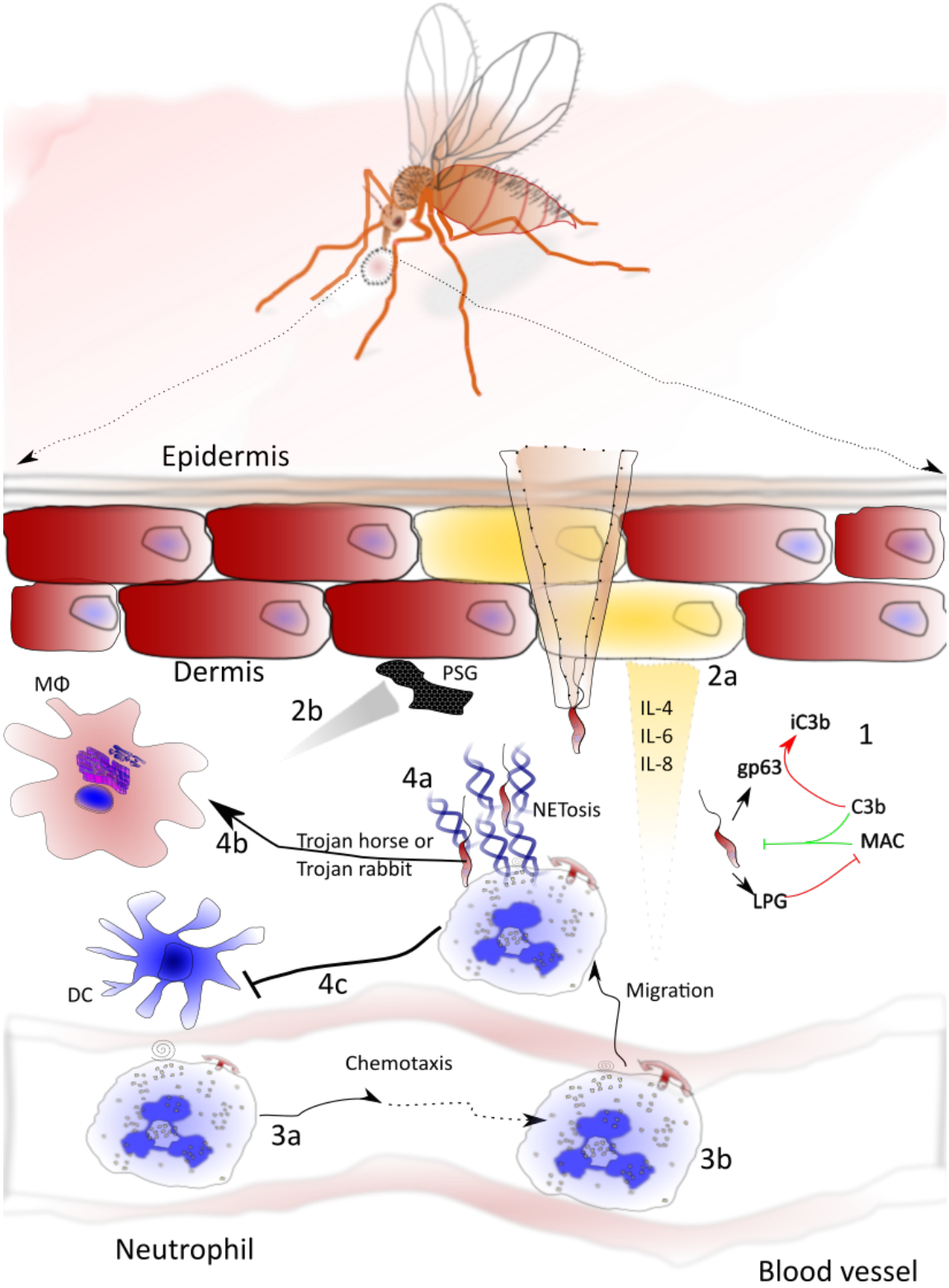

Figure 1-3: Early events at the site of the bite. The fly creates a hemorrogic pool during feeding, damaging skin cells including keratinocytes in the process. 1: the parasites avoids the complement system by LPG preventing membrane attack complex (MAC) binding and gp63 cleaving C3b into inactive iC3b. Red lines refer to the parasite inhibiting/diverting the anti-parasitic complement response (green lines). 2a: damaged keratinocytes release cytokines that interferes in the inflammatory response. 2b: PSG injected alongside parasites cause macrophage recruitment and interferes in function. 3a: CCL3 and 4 recruit neutrophils. 3b: Parasites cause selectin CD68L (rolling) to be down regulated and integrin CD18 to be upregulated to allow neutrophil migration. 4a: Neutrophil secretion of DNA (NETosis) can have positive or negative effects depending on parasite species. 4b: Neutrophils may provide silent entry into macrophages with parasites either inside ('Trojan horse') or along alongside ('Trojan rabbit') neutrophils. 4c: Apoptotic infected neutrophils can down regulate inflammatory DC responses.

1.3.3. Neutrophils

While macrophages, the definitive host cell, can phagocytise parasites directly, the tissue damage induced by insect biting results in a massive influx of neutrophils while the increased influx of macrophages occurs 2 days later. These poly-nucleated granulocytes are short-lived but upon infection their lifespan can be increased from ~6-10 hours to a few days. In order to exit blood circulation, they down regulate the selectin CD68L that is responsible for cell rolling, and upregulate the integrin CD18 that allows for transmigration **(Figure 1-3)** (Falcão *et al*. 2015). In the case of *L. major*, the parasites have been reported to delay apoptosis in human blood derived neutrophils by inhibiting the processing of procaspases in the infected cells, similar to what has been reported for toxoplasma (Aga *et al*. 2002). This was not found to be the case of *L. major* infected murine dermal neutrophils so cell type specific factors may be important (Ribeiro-Gomes *et al*. 2012).

Some species of parasites have been observed to avoid neutrophil killing mechanisms. *L. donovani* parasites for example, prevent lysosome fusion with the phagosome in a lipophosphoglycan (LPG, on the promastigotes surface) dependant manner (Gueirard *et al*. 2007). It has been proposed that neutrophils serve as a transient host and it has been reported that infected apoptotic neutrophils are phagocytised by macrophages that are recruited by the chemokine CCL3 and CCL4 (van Zandbergen *et al*. 2004). Furthermore, phagocytosis of the apoptotic neutrophil caused an increase in macrophage produced anti-inflammatory cytokine TGFß, which interferes with appropriate inflammatory parasite responses. This method of invasion that allows silent entry into the macrophage has been termed ‘Trojan horse’.

In contrast to the rapid motility reported for mosquito-transmitted *Plasmodium* sporozoites, which appear to actively seek out blood vessels; *L. major* parasites are relatively immobile, so it has been hypothesised that neutrophils can retrieve parasites from sites that professional phagocytes can’t access (Peters *et al*. 2008a). In this study, neutrophils were found to phagocytise the parasites efficiently with the parasites remaining viable. When these infected neutrophils or parasites were injected into naïve mice, equivalent infections were established. Furthermore, the authors observed that parasites were being

released from apoptotic neutrophils prior to being phagocytised, while the authors found no evidence, however for uptake of intact, infected neutrophils by macrophages. This result has led to the proposal of the 'Trojan rabbit' scenario where extracellular parasites alongside apoptotic neutrophils are phagocytised by macrophages **(Figure 1-3)** (Ritter *et al*. 2009). As for a role in infection, when Peters *et al* depleted neutrophils using a monoclonal antibodys (mAbs), a decrease in parasite burden was observed.

There have been conflicting results from studies examining the role of neutrophils with regards to *L. major* infection. A possible source of variation in studies investigating neutrophils role in leishmaniasis are the mAbs that have been used (Charmoy, Auderset, *et al*. 2010). RB6-8C5 depletes not only neutrophils but also affect other cells such as monocyte-derived macrophages, eosinophils, dendritic cells, and subpopulations of lymphocytes and monocytes. Other available mABs such as NIMP-R14 and 1A8 are more neutrophil specific. Thus studies where RB6-8C5 was used are difficult to interpret as other important leukocytes may have been depleted.

L. braziliensis triggers neutrophil activation resulting in reactive oxygen species generation, release of TNF-α and neutrophil elastase, and finally, neutrophil apoptosis **(Figure 1-3)** (Falcão *et al*. 2015). Interestingly the closely related species *L. amazonensis* are not as efficiently phagocytised as *L. braziliensis*, are not as potent at activating neutrophils and are more resistant to the neutrophils microbicidal mechanisms (Carlsen *et al*. 2015). However, depletion of neutrophils prior to infection with *L. amazonensis* increased parasite burden in Balb/c but not C57BL/6 mice (Sousa *et al*. 2014). Furthermore, in contrast to *L. major, L. amazonensis* caused a greater recruitment of neutrophils than in PBS infected mice.

With regards to *L. mexicana*, neutrophils have recently been shown to have a negative role in disease development (Hurrell *et al*. 2015). Using 2P-IVM in conjunction with Balb/c or C57BL/6 mice with neutrophils depleted with mAB 1A8, the authors observed that the absence of neutrophils led to lesion control. In addition the authors corroborated this finding by using genista mice, which lack mature neutrophils. The authors also demonstrated that *L. mexicana* induced neutrophils to form extracellular traps (NETs). These are DNA structures

coated with antimicrobial molecules and in the case of *L. mexicana*, had no impact on parasite survival (for review on role of NETs see (Hurrell *et al*. 2016). In the absence of neutrophils, parasites were found in monocytes, dendritic cells and macrophages and this was due to restored expression of monocyte specific chemokines such as CCL2. The authors next examined T-cell functions in the dermal lymph node. In the absence of neutrophils, the authors reported an increase in the levels of Th1 cytokines IFNγ and TNFα with no change in Th2 cytokines (IL-4 and IL-13). This led to the to proposal that in the context of *L. mexicana*, neutrophils provide temporary respite from dendritic cells and macrophages, and induce the development of a protective immune response that favours *L. mexicana* infection. Interestingly, even though *L. amazonensis* and *L. mexicana* both cause non-healing lesions in C57BL/6, only *L. amazonensis* are killed by NETs so there seems to be differences even between these closely related new world species (Guimarães-Costa *et al*. 2009; Hurrell *et al*. 2016).

The role of human neutrophils in the context of patients with cutaneous leishmaniasis (CL) caused by *L. braziliensis* has been investigated (Conceição *et al*. 2016). Here the authors used *in vitro* infection with *L. braziliensis* to examine differences in response of CL patient and health subjects neutrophils. CL patient neutrophils produced more ROS and higher levels of CXCL8 and CXCL9, which reflects an increased capacity to recruit T cells. These differences did not lead to parasite control they were not more proficient in phagocytosis or in being activated. Additionally, during infection any activation also occurred to an equal extent in bystander (non-infected) neutrophils. **(Figure 1-5)**. A summary of the recent studies examining the role of neutrophils in *Leishmania* infection is presented in **Table 3** (Adapted and updated from (Ritter *et al*. 2009)).

Table 1-2: Summary of studies examining the roles of neutrophils in Leishmania infection. Species and sub-strain of parasites used, neutrophil depleting antibody, mouse breed or human samples are specifies. Note that NIMP-R14 can deplete cells other than neutrophils. Updated from (Ritter *et al*. 2009).

Strain	*In vitro*/*in vivo*	Model	Result	Ref
L. major LV 39 (MRHO/Sv/59/P)	BALB/c, $3x10^6$ stationary promastigotes, SC C57BL/6, $3x10^6$ stationary promastigotes, SC	Depletion of neutrophils by NIMP-R14	Hampered the development of a Th2 response. Disease course is improved. Does not affect the development of a Th1 response or disease course	(Tacchini-Cottier *et al*. 2000)
L. major (MHOM/IL/80/Friedlin)	C57BL/6, exposition to infected sandflies	Depletion of neutrophils by RB6-8C5	Decreases the parasite burden at the infection site (4 weeks p.i.).	(Peters *et al*. 2008a)
L. major (MHOM/IL/81/FE/BNI)	Highly purified non-stimulated neutrophils infected with stationary promastigotes	Trojan horse model with human primary macrophages	Leishmanial transfer to macrophages induces amastigote development and TGF-ß production	(van Zandbergen *et al*. 2004)
L. major Friedlin strain FV1 (MHOM/IL/80/FN)	C57BL/6 and B6.SJL congenic mice, and RAG1-deficient OT-II CD4+ TCR transgenic mice	Depletion of neutrophils by RB6-8C5 or 1A8 mAb	Infected neutrophils are phagocytised by dendritic cells inhibiting their activation and subsequent priming of *L. major* specific $CD4^+$ T cells	(Ribeiro-Gomes *et al*. 2012)
L. donovani (MHOM/SD/00/1S-2D) and $lpg1^{-/-}$ and $lpg2^{-/-}$ mutants	Purified dog neutrophils or RB6-8C5 sorted C57BL/6 neutrophils both infected with stationary promastigotes	Trojan horse model with murine macrophages	LPG-dependent survival in C57BL/6 neutrophils enables silent transfer to murine macrophages	(Gueirard *et al*. 2007)
L. amazonensis (strain RAT/BA/74/LV78) *L. braziliensis (*strain LC1418)	C57BL/6, $3x10^6$ axenic amastigotes C57BL/6, axenic amastigotes (3: And 5:1 MOI)		Neutrophils better internalized. *L. braziliensis* amastigotes, *L. braziliensis* infection was a much more potent trigger for neutrophil activation. Neutrophils were able to kill *L. braziliensis* amastigotes, while *L. amazonensis* amastigotes, were highly resistant to this.	(Carlsen *et al*. 2015)
L. amazonensis (IFLA/BR/67/PH8)	C57BL/6, $1X10^6$ amastigotes, IV BALB/c, $1X10^6$ amastigotes, IV	Depletion of neutrophils by RB6-8C5 or 1A8 mAb	No influence on disease course. Increased parasite burden at infection site.	(Sousa *et al*. 2014)
L. braziliensis (MHOM/BR/01/BA788) *L. major* (WHOM/IL/80/Friedlin)	BALB/c mice stationary phase promastigotes (2:1 and 5:1 MOI)		Only neutrophils infected with *L. braziliensis* become activated and displayed markers of early apoptosis	(Falcão *et al*. 2015)
L. mexicana (MYNC/BZ/62/M379)	C57BL/6 BALB/c Neutropenic Genista mice	Depletion of neutrophils by 1A8 mAb or use of neutropenic genista mice	Neutrophil depletion leads to control of lesion development, increased recruitment of monocytes and dendritic cells and early control of parasites As above As above	(Hurrell *et al*. 2015)
L. braziliensis (MHOM/BR/LTCP11245)	Neutrophils isolated from CL patients and healthy individuals	*In vitro* infection (5:1 MOI)	CL neutrophils are more inflammatory producing higher ROS, CXCL8 and CXCL9. No observed difference in ability to phagocytise or con control parasite levels	(Conceição *et al*. 2016)

1.3.4. Macrophages: hosting the intracellular parasite stage

In order for the parasite to undergo its obligate intracellular stage, *Leishmania* parasites need to be phagocytised by residential macrophages or macrophages derived from recruited monocytes (bone marrow derived macrophages: BMDM or M_Φ). It is important to note that monocytes can act as effector cells as has been reported in the case where platelet activation attracts pro-inflammatory effector monocytes to sites of *Leishmania major* infection (Goncalves *et al*. 2011). While pro-inflammatory monocytes exhibit a strong respiratory burst upon infection, leading to early parasite control, macrophages need to be activated by IFNγ first to kill the parasites.

Common to all model infections examined to date is a PSG, which causes recruitment of macrophages (Rogers *et al*. 2009). Additionally, PSG causes the macrophage to upregulate arginase, which is a marker of alternatively activated macrophages. Macrophage activation can be described as a spectrum that at one extreme has 'Classically activated' or pro-inflammatory M1 macrophages and on the other extreme has the 'Alternatively activated' or anti-inflammatory M2 macrophages. A range of receptors including complement receptors (CR1 and CR3), mannose receptors (MR), fibronectin receptors and FcRγ receptors are responsible for pathogen uptake. The roles of different receptors in phagocytosis of *Leishmania* parasites is comprehensibly reviewed by (Shweash *et al*. 2011).

1.3.4.1. M1 macrophages

These cells have a role in the resistance against pathogens and tumours. Models of M1 macrophages include murine macrophages activated by a toll like receptor (TLR) agonist (e.g. Lipopolysaccharides (LPS)) or certain cytokines (TNFα/GM-CSF). Additionally, one of these stimuli, in combination with either prior or simultaneous IFNγ priming leads to a more pro-inflammatory M1 polarisation. M1 macrophages produce various pro-inflammatory cytokines including IL-1ß, IL-6, IL-12, TNFα and IFNγ as well as chemokines and growth factors. If IFNγ is used as a stimulus, these macrophages substantially upregulate surface MHC II (major histocompatibility complex class II) and produce nitric oxide via inducible nitric oxide synthase (*iNOS*).

1.3.4.2. M2 macrophages

Differentiation of macrophages into an M2 phenotype is driven by cytokines such as IL-4, which results in the up-regulation of CD206 (a MR) and galactose-type C-type lectin CD301 (Raes *et al*. 2005). The up-regulation of the arginase gene (*Arg1*) is a prototypical marker for murine macrophage alternative activation and in the context of *Leishmania* parasites; this diverts arginine away from *iNOS* and generates polyamines beneficial to parasite (Rogers *et al*. 2009). Additionally, IL-4 activation of macrophages directly suppresses the hallmarks of M1 macrophage activity, acting to inhibit both the respiratory burst (Abramson & Gallin 1990) and the production of pro-inflammatory cytokines (Levings & Schrader 1999).

1.3.4.3. Macrophage effector functions and evasion of these by the parasite

As previously mentioned gp63 favours the opsonic recognition of metacyclic promastigotes by macrophage by cleaving complement component C3b into its inactive form iC3b (Brittingham *et al*. 1995). Differentiation to metacyclic parasites results in the doubling of the phosphorylated disaccharide backbone repeats and addition of terminal arabinose to LPG oligosaccharide. This aids the parasite to bypass a broad-range pattern recognition receptors such as MR. Structural differences in LPG exist, with *L. major* LPG having a highly substituted nature (Pimenta *et al*. 1994). Species-specific differences in abundance of LPG and gp63 will also impact on host cell association. Additionally, the phase of the parasite's lifecycle is important for route of uptake. This is the case for lesion-derived amastigotes of *L. mexicana*, that have a paucity of LPG and gp63, and here uptake is regulated by FcRII-B2 (receptor Fc-domain of immunoglobulins) (Peters *et al*. 1995b).

Once within the phagosome of the macrophage, the parasites have to deal with oxidative stress. Early during phagosome formation NADPH oxidase is recruited, resulting in the generation of reactive oxygen species (ROS). *L. donovani* prevent this in a LPG dependant manner, as LPG deficient mutants were unable do so (Lodge *et al*. 2006). Whether this is the case for *L. mexicana* has not been investigated due to metacyclics of this species having relatively low levels of

LPG. Other factors such as calnexin and SNAREs are recruited from the endoplasmic reticulum and are essential for phagosome development.

A key step in phagosome maturation is acidification caused by lysosome fusion leading to the formation of the parasitophorous vacuole (PV). Lysosomes are hydrolase rich organelles that can sustain a low pH via a proton-ATPase **(Figure 1-4 (B))**. LPG inhibits this process in the case of *L. donovani* (Vinet *et al.* 2009). Here LPG excluded the exocytosis regulator Synaptotagmin (Syt) from the phagosome, which in turn, prevented the recruitment of the proton-ATPase and hydrolase cathepsin D.

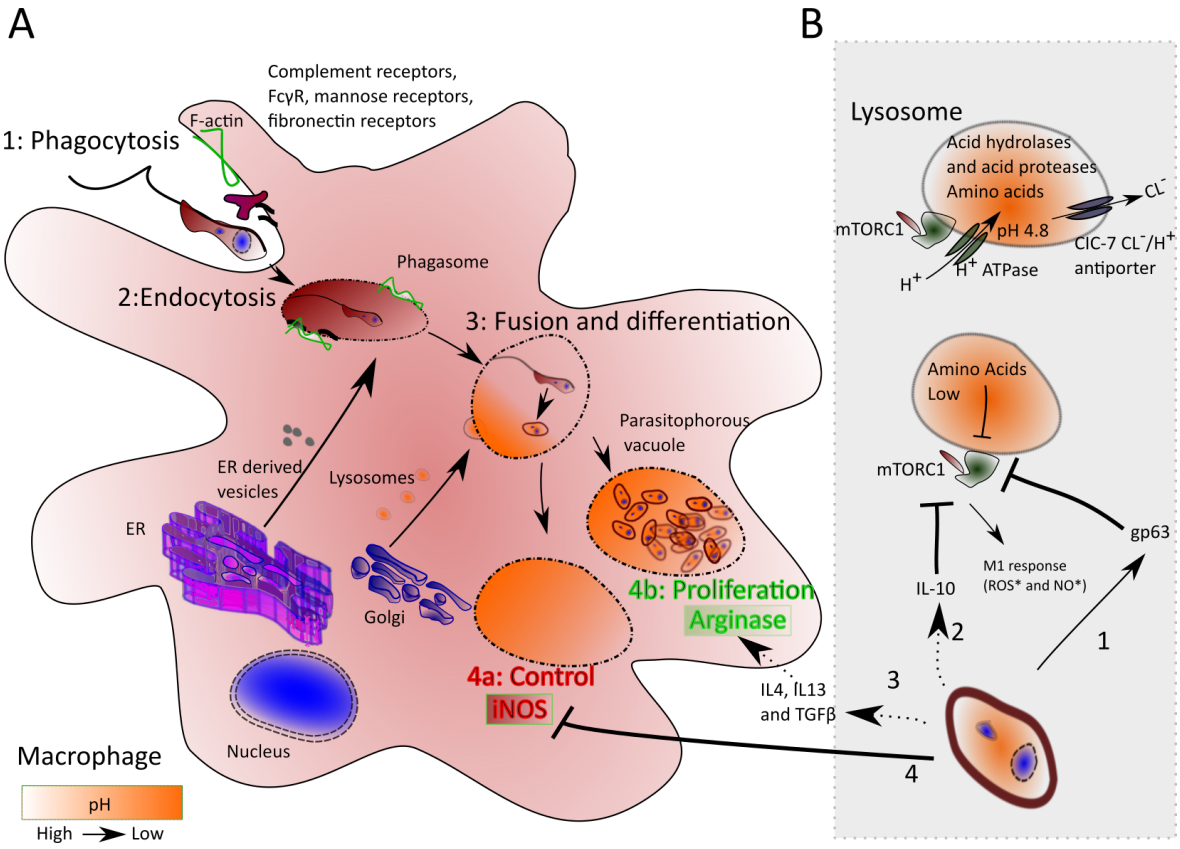

Figure 1-4: (A) Phagocytosis of metacyclic parasite.
1: Phagocytosis is mediate by a variety of surface receptors, 2: Endosome is formed the recruitment of NADPH oxidase occurs at this point, 3: vesicles from endoplasmic reticulum shuffle SNAREs and calnexin to the endosome while lysosomes, which originate from the Golgi, fuse and cause acidification. This decrease in pH as well as changed temperature drives differentiation of metacyclic into amastigote form. Depending on host-pathogen interactions there can either be, 4a: parasite control mediated by iNOS or, 4b: parasite proliferation driven by Arginase. (B) Parasite manipulation of host. Lysosomes are acid vesicles that contain acid hydrolases and proteases and amino acids (aa). The lysosome's pH is maintained by a proton ATPase and a chloride antiporter. Additionally, mTORC1 acts as an aa sensor that activates inflammatory pathways during infection. Other than inhibiting NADPH oxidase recruitment to phagosome and delaying lysosome fusion, *Leishmania* parasites have been shown to 1: secrete gp63 protease to cleave mTORC1, 2: upregulate IL-10, which inhibits mTORC1, 3: upregulate IL-4, IL-12 and TGF-ß resulting in increased Arginase activity, 4: down regulate iNOS activity either via gp63 or LPG.

After the completion of phagocytosis, the main effector function of macrophages is inducible nitric oxide synthase (*iNOS*) **(Figure 1-4, 1-5)**(Wang *et al*. 2009a). Using arginine as a substrate, *iNOS* generates reactive nitrogen species (RNS) including nitric oxide ($NO^{\bullet}$) and citrulline as a by-product. ROS can combine with $NO^{\bullet}$ to generate peroxynitrite (ONO_2^-). $NO^{\bullet}$ can diffuse across cell membranes, it can mediate parasite killing in both immune cells with *iNOS* activity and bystander cells (Olekhnovitch *et al*. 2014). Olekhnovitch *et al* found that protection was associated with the total levels of $NO^{\bullet}$ produced and was not cell extrinsic. The authors demonstrated this by setting up infected cultures where *iNOS* expressing cells made up a small fraction, they were infected as readily as *iNOS* negative cells. When the fraction was increased, all cells were equally protected.

LPG from *L. major* has been found to inhibit *iNOS* upregulation (Proudfoot *et al*. 1996). In contrast to this, *L. mexicana* promastigotes activate MAP kinase signalling through a TLR-4 dependent mechanism to prolong COX-2 and *iNOS* expression, and enhance PGE2 and $NO^{\bullet}$ production (Shweash *et al*. 2011). Interestingly, these effects were required for the parasites upregulation of host *Arg1* as well as the inhibition of IL-12 upregulation. The role of $NO^{\bullet}$ in humans is less clear. In the case of *L. chagasi*, as $NO^{\bullet}$ could not be measured in human cell cultures but *iNOS* inhibitor still abrogated IFNγ mediated parasite clearance (Gantt *et al*. 2001). Thus there is mixed evidence on the role of $NO^{\bullet}$ in humans.

L. mexicana amastigotes have been shown to inhibit LPS induced IL-12 production via a cysteine peptidase B (CPB) mediated degradation of the NF-κB pathway (Cameron *et al*. 2004). *Leishmania* also utilise a CPB-positively regulated metalloprotease gp63, which is abundantly expressed on the cell surface of promastigotes (Casgrain *et al*. 2016). The protease GP63 has numerous host targets that are critical for the hosts pro-inflammatory response including NF-κB and mTORC1 (Gregory *et al*. 2008; Halle *et al*. 2009). The result of NF-κB cleavage was a generation of a novel heterodimer that translocate to the nucleus, driving expression of pro-inflammatory cytokines such as CXCL2, CCL2, CCL3 and CCL4. Interestingly this effect was restricted to pathogenic strains including *L. mexicana*, *L. donovani* and *L. major* but not in the non-pathogenic strain *L. tarentolae*.

Finally, the *Leishmania* parasite combines various defence mechanisms to cope with oxidative stress caused by ROS and RNS (Van Assche *et al*. 2011). These include peroxidases, which reduce H_2O_2, the trypanothione/trypanothione reductase system that is unique to trypanosomatid parasites, pentose phosphate pathway metabolism that maintains intracellular NADPH levels and the cellular redox balance, and superoxide dismutase (SODs), which catalyse the dismutation of superoxide (O_2-) into oxygen and hydrogen peroxide. *Leishmania* also expresses an unusual plant-like ascorbate peroxidase: an enzyme that transfers electrons from ascorbate to H_2O_2 during peroxide detoxification.

1.3.5. Dendritic cells: sentinels bridging the innate and adaptive immune system

Much research on the role of dendritic cells (DCs) has focused on the parasite species causing CL in the Old world, *L. major*. The role of DCs in New world CL causing species is quite different. It the following sections, the two are separated.

1.3.5.1. *Leishmania major*:

There has been some work showing that dermal dendritic cells (dDCs) harbouring parasite antigens, migrate out of the skin and transport the antigens to the draining lymph node (dLN) (Ng *et al*. 2008; Ritter *et al*. 2004). Ng *et al* using 2P-IVM showed that shortly after parasite inoculation motile dDCs decreased velocity to phagocytise parasites.

It has been demonstrated that at 3 to 4 weeks after infection two new subsets of DCs make up the majority in cells in the popliteal lymph nodes and increases of these subsets correspond with a similar increase in monocytes (León *et al*. 2007). The authors demonstrated that one of the new subsets were monocyte derived DCs (Mo-DCs) that differentiated at the site of infection and the other were monocytes that matured at the lymph nodes. This dermal-derived subset potently induced CD4+ and CD8+ T cell production of IFNγ **(Figure 1-5)**. Furthermore, the time-points examined (3-4 weeks) were the same time-points where C57BL/6 mice decrease IL-4 levels versus IFNγ in comparison to BALB/C mice. As the latter event is critical to controlling disease progression, the authors proposed that DCs are important for parasite control. The recruitment of

these monocytes requires CCL3 produced by neutrophils once again highlighting the complexity of cell-cell interactions and dependencies (Charmoy, Brunner-Agten, *et al*. 2010). Infected dendritic cells migrating to the lymph node in a CCR7-dependent manner resulting in LN hypertrophy **(Figure 1-5)** (Carvalho *et al*. 2012). Mice (C57BL/6) unable to recruit cells to the lymph node (selectin $CD62L^{-/-}$) were more susceptible to infection. The authors were unable to explain why only bystander (non-infected cells) upregulated CCR7. This CCR7 signalling was dependent on TLR9 as $TLR9^{-/-}$ dendritic cells migrated less efficiently to the draining lymph node and had decreased CCR7 levels. Furthermore, the mice exhibited a deficit in lymph node expansion following *L. major* infection, as well as increased susceptibility. Finally, there has been some evidence for a supportive role for natural killer cells (NK) in activating DCs (Remer *et al*. 2010). Co-culture of DC with NK led to NK-DC- cross activation and an induction of IFNγ while depleting NK (using anti-asialo antiserum) during vaccination of BALB/C mice with conditioned DC resulted in reduced protection.

1.3.5.2. New world species:

In the context of *L. major*, C57BL/6 mice infected via the ear pinnae have been used to model the self-resolving form of the disease as they mount a vigorous Th1 response and resolve their lesions. C57BL/6 mice infected with *L. mexicana* however, fail to do the same and studies have been carried out to elucidate the mechanisms responsible (Petritus *et al*. 2012; Hsu & Scott 2007). Petritus *et al* showed that fewer monocytes are recruited to the site of infection in the case of *L. mexicana* and those that differentiated into Mo-DCs, had lower *iNOS* activity and were less efficient at migrating to the dLNs. IL-10 was found to have a role inhibiting the Th1 response as treatment of *L. mexicana* infected mice with an anti-IL-10R antibody resulted in increased recruitment of monocytes to the lesion along with greater production of IFNγ and increased *iNOS* positive cells. Hsu *et al* demonstrated that while there was no difference in the inducement of T cell proliferation between *L. mexicana* and *L. major*, the former failed to cause LN hypertrophy, had lower absolute numbers of T-cells (Hsu & Scott 2007). These results were associated with fewer cells migrating to the LN. Additionally, T-cells responding to *L. mexicana* infection were less able to differentiate into IFNγ producing cells. The role of NK cells has been investigated in the context of *L. amazonensis* where co-culture of NK cells have been shown to activate

infected DCs (Sanabria *et al*. 2008). When activated NK cells were injected into infected mice, there was an increase in activated DCs present at lymph nodes and a decrease in parasite burden.

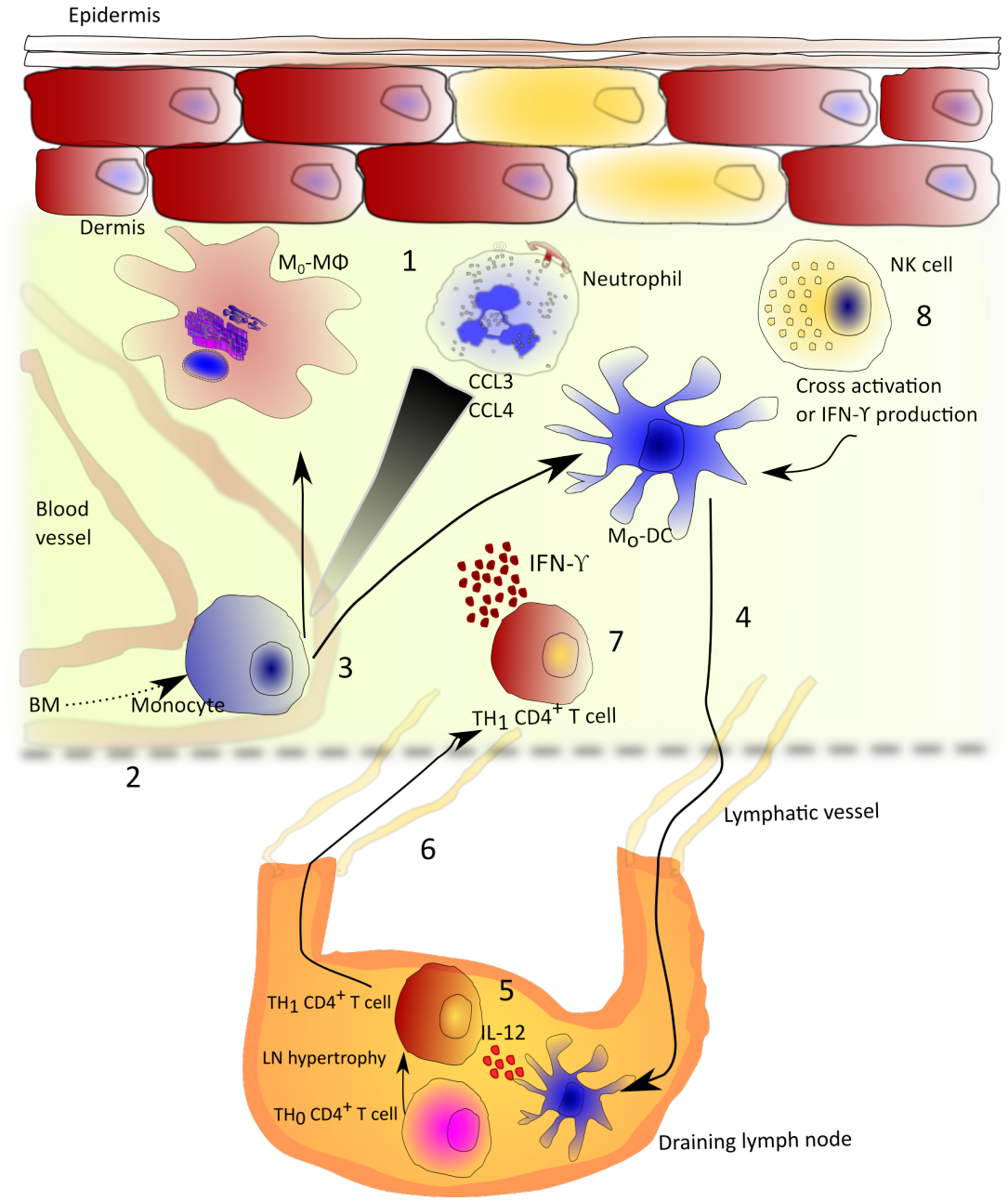

Figure 1-5: Engagement of the adaptive immune response to resolve disease. 1: Infected neutrophils secrete chemokines CCL3 and CCL4. 2: these chemokines recruit monocytes from bone marrow. 3: upon arrival monocytes can differentiate into macrophages or dendritic cells (DCs). 4: Dendritic cells that take up parasite antigen can migrate via lymphatic vessels to the draining lymph node (dLN). 5: Here DCs can secrete IL-12, which causes dLN hypertrophy and naive TH0 CD4+ cells to mature into pro-inflammatory Th1 CD4+ T-cells by around 1 week after infection. 6: Th1 CD4+ T-cells migrate to the site of infection. 7: IFNγ secreted by these cells actives macrophages, causing them to produce sufficient nitric oxide for parasite clearance. 8 Natural killer (NK) cells are another source of IFNγ in Leishmania infection, which can cause cross activation of DCs.

1.3.6. T-Cells

The immunological spectrum observed in patients with leishmaniasis has individuals at both extremes with regard to aberrant T-cell responses. It extends from individuals with delayed-type hypersensitivity (DTH) and high levels of IFNγ, to individuals lacking a DTH response but having a strong humoral response (Scott & Novais 2016). Thus patients without a T cell response exhibit a severe disease called diffuse cutaneous leishmaniasis (DCL) whilst at the other end of the spectrum, patients with an exaggerated immune response also experience a pathological condition known as mucosal cutaneous leishmaniasis (MCL). While $CD8^+$ T-cells do have roles in Leishmaniasis this section will focus on the well-studied $CD4^+$ T-cell. A detailed description of subtypes such as effector T cells, central memory T cells (upon secondary stimulation cells differentiate into effector T cells), and tissue-resident memory T cells, some of which are important in the context of immunity and vaccine development is reviewed elsewhere (Scott & Novais 2016).

In classical animal models of *L. major* infection, parasite-activated $CD4^+$ T cells rapidly proliferate in the expanded dLNs, differentiate and secrete specific cytokines. Th1 (pro-inflammatory) cells secrete IL-2, IFNγ and TNFα, leading to macrophage activation and parasite elimination. Conversely, the Th2 (anti-inflammatory) response is associated with IL-4, IL-5 and IL-13 production, leading to increased parasitaemia. To target these parasites with immunomodulatory agents, the mechanisms of host immunity and of parasite pathogenicity need to be thoroughly examined. For this purpose, mouse models are widely used. However, as seen above for other immune cells, the results obtained with these models are influenced by several experimental parameters, such as the genetic background of the mouse, parasite species and subspecies, inoculation site of infection, parasite dose and use of needle or fly host for parasite inoculation (Uzonna *et al*. 2004).

Upon inducement an appropriate Th1 pro-inflammatory response, the expansion of the dLN is required for disease resolution in the case of *L. major* **(Figure 1-5)** (Carvalho *et al*. 2012). As mentioned above, this process is driven by the migration of dendritic cells from the site of the bite to the dLN (Hsu & Scott 2007). Here they (DCs) induce IFNγ-upregulation in $CD4^+$ Th1 cells by antigen

presentation and release of IL-12. This process is perturbed by *L. mexicana* where it has been shown that cysteine protease B (CPB) deficient parasites induce a Th1 response and as a result, fail to establish infection in susceptible CH3 mice (Buxbaum *et al*. 2003).

To inhibit an appropriate Th1 response, *L. mexicana* induces upregulation of IL-10. Treating mice infected with *L. mexicana* with an anti-IL-10R antibody resulted in parasite control (Petritus *et al*. 2012). It has been shown recently that IL-10 is produced by CD4+ and $CD8^+$ T-cells (Buxbaum 2015). Interestingly, CD4-cre IL-$10^{flox/flox}$ mice lacking IL-10 from T cells (both $CD4^+$ and $CD8^+$) heal their *L. mexicana* lesions, and control parasitemia. Additionally, mice lacking IL-10 from macrophages and granulocytes still develop chronic disease, like their wild-type C57BL/6 counterparts.

A key cytokine in disease resolution is IFNγ. When purified, naive $CD4^+$ T cells were transferred into Thy1-disparate C57BL/6 or IL-10-deficient recipient mice, it was found that alongside poor dLN hypertrophy, IFNγ producing percentages of both $CD4^+$ and $CD8^+$ responding T cells remained greatly diminished after four weeks following *L. mexicana* infection (Hsu & Scott 2007). Hsu *et al* also found that the co-administration of CpG-containing oligodeoxynucleotides at the time of infection overcame this IFNγ deficit and promoted disease resolution. CpG-containing oligodeoxynucleotides function as a ligand for toll-like receptors 9 (TLR9) expressed on the surface of dendritic cells. As mentioned earlier, $TLR9^{-/-}$ dendritic cells migrated less efficiently to the draining lymph node and have decreased CCR7 levels (Carvalho *et al*. 2012). Thus it appears the migration of professional antigen presenting cells such as DC to the dLN and the subsequent interactions with and activation of $CD4^+$ T- cells is critical for a successful Th1 response.

It will be important that further studies comparing disease resolution of different parasite species are carried out to determine if the *L. major* Th1 vs. Th2 paradigm of pathogenesis and protection holds true for New World CL.

1.4. Omics: A short and recent history

Traditionally 'Omics', has referred to genomics, transcriptomics, proteomics and metabolomics but this has been extended to include closely related fields such as epigenetics and lipid-omics. Dr. Thomas Roderick, a geneticist at the Jackson Laboratory, first coined the word genomics in 1986 when discussing a name for a new journal (Yadav 2007). The word genome is much older, its creation being attributed to Hans Winkler who used it to describe a haploid chromosome set by making a portmanteau of the words gene and chromosome. Today genomics refers to the complete genetic makeup of an organism. The other omics followed much later when, in 1995, Marc Wilkins coined the word 'proteomics' to describe an entire organism's protein complement. Integration of the different omics will be invaluable in discovering systems emergent properties. These are features of a system, which only become observable when the system is studied as a whole and not as the sum of its parts. In the following section, the background and current state of the different omics will be covered. Metabolomics will be covered in more detail, as it was the most important and commonly used technique for this thesis.

1.4.1. Genomics

One of the earliest forms of nucleotide sequencing was RNA sequencing which led to Bacteriophage MS2 genome being published by Walter Fiers group in 1976 (Fiers *et al*. 2004). RNA sequencing was initially more amenable due to the wide array of RNA editing enzymes available at the time. A seminal moment in DNA sequencing came with the chain-termination method developed by Frederick Sanger and co-workers in 1977 (Sanger *et al*. 1977). While this method made possible the sequencing of the human genome, next generation sequencers (NGS) have superseded it. In 2004, 454 Life Sciences released a parallelized version of pyrosequencing that was 6 times cheaper than Sanger sequencing. Today sequencing by synthesis (Illumina), which uses reversible dye-terminators technology is the most widely used technique for genome sequencing. While these techniques require amplification of template, PacBio and Oxford Nanopore offer single molecule real time sequencing platforms. These platforms give longer read lengths, which are extremely useful for *de novo* genome sequencing.

Genome assembly is a computationally intensive task, which today, is executed by specialized algorithms such as Bowtie (Trapnell *et al*. 2012).

1.4.2. Transcriptomics and epigenetics

RNA and DNA sequencing protocols are similar once a RNA 'Poly (A)' library has been prepared. Critical to this is reverse transcriptase, a viral enzyme that was independently discovered in 1970 by Howard Temin and David Baltimore. PolyA selection excludes non-coding RNAs and reverse transcriptase creates a complementary DNA (cDNA) that is further fragmented to reach the desired fragment length of the sequencing system. NGS platforms also can be used to sequence the 'methylome'. This is an important epigenetic modification of cytosine (typically in promoter regions) that typically acts to repress gene transcription. Library preparation consists of bisulfite treatment of some of the DNA, which converts cytosine residues to uracil, but leaves 5-methylcytosine, which is read as a cytosine. Thus the DNA that has been treated with bisulfite retains only methylated cytosine, while non-methylated sequences are read as thymine. This approach gives single-nucleotide resolution information about the methylation status of a segment of DNA.

1.4.3. Metabolomics

Metabolomics is a recent and rapidly growing area of research. Primitive examples of metabolomics can be dated back to 1500-2000 BC in ancient China where doctors used ants to detect abnormal glucose levels in patients urine (van der Greef & Smilde 2005). In the middle ages "urine charts" that were based on colours, tastes and smells of urine were used to diagnose various medical conditions. The concept of a metabolic profile was advanced by Roger Williams who, in the late 1940s, used hundreds of thousands of paper chromatographs to look for disease-linked patterns in urine and saliva. The term "metabolic profile" was first introduced in 1971 when Horning *et al* demonstrated that gas chromatography-mass spectrometry (GC-MS) could be used to analyse compounds present in human urine and tissue extracts (Horning & Horning 1971). The term metabolomics was first coined in 1998 (Oliver 1998). Metabolomics is defined as the measurement of small molecules (Mr<1200) within a given system and the importance of this area of research is being increasingly appreciated.

The central dogma of molecular biology first proposed by Crick in 1956 has been further refined to show the complex regulatory networks that act at transcription, replication, translation and post translational modifications.

Metabolism is the closest level to phenotype, with metabolites acting as building blocks of cell structure, effector molecules, products and cofactors of enzymatic reactions **(Figure 1-6)** and thus is an invaluable readout. Today there are various techniques available to measure pathways including carbohydrate metabolism, lipid metabolism, nucleotide metabolism and amino acid metabolism. These two general approaches called Untargeted metabolomics and Targeted metabolomics. Untargeted metabolomics gives a qualitative metabolic profile of a system, and while aiming to maximise coverage, it can be biased by sample preparation and choice of platform. This approach is useful for hypothesis generation and discovery of novel mechanisms of drug resistance (Vincent *et al*. 2010). Targeted metabolomics is used to focus on a specific pathway. By using stably labelled isotopes, metabolites fate can be traced while spiking samples with varying concentrations of labelled metabolite can allow for quantification. By spiking samples with extracts of *E.coli* grown on labelled glucose in conjunction with a calibration curve, it has been possible to quantify up to 65 metabolites (Kim *et al*. 2015a). Targeted metabolomics can be regarded as hypothesis testing. These initial hypotheses can be derived from previous investigations, including untargeted metabolomics.

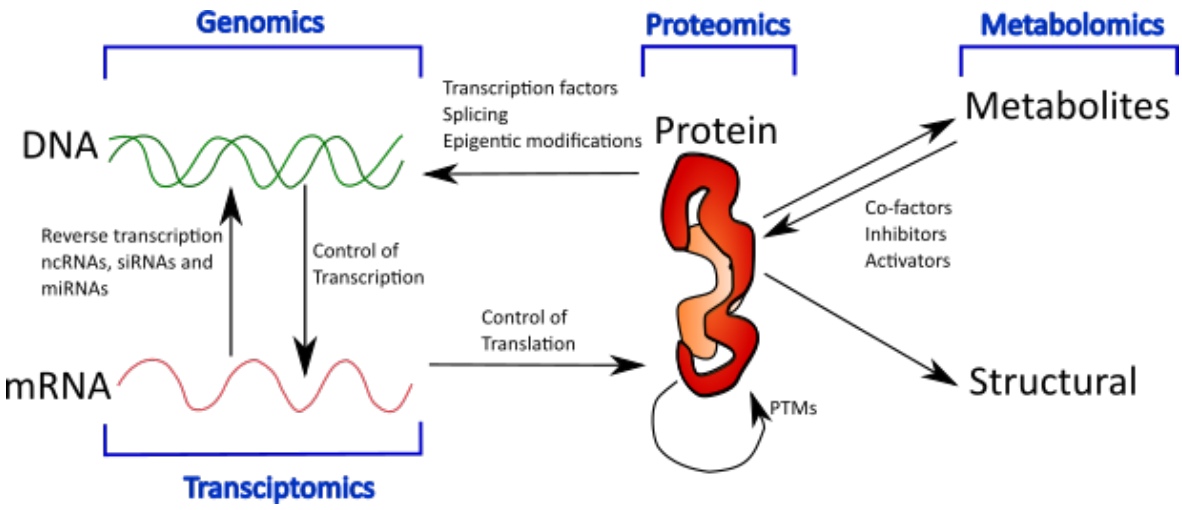

Figure 1-6: How the Omics technologies can cover all levels and directions of the central dogma of molecular genetics.

1.4.4. Sample preparation

The hypothesis to be tests is critical to this step in that it determines if a targeted or untargeted approach is required **(Figure 1-7).** Additionally, the solvent used will determine how well certain metabolite classes are detected (Sellick *et al*. 2010). As metabolism is by its nature quite unstable, rapid quenching is essential to slow or stop metabolism (Sellick *et al*. 2010). This involves removing medium, rapidly cooling sample and adding extraction solvent such as methanol, hot ethanol or chloroform/methanol/water. If cells are in suspension, samples can be quickly cooled using a dry ice ethanol bath before centrifuging. For this project cold chloroform/methanol/water (1:3:1) was used, as this provides good coverage and is stable for oxidation sensitive metabolites such as trypanothione (t'Kindt *et al*. 2010). Essential technical controls include a solvent blank and pooled sample. The pool can be used in a "burn" at the prior to samples to coat columns in matrix similar to sample, and in between samples to ensure instrument reproducibility and stability of samples. Finally, use of internal (labelled) standards in extraction solvent can reveal unequal evaporation in samples.

1.4.5. Platforms

While NMR offers absolute quantification, coverage is quite low when compared to mass spectrometry (MS) systems. MS measures the mass to charge ratio of metabolites and accurate mass allows for the assignment of a chemical formula. A combination of either gas (GC-MS) or liquid (LC-MS) chromatography with a MS platform can be used. In GC-MS the sample is usually ionised directly (EI), or indirectly (CI) by an electron beam. LC-MS is useful for thermally unstable molecules that are soluble in the LC's mobile phase while GC-MS is applied mainly for the analysis of volatile compounds. For life sciences, LC-MS is widely used as it has much wider coverage. However there are many biological important classes of metabolites that do not readily yield derivatives that are needed for GC.

1.4.6. Liquid Chromatography

This method allows for molecules of the same mass to be separated allowing for more accurate annotation. Additionally, the initial separation provided can reduce ion suppression and matrix effects, thereby reducing chemical interactions within samples (Cubbon *et al*. 2010). Ion suppression is where the ionisation of one molecule inhibits that of another, thereby limiting its ability to be detected. Separation occurs in a column that consists of a stationary phase and mobile liquid phase carrying the sample. The physiochemical properties of these phases determine the target classes of metabolites. For MS, High-performance liquid chromatography (HPLC) columns are preferred. HPLC uses smaller sorbent particles (2–50 μm), giving it superior resolving power.

Three common types of LC are partition chromatography, normal phase (NP-HPLC) and reversed phase HPLC (RP-HPLC). NP-HPLC has a polar stationary surface and a non-polar, non-aqueous mobile phase. RP-HPLC has a non-polar stationary phase and an aqueous, moderately polar mobile phase. Finally, partition chromatography gives separation from interactions with a solvent retained on the surface of column matrix or with the matrix itself. A variant of normal phase liquid chromatography that partly overlaps with ion chromatography and reversed phase liquid chromatography is hydrophilic interaction chromatography (HILIC). HILIC uses a hydrophilic stationary phase and a water-acetonitrile mobile phase. RP-HPLC uses a decreasing gradient of polar solvent to elute polar compounds first, which is good for lipophilic compounds while NP-HPLC uses an increasing gradient and is better for polar compounds. HILIC uses a normal-phase type of separation but uses reversed-phase type eluents **(Figure 1-7).**

Stationary phases use functional groups such as a zwitterionic functional group, which carry both positive and negative charges that limit interactions with charged metabolites or octadecyl carbon chain (C18), which is good for lipid separation (Di Palma *et al*. 2011). For our work a ZIC-pHILIC column was used as it gives good separation for both polar and non-polar metabolites and thus was our method of choice (Cubbon *et al*. 2010). The silica-containing ZIC-HILIC column can be used but while it can separate polyamines well, it is inferior for phosphosugars.

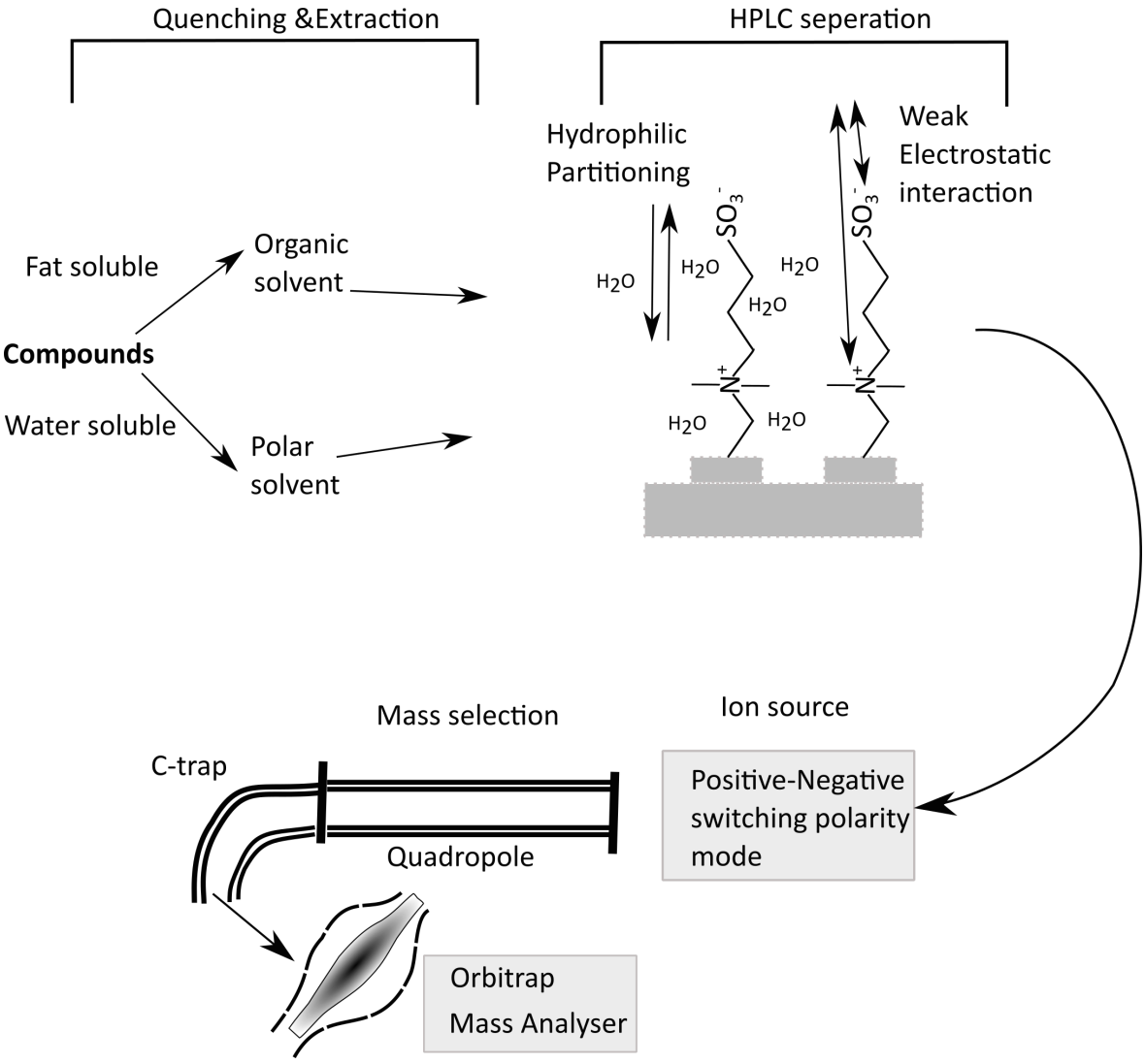

Figure 1-7: Schematic outlining of a typical metabolomics experiment. Solvent choice is critical in determining the types of metabolites that will be best covered. For an example of liquid chromatography, the ZIC-pHILIC system used in this study is shown. Here the presence of zwitterionic ligands and water allow for a wide range of metabolites to be separated in reverse phase elutions. The Orbitrap MS platform shown here was used in this study. Briefly, the ion source switches between positive and negative mode for ionisation of a maximum number of metabolites. Ions are selected based on mass in the quadropole and diverted via a C-trap quadropole for accurate mass measurements in the Orbitrap detector.

1.4.7. Ionisation and detection

In order for metabolites to be detected via their mass to charge ratio, they must first be ionised. A commonly used method is electrospray ionisation (ESI), which operates in positive (adds proton), negative (removes a proton) or switching (between positive and negative) modes **(Figure 1-7)**. The latter mode is preferable as samples containing acidic compounds such as phosphates that are more stable when deprotonated and thus will be detected in negative mode while the opposite is true for amines, which are detected in positive mode (Watson 2010; Yuan *et al*. 2012). In addition to isomers, common unwanted ion

species include multi-charged species and adducts (salt, or fragments generated in source) can complicate metabolite identification. The use of authentic standards and targeted fragmentation of select features can increase confidence in identifications. Nevertheless, the coverage of each platform is limited by the presence of unstable metabolites and those outwith their mass or detection range.

Many different mass-analysers are used, each offering different accuracy and resolution. Commonly used mass-analysers include Quadrupoles that filters ions based on mass and charge, Time of flight (TOF) instruments that accelerate ions and measure time taken to reach a detector and Orbitrap platforms that record the current generated by a ion's oscillation back and forth along central electropole (Dunn 2008). A hybrid Orbitrap instrument was used for this project as it offers achieves ultra-high mass accuracy (as low as 0.21 parts per million (ppm)) and a resolving power greater than 100,000 fwhm (full width at half maximum) at a scan speed of three spectrum per second **(Figure 1-7)**. The qExactive used here uses a quadropole to select precursors and a C-trap (trapping quadropole) for injection into the Orbitrap **(Figure 1-7)**. The accurate mass allows for the assignment of mass spectral featured to few (isomers) or even one metabolite.

1.4.8. Data analysis

Analysis often proceeds by converting instrument propriety data files to a format that is amenable open source software. Subsequently features are selected that meet arbitrary thresholds for abundance, retention time, shape of chromatogram peak, and relative standard deviation (RSD) within replicates. Choosing each threshold is essential in determining the trade-off between false positives and false negatives. Furthermore, gaps in chromatographic peaks can be filled, and additional features be annotated, especially for related peaks (ESI artefacts such as Isotopes, adducts, fragments, and multiply-charged species) (Scheltema *et al*. 2008). Use of an appropriate solvent blank can be used to define detection limit and pooled samples across the experimental batch can be used to for batch correction algorithms and correct for instrument drift across a run (Dunn 2008). Setting a common system for denoting confidence in

metabolite identifications has been advanced by the Metabolomics Standards Initiative (MSI) (MSI Board Members, 2007).

Statistical analysis can be carried out prior or after metabolite identification. However, by filtering out non-metabolites, the false discovery rate is decreased. Using authentic standards as part of a batch helps identifying matching metabolites in samples as well as prediction of other metabolites retention time based on their physio-chemical properties. Essential to identification are compound databases. Examples of these are Human Metabolome Database (HMDB), MZCLOUD, ChemSpider and Kyoto Encyclopedia of Genes and Genomes (KEGG) (Vinaixa *et al*. 2016). While these are comprehensive, a match here does not preclude the possibility of an alternative ion, fragment or isomer.

According to the MSI, high confidence can be achieved by measuring accurate mass and retention time data and comparing it to that of authentic standards (Sumner *et al*. 2007). Furthermore, it is possible to increase confidence in metabolite identifications by fragmenting a metabolite to provide information about its structure.

While use of multi-variate analysis and statistics is essential to obtain confidence intervals and fold-changes, these metabolites belong to pathways and sometimes occur in multiple pathways. Furthermore, metabolites can act in positive or negative feedback loops, and inhibit or induce enzymes in other pathways. To get a meaningful biological interpretation of complex samples, it is essential to explore alterations across entire pathways. Tools such as PATHOS and MetaboAnalyst allow for such analysis (Leader *et al*. 2011; Xia *et al*. 2015). Furthermore, integration of data from different omics can reveal novel discoveries that would not be possible to make from the individual data sets (Jha *et al*. 2015). Finally, there has been a push recently to create data depositories such as MetaboLights (Haug *et al*. 2013). These will be essential to not only archive data, but also create a record of intermediate and final files from data processing pipelines, methodologies, and software (version). Such information will be invaluable in creating highly reproducible results.

1.5. Omics and macrophage function

1.5.1. Transcriptomics: insight into the role, origin and differentiation of macrophages

Macrophages are pivotal to innate immune responses in a diverse range of tissues including the brain, liver, spleen and lung. During challenge, many of these macrophages originate from bone marrow monocyte precursors. An additional population are tissue macrophages. These arise from primitive hematopoietic progenitors present in the yolk sac during embryonic development independently of the monocyte lineage that persists in tissue up to at least 4 months age. There is a new dogma called homeostasis where monocytes differentiate into a long-lived, macrophage that can undergo non-stochastic self-renewal (Bain *et al*. 2016). These cells increasingly replace the embryonic population with age in a process that is highly gender dependent.

As well as macrophages, a highly similar cell type, dendritic cells (DCs) are also present. DCs can be identified by their ability to migrate to the lymph node to present antigens and activate T-cells. Transcriptomics has offered invaluable insight into elucidating the contribution of organ environment and lineage to macrophage cell function as well as differentiating them from DCs (Gautier *et al*. 2012). Gautier *et al* found that only several hundred mRNA transcripts are selectively expressed by macrophages when compared to dendritic cells. Many of these were absent in some of the macrophage from different tissues. On the other hand some that were expressed were specific to certain tissues such as transcription factor GATA-6 in peritoneal macrophages. This information is crucial in modelling diseases that are restricted to certain tissues.

As mentioned in **1.3.4**, macrophages polarisation has traditionally been considered to result in the generation of classically activated, inflammatory (M1) or alternatively activated, anti-inflammatory (M2) effector cells. Recently it has become apparent that these phenotypes are edges of spectrum (Xue *et al*. 2014). In this key study, the authors examined the transcriptional profile of human macrophages polarised to M1 or M2 phenotypes using a diverse range of stimuli. Correlation network analysis revealed that, while for the most part, the transcription profiles was largely bipolar, the addition of either free fatty acids,

high-density lipoprotein (HDL), or combinations of stimuli associated with chronic inflammation, a spectrum of distinct macrophage-activation signatures became apparent. This spectrum became more apparent when multiple time-points were included in analysis. Interestingly, these signatures were absent in human lung macrophages taken from smokers and patients with chronic obstructive pulmonary disease (COPD). Such phenotypes are difficult to reproduce using standard protocols where limited stimuli (and combinations) and time points are used.

1.5.2. Immuno-metabolomics: an essential rewiring

Immuno-metabolism is a recent and rapidly growing area of research with the discovery that changes in cell metabolism not only occur to meet the need for metabolic end products but also are necessary for inflammatory and anti-inflammatory effector functions of macrophages, dendritic cells and T-cells (O'Neill & Pearce 2016). Immuno-metabolism is distinct from anabolism and catabolism, in that it describes how metabolites control transcriptional and post-transcriptional events.

Otto Warburg first recognised this phenomenon when he observed cancer cells upregulate glycolysis to meet ATP demands, as well as NADPH and nucleotides from the pentose phosphate pathway (PPP). This phenomenon is known as the Warburg shift and occurs in inflammatory, LPS stimulated macrophages. While the LPS induced upregulation of both glucose transporter GLUT1 (Fukuzumi *et al*. 1996), and arginine SLC7A2 has been known for some time **(Figure 1-8)**, the mechanisms and functional importance has only become apparent with the advent of immune-metabolism.

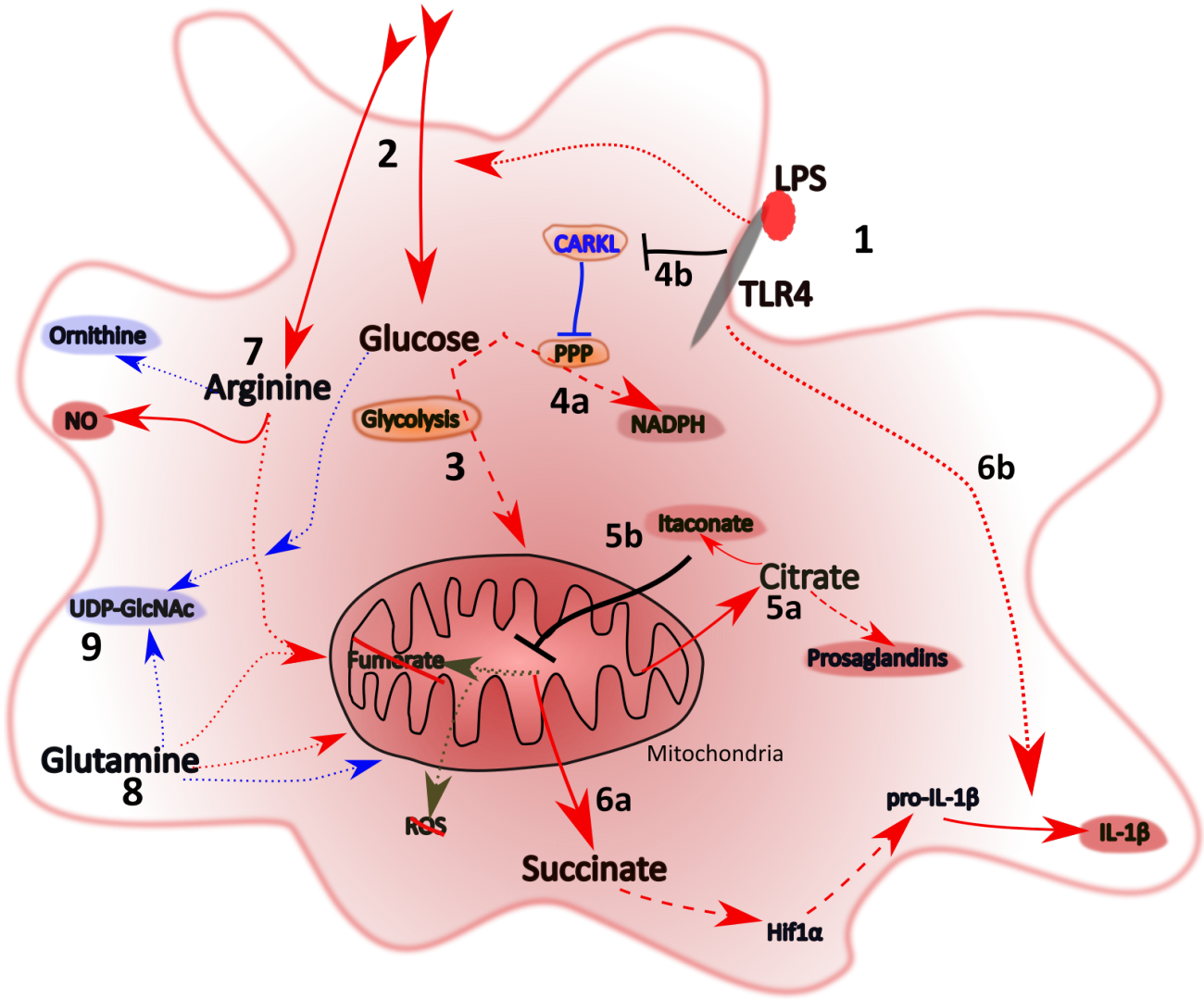

Figure 1-8: Summary of metabolites and pathways the alteration of what required for macrophage effector functions. Red represents pro-inflammatory M1 changes and blue represents anti-inflammatory M2 changes. 1: LPS binding to TLR4 is shown as an example of a M1 stimulus. 2: LPS causes up regulation of Glucose and Arginine uptake. 3:flux is increased through glycolysis. 4a flux is increased through the pentose phosphate pathway (PPP) for NADPH and nucleotide generation. 4b: LPS inhibits the kinase CARLK, which itself prevents flow between glycolysis and the PPP. CARLK is upregulated in IL-4 treated M2 macrophages. 5a: citrate accumulates and is diverted for prostaglandins and Itaconate synthesis. 5b. Itaconate inhibits conversion of succinates into fumarate thereby preventing ROS formation and excessive inflammation. 6a: Accumulated succinate induces HIF-1, which up regulates the M1 cytokine IL-1B. 6b: LPS activates the inflammasome that processes pro-IL-1B in to its active form. 7: In M1 cells arginine is converted into nitric oxide and citrulline via *iNOS*, the latter, helps replenish fumarate via the arginino-succinate shunt. In M2 cells arginine is diverted to ornithine via arginase. 8: in M1 cells, glutamine supplements the TCA cycle via the GABA and argino-succinate shunt. 9: IM2 cells divert glutamine to UDP-GlcNAc synthesis, which is important for pathogen recognition receptors.

In a seminal study, Tannahill *et al* used targeted metabolomics to show that LPS increases flux through glycolysis and induced an accumulation of succinate in bone marrow derived macrophages (BMDM) **(Figure 1-8)**. This increase in succinate induces the HIF1α transcription factor that binds to the promoter of the pro-inflammatory cytokine IL-1β, driving its expression (Tannahill *et al*. 2013). Succinate can also serve as a substrate for succinylation. This is a post-translational modification of proteins in which a succinyl group is added to a lysine residue. LPS increases succinylation of multiple proteins including the glycolytic enzyme glyceraldehyde 3-phosphate dehydrogenase (GAPDH), as well as malate dehydrogenase (MDH), lactate dehydrogenase (LDH), and glutamate carrier. The impact of this on these enzymes functions remains to be elucidated.

Succinate induced pro-IL-1β needs to be processed by the NLRP3 inflammasome, which itself requires glycolysis to function (Moon *et al*. 2015). Following up on these findings, Jha *et al* used integrated untargeted metabolomics and transcriptomics to reveal important pro- and anti-inflammatory metallic modules (Jha *et al*. 2015). In validation experiments using labelled glucose and glutamate, the authors found that, in addition to a succinate accumulation, there is a break in the TCA cycle after citrate caused by down-regulation of isocitrate dehydrogenase (*Idh*) **(Figure 1-8)**. This led to citrate being diverted towards prostaglandin synthesis and Irg1-catalysed production of the anti-microbial itaconate. These breaks in the TCA cycle are replenished by glutamate via the GABA shunt and by glutamate and arginine via the arginino-succinate shunt. The latter reaction links *iNOS* to the TCA, where citrulline combines with asparte (from glutamate) to form fumarate.

Not only can itaconate inhibit the glyoxylate shunt in *Salmonella typhimurium* and *Mycobacterium tuberculosis*, it recently been shown to inhibit succinate dehydrogenase (*Sdh*), causing increased succinate levels (Lampropoulou *et al*. 2016). Macrophages from mice deficient in *Irg1* have increased inflammatory responses to LPS implying an additional regulatory role in limiting inflammation. Lampropoulou *et al* combined a flux balanced analysis (FBA) model with RNAseq data to show that increased itaconate levels caused increased lactate production and decreased flow through *Sdh*. Itaconate also prevents any accumulated succinate being rapidly oxidized, generating ROS via reverse electron transfer

(RET) at complex I **(Figure 1-8)**. In alternatively activated M2 macrophages, there is an upregulated arginase and intact TCA cycle that is supplemented via glutamine. Glutamine and glucose are also diverted to UDP-GlcNAc production (Jha *et al*. 2015). UDP-GlcNAc is used in the glycosylation of lectin or mannose receptors, which are essential for pathogen recognition.

Finally, the PPP has an important role in phagocytes in that in that it provides NADPH that is used by NADPH oxidase to produce ROS as well as Ribose-5P for nucleotides and nucleic acid synthesis. Additionally, it is used in the glutathione-glutathione disulphide (GSH-GSSH) anti-oxidant system, which is needed to protect macrophages from the reactive oxygen and nitrogen species produced during inflammation. An additional regulatory role was found for the PPP with the discovery of the sedoheptulose kinase CarlK (Haschemi *et al*. 2012). CarlK catalyses an orphan reaction in the non-oxidative part of the PPP, generating seduheptolose-7-phosphate (S7P) from sedoheptulose. LPS inhibits this while M2 stimulus such as IL-4 increases it **(Figure 1-8)**. Haschemi *et al* proposed that CarlK, which acts in an ATP dependent manner, facilitates input of glycolytic 3 carbon phospho sugars by generating the rate limiting S7P. The source of sedoheptulose, where the enzyme is located, how it precisely decreases PPP flux, and how mechanistically influences cell function remains to be determined.

1.5.3. Leish-omics: recent breakthroughs

Omics technologies have been key to showing changes that take place when the parasite moves from the fly to the mammalian host. This move results in an increase in temperature and a decrease in pH. By using ^{13}C-stable isotope-metabolomics and $^{2}H_2O$ labelling, Saunders *et al* showed that *L. mexicana* parasites reduce glucose and amino acid uptake when transformed into amastigotes (*in-vitro* and *in-vivo* models) (Saunders *et al*. 2014). Instead the parasites display a stringent metabolic phenotype characterised by increased fatty acid ß-oxidation and glutamate synthesis but generally less profligate use of most metabolites and reduced secretion of metabolic end products. Use of inhibitors showed that the increased fatty acid ß-oxidation and glutamate synthesis are essential to infection progressing.

Some work has been done on determining the key metabolic differences between *L. mexicana, L. major* and *L. donovani* (Westrop *et al*. 2015). While multiple differences were observed in levels of intracellular and secreted (extracellular) metabolites, interestingly, novel arginine and tryptophan utilising pathways were found, of which the former is studied further in this project. Interestingly one novel metabolite, indole pyruvate, which is a transamination product of tryptophan, has also been found to be secreted by bloodstream form of *T. brucei* (McGettrick *et al*. 2016). This study showed that this process is essential in bloodstream forms, and, importantly, revealed an immunomodulatory role. Indole-pyruvate was found to prevent LPS-induced Warburg shift in macrophages (McGettrick *et al*. 2016). This effect was mediated by the degradation HIF-1α, ultimately resulting in a decrease of IL-1β levels.

Metabolomics has also been used to explore the interface of the host pathogen relationship. A ^{1}H NMR spectroscopy approach has been previously used to examine the profile of *L. major* infected BMDM (BALB/c) (Lamour *et al*. 2012). Differences were detected in only 7 out of 34 metabolites including alanine, citrate and succinate. A summary of the various comparisons is shown in **Table 1-3**. This study was limited by the low coverage of ^{1}H NMR. Another limitation was the lack of an attenuated control. The latter is important in differentiating between general infection responses and *Leishmania* specific responses.

Table 1-3: Summary of altered metabolites from Lamour *et al*. Metabolites with increased levels in the various pairwise comparisons are in bold, while those decreases are *italicised*.

	M0+		M1+		M2+	
	Intracellular	**Medium**	**Intracellular**	**Medium**	**Intracellular**	**Medium**
M0	**Acetate** **ß-alanine** **Citrate** **Creatine** **Creatine-P** **Lactate** **Glycine** **GPC** **PC** **Taurine**	**Succinate**				
M0+			**Lactate** **GPC** *Glucose* *Taurine* *Creatine-P*	**Lactate** **Pyruvate** *Alanine* *Glucose* *Glycine*	**Creatine** **Creatine-P**	**Arginine** **Citrate** **Lactate** *Acetate* *Glucose* *Glycine* *Pyruvate*
M1			**Creatine**	**Acetate** **Alanine** **Fumarate** **Pyruvate** **Succinate**		
M2					**Acetate** **ß-alanine** **Citrate** **Creatine** **Creatine-P** **Lactate**	**Acetate** **Alanine** **Arginine** **Fumarate** **GPC** **PC** **Pyruvate** **Succinate** *Citrate* *Glucose*

For such a control, γ-irradiated parasites were included in a recent study examining *L. infantum* infected BMDM (Moreira *et al*. 2015). Moreira *et al* found that the live parasites induced a temporary metabolic shift to the aerobic glycolytic state in macrophages (6 hours post infection), which later reverted to mitochondrial metabolism (18 hours post infection). These changes were detected at transcript (quantitative PCR (qPCR) of glycolytic genes) and at the level of lactate secretion and oxygen consumption. These modulations related to the upregulation of the glucose transporter (Slc2a4 [GLUT1]) and the energy metabolism transcriptional co-activator (Ppargc1a), all of which are essential for parasite growth. Specifically, this metabolic manipulation was shown to require

Sirtuin1 (SIRT1) and a liver kinase B1 (LKB1)/ AMP-activated protein kinase (AMPK) axis as macrophages from mice deficient in LKB1 or AMPK were more efficient in clearing parasites. This axis relies on these three enzymes, which are key energy sensors to switch energy metabolism from glycolysis to mitochondrial oxidation. AMPK acts central cellular signalling hub involved in the regulation of energy homeostasis while LKB1 is an upstream activator. SIRT1 acts by deacetylating key targets (including LKB1) in response to intracellular NAD^+ levels fluctuations. Thus in the case of *L. infantum*, it seems that upon infection the parasites up-regulates glycolysis leading to an increase in the AMP/ATP ratio and a decrease NAD^+/NADH ratio. The result of this is that infected macrophages are initially subjected to the M1 associated Warburg shift that causes a deficit of the energetic and redox status. Later in infection this results in a SIRT1 activating LKB1 that, alongside the increased AMP/ATP ratio, engages AMPK to shift metabolism mitochondrial oxidative phosphorylation.

Recent studies of the transcriptome of *Leishmania*-infected macrophages have given insight into not only how the parasite manipulates the host, but also what changes that occur during the parasites life cycle. Fiebeg *et al* recently published the transcriptome of *L. mexicana* in promastigotes, axenic and intracellular (amastigotes in BMDM) forms (Fiebig *et al*. 2015). By including genome-wide mapping of trans-splice sites and poly-A addition site, the authors proposed a revised genome annotation with over 900 novel genes. There was over 3000 differentially expressed genes between extracellular and intracellular parasites with flagellum-associated genes being down regulated while upregulated ones included transporters and peptidases.

El-Sayeda's group focused on both host (murine) and parasite (*L. major*) over the first 72 hours of infection (Dillon *et al*. 2015). The authors reported that it was during early infection (4 hours) the most dynamic responses were seen in hosts and parasites transcriptome. Significantly upregulated transcripts included those involved in pro- or anti-inflammatory immune responses, and glycolysis, while genes involved in lipid metabolism and Fc gamma receptor-mediated phagocytosis were down regulated. In the parasite, oxidative stress response genes were upregulated while significantly down regulated genes were in pathways such as translation, cell signalling, and flagellum structure. In a

subsequent study, El-Sayeda's group followed up this experiment in human macrophages including *L. major, L. amazonensis* as well as latex beads to subtract the general phagocytosis effect (Fernandes *et al*. 2016). After accounting for phagocytosis, 4 hours post infection displayed the most drastic changes in both host and the two parasite species. Furthermore, there was a large degree of overlap when the authors compared their data on human and murine-specific (Dillon *et al*. 2015) differentially expressed genes which gave a list of genes that make up an infection signature.

Recently, an Illumina methylation specific array was used to examine *L. donovani* infected THP-1 cells (Marr *et al*. 2014). Excluding hits that were present in their heat-killed control, the authors obtained a high confidence set of 443 altered CpG sites that correlated with live *L. donovani* infection. Notable genes that had altered sites in promoter regions were in host defence pathways such as the JAK/ STAT signalling pathway and the MAPK signalling pathways. While the biological relevance of cell lines may be an issue, it does seem that the live parasite can down-regulate appropriate immune responses.

The combination and integration of -omics approaches i.e. untargeted metabolomics and RNAseq has not yet been performed in the case of *Leishmania* infection. In regards to metabolomics, previous studies have utilised low coverage techniques such as ^{1}H-NMR or focused exclusively on central carbon metabolism heavily depending on assays such as oxygen production and lactate secretion, and qPCR. On the other hand, transcriptomics studies have given high coverage but cannot show if altered gene expression acts at the phenotypic level. As previously mentioned, integrated approaches can reveal changes that are of importance or contexts that are not obvious in the individual datasets. In **chapter 4** of this thesis this strategy is used in order to build a comprehensive model of the *Leishmania*-infected macrophage.

1.6. Aims

A primary limitation of Leishmaniasis treatment is the poor understanding of the immune responses that occur in disease resolution and disease progression. Parasite species and highly variable immune responses between individuals can and does compound the determining of appropriate host responses to infection, and how the parasite avoids them. A more immediate and obvious gap in knowledge is how the parasite manipulates host cells such as the macrophage. While past studies, using narrowly focused approaches, have revealed invaluable information, these cannot give the coverage that omics offers.

Immune-metabolism is a recent and rapidly growing area of research. Metabolites that previously thought of as fuel or building blocks have now been shown to have signalling purposes, and changes in certain pathways are essential to cell's effector functions. In the context of inflammation, multiple stimuli are present and so far there is a lack of understanding of the contribution of these cues to phenotype. Whether these metabolic shifts are also induced/supressed in *Leishmania* infection has yet to be determined. A detailed and integrated model of the metabolism and transcriptome of the host cell infected with live parasites will allow for this to be assessed.

This projects aims to:

1. Develop a system for measuring the metabolome of macrophages that accounts for the effects of different stimuli on cell size or numbers.

2. Apply this system to differentiate the contribution of inflammatory stimuli alone or in combination, to identify metabolic shifts that are essential for immune cell function

3. Generate a metabolic model of the *Leishmania* infected macrophage; specifically, to model differences stimulated by the live parasite

4. Generate a high resolution transcriptome of the *Leishmania* infected macrophage and integrate it with the metabolic model

5. Use stably labelled isotope-metabolomics to validate and investigate arginine metabolism in the *Leishmania* parasite

2 Materials and methods

2.1 Bacterial strains and culture

2.1.1 *E.coli* strains used

For routine ligations, the DH5α competent cells (Invitrogen) were used. This strain has been genetically modified as follows: It has a lacZ Delta M15 mutation that allows for blue-white screening of recombinant cells. It also has an endA1 mutation, which causes lower endonuclease degradation. This ensures higher plasmid transfer rates. Finally, it has a recA1 mutation that reduces homologous recombination hence giving a more stable insert. MAX Efficiency® DH5α ™ Competent Cells (Invitrogen), which have a higher transformation efficiency, were used for all transformations that had low efficiency. For overexpression of recombinant protein, the Rosetta strain of *E.coli* was used.

During the project at the OPPF in Harwell all InFusion reactions were transformed into the Omnimax *E.coli* Strain (Invitrogen). In addition to the mutation, these strain lack the *E. coli* K12 restriction systems (mcrA Δ(mrr hsdRMS-mcrBC) which allows for the transformation of highly methylated DNA Furthermore, this strain is resistance to T1 and T5 phage infection as a result of its tonA genotype. For overexpression in *E.coli* at the OPPF the Lemo21 DE3 strain (New England Biolabs) and the Rosseta 2 pLacI (Novagen) were used. In the former strain T7 polymerase is induced by IPTG. Furthermore, the activity of the T7 polymerase is further modulated by its natural inhibitor T7 lysozyme, which is expressed from the rhaBAD promoter. T7 lysozyme levels can be finely controlled by the titration of L-rhamnose. The *P. aeruginosa* stain from which the dimethylarginase was cloned was strain PAO1.

2.1.2 Transformations

Prior to transformation the bacterial stabilate(s) (50 µL) was thawed on ice. Plasmids or ligations were added to stabilate and left on ice for 15 minutes. Cells were then subjected to heat-shock (1 minute 42ºC), then returned to ice for 3 minutes. 250 µL of SOC medium was then added to each transformation and the cells were incubated at 37ºC for 30-60 minutes. SOC is composed of Super Optimal Broth (SOB medium), which is a nutrient-rich bacterial growth

medium, with glucose added for catabolite repression. Subsequently 100 µL of the transformation was plated on selective Lysogeny broth (LB)-agar plates containing appropriated antibiotic (Ampicillin 150 µG/ml; Kanamycin 60 µG/ml (Sigma) before overnight incubation at 37ºC. For plasmids generated using the NEBuilder® HiFi DNA Assembly Cloning Kit, heat shock was 30 seconds, 950 µL of SOC was added, and incubation was 60 minutes.

During the project at the OPPF in Harwell 3 µL of the Omnimax *E.coli* Strain (Invitrogen) was added to In-Fusion® generated plasmids. This mix was left for 30 minutes on ice, heat-shocked for 30 seconds, 42ºC, then left for 2 minutes on ice. 300 µL SOC was added and left for 1 hour at 37ºC with shaking at 225 RPM. The transformants were added to 24 well plates containing the following: 1 mL of LB agar with X-galactose (allows for blue/white selection), IPTG, carbenicillin (Sigma: 50 µG/mL) (similar to ampicillin but less susceptible to pH degradation, thus better for growing longer). The amount of cells added was 25 µL per well or a 1/5 dilution (5 µL cells plus 20 µL LB). Plates were rotated to spread cultures, left ~10 minutes to air dry and incubated overnight at 37ºC.

2.1.3 Bacterial culture and stabilities

Unless otherwise stated all stains were grown in LB. Here individual colonies were inoculated into LB with the appropriated antibiotic (Ampicillin 150 µg/ml; Kanamycin 50 µg/ml (Sigma). For protein over-expression outwits the OPPF project, 1 mM IPTG (Sigma) was used for a 4-hour induction at 37ºC with shaking at 225 rpm. For long-term storage of *E. coli* stocks containing plasmid, 700 µL of overnight culture was added to 300 µL glycerol and stored at -80ºC.

During the project at the OPPF in Harwell, to amplify plasmids in *E. coli*, 2 colonies from each well were picked and put in a 96 deep-well with 1.2 mL Power Prime Broth™ (AthenaES™) and incubated overnight (37ºC with shaking at 225 RPM). For overexpression, both Power Prime Broth™ with chloramphenicol (34 µG/mL) & carbenicillin (50 µG/mL) and 71491 | Overnight Express™ Instant TB Medium with chloramphenicol (34 µG/mL) & carbenicillin (50 µG/mL) were used. 150 µL of overnight culture was added to 3 mL in 24 deep-well plates, and these were incubated at 37ºC, 600 RPM until OD600 was ~0.5. At this point cells were in Power Prime Broth™ had 1 mM IPTG added, and all cells were then

incubated overnight (cells were in Power Prime Broth™ were incubated at 20ºC with shaking at 600 RPM, while cells in auto-induction medium were incubated at 25ºC.

2.1.4 Plasmid purification from *E. coli*

Plasmids were purified from 5 mL overnight cultures using the Macherey Nagel Nucleospin® Plasmid kit according to manufacture's instructions. During the project at the OPPF in Harwell a QIAGEN BIOROBOT 8000 was used in combination with a Wizard® SV 96 Plasmid DNA Purification System Automated protocol (with Qiagen Biorobot 8000) to carry out plasmid purification on 1 mL cultures.

2.2 Molecular biology

2.2.1 Polymerase chain reaction (PCR)

Oligonucleotides were designed using the NCBI primer designing tool and synthesized by MWG Eurofins Genomics (Ebersber, Germany). For screening *E. coli* colonies, GoTaq® G2 polymerase (Promega) was used according to manufacture's instructions. For cloning of genes for the purpose of overexpression or gene replacement where an enzyme with proofreading capability was required, Phusion® High-Fidelity DNA Polymerase (New England Biolabs) was used according to manufactures instructions. For certain reactions, annealing temperatures were determined using a temperature gradient and for all reactions, extension time was adjusted for different product lengths.

During the project at the OPPF in Harwell all reactions were carried out in 96 well micro-plates. Polymerase chain reactions using Phusion Flash Mastermix (NEB) were set up on ice following the manufacturer's protocol. Reactions typically contained 25 µL (bringing it to a final concentration of 1X Phusion Flash Mastermix) 2X Phusion Flash Mastermix, 17 µL sterile H_2O, 3 µL (10 µM) of each primer and 2 µL of template. For these samples, the following protocol was used: 98˚C 10 seconds, 29 cycles (98˚C 1 second, 60˚C 5 seconds 72˚C 30 seconds), 72˚C 2 minutes. For gene blocks, KOD Xtreme™ Hot Start DNA Polymerase (Merck-Millipore) were used according to the following protocol:

94°C 2 minutes, 29 cycles (98°C 10 seconds, 68°C 30 seconds 68°C 30 seconds), 68°C 2 minutes.

2.2.2 Agarose gel electrophoresis

PCR products or digested DNA was separated on 1% Agarose-TAE gels (Invitrogen, UltraPure) containing a 1 in 20,000 dilution of SYBR® Safe (Invitrogen). The PCR band (s) restriction digest profile was compared to those of a Promega 1kb DNA ladder. Gels were cast in the required size using moulds. DNA was prepared by addition of 6x Loading Buffer (Promega) and loaded into wells. Gels were run at between 80-100 V for 30-60 min depending on the DNA fragment size or separation needed. The method for generating a 2% gel used below was identical. Gels were imaged using an UVP Bio doc-it®.

During the project at the OPPF 1.5% TAE agarose gels were used, (Sybersafe 1/20,000), 100 V for 40 minutes. 2 µL of loading dye (0.25%w/v Bromophenol Blue in 30%v/v Glycerol) was added to each sample. 5 µL of Hyperladder I (BioLine BIO-33025/BIO-33026) was used as a reference.

2.2.3 RNA isolation from cultured cells

Mid-log phase parasites (5 x 10^7 cells) were harvested by centrifugation (10 min at 1,200 RCF). The pellet was resuspended in 1 mL Trizol (Invitrogen) and samples stored at -80°C until RNA isolation. For RNA isolation, to 1 mL of cells in Trizol 200 µL of chloroform was added and mixed thoroughly by vortexing. After centrifuging (12,000 RCF, 15 min, 4°C), the mixture separated into a lower red phase (phenol – chloroform: Protein), an interphase (DNA), and an upper colourless aqueous phase (RNA). The upper colourless aqueous phase was removed and transferred to a NucleoSpin® RNA mini spin column (Machery Nagel). The subsequent steps, including the on-column DNA digest, were carried out according to manufacturer's instruction. RNA was eluted in RNAse free water and concentration was measured using a Nanodrop 1000 spectrophotometer (Thermo Scientific), with the method RNA-40.

2.2.4 Reverse transcription

For reverse transcription reactions, 1 µg of RNA sample was mixed with 250 ng random primers (Sigma), 1 µL of dNTPs (10 mM, Promega) and dH_2O to a final volume of 14 µL. To remove secondary structures, the sample mix was heated (65°C, 1 min) and immediately placed on ice. To synthesise cDNA 6 µL RT-mix (containing 5x First-Strand Buffer, 0.1 M DTT and SuperScript III reverse transcriptase (Invitrogen) was added to the sample and incubated for 25 min at 25°C, and then for a further 30 min at 50°C. The reverse transcriptase was inactivated by heating (70°C, 15 minutes). Finally, complementary RNA was removed by adding 1 µL of *E. coli* RNaseH (2U) and incubating at 37°C for 20 minutes. Samples were prepared in duplicate, with one sample set containing dH_2O instead of SuperScript III RT as negative control. Samples were stored at -20ºC until subjected to Real time PCR.

2.2.5 Real-time PCR

SYBR® Green PCR Mastermix (Applied Bioscience) and 96-well plates (Life technologies: MicroAmp® optical 96 well reaction plates) were used for relative quantitative PCR. Sample setup included three biological replicates of each sample (+/- reverse transcription reaction) for the transcript of interest. Water controls (non temple control) were used to detect contamination. Amplification of cDNA was performed using Applied Biosystems Prism 7500 Real Time PCR system, the default thermocycling settings (ddCt (Absolute quantification: Relative Quantification for RT-PCR)), with the reaction volume set to 25 µL, and marker set to SYBR. A melt curve analysis step was added to check that only primer pairs were forming a single product. Raw data was analysed using Applied Biosystems 7500 SDS Real-Time PCR systems software. Specific real-time PCR primers for target genes were designed using the GenScript Real-time PCR (TaqMan) Primer Design tool (https://www.genscript.com/ssl-bin/app/primer). For novel oligos, primer efficiency was tested on *L. mexicana* genomic DNA to verify it was >95%. Primer *L. mexicana* genomic DNA was used to test primer efficiency (doubling dilutions from about 2 ng/25 µl). A standard curve was generated by plotting $\log_{10}$[gDNA] vs Ct. The slope of this curve was used to calculate the efficiency (E) with the formula:

$E=10^{-1/slope}$

% Efficiency=(slope-1) x 100% = efficiency%

2.2.6 Purification of PCR products

PCR products were purified using NucleoSpin® Gel and PCR Clean-up (Machery Nagel) according to manufacturer's instructions. In order to purify DNA fragments from agarose gels the DNA was visualised using a DarkReader blue light transilluminator (Clare Chemical) and the band excised using a sterile scalpel blade.

During the project at the OPPF PCR purification was carried out using Agencourt AMPure XP magnetic beads (Beckman Coulter, Inc.) were used with a MWG Bilatest Seperator M96 small volume. Briefly 1.8 volumes of beads (81 µL) was added to each PCR reaction in a 96 well plate. The plate was then left for 2 minutes on the separator, the supernatant discarded and 200 µL of 70% ethanol was added. After a 2-minute incubation on the separator, the supernatant was discarded and the ethanol was repeated. Again the supernatant was discarded and the plate was left to air dry for 10 minutes. The DNA-magnets mix was resuspended in 30 µL of dH_2O. After a further 2-minute incubation, the DNA was transferred to a new 96-well plate.

2.2.7 Quantification of DNA concentration and purity

A NanoDrop 1000 Spectrophotometer (Nanodrop-Thermo) was used to quantify DNA concentration and purity (A NanoDrop 8000 Spectrophotometer (Nanodrop-Thermo) was used at the OPPF in Harwell). The ratio of absorbance at 260 nm and 280 nm was used to assess DNA purity. A ratio of ~1.8 is generally accepted as "pure" for DNA while the presence of contaminants such as phenol or protein can lower this. The ratio of absorbance at 260 nm and 280 nm was used as a secondary measure of nucleic acid purity. Expected 260/230 values for "pure" nucleic acid are often higher than the respective 260/280 values. Concentration was given as ng/µL.

2.2.8 DNA isolation from cultured cells

For *Leishmania* parasites, ~10 mL of mid-log culture was pelleted by centrifugation, washed with PBS, and the genomic DNA isolated using a Nucleospin Tissue kit (Machery-Nagel®) according to manufacture's instructions.

2.2.9 Ethanol precipitation of DNA

To each sample of DNA, 1/10 volume of sodium acetate (3 M, pH 5.2) was added. After mixing, 2.5 volumes of ice cold 100% ethanol were added. After mixing samples were placed in -80ºC for a minimum of 20 minutes. The precipitated DNA was pelleted by centrifugation (18,000 RCF, 4ºC). The supernatant was removed and the pellet washed with 1 mL of 70% ethanol. The precipitated DNA was again pelleted by centrifugation (18,000 RCF, 4ºC), the supernatant removed and the pellet was left to air-dry briefly. Finally, the pellet was resuspended in 20 µL sterile water.

2.2.10 Plasmid and Oligo design

The relevant DNA sequences were retrieved from TriTrypDB in FASTA format (http://tritrypdb.org/tritrypdb/) and imported into CLC-Genomics Workbench 6. In the case of overexpression of the *P. aeruginosa* protein, the gene symbol is PA1195 and the Fasta sequence can be retrieved from NCBI gene (ID: 883112). Oligos were designed using the NCBI primer blast tool (https://www.ncbi.nlm.nih.gov/tools/primer-blast/) to ensure optimal binding and specificity.

During the project at the OPPF codon optimisation against *E. coli* K12, HEK293 and *Drosophila melanogaster* was first carried out using the online Jcat tool (http://www.jcat.de/). Dr Louise Bird further modified the output of this in order to ensure compatibility with the InFusion (Clontech) system. The final codon-optimised sequences were ordered from IDT® as sequence-verified genomic blocks (gBlocks®). Dr Louise Bird also used the InFusion primer design tool to select oligos which were ordered from IDT® in the form of 96 well oligo plates. This, and following protocols were conducted at the OPPF in accordance with established protocols (Berrow *et al*. 2007; Bird 2011; Bird *et al*. 2013; Nettleship *et al*. 2009; Nettleship *et al*. 2015).

Table 2-1: List of primers used for real-time PCR in this study.

Name	Sequence	Comment
MB1026	CGGCTATGACATCGAGCTTA	*Lmxm.08.1225* fw (qPCR)
MB1027	GACACGTCCTCCACAAACAT	*Lmxm.08.1225* fw (qPCR)
OL4595	GATCGCACTGAGGAGGGTAT	*LmxM.18.0360* fw (qPCR GPI)
OL4595	GTGGTCGAACTCTTGCAGAA	*LmxM.18.0360* rv (qPCR GPI)
Arg1 fw	AGTGTTGATGTCAGTGTGAGC	Arg1 fw (Murine)
Arg1 rv	GAATGGAAGAGTCAGTGTGGT	Arg1 fw (Murine)
Arg2 fw	ACCAGGAACTGGCTGAAGTG	Arg2 fw (Murine)
Arg2 rv	TGAGCATCAACCCAGATGAC	Arg2 fw (Murine)
18s fw	GTAACCCGTTGAACCCCATT	18s fw (Murine, housekeeping)
18 s rv	CCATCCAATCGGTAGTAGCG	18s rv Murine, housekeeping)

Table 2-2: List of primers used for cloning this study. Start codons are underlined and bold, stop codons are bold, underlined and red. 3' his-tag is highlighted in grey #: The OPPF id is given for each primer and the last column refers to the plasmid (Table2-4) within which it is inserted. GPI8 primers were obtained from Prof. Jeremy Mottram, Arginase primers from Dr Mariola Kurowska-Stolarska and 18 s primers from Prof.Iain McInnes.

Name	Sequence	Comment
MB1028	CAGGATCCCAT**ATG**TTCAAGCACATCATCGCTCG	P. aer POA1 fw (DDAH, BamHI)
MB1029	CGGAATTC**TCA**GAAGCGCAGCGACATG	P.aer POA1 rv (DDAH, EcoRI)
MB1030	GCCCCGGG**ATG**ATCGAGGACGGCTATGA	*LmxM.18.0360* fw (Episomal: No tag, XmaI)
MB1031	GCGGATCCCTACGCGCTGTAGC**TCA**GAA	*LmxM.18.0360* rv (Episomal: No tag, BamHI)
MB1032	GCCCCGGG**ATG**ATCGAGGACGGCTATGA	*LmxM.18.0360* fw (Episomal: 3' tag XmaI)
MB1033	GCGGATCCCTAGTGGTGGTGGTGGTGGTGCGGGCCCTGAAACAGCACCTCCAGCGCGCTGTAGC**TCA**GAA	*LmxM.18.0360* rv (Episomal: 3' tag, BamHI)
OPPF17669F	AGGAGATATACCATGATCGAGGACGGCTACGACATCGAGC	Harwell 1 Fw
OPPF17669R	GTGATGGTGATGTTTGGCGCTGTAGCTCAGCAGGCTG	Harwell 1 Rv
OPPF17671F	AAGTTCTGTTTCAGGGCCCGATCGAGGACGGCTACGACATCGAGC	Harwell 2 Fw
OPPF17671R	ATGGTCTAGAAAGCTTTAGGCGCTGTAGCTCAGCAGGCTG	Harwell 2 Rv
OPPF17673F	CATCAGTTCTGCATGCTATCGAGGACGGCTACGACATCGAGC	Harwell 3 Fw
OPPF17673R	GTGATGGTGATGTTTGGCGCTGTAGCTCAGCAGGCTG	Harwell 3 Rv
OPPF17677F	CATCAGTTCTGCATGCTATCGAAGACGGTTACGACATCGAACTGATC	Harwell 4 Fw
OPPF17677R	GTGATGGTGATGTTTAGCAGAGTAAGACAGCAGAGAGCAGCAGG	Harwell 4 Rv
OPPF17677F	CATCAGTTCTGCATGCTATCGAAGACGGTTACGACATCGAACTGATC	Harwell 5 Fw
OPPF17677R	GTGATGGTGATGTTTAGCAGAGTAAGACAGCAGAGAGCAGCAGG	Harwell 5 Rv
OPPF17665F	AAGTTCTGTTTCAGGGCCCGATCGAAGACGGTTACGACATCGAACTGATC	Harwell 6 Fw
OPPF17665R	ATGGTCTAGAAAGCTTTAAGCAGAGTAAGACAGCAGAGAGCAGCAGG	Harwell 6 Rv

Table 2-3: List of primers used for sequencing or analysis (insert orientation) in this study. SP6 and T7 were use to sequence episomal over-expresser genes in pGEMT-Easy, while MB0212 and MB479 were used to the final construct (in pGL1002). T7 and T7 terminator was used to sequence *P. aer* or *L. mexicana* gene (Lmxm.08.1225) in pET28a (+).

Name	Sequence	Comment
MB0095	CTGGATCATTTTCCGATG	Leishmania ITS1 (S)
MB0096	TGATACCACTTATCGCACTT	Leishmania ITS1 (AS)
MB0215	TAATACGACTCACTATAGGG	T7
MB0663	GCTAGTTATTGCTCAGCGG	T7 terminator*
MB0213	TGTCTCTTGTCGGTGCTCAC	pXG Fw (Episomal)
MB479	GAGCACAACACCAAGACGGG	pXG Rv (Episomal)
T7**	GACCGAAATTACGACTCACTATAGGG	OPPF-provided primer

Table 2-4: List of plasmids generated in this study. The pET28a (+) plasmid was used for overexpressing the *P. aeruginosa* protein, pGL1002 was used for episomal overexpressors and pOPIN series was used at the OPPF. Molecular weight (MW) is in kDa. POI = protein of interest, His6 = His6 tag, His8 = C-terminal His8 tag, 3C = Rhinovirus 3C protease site, GST = Glutathione-Stransferase, TRX = E. coli Thioredoxin reductase, RPTPmu = receptor-type tyrosine-protein phosphatase mu, eGFP = enhanced Green Fluorescence Protein. * PDB id for P. aeruginosa gene. Abr refers to antibiotic resistance marker, the second one, if any is for in mammalian cells.

Name	Gene	MW	Ab^r	MW tag	MW	Codon usage	Backbone	Comment
pMB234	*P.aer (1h70*)*	28.5	Kanamycin	~1	29.5	N/A	pET28a (+)	HIS6-POI
pMB235	*Lmxm.08.1225*	26.6	Ampicillin/G418	0	26.6	N/A	pGL1002	No tag
pMB236	*Lmxm.08.1225*	26.6	Ampicillin/G418	~1	27.6	N/A	pGL1002	POI-HIS6
pMB237	*Lmxm.08.1225*	26.6	Ampicillin/G418	~1	27.6	HEK293	pOPINEneo	POI-3C-HIS8 (1)
pMB238	*Lmxm.08.1225*	26.6	Ampicillin	~1	27.6	HEK293	pOPINF	HIS6-3C-POI (2)
pMB239	*Lmxm.08.1225*	26.6	Ampicillin	~3.6	30.2	HEK293	pOPINTolB	SS [TolB]-POI-KHIS6 (3)
pMB240	*Lmxm.08.1225*	26.6	Ampicillin	14	40.6	Bac/insect	pOPINTRX	HIS6-TRX-3C-POI (4)
pMB241	*Lmxm.08.1225*	26.6	Ampicillin	~5.2	31.8	Bac/insect	pOPINH	SS [RPTPmu]-HIS6-3C-POI (5)
pMB242	eGBP*	32.7	Ampicillin	N/A	32.7	N/A	pOPINE-3C-GFP	Empty vector control (+GFP)
pMB243	*Lmxm.08.1225*	26.6	Ampicillin	~5.2	31.8	*E.coli*	pOPINH	SS [RPTPmu]-HIS6-3C-POI (6)

Table 2-5: Gene blocks used in this study: Codon optimisation is as described above.

Name	Sequence
E. coli	ATCGAAGACGGTTACGACATCGAACTGATCGAACTGCCGGCTCTGAACGAACTGCCGGACTCTATGTTCGTTGAAGACGTTTCTATGATCTACAACA CCTGCGCTGTTATCACCCGTCCGGGTGCTCCGTCTCGTCGTCCGGAAGTTGACCCGATCCTGGACACCGTTACCGCTCTGCGTCAGGAACACTACCGTAT CTAAATACGTTTTCGTTGGTAAATCTACCCGTTCTAACGACTCTGGTTACCTAAATACGTTTTCGTTGGTAAATCTACCCGTTCTAACGACTCTGGTTAC GAACAGCTGCGTGACTACCTGGGTAAACACGGTCTGGAATGCGTTCAGTGCGTTGTTAAAAACTGCCTGCACCTGAAATGCGCTGTTACCTTCCTGTCTG AAAACACCCTGCTGGTTTCTCCGAAATGGGTTGACCCGGGTATCTTCACCTCTCGTGGTTTCAAAGTTGTTGAAGTTGACTCTAACGAACCGGCTTCTGC TAACGTTCTGTCTTTCTCTGCTGAAAAAAACGGTAAACCGCTGCGTACCATCGTTACCGCTGCTGAATTCCCGGGTACCGCTTCTCGTGTTGAAGCTTTC GCTGAAGAAGAAACCGCTCAGGGTCGTCCGACCCGTCAGGTTGTTCTGAAAGCTGACGAAATCGCTAAAGCTGAAGGTTCTCTGACCTGCTGCTCTCTGC TGTCTTACTCTGCTTAA
Hek293	ATCGAGGACGGCTACGACATCGAGCTGATCGAGCTGCCCGCCCTGAACGAGCTGCCCGACAGCATGTTCGTGGAGGACGTGAGCATGATCTACAACA CCTGCGCCGTGATCACCCGCCCCGGCGCCCCTAGCCGTCGTCCTGAGGTGGACCCCATCCTGGACACCGTGACCGCCCTGCGCCAGGAGCACTACCGCAT CTGCGAGCCCGGCACCGTGGACGGCGGCGACGTGATGCACGTGGCCAACAGCAAGTACGTGTTCGTGGGCAAGAGCACCCGCAGCAACGACAGCGGCTAC GAGCAGCTGCGCGACTACCTGGGCAAGCACGGCCTGGAGTGCGTGCAGTGCGTGGTGAAGAACTGCCTGCACCTGAAGTGCGCCGTGACCTTCCTGAGCG AGAACACCCTGCTGGTGAGCCCCAAGTGGGTGGACCCCGGCATCTTCACCAGTCGTGGCTTCAAGGTCGTGGAGGTGGACAGTAACGAGCCTGCCAGCGC CAACGTGCTGAGCTTCAGCGCCGAGAAGAACGGCAAGCCCCTGCGCACCATCGTGACTGCTGCTGAGTTCCCTGGTACCGCTAGCCGCGTGGAGGCCTTC GCCGAGGAGGAGACCGCCCAGGGCCGCCCCACCCGCCAGGTGGTGCTGAAGGCCGACGAGATCGCCAAGGCCGAGGGCAGCCTGACCTGCTGCAGCCTGC TGAGCTACAGCGCCTAA
Bac/insect	ATCGAGGACGGCTACGACATCGAGCTGATCGAGCTGCCCGCCCTGAACGAGCTGCCCGACAGCATGTTCGTGGAGGACGTGAGCATGATCTACAACA CCTGCGCCGTGATCACCCGCCCCGGCGCCCCTAGCCGTCGTCCTGAGGTGGACCCCATCCTGGACACCGTGACCGCCCTGCGCCAGGAGCACTACCGCAT CTGCGAGCCCGGCACCGTGGACGGCGGCGACGTGATGCACGTGGCCAACAGCAAGTACGTGTTCGTGGGCAAGAGCACCCGCAGCAACGACAGCGGCTAC GAGCAGCTGCGCGACTACCTGGGCAAGCACGGCCTGGAGTGCGTGCAGTGCGTGGTGAAGAACTGCCTGCACCTGAAGTGCGCCGTGACCTTCCTGAGCG AGAACACCCTGCTGGTGAGCCCCAAGTGGGTGGACCCCGGCATCTTCACCAGTCGTGGCTTCAAGGTCGTGGAGGTGGACAGTAACGAGCCTGCCAGCGC CAACGTGCTGAGCTTCAGCGCCGAGAAGAACGGCAAGCCCCTGCGCACCATCGTGACTGCTGCTGAGTTCCCTGGTACCGCTAGCCGCGTGGAGGCCTTC GCCGAGGAGGAGACCGCCCAGGGCCGCCCCACCCGCCAGGTGGTGCTGAAGGCCGACGAGATCGCCAAGGCCGAGGGCAGCCTGACCTGCTGCAGCCTGC TGAGCTACAGCGCCTAA

2.2.11 Ligations

Ligations were carried out at 16ºC, overnight using a T4 DNA ligase (Promega) and the 10x Ligase Buffer supplied with it. The backbone: insert ratios used were 1:1 or 1:3 in a 10 µL volume. Some inserts were sub-cloned into pGEMT-Easy (Promega) if ligation efficiency was low.

2.2.12 DNA sequencing

MWG Eurofins (i54 Business Park, Valiant Way, Wolverhampton, WV9 5GB) carried out Sanger DNA sequencing on a 96-capillary Applied Biosystems model 3730XL DNA sequencer using a SmartSeq kit. Forward and reverse reads were routinely obtained. For sample preparation in dH_2O, plasmids and PCR template were prepared at 50-100 ng/µL and 5-10 ng/µL respectively in a total volume of 15 µL (including 15pmol of relevant primer). Results (.scf format) were analysed using CLC-Genomics Workbench 6 (CLC Bio), aligning reads to a relevant reference sequence, and viewing sequencing traces. During the project at the OPPF sequencing was carried in house at the University of Oxford.

2.2.13 Cloning of *P. aeruginosa* DDAH

Gene was amplified using Phusion high fidelity polymerase (New England Bioscience (NEB)) according to manufactures instructions. The PCR protocol was as follows: 98ºC denaturing 30 second, 34 cycles (98ºC denaturing for 30 seconds, 70ºC annealing for 30 seconds. 72ºC extension for 30 seconds), 72ºC, 5 minutes for final extension. PCR product was purified as above and sub-cloned into pGEMT-easy vector (Promega) and transformed into DH5α *E. coli*. Mini-prepped PCR product (in pGEMT EASY) and pET28a (+) vector were digested with *NdeI* (NEB) and *EcoRI* (NEB). pET28a (+) was then treated with Antarctic Phosphatase (NEB). This step was as follows: 5.7 µL 10x Antarctic phosphatase buffer and 1 µL phosphatase were mixed with 50 µL digested vector. The sample was then heated to 60 minutes at 37ºC then 70ºC for 5 minutes. All products were gel purified and ligated overnight at 16ºC (Promega, T4 ligase). Ligations were transformed into DH5α *E. coli*. PCR positive (SP6 and T7 primers) colonies were grown (5 mL LB) overnight, and mini-prepped. Finally, the isolated plasmid

was sent for sequencing (T7 and T7 terminator primers) at MWG Eurofins prior to transformation into the Rosetta *E.coli* strain for over-expression work.

2.2.14 Generation of episomal overexpression plasmids

Gene was amplified using Phusion high fidelity polymerase (New England Bioscience (NEB)) according to manufactures instructions. The PCR protocol was as follows: 98ºC denaturing, 34 cycles (98ºC denaturing for, 69ºC annealing for 30 seconds. 72ºC extension for 30 seconds), 72ºC, and 5 minutes for final extension. PCR product was purified as above and sub-cloned into pGEMT-easy vector (Promega), transformed into DH5α *E. coli* and subsequently mini-prepped as described above. As there was a conflict of restriction sites, genes were digested out using *SpeI*, then blunt-ended using DNA Polymerase I, Large (Klenow) Fragment (NEB M0210). Briefly DNA was dissolved in 1x NEBuffer (supplied with polymerase) supplemented with 33 µM of each dNTP. 1 unit of Klenow was added per microgram DNA mix and incubated for 15 minutes at 25˚C. Reactions were stopped by adding EDTA to a final concentration of 10 mM and heating for 20 minutes at 75˚C. The reaction was cleaned up and eluted into 20 µL, prior to digestion with *Bam HI* HF (NEB). The pGL1002 was digested with *BamHI* HF and *SpeI*, treated with Antarctic Phosphatase. The remaining steps, including ligation, and transformation into DH5α *E. coli* are as described above. Final plasmids were sent for sequencing (MB0213 and MB0479 primers) at MWG Eurofins prior to transfections.

2.3 Biochemical methods

2.3.1 SDS page

Samples were typically diluted according to OD600 or protein content (Bradford reagent, Biorad). Diluted samples were mixed 3:1 (sample: loading dye) with a 4x stock of loading buffer (2.0 ml 1 M Tris-HCl pH 6.8, 0.8 g SDS, 4.0 ml 100% glycerol, 0.4 ml 14.7 M ß-mercaptoethanol, 1.0 ml 0.5 M EDTA, 8 mg bromophenol Blue) and denatured (95ºC, 10 minutes). Samples were run on NuPAGE Novex 4-12% Bis-Tris Protein Gels, 1.0 mm, 12-well (Thermo), using NuPage MES SDS running buffer (Thermo) ensuring that milliamps (mA) did not

exceed 120 mA. To determine protein size, a dual colour marker protein precision plus ladder (Biorad) was run alongside samples.

During the project at the OPPF 24 well gels were used as well as wide and low range his-tagged markers (Sigma S8445 and M3913). For *E.coli* experiments a 1 µL of His-tagged Protein Standard (BenchMark™ Thermo) was run alongside Precision Plus dual colour marker.

2.3.2 Western blotting

Protein was transferred to Amersham Hybond ™ ECL membranes (GE Healthcare) using the Novex XCell II™ Blot module (Thermo) using manufactures instructions. Membranes were blocked for one hour at room temperature with 5% milk in PBS-T (PBS with 0.05% Tween-20). Membranes probed with the relevant primary antibody overnight at 4°C, washed three times with PBS-T, and probed with relevant primary antibody for one hour at room temperature. Membranes were then washed three times with PBS-T. The Pierce ® ECL Western blotting substrate (Thermo) was used on membranes according to manufactures instructions and chemiluminescence visualised using the Amersham Hyperfilm ™ ECL (GE Healthcare) on a Xomat (Konica Minolta, Cat no. SRX-101A). Primary antibodies used in this study include a monoclonal anti-polyhistidine (Mouse, Sigma: H1029) or polyclonal anti-transketolase (rabbit, Barrett group). Secondary antibody used was anti-mouse (Promega: W4021) or anti-rabbit (Pierce: 31464).

During the project at the OPPF the protocols were similar except that an iBlot (Invitrogen) was used with iBlot® Transfer Stack, nitrocellulose for transfers and the Amersham ECL Prime Western Blotting detection reagent was used to detect chemiluminescence. The primary antibody used was the MAB050 anti-his-tag Monoclonal Mouse IgG1 (R&D Biosystems) and the secondary used was Anti-Mouse IgG (Sigma: A9044).

2.3.3 Coomassie blue, Ponceau SYPRO ruby (Thermo) and silver staining of protein gels

25 g of Coomassie Brilliant Blue (Thermo) was dissolved in 250 mL of the following solution: Methanol (50% [v/v]) Glacial acetic acid (10% [v/v]) H2O

(40%) the solution was stirred for ~1 hour and then passed through a 0.2 µM filter (Merck Millipore). Gels were stained for a minimum of 30 minutes, and de-stained using the following solution: H_2O, methanol, and acetic acid (50/40/10: v/v/v). Gels were imaged using a Thermo Scientific myECL Imager. Ponceau S (Thermo, 0.1w/v, 5% Acetic acid, 20 min) was used to confirm successful transfer of proteins to membrane. SYPRO ruby (Thermo) was used according to manufactures instructions and gels imaged on a Typhoon scanner (GE healthcare) in acquisition mode (Protocol: 6130 BP30 Deep purple SYBERPROGreen). For silver staining, the SilverQuest™ Silver Staining Kit (Thermo) was used according to manufacture's instructions.

2.3.4 Nickel affinity chromatography

A pellet from 110 mL of culture (OD600 = 2.407) thawed on ice was resuspended in 5 mL of 100 mM sodium phosphate buffer (pH7, 1x PIC (Roche EDTA free), 100 µL lysozyme (Sigma), 2 µL Benzonuclease (Sigma, 500 U)). Sample was sonicated (MSE Soniprep with 19 mM (3/3') probe, 8 cycles x 30s on/off, medium amplitude [14 microns]). The insoluble fraction was sedimented by centrifugation (4ºC, 9500 RCF, 15 minutes) and supernatant stored at -20ºC until processed further.

Protein was purified using a HisTrap HP 5 ml Ni Sepharose column (GE Healthcare) on an AKTAprime plus (GE Healthcare) with binding buffer containing 200 mM NaCl, Tris HCl 50 mM, 10 mM imidazole (Sigma) pH7.5, and eluting into same buffer containing 500 mM imidazole (16 minute gradient). The five 2 mL fractions containing most protein were pooled and protein was dialysed (Spectrum labs Spectr/Por® MCWO 6-8000) into 100 mM phosphate buffer, pH6.8 [2x1L] [1hr first, then overnight] to remove the 500mM imidazole and any L-citrulline/urea present. Protein was concentrated using a concentrator (Vivaspin 20, 5,000 MCW cut off, 4,000 RCF, 4ºC) and diluted to yield a (4.3 mg/mL) solution consisting of 100 mM sodium phosphate buffer pH6.8, 15% glycerol (cryoprotectant to stabilizes protein), which was stored at -80ºC.

During the project at the OPPF for HEK 293 cells, supernatant was removed (secreted sample), plate stored at -80°C for 30 minutes. Plates were defrosted

and 150 µL of lysis buffer (50µL NPI-10 + DNase (Sigma, 8000U) + 50µL protease inhibitors SIGMA P8340) were added to each well and left shaking for 30 minutes (300RPM, 20ºC). 10 µL of the resulting homogenate was added to a 96well plate (total protein). The remaining homogenate was transferred to the 96-deep well plate and centrifuged (6000 RCF, 30 minutes). 10 µL of supernatant (soluble fraction) was then mixed with 10 µL of SDS-PAGE sample buffer.

For *E. coli* samples, 1 mL of overnight culture was transferred to two 96 deep well blocks, centrifuged (6000 RCF, 10 minutes) and supernatant was discarded. Samples were frozen (-80ºC, 20 minutes) and processed using a QIAGEN BIOROBOT 8000 with the following reagents NP-10, NP-20, DNASE/Lysosyme mix, GE beads (His Mag sepharose Ni, 1 mL). The protocol included a 30 minute centrifugation step (6000 RCF) after lysis and samples were eluted in 250 mM imidazole.

2.3.5 2'-5' -ADP agarose affinity chromatography

The aim of this experiment was to try and reproduce the findings of two previous publications (Basu *et al*. 1997; Genestra *et al*. 2006). 5 x 10^{10} mid log promastigotes were harvested by centrifugation (1200 RCF, 4ºC, 10 minutes). Cells were washed once with PBS, re-suspended in 4 mL of 0.25 M sucrose, 5 mM KCl with 0.5 mM PMSF and 1 PIC (Roche, EDTA free) tablet and freeze-thawed 4 times on dry ice ethanol bath. Debris was centrifuged (1000 RCF, 20 minutes, 4ºC), and supernatant subjected to ultra-centrifugation (100,000 RCF, 1hr, 4ºC). Supernatant was ejected onto 2' 5' ADP agarose column. 5 mL of 2' 5' ADP agarose powder (Sigma A 3515) was packed into a 5 mL column according to manufacture's instructions using Buffer A (10 mM Tris-HCL, 1 mM DTT, 1 mM EDTA, 0.5 mM L-Arginine). Column was washed with 20 mL of Buffer A. Next the column was washed with 20 mL Buffer A (+ 0.5 M NaCl), 20 mL Buffer A (+ 0.5 mM NADH), then 20 mL Buffer A (+ 0.5 mM NADP (Sigma), and finally, 20 mL Buffer A. To elute target protein (S) 10 mL of Buffer A (+ 10 mM NADPH (Sigma), 10% w/v glycerol + 3 µM H_4B (Sigma)) was used. Samples were frozen until subsequent anion exchange step was carried out. Fractions A4-7, A8-11, Elutes from NACL, NADH, NADP and concentrated to 750 µL and loaded onto anion exchange column (Whatman: DE-52) Colum was washed 3 times with 80 mM NaCl

(10 mL-20 mL) and target protein eluted using 2 injections of 150 mM NaCl, 3 µM biopterin (10-30 mL).

2.4 Animals

2.4.1 Mouse strains

For all experiments, wild-type male C57 BL/6 mice (age 8-12 weeks), were used. Mice were purchased from Harlan, and kept at the Central Research Facilities, University of Glasgow, Glasgow, U.K. All mice were maintained under standard animal house conditions in accordance with local and home office regulations.

2.5 Culturing of murine (primary and cell line) cells

Detailed standard protocols of culturing mammalian cells at the OPPF are available online (https://www.oppf.rc-harwell.ac.uk/OPPF/protocols/). Methods described below are based on a previous publication (Weischenfeldt & Porse 2008).

2.5.1 Culturing of L929 cells

A vial of frozen cells was removed from liquid nitrogen storage and allowed to thaw in an incubator (37ºC, 5% CO_2). Cells were resuspended in 5 mL cRMPI and then transferred into a vented T25 flask (Corning) and returned to incubator. Once confluent, medium was removed by aspiration. To each plate 6 mL of ice-cold dPBS (Thermo, Magnesium and Calcium free) was added for 1-2 minutes. Cells were detached by gentle scraping (Greiner bio-one Cat-No: 541 070), and transferred to a 50 mL falcon tube. Cells were pelleted by centrifugation (300 RCF, 5 min) and resuspended in cRMPI (15 mL), and then transferred into a vented T75 flask (Corning) and returned to incubator. Once confluent, the process was repeated, this time transferring cells in a volume of 30 mL to a vented T150 flask (Corning). Once this culture was complete the process was again repeated, transferring cells into 5 T150 vented flask (Corning) each containing 100 mL. Four days after the cells had reached confluence the supernatant was collected. Briefly, supernatant was passed through two separate 0.2 µM filters (Merck Millipore: Stericup® and Steritop®, vacuum driven) and divided into 40 mL aliquots. These were stored at -20ºC until used.

In order to quantify M-CSF levels, a Mouse M-CSF DuoSet (R&D Systems) was used with L929 supernatant, according to manufacturer's instructions.

2.5.2 Culturing of bone marrow derived macrophages (BMDM)

Mice were culled using cervical dislocation on day 0. First, dissection kit and mouse were sprayed with 70% ethanol. Legs were removed from mice and surrounding tissue was stripped off using scalpel and bones transferred to a 5 mL bijou tube (Thermo) containing RPMI. The subsequent steps were carried out in a sterile tissue culture hood.

Bones were cut at each end and a 5 mL syringe (BD Plastipak) with 23-gauge needle (Kenke Sass Wolf Fine-Ject®) was used to flush out bone marrow out of leg bone with complete RPMI (cRPMI) into a 9 cm petri dish (Thermo). Any clumps were broken up by repeating the passing through syringe and finally, through a 70 μM cell strainer (Easy strainer™ Greiner bio-one) in to a 50 mL falcon tube (Corning). Cells were pelleted by centrifugation (300 RCF, 5 min) and resuspended in cRMPI (10-20 mL) to obtain a density of 6-7 x 10^6 cells/mL. Cell number was calculated using Trypan blue exclusion (1:1 cells: Trypan blue (Sigma)) to ensure that >95% were viable. Next 1 mL of bone marrow suspension, 2 mL of L929 supernatant and 7 mL cRPMI were added to fresh 9 cm petri dishes. Subsequent culturing took place in an incubator (5% CO2, 37ºC). Three days later (day 3) 5 mL cRMPI and 2 mL L929 supernatant were added. On day 6 BMDM were harvested.

Medium was removed by aspiration and plates were washed once with warm dPBS (Thermo, Magnesium and Calcium free) to remove remaining non-adherent cells. To each plate 6 mL of ice-cold dPBS was added for 1-2 minutes. Cells were detached by gentle scraping (Greiner bio-one Cat-No: 541 070), transferred to a 50 mL falcon tube. Plates rinsed once more with 6 mL of ice-cold dPBS, transferring the same 6 mL between plates to collect remaining cells. Cells were pelleted by centrifugation (300 RCF, 5 min), resuspended in an appropriate volume of cRMPI (10-20 mL) and viable cell number was calculated using Trypan blue exclusion. Cell density was then adjusted by dilution to desired density (10^6 cells/mL in this study). Next cells were left to re-adhere overnight in tissue culture plates. Typically 6, 12, 24, 48 and 98 flat well plates were used. These

were purchased from Costar, with the exception being the 48 well plates, which were purchased from CytoOne. If cells were being used for *Leishmania* infections, they were left overnight at 32ºC, 5% CO_2 prior to infections the next day.

2.5.3 Immune-stimulation of BMDM

The stimuli used were murine IFNγ (Peprotech, 315-05), LPS (Sigma: *E. coli* 0111:B4, Ref L2630) and murine IL-4 (Ebioscience: 14-8041). IFNγ (100 U/mL: 0.02 μG/mL) was typically added for overnight stimulation, after which LPS (100 nG/mL) or IL-4 (20 ng/mL) was added for indicated times. If different concentrations were used, these are indicated. Note that LPS and IL-4 were added to wells without replacing medium (i.e. IFNγ was not removed). Cytokines (including IFNγ) and LPS were replaced after the washed in **Chapter 4**.

2.6 Culturing of *L. mexicana* cells

2.6.1 Species identification

In order to ensure that the parasites used in this study were *L. mexicana*, a simple PCR based strategy was used (Schonian *et al*. 2003). Briefly a repeat region from the 18S ribosomal locus was amplified by PCR using oligonucleotides MB00095 and MB00096, and gel purified as described above. The purified DNA was digested with Hae III (Promega) and the products separated on 2% Agarose-TAE gel (Lonza NuSieve® GTG® agarose) containing a 1 in 20,000 dilution of SYBR® Safe (Invitrogen). The restriction digest size profile was compared to those of a Promega 100 bp DNA ladder and the referenced publication, thus enabling identification of the species.

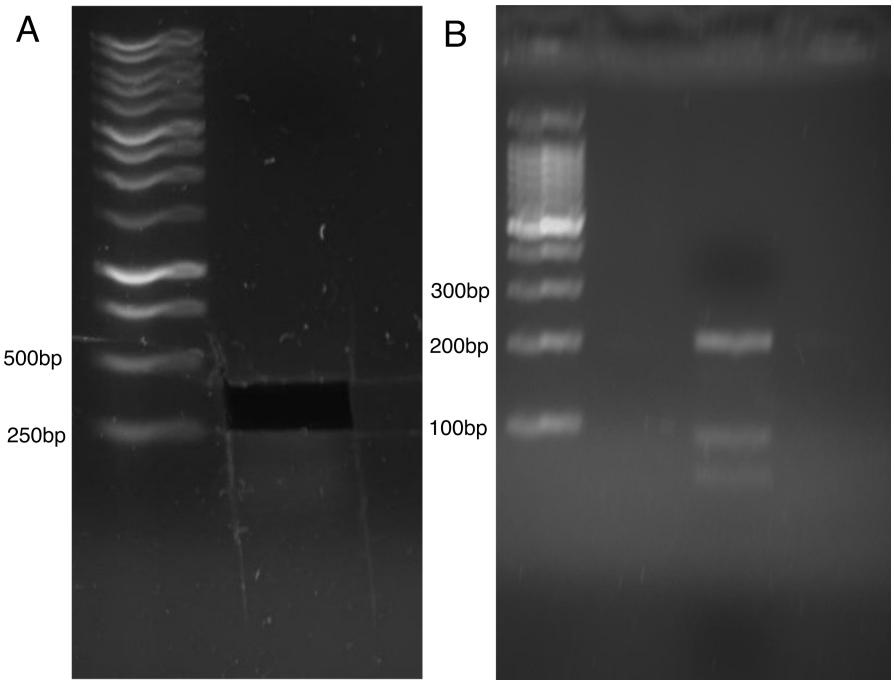

Figure 2-1: Species identification of *L. mexicana*. A: 18S ribosomal locus amplified by PCR using oligonucleotides MB95 and MB96. A Promega 1kb DNA ladder was used and band cut out for purification of DNA. B: DNA was digested with Hae III and separated on a 2% Agarose gel alongside a Promega 100bp DNA ladder.

2.6.2 Culture of promastigotes

L. mexicana (MNYC/BZ/62/M379) were grown in modified Eagle's medium (HOMEM, Invitrogen) supplemented with 10 % (v/v) heat-inactivated foetal calf serum (HiFCS, Invitrogen) and 1 % (v/v) penicillin streptomycin solution (Sigma) at 25ºC. The episomal over-expressor transgenic parasites were maintained in G418 (Sigma) at 50 µg/mL. When referring to the stage of growth of cultures, mid-log phase corresponds to 2-7 x 10^6 parasites/mL and stationary phase to >1.5 x 10^7 parasites/mL. Cells were passaged weekly by counting parasites, and readjusting density to 1-5 x 10^5-10^6 cell/mL. For counting, 25 µL parasites were mixed with 25 µL 2 % formaldehyde (in PBS) and mixed by pipetting. Cells were placed in a Neubauer haemocytometer (Weber Scientific), allowed 3 minutes to settle prior to counting under a light microscope. For all infections, passage number 2-3 (number of passages since retrieved from Balb/c mouse) was used. For infections cells were seeded to insure that parasites had reached stationary phase 2 days prior to infection. For all cultures, non-vented flasks (Corning, 25 or 75 mL) were used.

2.6.3 Transformation and culture of axenic amastigotes

Medium was made according to a previous publication (Bates *et al*. 1992). Growth medium consisted of Schneider's Drosophila Medium (Thermo) supplemented with 20% (v/v) foetal calf serum (HIFCS, Invitrogen) and 1 % (v/v) penicillin streptomycin solution (Sigma). The pH of this medium was adjusted to 5.4 prior to sterile-filtering via a 0.2 µM filter (Merck Millipore: Stericup® and Steritop®, vacuum driven). Stationary phase (5 day old culture) of *L. mexicana* were subculture into the above medium at a density of $1x10^6$/mL at 32.0˚C, 5% CO_2 in vented flasks (Corning, 25 mL). Parasites were sub-cultured weekly. For metabolomics the initial cell density was 10^6 cells/mL.

As axenic amastigotes tend to clump, they were disrupted for the purposes of counting or sub-passaging by passing the cells 3 times through a 26-gauge needle.

2.6.4 Heat-killing of *L. mexicana* parasites

This protocol was carried out after labelling of parasites for FACS enrichemnet (see **2.7.2**) to minimise handling of heat-killed cells. The temperatures that were trialled were 42ºC for 6 and 12 minutes, 46ºC for 6 minutes, 48ºC for 6 and 12 minutes, 56ºC for 6 minutes and 65ºC for 45 minutes. The lowest temperature that reliably gave heat-killed parasites was 48ºC for 12 minutes. Parasites were resuspended in a single cell solution by passing three times through a 23-gauge needle in a volume ≤ 250 µL. The heat-killing was carried out in a water bath with the parasites in 0.5 mL micro-tubes (Sarstedt). Parasites were then transferred to a vented T25 flask (Corning), a density of $1x10^6$/mL in a volume of 10 mL in cRMPI. Flasks were placed in at 32.0˚C, 5% CO_2 in vented flasks (Corning, 25 mL) and counted daily.

2.6.5 Creating stabilates of *L. mexicana* parasites

Stabilates were prepared by mixing 500 µL cells with a pre-chilled mixture of 500 µL consisting of HOMEM, 20 % HIFCS and 10 % DMSO in a 1.5 ml cryovial. These were stored at least overnight at -80ºC before transferring to liquid nitrogen.

2.6.6 Macrophage infection

Bone marrow derived macrophage were adhered overnight either in 48 well plates or 9 cm petri dishes (for FACS enrichment) at a density of 10^6 cells/mL in complete RMPI at 32ºC in 5 % CO_2. Macrophages were then infected with *L. mexicana* metacyclic promastigotes at a ratio of 10 parasites per macrophage for hour hours. At this point, medium was removed from plates by aspiration and wells were washed three times with RMPI (pre warmed to 32ºC). To each well, cRMPI was added and plates were returned to the incubator until processing for metabolomics. For petri dishes (FACS enrichment) the subsequent steps are described below.

2.6.7 Transfection of *L. mexicana* parasites

For each transfection, 5 x 10^7 cells in mid-log phase of growth were pelleted by centrifugation (1200 RCF, 10 min, 4ºC), washed once with ice cold PBS, resuspended in 100 µL of ice cold transfection buffer (90 mM Na-PO_4, 5 mM KCl, 50 mM HEPES, 0.15 mM $CaCl_2$, pH7.3) and transferred to a 1 mL cuvette (Bio-rad: GenePulser® cuvette 165-2086). A minimum of 10 µg DNA in 20 µL sterile dH_2O were added to the cells and tapped gently to mix. Cells were electroporated using the U-033 program on an Amaxa system (Amaxa AG, Köln, Germany) before being transferred to 10 mL pre-warmed complete HOMEM. The culture incubated overnight at 25ºC to allow recovery. A negative control was performed where 20 µL dH_2O was added instead of DNA. The following day appropriate antibiotics were added to select for successful transfectants. As an episomal over-expressor is not a stable phenotype, drug resistant parasites were passaged once before making stabilates alongside the wild-type control.

2.7 Flow cytometry

An overview of the FACS antibodies and dilutions used in this study are given in **Table 2-6**.

Table 2-6: Anti-mouse antibodies, viability and proliferation dyes used in current study.

Marker	Flurophore	Clone	Dilution	Manufacturer	Channel	Isotype
Cd11b	Brilliant violet 510	M1170	5 µL/10^6 cells/100 µL	Biolegend	V2	Rat IgG2a, κ
F4/80	Brilliant violet 421	BM8	5 µL/10^6 cells/100 µL	Biolegend	V1	Rat IgG2a, κ
Live/dead	APC-cy7 Efluor 780	N/A	1 µL/1 mL cells	Ebioscience	R2	N/A
Proliferation	APC-eFluor 670	N/A	5 µM ($6x10^7$ promastigotes/	Ebioscience	N/A	N/A

2.7.1 Characterisation of bone marrow derived macrophages

For cell surface staining, 10^6 cells were detached from plates as described in **2.5.2**, transferred to 5 ml FACS tubes (BD Falcon), washed with 1 mL twice with dPBS (Mg and CL free, 1 mM EDTA). Viability staining was executed using APC-eFluor 670 (Ebioscience) according to manufactures instructions. This protocol ends with cells in FACs buffer (PBS, 1 mM EDTA, 2 % FBS). After this step, cells were re-suspended, 50 µL of a 1:100 dilution of Fc Block (BD Bioscience) added and the cells incubated for 15 minutes at 4ºC. Antibodies for were diluted in FACS buffer and 50 µL of this mix added to each tube and incubated for 20 minutes at 4ºC in the dark (in a fridge). Cells were subsequently washed with 1 mL of FACS buffer and centrifuged (300 RCF, 5 minutes). Cells were then re-suspended in 300 µL FACS buffer, and passed through a 100 µM cell strainer (Easy strainer™ Greiner bio-one) prior to running on a MACSQuant (Miltenyi) as described in **Chapter 3**. For these experiments, alongside fluorescent–1 (FLO-1) controls, compensations beads (eBioscience: OneComp eBeads) were used with each antibody, according to manufactures instructions.

2.7.2 FACS enrichment of infected cells

Protocol is adapted from previous publication with no carboxyfluorescein succinimidyl ester (CFSE) used (Moreira *et al*. 2015). Required number of cells were taken, pelleted by centrifugation (1200 RCF, 5 minutes) and supernatant discarded. Cells were wash twice in dPBS (Mg and CL free), and then re-suspended (passed through 23-gauge) in single cell solution at $6x10^7$ promastigotes/mL. Cells were stained for 5 minutes with 5 µM eFluor670 (in dark, 25ºC). Reaction was stopped by adding 5 volumes of ice-cold cRPMI, incubating on ice for 5 minutes. Cells pelleted by centrifugation (1200 RCF, 5 minutes) and medium discarded. Cells were re-suspended an equal volume of ice-cold cRPMI, pelleted by centrifugation (1200 RCF, 5 minutes) and finally, resuspended (passed through 23-gauge) at a density suitable for heat-killed. Infection was allowed to proceed for 4 hours (32ºC, 5% CO_2) in petri dishes containing BMDM (10^6 cells/mL) after which medium was removed.

To each plate, 6 mL ice-cold dPBS (Mg and CL free) was added for 3 minutes, and cells detached by scraping. Cells were washed once with PBS, re-suspended in FACs buffer (2% FCS in dPBS (Mg and CL free)) and passed though a 100 µM cell strainer into FACS tubes (BD Falcon). Note that EDTA was not used at any point of this protocol. Samples were stored on ice until processed. An FACS Aria I and III (BD Biosciences) were calibrated (auto-compensation) using same samples (Non-infected, infected and heat-killed infected). Cells were sorted into 15 mL falcon tubes containing RPMI+50% HiFCS). After collecting all samples, cells were pelleted centrifugation (300 RCF, 5 minutes), and resuspended in cRMPI. Cell number was calculated using Trypan blue exclusion (1:1 cells: Trypan blue (Sigma)) to ensure that >90% were viable. Finally, cells were seeded at a density of 10^6 cells/mL in a volume of 200 µL in 48 well plates. Plates were placed in incubator (32ºC, 5% CO_2) to allow infection to resume.

2.7.3 Data and analysis

Data was imported into FlowJo 10.0.8r1 (Treestar) for analyses. Cell size (Forward scatter versus side scatter) and viability (EF780), single stained samples, Compensation beads and FMO-1 were used where relevant.

2.8 Phenotypic analysis of BMDM

2.8.1 ELISA

Cytokine expression was tested in *in vitro* culture supernatants. ELISAs were carried out according to the manufacturer's protocols. In general, 96-well half or full volume high-binding plates (Fisher Scientific) were coated with capture antibody in recommended coating buffer and incubated overnight at a temperature recommended by the manufacturer. For IL-6 ELISA, a 1/8 dilution in assay diluent was used to insure samples were in linear range of assay. After incubation with detection antibody and streptavidin- horseradish peroxidase (HRP) and subsequent washing, TMB substrate was added to wells and incubated at room temperature (in dark) until development of standards appeared middle of this linear phase of amplification (i.e. when it was possible to visually note the differences in the different concentrations). The reaction was then stopped using 4N sulphuric acid, and plates read at 450 nm with wavelength correction applied by subtracting the absorbance at 570 nm using a Tecan Sunrise® plate reader. See **Table 2-7** for a list of ELISA kits used in the current study. Medium incubated in empty wells were used as matrix blanks.

Table 2-7: ELISA kits used in current study.

Cytokine detected	Manufacturer	Detection range
M-CSF	R&D Systems	15.6-1000 pg/mL
IL-6	BD Biosciences	15.6-1000 pg/mL
MCP-1	Affymetrix Ebioscience	15.0-2000 pg/mL

2.8.2 Luminex

The Cytokine Mouse 20-Plex Panel (Thermo: LMC0006) was used according to manufactures instructions with the exception being that the reagents were dilutes as to spread the assay over two plates (using Extracellular Protein Buffer Reagent Kit for Mouse or Rat, LMB0001). Standard protocols provided by the Institute of Infection, Immunity and Inflammation's Flow Cytometry Facility

were used (see http://www.gla.ac.uk/media/media_264279_en.pdf and http://www.gla.ac.uk/media/media_265386_en.pdf for more information) Medium incubated in empty wells were used as matrix blanks. Plates were read using Biorad Bio-Plex 100 and data acquired and analysed using Bio-Rad's Bio-Plex software version 4.1TM. 4 biological replicates were used in this assay.

2.8.3 Greiss assay

Supernatant was transferred to 96 well plate, centrifuged (300 RCF, 5 minutes) and 50 µL transferred to a new 96 well plate. Standard curves were made using a serial dilution of 0.1 M Nitrite (Sigma). The concentrations used were 100, 50, 25, 12.5, 6.25, 3.125 and 0 µM. To the samples and standards, 100 µL of Greiss reagent (Sigma: 03553) was added until development of standards appeared middle of this linear phase of amplification. Plates were read at 570 nm using a FLUOstar OPTIMA micro-plate reader (BMG Labtech). Medium incubated in empty wells were used as matrix blanks.

2.8.4 MTT assay

The Vybrant® MTT Cell Proliferation Assay Kit was used to determine the toxicity of L-argininic acid and L-pipecolic acid (American Custom Chemical Corporation). 1.25 and 20 mM were the concentrations used and the positive control was 2% formaldehyde (final concentration). The protocol was carried out according to manufacture's instructions (Quick protocol option) using DMSO to re-solubilise formazan crystals. Absorbance was read at 540 nm using a FLUOstar OPTIMA micro-plate reader.

2.9 Enzymatic synthesis and assays

2.9.1 Synthesis of 2 keto-arginine

Synthesis was modified from (Wellner & Meister. 1960). Briefly 30 mg L-amino oxidase (Sigma: dried venom) 0.2 grams arginine, 47,000 U catalyse (Sigma: bovine), 0.39 µM FAD pH 7.2 were mixed together in a volume of 21.4 mL in a 100 mL conical Erlenmeyer flask. The pH was adjusted to 7.6 with 1 N HCI. The flask was plugged with cotton, left shaking overnight at 37°C. After 6 hours, another 47,000 U catalyse was added. Protein was removed by passing through a

Vivaspin 20 tube (5,000 MCW cut off, 4,000 RCF). The elute was concentrated by evaporation with a Savan DNA120 speed vac concentrator (Thermo) under vacuum, medium heat, to about 6.4 mL. For a control, a 1/10 amount of the above reagents minus L-arginine was put through the same protocol. For LC-MS analysis, samples were diluted to 100 µM (of a theoretical 100% efficient yield) in Chloroform/Methanol/dH_2O, 1:3:1).

2.9.2 Assay for L-citrulline detection

All non-radioactive / non LC-MS methods detect ureido compounds use diacetylmonoxime in strong acid for the colorimetric determination of citrulline. These assays also detect carbamyl aspartate and urea. The assay used here was adapted from a previous study (Prescott & Jones 1969) to a 96 well format. Note that for experiments using ADI, reactions took place in glass tubes, 1 mL volume, and standards and blanks were developed alongside these in 1 mL tubes, before transferring to cuvettes (Fisher Scientific FB55147) for measurement in at Shimadzu UV-2550 spectrometer. While this assay lacks the dynamic range of alternative protocols (Knipp & Vašák 2000), it is highly sensitive in our hands, reproducibly detecting in the low (<50) µM range. Briefly, 100 µL enzymatic reactions were set up in a 96 well plate. For ADI, the indicated amount of commercial *Mycobacterium arginini* ADI (Abcam®) was added (5 µL of 0.1 mg/mL stock) to a volume of 1 mL consisting of 50 µM L-arginine in dH_2O. Samples were incubated at 37ºC for 60 minutes. 70 µL Urease (Sigma Jack bean 10 mg/mL in 0.2 M sodium phosphate buffer) was added for a further 10 minutes at room temperature. Buffer controls and a L-citrulline standard curve were set up on same plates. The L-citrulline standard curve included the following concentrations: 200, 100, 50, 25, 12.5, 6.25, 3.125 and 0 µM.

For DDAH assay, 2.5 µL of enzyme (4.3 mg/mL) was added to 100 µL solution of 100 mM Na_2HPO_4, pH 6.5, containing 100 µM ADMA (Cayman Chemical, stock was 10 mM in 100 mM Na_2HPO_4, pH 6.5). Samples were incubated at 37ºC for 60 minutes. Buffer controls and a L-citrulline standard curve were set as above.

Two colour development solutions are used in the assay. Solution A is an antipyrine/H_2SO_4 (50% v/v) reagent that is stable at room temperature. Briefly, 50 mL stock H_2SO_4 (Sigma, 17.8 M) was slowly added to 25 mL dH_2O. Next 25 mL

was added to this mix, ensuring solution did not over heat. Once solution cooled down to room temperature, antipyrine (Sigma) was added (5 g/L). Solution B consists of 0.80 gram of diacetymonoxime (Sigma) in 100 mL of 5% (v/v) acetic acid (Sigma). This oxime reagent was stored at 4ºC in a dark bottle covered with aluminium foil. It was made fresh every three weeks.

Immediately before use, 2 volumes of Solution A was mixed with 1 volume of Solution B. To each well, 100 µL of this mixture was added (or 1 mL to tubes), and the plate placed in an oven at 60ºC for 3 hours. Plates were read on a FLUOstar OPTIMA micro-plate reader, measuring 485 nm excitation, 460 nm emission.

2.9.3 G6PDH assay

Assay was carried out according to previous publication (Maugeri *et al*. 2003). Cells were lysed for one hour on ice in 10 mM Tris HCl buffer (pH 7.4, PIC (Roche, EDTA free), 0.4% Triton-X100 (Sigma). Debris was pelleted by centrifugation (18,000 RCF, 4ºC, 15 minutes) and 100 µL supernatant transferred to each cuvette (Fisher Scientific FB55147). Reactions were measured in quartz cuvettes and contained 50 mM Triethanolamine, pH7.5, 5 mM MnCl2, 0.5 mM NADP and 2 mM glucose 6-phosphate. Reactions were initialised by adding NADP after the 5 minutes allocated to allow measurements to stabilise. The assay was performed at 30ºC and absorbance read at 340 nM using a Shimadzu UV-2550 spectrometer. The positive control was 1 µL of G6PDH, (Sigma, *Leuconostoc mesenteroides* 0.0034 mg of enzyme/2.66 units added). Bradford reagent (BioRad) was used according to manufactures instructions with same sample to determine protein content.

2.10 Metabolite extractions

2.10.1 Preparation of LC-MS samples for *L. mexicana* parasites

Protocol for amastigotes and procyclic promastigotes are identical except that 2 x 10^8 cells are used for the former, and 1 x 10^8 cells for the latter. Note that for all stable isotope labelling experiments, parasites were grown in 50% labelled medium. This medium was made by adding an equal concentration of labelled or non-labelled amino acid to either stock HOMEM or axenic amastigote medium.

Note that the concentration of L-arginine was 1.01 mM in HOMEM. This means that the amino acids concentration was 2x in all samples these experiments. In the axenic amastigote medium, SDM makes up 80% of the medium (20% serum). As the concentration of L-arginine is 2.3mM in SDM and it was assumed that there is some L-arginine present in serum, so 2mM labelled or non-labelled amino acid was added.

Parasites were counted and required number of cells collected in 50 mL falcon tubes. Samples were quenched by immersing tubes in a dry-ice ethanol bath and a thermometer was used to mix samples and ensure samples did not freeze. In our hands, quenching until thermometer reads 10ºC is sufficient to cool samples near to 0ºC without freezing. Cells were pelleted by centrifugation (1200 RCF, 10 minutes, 4ºC). Spent medium as removed by aspiration. Pellets were resuspended in 1 mL of ice cold PBS, transferred to 1.5 mL micro-tubes and again pelleted by centrifugation (1200 RCF, 10 minutes, 4ºC). PBS was discarded and pellets extracted by re-suspending in ice-cold extraction solvent (chloroform/methanol/water, 1:3:1).

Cells were left shaking (1 hour, 4ºC). To make a solvent blank, 200 µL of extraction solvent was added to an empty 1.5 mL micro-tube and processed alongside these samples. Solvent was then transferred to 1.5 mL micro-tubes (Sarstedt), and centrifuged (18,000 RCF, 15 minutes, 4ºC). Supernatant was immediately transferred to 2 mL screw-cap tubes (Sarstedt) or glass vials for LC-MS analysis (Chromacol SV-S11G). Sample from each tube was transferred to a new screw-cap tube for pooled sample. The amount taken was calculated so that there would be sufficient pooled sample to coat the pHILIC column (6 injections) and to be injected after every 4 samples. At this point, samples were capped with Argon, and then stored at -80ºC until LC-MS analysis.

In the case where spent medium analysis was required, 5 µL was extracted in a volume of 200 µL extraction solvent and processed as above. For these experiments, medium was left in an empty well for duration of experiments to give fresh medium samples.

2.10.2 Preparation of LC-MS samples for BMDM

10 µL of medium was transferred to a 48 well tissue culture plate, which was kept on ice. When time permitted, this plate was centrifuged (300 RCF for 5 minutes, 4ºC) and supernatant transferred to new plate for extraction or storage (-80ºC).

Remaining medium was aspirated and cells were washed once with dPBS (Magnesium and Calcium free, no EDTA), aspirating immediately. Ice-cold extraction solvent (CMW: chloroform/methanol/water, 1:3:1) was added to each well, including an empty well (for solvent blank), and cells were left shaking (1 hour, 4ºC). Solvent was then transferred to 1.5 mL micro-tubes, and centrifuged (18,000 RCF, 15 minutes, 4ºC). Supernatant was immediately transferred to 2 mL screw-cap tubes. Sample from each tube was transferred to a new screw-cap tube for pooled sample. At this point, samples were capped with Argon, and then stored at -80ºC until LC-MS analysis.

For **Chapter 3**, 3 million macrophages were seeded at a density of 10^6 cells/mL and extracted in a volume of 400 µL CMW. In **Chapter 4**, for FACS enriched samples, 200,000 macrophages were seeded at a density of 10^6 cells/mL (250 µL) and extracted in a volume of 250 µL CMW. For non-FACS enriched samples, 250,000 macrophages were seeded at a density of 10^6 cells/mL (250 µL) and extracted in a volume of 250 µL CMW.

2.10.3 Calculation of protein content post-extraction

To each well, NaOH (0.1 M, 400 µL/10^6 cells) was added. The plate (s) were left shaking (15 minutes 4ºC). Plates were next centrifuged (300 RCF, 5 min) and 10 µL of supernatant transferred to a 96 well plate. To the same plate, a 10 µL of a BSA (Sigma) dilution series (2 fold: 0.5-0 mg/mL in 0.1 M NaOH) was added. Finally, 190 µL of Bradford reagent (BioRad) was added to each plate on top of samples and standards. Absorbance was measured at 595 nm using a FLUOstar OPTIMA micro-plate reader.

2.11 Statistical analysis

Statistical analysis was carried out as described in text using Graphpad Prism. Otherwise, MetaboAnalyst or Deseq2 were used as described. For targeted LC-MS, 3 replicates were used while 3-4 replicates were used for untargeted metabolomics. ELISAs, Greiss assays, MTT assays, Luminex assays and qPCRs were conducted on 3-4 biological replicates.

2.12 LC-MS

Note that experiments in Chapter 3 and the U^{13}C-L-arginine labelling promastigote studies used extraction solvent using 1 µM internal standards (theophylline, 5-fluorouridine, Cl-phenyl cAMP, N-methyl glutamine, canavanine and piperazine).

The sample platform chosen for this project was liquid chromatography coupled with mass spectrometry. All samples were separated with high performance liquid chromatography (HPLC) on a Dionex Ultimate 3000 RSLC system (Thermo) using ZIC-pHILIC (Merck) column. The mass spectrometry platform used was a qExactive Orbitrap mass spectrometer (Thermo), the exception was the dilutions of the episomal over-expressors, which were run on a FUSION MS qExactive Orbitrap mass spectrometer (Thermo). Analysis was performed in positive and negative mode; using 10 µL injection volume and samples were maintained at 4ºC during analysis. A linear biphasic LC gradient was conducted from 80% B to 20% B over 26 minutes, where solvent B was acetonitrile and solvent A was 20 mM ammonium carbonate in water. The flow rate was 300 µL/min, and column temperature maintained at 25ºC. For longer LC protocol the gradient was identical except that it was over 46 minutes. Each sample was run in a randomized order, with a pooled sample run between every 4 samples, according to previously published methods (Vincent *et al*. 2010).

The MS set up was calibrated [Thermo calmix (Pierce™ calibration solutions from Thermo Scientific) with masses at lower m/z; 74.0393 m/z ($C_2H_6NO_2$: +) and 89.0244 ($C_3H_5NO_3$: −)] in both ionization modes before analysis and a tune file targeted towards the lower m/z range was used. Full scan (MS1) data was acquired in both ionization modes in profile mode at 50,000 resolution (at m/z

range 70-1400), an automatic gain control (AGC) target of 106 cts, with spray voltages +4.5 kV (capillary +50 V, tube: +70 kV, skimmer: +20 V) and −3.5 kV (capillary -50 V, tube: -70 kV, skimmer: -20 V), capillary temperature 275ºC, probe temperature 150ºC, sheath gas flow rate 40, auxiliary gas flow rate 5 a.u., and a sweep gas flow rate of 1 a.u. For fragmentation analysis the settings are in **Supplementary File 2-1** and analysis conducted using mZCloud.

Data analysis was performed using the MzMatch (Scheltema *et al*. 2008) and IDEOM (Creek *et al*. 2012) software packages for untargeted analysis. The Xcalibur (Thermo) software package was used for targeted peak picking and exporting fragmentation spectrums which were used as queries with which to search mZCLOUD (Vinaixa *et al*. 2016). A mixture of 240 standards (in three separate mixes), covering a range of metabolic pathways, was run alongside each sample batch to allow metabolite "identifications" to be made (MSI level 1).

According to the metabolomics standards initiative (MSI), metabolite identifications (MSI level 1) are given when more than one feature matches an authentic standard (i.e., mass and retention time) and annotations are made when matching to a metabolite is made by mass only (MSI level 2) (Sumner *et al*. 2007). Peaks were visually interrogated on the identification tab, with some "metabolites" removed at this stage. To avoid the lipid bolus, a 4.2-minute retention time cut off was applied. As lipids and peptides are not reproducible detected, these were removed from statistical analysis. If available, fragmentation data was used to strengthen confidence in identifications

Statistical analysis was conducted using MetaboAnalyst (One way ANOVA with false discovery rate correction) or Graphpad Prism (One way ANOVA with Tukeys correction for pairwise comparisons).

2.13 RNA seq

Glasgow Polyomics carried out library prep and sequencing. Quality of samples was verified using a Bioanalyser 2100 (Agilent) and accurate quantity determined using a Qubit® (Life technologies). A poly A selection was carried out with the SMART-Seq v4 Ultra low Input RNA kit (Clontech) followed by the Nextera XT kit

(Illumina). The SMARTer kit selects poly A RNA and creates cDNA then the Nextera XT kit fragments the DNA, adds the adapters and amplifies adapter-fragments by PCR to form the final library. The average size of the first-stranded library was 467bp (average size of the library was determined by the Bioanalyzer). Samples were run on the NextSeq™ 500 platform to obtain approximately 50 million paired end reads (2 x 75bp). Raw data was loaded onto the Galaxy server (hosted by Glasgow Polyomics) (Afgan *et al*. 2016).

Quality investigated using Fastqc (Andrews 2010) and raw files aligned to the mouse mm10 genome using HISAT2 (Kim *et al*. 2015b). Htseqcount (Anders *et al*. 2015) was used to extract counts per gene. The counts were downloaded to be run on a local instance of Deseq2 (1.10.1) (Love *et al*. 2014). Overlap between pairwise comparisons and likelihood ratio test (LRT) DE genes (adjusted p-value < 0.05) was mapped using Venny (Oliveros 2015). For pathway analysis, the filtering described in **Chapter 4** was done in Excel (Microsoft). Similarly, filtering to get a list of detected (in at least 2 replicates of one condition) was done in Excel. Pathway analysis was conducted using the web version of Graphite Web (Sales *et al*. 2013) uploading the background and the indicated lists of DE genes with their respective Log_2 fold change values. To map mouse to human IDs, Biomart was used (Durinck *et al*. 2009). Raw files and workflow (Raw→Hisat2→HTseqcount, Raw→ Fastqc) is available on request on the Galaxy server hosted by Glasgow Polyomics. Final (including SPIA pathway analysis) and intermediate files, r code (Deseq2 session), are all contained within **Supplementary File 2-2**.

2.14 Phylogenetic and structural analysis of *Lmxm.08.1225*

2.14.1 Clustal Omega and Phyre^2

Homologs from species with DDAH activity were downloaded from BRENDA. A select list of ADI sequences was chosen from species with confirmed ADI activity on BRENDA. This was so to better match the alignment from a previous publication (Knodler 1998). For analysis on Phyre^2 the sequence for *Lmxm.08.1225* was uploaded and default settings were selected.

Table 2-8: Genes used in Clustal Omega analysis. Note that ID refers to NCBI Reference Sequence or UniProtKB/Swiss-Prot*.

Name	Protein	Species	ID
DDAH1_HUMAN	DDAH	*Homo sapiens*	NP_036269.1
DDAH2_HUMAN	DDAH	*Homo sapiens*	XP_011512750.1
DDAH1_BOVINE	DDAH	*Bos taurus*	NP_001095671.1
DDAH2_BOVINE	DDAH	*Bos taurus*	XP_005223736.1
DDAH1_MOUSE	DDAH	*Mus musculus*	NP_081269.1
DDAH2_MOUSE	DDAH	*Mus musculus*	XP_006524675.1
DDAH1_RAT	DDAH	*Rattus norvegicus*	NP_071633.1
DDAH2_RAT	DDAH	*Rattus norvegicus*	NP_997697.1
DDAH1_Rabbit	DDAH	*Oryctolagus cuniculus*	XP_002715931.2
DDAH2_X1_ Rabbit	DDAH	*Oryctolagus cuniculus*	XP_008260806.1
DDAH2_X2_ Rabbit	DDAH	*Oryctolagus cuniculus*	XP_008260808.1
DDAH_Dog	DDAH	*Canis lupus familiaris*	XP_005622043.1
DDAH_Chicken	DDAH	*Gallus gallus*	NP_989713.1
DDAH1_ Mycobacterium tuber	DDAH	*Mycobacterium tuberculosis*	WP_023643926.
DDAH_ Streptomyces coel	DDAH	*Streptomyces coelicolor*	NP_630791.1
DDAH_P. aer	DDAH	*Pseudomonas aeruginosa*	NP_249886.1
Giardia_intest_AD	ADI	*Giardia intestinalis*	Q27657*
Pseudomonas_aer_AD	ADI	*Pseudomonas aeruginosa*	P13981*
Mycoplasma_arg_AD	ADI	*Mycoplasma arginini*	P23793*
Lactococcus_lac_AD	ADI	*Lactococcus lactis*	P58013*
NOS2_Human	NOS2	*Homo sapiens*	P35228

3 A stimulus specific metabolic signature of inflammatory macrophage

3.1 Introduction

Immune-metabolism is a rapidly growing area of research, whose importance is increasingly recognised across the immunology discipline. The complexity of cellular metabolism has been the main challenge when it comes to trying to relate metabolism to cell function. This complexity stems from the vast number of metabolites (thousands), the multiple pathways in which they occur, and the complex regulation of enzymes that modulate these pathways. A plethora of studies are now investigating and discovering the mechanisms by which metabolites modulate the function of key innate immune cells such as macrophages and dendritic cells (DCs) (Tannahill *et al*. 2013; Jha *et al*. 2015; Lampropoulou *et al*. 2016). In these cells metabolites act not only as precursors for anabolic and catabolic process but engage intracellular and extracellular signalling pathways to drastically alter the cell phenotype.

In the **1.5.2** the way in which inflammation leads to an altered energy metabolism consisting of an increased flux through glycolysis and the PPP, as well as a fragmented TCA cycle is introduced. These perturbations are required to meet the inflammatory cells' demands for ATP, NADPH, and ribonucleotide precursors. These events are initiated by ligation of immune signalling molecules or pathogen antigen to receptors such as pattern recognition receptors (PRRs), cytokine receptors or antigen receptors. Inflammatory macrophages (M1) also cause accumulation of or upregulate the production of metabolites such as succinate and itaconate, which have effector functions. Itaconate is produced from citrate that accumulates as a result of the downregulation of isocitrate dehydrogenase (Jha *et al*. 2015). Citrate is also diverted towards prostaglandin synthesis. Itaconate has been demonstrated to inhibit isocitrate lyase, which is part of the glycoxylate shunt in bacteria (Michelucci *et al*. 2013).

In contrast to M1 macrophages, anti-inflammatory (M2) macrophages rely on oxidative phosphorylation with an intact TCA cycle that is supplemented by glutamine. Certain key metabolic processes are differentially regulated in anti-inflammatory macrophages. This is illustrated by M2 macrophage expression of a

specific phosphofructokinase isoform, PFKFB1 (also known as fructose bisphosphatase 2 (FBPase2)) that is much less active than the u-PFK2 isoform, which is expressed in M1 macrophage (Kelly & O'Neill 2015; Rodríguez-Prados *et al*. 2010). In M1 macrophages Fructose-2, 6-bisphosphate synthesis is driven by u-PFK2. Fructose-2, 6-bisphosphate activates glucose breakdown in glycolysis by activating the glycolytic enzyme 6-phosphofructo-1-kinase.

Additionally, M2 macrophages increase uptake of triglycerides using the CD36 receptor. The triglycerides are subsequently hydrolysed by lysosomal acid lipase to yield lipids, which in turn are used for fatty acid oxidation (Huang *et al*. 2014). M2 macrophages divert glutamine metabolism to UDP-GlcNAc production (Jha *et al*. 2015). This is critical for the glycosylation of lectin and mannose receptors, which are required for pathogen recognition. Jha *et al* confirmed this by showing that both glutamine deprivation (in cell culture medium) and an inhibitor of N-glycosylation decreased M2 polarisation.

The effects of immune-modulating metabolites are not confined to within the cell producing them. Immune cells possess extracellular receptors such as G protein–coupled receptors (GPCRs) that enable them to detect extracellular metabolites. One example of this is where DCs detect extracellular succinate via the succinate receptor GPR91. When activated, this receptor triggers an increase in intracellular Ca^{2+} and this combines with TLR3 or TLR7 signalling to enhance DC activation and migratory ability (Rubic *et al*. 2008).

The microbiome is an additional source of immunomodulating metabolites. A key example of this is the short chain fatty acid butyrate, which is produced by commensal bacteria in the gut. Butyrate can bind to GPCRs on macrophages and DCs. It was recently shown that butyrate facilitates M2 macrophage polarization, *in vitro* and *in vivo* (Ji *et al*. 2016). This led to macrophages that were tolerogenic, and had increased migrational and wound healing capacity. The authors proposed that an H3K9 acetylation/STAT6-signalling pathway was responsible for upregulated arginase activity, which was the key mechanism responsible for these anti-inflammatory phenotypes.

The overall aim of the work in this project is to establish a model of metabolism within the *leishmania*-infected macrophage. Prior to this a robust protocol was

required to measure the metabolic profile of inflammatory macrophages that could reproduce previously validated findings. A classical inflammatory (M1) macrophage model was used to establish the immune metabolism therein. This involved use of a commonly used M1 stimulus; IFNγ and LPS. The former is an immune stimulus while the latter represents a pathogen challenge.

To generate M1 macrophages in the previously mentioned immune-metabolic studies, Tannahill *et al* used LPS and Jha *et al* used IFNγ + LPS. These studies have not, however, distinguished between what these stimuli do on their own and what they do together. An obvious example is the argino-succinate shunt, which Jha *et al* showed is upregulated to replenish a fragmented TCA cycle in M1 macrophages. An essential part of this shunt is L-citrulline generated by iNOS, and this enzyme is maximally upregulated in the presence of macrophages treated with both IFNγ + LPS. It is not expected this to occur to the same extent in cells rerated with either stimulus on their own. To address this gap in the literature, four conditions were used; non-stimulated cells, IFNγ primed cells, LPS treated cells and cells that were both IFNγ primed and LPS treated. The reasoning behind this was to systematically determine the immune-metabolic processes that were driven by the immune system (IFNγ), a pathogen (LPS) or the interaction of both (IFNγ + LPS). This knowledge will be essential if deciding to target inflammation via the pathogen, immune system, or both.

3.2 Results

3.2.1 Characterisation of the bone marrow derived macrophages (BMDM) system

3.2.1.1 Evaluation of L929 supernatant.

To generate bone marrow derived macrophages (BMDM) bone marrow was taken from 8-12 weeks old male C57 BL/6 mice. To differentiate myeloid precursors from murine bone into macrophages, supernatant from the L929 murine fibroblast cell line was used (see **2.5**). The key differentiation factor present in L929 conditioned medium is macrophage colony-stimulating factor (M-CSF) (Weischenfeldt & Porse 2008). This is a lineage-specific growth factor, which is responsible for the proliferation and differentiation of committed myeloid progenitors (i.e., monocytes) into cells of the macrophage/monocyte lineage.

20% L929 supernatant was routinely used during the 7-day differentiation but in order to get a more informative characterisation an M-CSF ELISA was used (**2.8.1**) to provide a quantitative readout on the amount of M-CSF typically used during this experiment **(Figure 3-1)**. The results demonstrate that there is batch-to batch variation, however, the amount of M-CSF in the L929 supernatant ranges between 165 pg/mL to 285 pg/mL. Thus, depending on the batch used the cultures will be receiving 33-57 pg/mL; less than a half log difference.

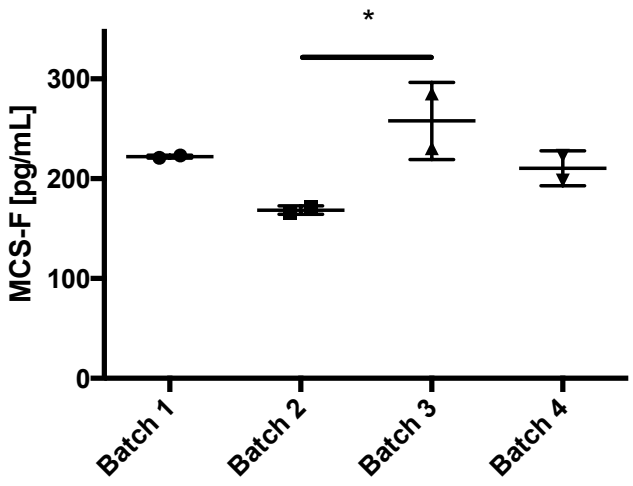

Figure 3-1: MCS-F of 4 batches of L929 supernatant was quantified using ELISA. A one-way ANOVA with a Tukeys multiple comparison test was used to test for significance ($p<0.05$). Andrew Pountain and Clément Regnault assisted with this experiment.

3.2.1.2 Flow cytometry profiling of BMDM

To assess the purity of BMDM, flow cytometry was used (**2.7.1**). In our protocol the APC-eFluor® 780 (eBioscience) viability dye that is excluded from live cells was used **(Figure 3-2a)**. The cells used in this experiment were generated as described in **2.5** and left overnight (37ºC, 5% CO_2) to re-adhere. It is worth noting that removing cells from tissue culture plates was not done for any metabolomics experiments presented in this chapter, so the cell death shown in **Figure 3-2 c** is not necessarily indicative of the situation in other experiments at the point of sample preparation. Furthermore, for all experiments, viability of all cells at time of seeding was, as is standard, verified to be >95% using trypan blue exclusion. The receptors assessed to evaluate purity were CD11b and F4/80, which are commonly used macrophage markers. As can be seen in **(Figure 3.2(d-l)),** the vast majority of differentiated cells were macrophage. Dendritic cells can also express these markers but require either granulocyte-

macrophage colony stimulating factor (GM-CSF) or FLT-3L for their differentiation.

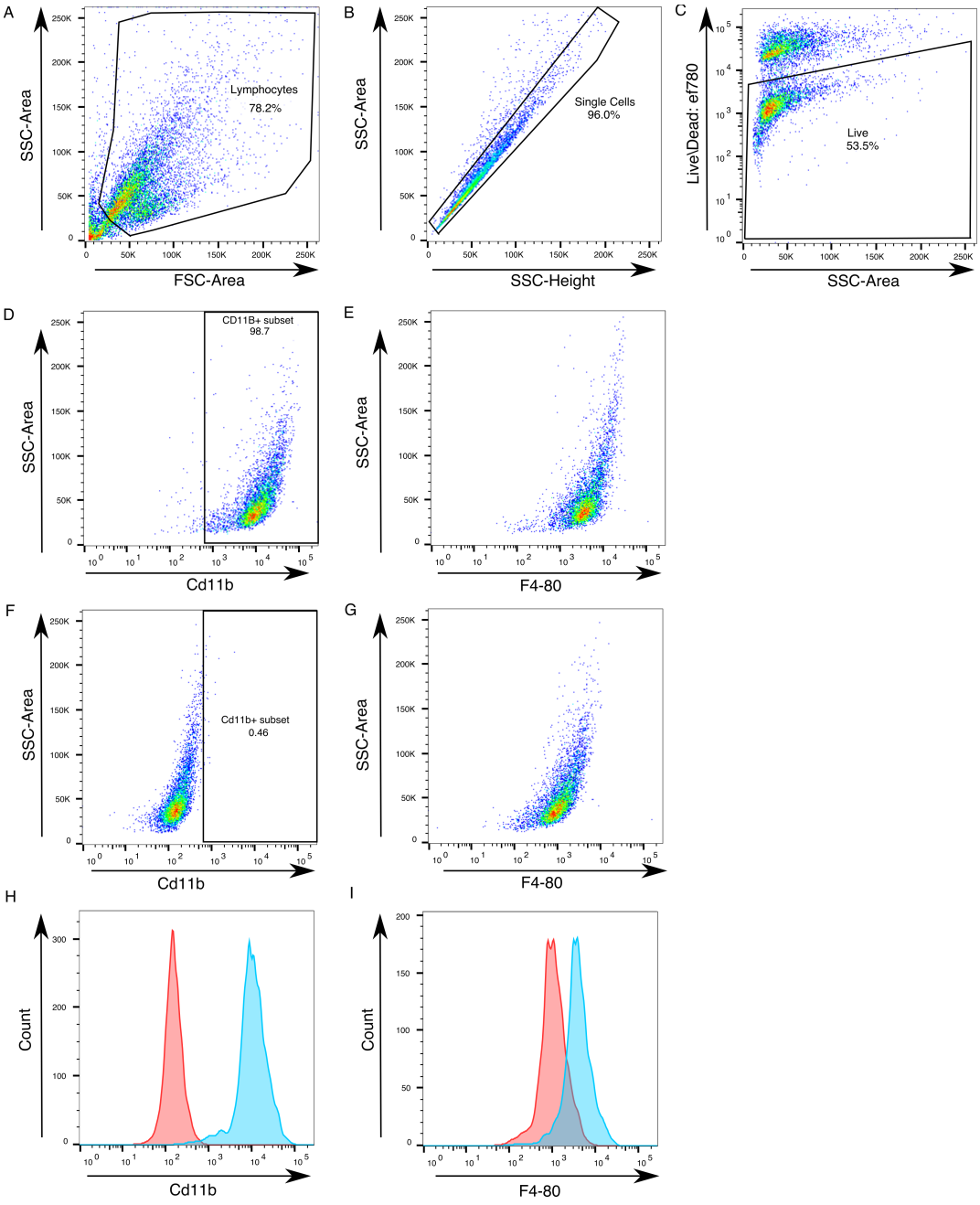

Figure 3-2: Flow cytometry characterisation of cultured macrophage: A: Selecting population based on forward scatter area (FSC-Area) against side scatter area (SSC-Area). B: Gating on single cells using SSC-Area against side scatter area (SSC-Height). C: Gating on live cells using gating on cells negative for the viability dye Ef780. D: Gating on Cd11B^{+} cells then, E: characterising presence of F4-80. F: Fluorescence -1 (FLO-1) control for Cd11b and, G: F4-80. H: Histogram overlay of D (blue) and F (red). I: Histogram overlay of E (blue) and I (red). Results are representative of 3 biological replicates. Andrew Pountain and Clément Regnault assisted with this experiment.

3.2.1.3 Cytokine profile and nitric oxide production

In order to validate the BMDM obtained from *in vitro* culturing several standard immunological assays were used to characterise them. To generate polarised macrophage either LPS, IFNγ prior to LPS, or IL-4 were used. IFNγ, LPS or IFNγ plus LPS are routinely used to generate pro-inflammatory macrophages. These pro-inflammatory cells express a plethora of inflammatory cytokines. A prior stimulus with IFNγ is required to obtain detectable iNOS activity and upregulation of MHC-II receptors. On the other hand IL-4 is used to generate anti-inflammatory macrophage that have higher arginase activity and upregulation of mannose and lectin receptors.

To profile a large number of cytokines the Luminex 20-plex assay (Invitrogen) was used. This allowed us the profiling of 20 cytokines in supernatant from BMDM that were stimulated with either nothing (naïve), LPS or IL-4 for 6 hours. Out of all cytokines evaluated, only six were reproducibly detected in the inflammatory macrophage cultures **(Figure 3-3)**. These include classical M1 cytokines such as TNF-α and IL-6. Although not performed, the author anticipates that, based on the literature that if the supernatants were collected at a later time-point, or if the cells had been co-stimulated with IFNγ prior to LPS, additional cytokines would have been detected. It is important to note that no cytokine were detectable in naive or anti-inflammatory macrophages. While some mMCP-1 was detected in some of the M2 macrophages, the levels in M2 were not significantly (one-way ANOVA, Tukeys multiple comparison test) different to those in M0 macrophages.

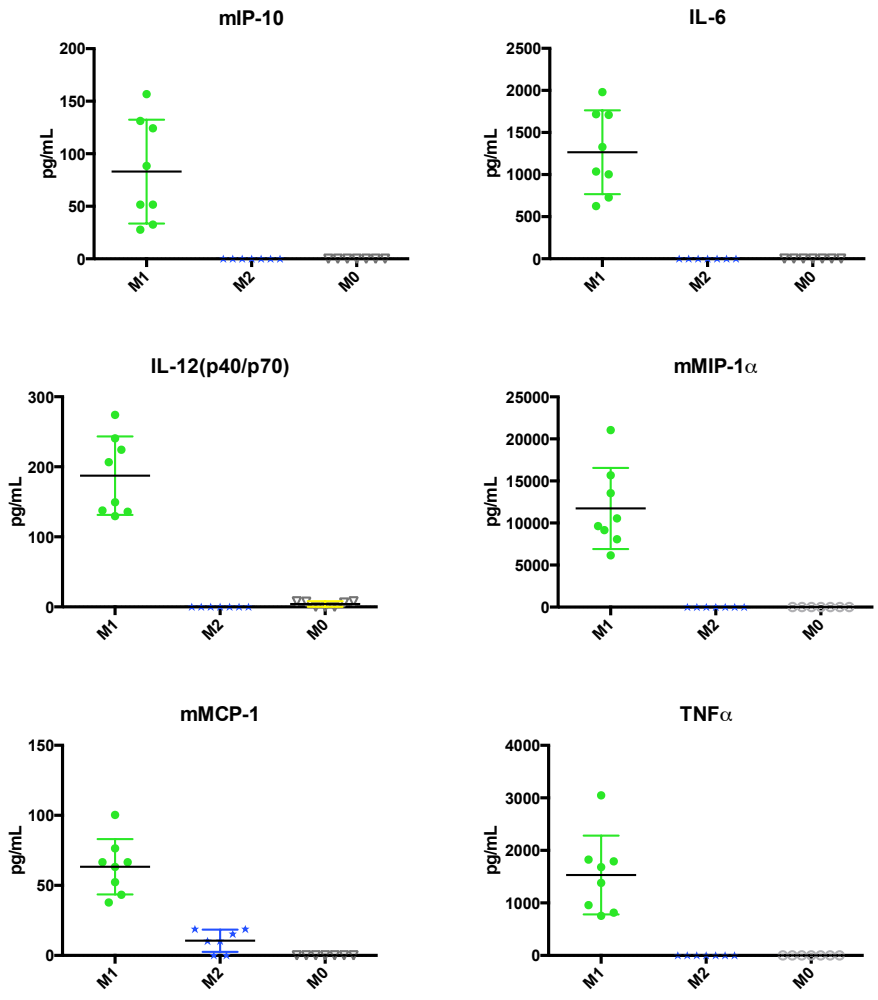

Figure 3-3: Generated BMDM produce pro-inflammatory cytokines in response to LPS. BMDM were stimulated for 6 hours in the presence of LPS (100 ng/mL). Supernatants were analysed using the Luminex murine 20-plex kit (Invitrogen) as described in materials and methods. M2 macrophages were stimulated with IL-4 for the same amount of time. 4 biological replicates (each in 2 technical duplicates) are included in analysis. Andrew Pountain and Clément Regnault assisted with this experiment.

Furthermore, for the inflammatory BMDM, the IL-6 data produced in the Luminex assay was validated using an ELISA using the same supernatants (**Figure 3-4a).** While the anti-inflammatory cytokines IL-4 and IL-10 were profiled in the assay, the latter was not detected and the former was not appropriate as it was used for stimulation of the anti-inflammatory phenotype. IL-4 primes the cells to respond in an anti-inflammatory manner but phenotypic changes are more obvious when they are challenged with an immune stimulus (i.e. lipopolysaccharides (LPS)). The experiment was repeated with a 24 h IL-4 stimulation and arginase (*Arg1*) levels were quantified using qPCR (**Figure 3-4b**) as is a classical M2 marker. The *Arg2* transcript was also profiled as this has been reported to be pro-inflammatory (Yang & Ming 2014) as well as being

upregulated in both M1 and M2 macrophages (Jha *et al*. 2015). For *Arg1* the results are as expected with strong upregulation in IL-4 treated macrophages while M1 macrophages had higher, albeit variable *Arg2* expression levels. Finally, as iNOS activity was not reproducibly detected in the absence of IFNγ (**Figure 3-5a)**, the Griess assay (**2.8.3**) was carried out on cells primed with IFNγ overnight and LPS for 24 h. As expected, this was sufficient to obtain detectable iNOS activity (**Figure 3-5b)**. In summary, the protocol used to generate BMDM yields cells that display surface markers typical of macrophages. Furthermore, when stimulated to M1 or M2 phenotypes, these cells display cytokine/ and transcript profiles, that are characteristic of these polarised macrophages.

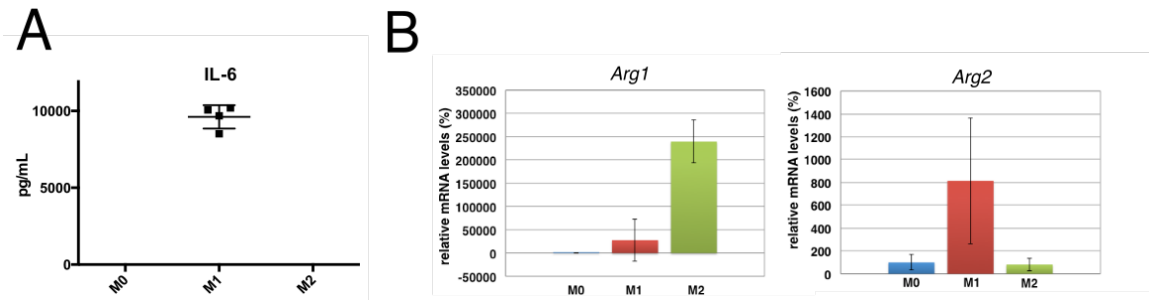

Figure 3-4: Characterisation of macrophages A: IL-6 quantified by ELISA on the same supernatants used for Luminex assay. BMDM from four biological replicates are shown here. IL-6 was not detectable in M0 or M2-treated BMDM. B: Results of qPCR of *Arg1* and *Arg2* expression in BMDM. Results are indicative of 3 biological replicates. The D-Delta method was used, normalising to the18S ribosomal transcript. Andrew Pountain and Clément Regnault assisted with this experiment.

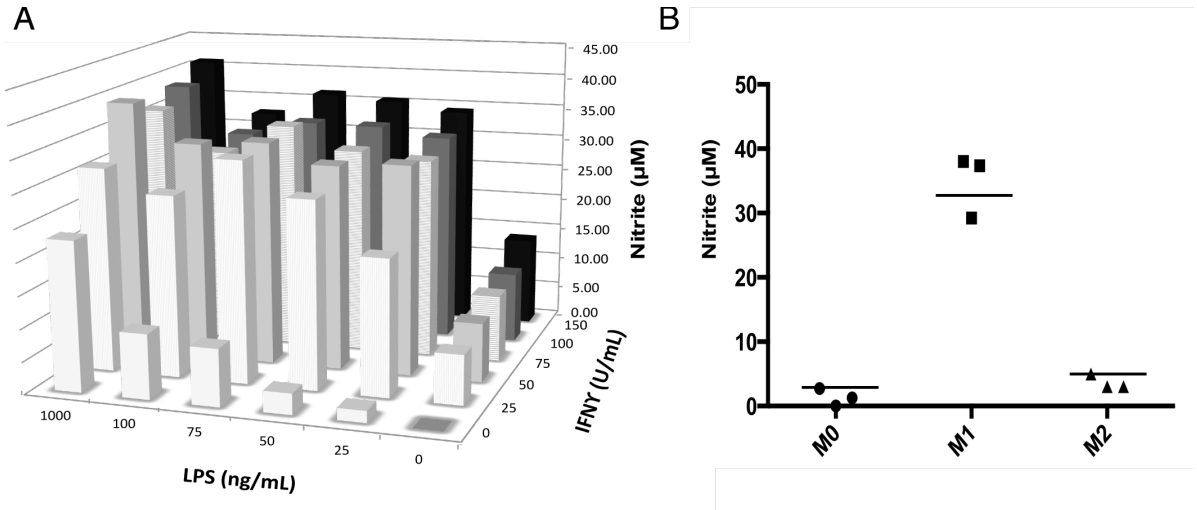

Figure 3-5: Nitric oxide production by inflammatory macrophages. A: cells were primed with IFNγ (indicated amounts) overnight, then LPS (indicated amounts) for 24h. Nitrite was quantified using the Griess assay. Results are indicative of 3 independent experiments. B: Cells from 3 biological replicates were treated IFNγ (100 U/mL) overnight, then LPS (100 ng/mL) for 24h and nitrite quantified using Griess assay. Andrew Pountain and Clément Regnault assisted with this experiment (part B).

3.2.1 Development of a BMDM extraction protocol

3.2.1.1 Normalising to protein content

A major issue with metabolomics is ensuring that samples in different treatment groups are comparable. Compounding this are treatments causing loss of metabolites due to cell death or alterations in cell size. The author noticed early during our studies that the presence of IFNγ led to increased cell density with fewer non-adherent cells. This may be due to IFNγ promoting cell survival. This is a concern as it is not advisable to normalise at the point of data analysis, as many metabolites do not have the same linear range. As macrophages are adherent it is not feasible to count cells prior to extraction. Furthermore, cells of reduced adherence would be more likely to be counted if attempting this, as they would be easier to remove.

To remove macrophages, either disassociation buffer, which contains EDTA or trypsin, are often used but this would interfere with macrophage function by cleaving extracellular receptors or depleting ions such as Ca^{2+} or Mg^{2+}. Ideally the aim was to process samples rapidly *in situ* and to this end a method developed that allows the use of protein that was precipitated during extraction as an estimate of cell number at the time of extraction. To this end 0.1 M NaOH was used to solubilise precipitated protein and this was demonstrated to give a read out in the Bradford assay that corresponded to the number of cells present (**Figure 3.6a)**. This allowed the author to confirm that the existing cell culturing protocol was leading to samples that were not comparable (**Figure 3.6b).**

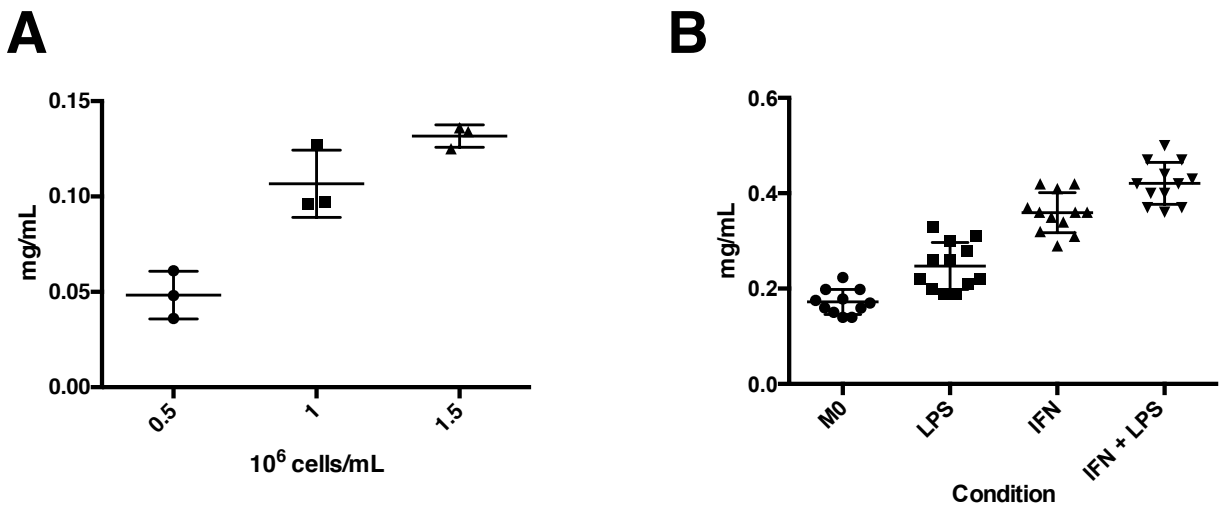

Figure 3-6: Method of quantifying protein content (mg/mL) post extraction. A: Macrophages were seeded at densities indicated and protein content quantified post extraction. Results are representative of two independent experiments. B: The same protocol was employed post extraction on cells cultured using a standard protocol. Two sample groups were primed with IFNγ (100 U/mL) overnight, then LPS (100 ng/mL) for 4h (IFN LPS) while the other sample did not get LPS (IFN). One group of samples were treated with LPS without prior IFNγ stimulation (LPS) while Un is non-treated. Cells not receiving a given stimulus received an equal volume of cRPMI. Units were determined using BSA standards in Bradford assay.

3.2.1.2 Modified culture protocol to ensure equal cell numbers

One option available was to correct for unequal cell numbers by adding solvent after the post-extraction Bradford assay. However, adding extraction solvent to correct after the initial extraction is not ideal, as more pipetting error would be introduced and the retrospectively added extraction solvent wouldn't be subject to the same conditions. Furthermore, cell density effects will complicate any interpretation of experiments carried out in such a manner. By modifying our protocol with the addition of a warm PBS wash to reduce the number of non-adhered cells present, the result was that each group had a more similar protein content (**2.10.2**). This was true for the samples used in the metabolomics data presented in the following sections (**Figure 3.7a**). Inflammatory macrophages have been shown to be larger and to have higher protein content (Jha *et al*. 2015; Meiser *et al*. 2016), but as the majority of our LPS stimulations were less than 6 hours this effect should be minimal. Nevertheless, by accurately quantifying protein content it was possible to be reasonably sure that conditions were comparable and aware of when they are not.

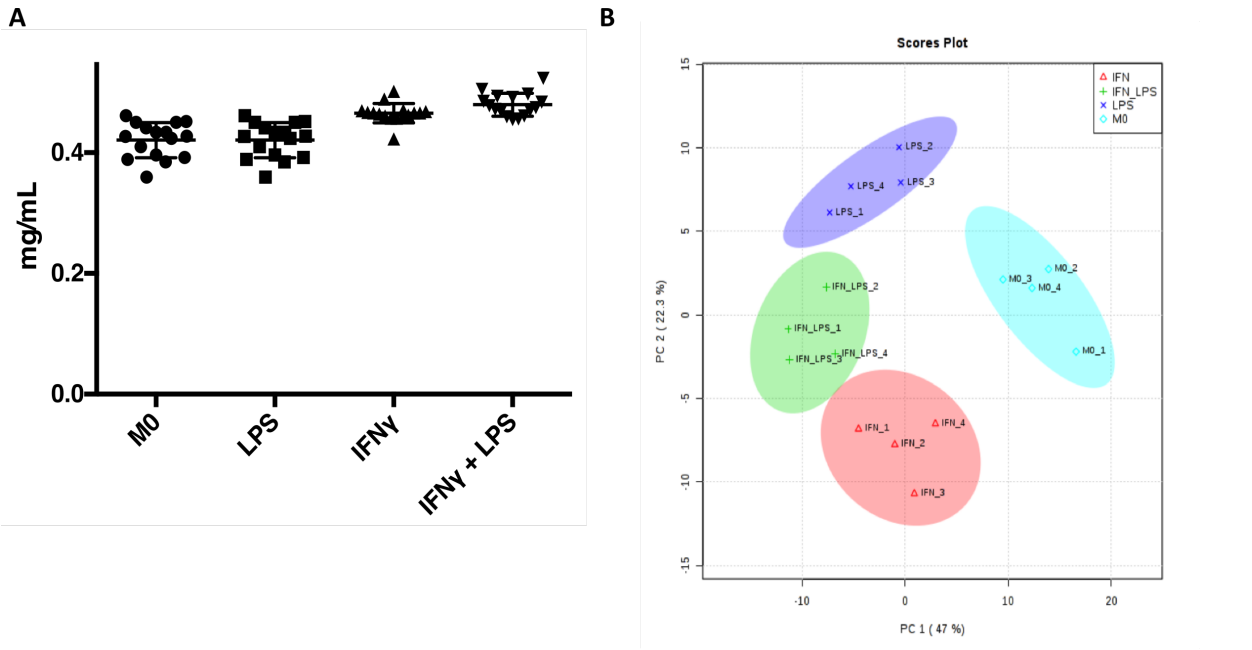

Figure 3-7: Modified protocol ensures that samples from different conditions are equivalent. A: Bradford assay carried out post extraction on samples that were used for the analysis that is shown in section **3.2.2**. 16 samples (four from each technical replicate) were measured B: PCA on same samples. Data was log transformed prior to analysis. MetaboAnalyst 3.0, which utilises the pcaMethods Bioconducter package (Stacklies *et al*. 2007) was used to construct PCA plots. 95% confidence intervals are highlighted by the respective background colour. Units were determined using BSA standards in Bradford assay.

3.2.2 The metabolome of multiple inflammatory macrophages

3.2.2.1 Initial data analysis and filtering

Once our culturing techniques and sample preparation were optimised, these methods were applied to interrogate the metabolome of M1 macrophages. Specifically the aim was to determine the relative contribution of IFNγ and LPS, either alone or in combination to immune-metabolism. The conditions used were non-stimulated cells, IFNγ primed cells, LPS treated cells and cells that were both IFNγ primed and LPS treated. Note that IFNγ (100 U/mL) priming took place over night (16 h) and LPS (100 ng/mL) was added for 4 h the next day. Samples were prepared as described in **2.10.3** and LC-MS performed as described in **2.12**.

Initial data analysis was carried out using the IDEOM pipeline (**2.12**). Prior to statistical analysis putatively identified metabolites were filtered based on integrity of peak shapes (first column in IDEOM comparison tab). This includes annotated peaks that were shoulders or noisy peaks where statistical interpretation of peak area did not appear reliable. This approach reduces the

number of false negatives that typically affect large data sets. Next peptides, which are not reproducible in our system were filtered out. Finally, a 250-second retention time cut-off was used as most lipids elute from the column as a bolus during this time. This was done because lipids are not separated by retention time on our LC-MS method and thus, their identification is not reliable. Furthermore, the number of metabolites not attributed to any biological pathway is extremely high during this time window and could actually be a lipid or a fragment of one.

Finally, ß-alanine and L-alanine could be separated based on retention time but the gap was too small for standard settings within the Ideom pipeline (Creek *et al*. 2012). For these metabolites, a custom method was written in Xcalibur (Thermo) where an appropriate retention time window (±30 seconds of authentic standard) was used to obtain an accurate peak area measurement. The global application of the retention time window used here in the Xcalibur method to IDEOM would have been too restrictive and thus, was not done. The result of the filtering in IDEOM and the Xcalibur method was a list of 233 metabolites. The identity of 74 of these was confirmed using authentic standards (MSI level 1). PCA analysis was carried out on MetaboAnalyst and show that that conditions clearly separate (**Figure 3-7b**).

We initially analysed the experiment using the commonly used one-way analysis of variance (ANOVA), with a false discovery rate (FDR: Benjamini–Hochberg) threshold of ≤0.05 on MetaboAnalyst. Note that the input files for additional analysis are in **Supplementary File 3-(2-3) (Kegg IDs are shown, metabolite name is in Supplementary File 3-1)**. Several of the perturbed metabolites are in pathways that are important for immune function (**Table 3-1**), confirming the validity of our cell culture and LC-MS sample preparation protocol. The metabolites in this table are increased by one or both stimuli (**Supplementary File 3-4**). The contribution of both is discussed in more detail the following sections.

Some of these are well known pathways such as oxidative stress response, the pentose phosphate pathway (PPP), CD38 calcium signalling and folate metabolism (Duch & Smith 1991; Haschemi *et al*. 2012; Qiao *et al*. 2007; Willmott *et al*. 1996). Upon up-regulating the production of reactive oxygen

species (ROS), macrophages utilise glutathione disulphide (GSSG) by reducing it to two molecules of glutathione with reducing equivalents from the coenzyme NADPH. Gluthathione (GSH) scavenges ROS, regenerating GSSG with water as a by-product.

Inflammatory macrophages have enhanced glycolysis resulting in lactate accumulation (Tannahill *et al*. 2013). Central carbon metabolism has recently been the focus of much research into immune-metabolism and the previously reported increases in glycolysis and the TCA cycle are present in the data presented here. Accumulation of itaconate has been shown to inhibit succinate dehydrogenase leading to increased succinate levels (Lampropoulou *et al*. 2016).

Thymidine degradation by thymidine phosphorylase leads to accumulation of 2-Deoxy-D-ribose 1-phosphate. This is subsequently phosphorylated to yield 2 Deoxy D-ribose-5-phosphate that is then cleaved by deoxy-D-ribose phosphate aldolase to acetoaldehyde and glyceraldehyde 3-phosphate ultimately leading to pyruvate production. 2-deoxy-D-ribose has previously been shown to cause the proteasomal degradation of HIF-1α in a human leukaemia cell line (Ikeda *et al*. 2013). It is important to note that as we do not have an authentic standard we cannot preclude the possibility that 2 deoxy D-ribose-5-phosphate is instead 2 deoxy D-ribose 1-phosphate.

In the next section the results of our implementation of a general linear model (GLM), which was used as it allowed the incorporation of an interaction term, are discussed. 108 metabolites had a false discovery rate (Benjamini-Hochberg) of <(0.05) from the ANOVA while only 85 metabolites met the same threshold in the GLM (**Supplementary File 3-4)**. Thus it is reasonable to consider both methods appropriately stringent considering the overlap in the metabolites found to be perturbed (Unique to the ANOVA are (R)-lactate (corrected GLM p value: 0.057) and 2 deoxy D-ribose-5-phosphate (corrected GLM p value: 0.07)).

In conclusion, perturbations of metabolites, which have previously been shown to be essential for immune-metabolism were detected here, thus confirming the validity of our methodology. Furthermore, both approaches (ANOVA and GLM) detect significant changes in carnitine, pyrimidine and purine metabolism, which have not been interrogated in the context of M1 macrophage metabolism (see

Supplementary File 3.4 (GLM results were used for formal pathway analysis)). The nature of these perturbations is described in the following sections. In the next sections a GLM was used to determine the contribution of the inflammatory stimuli used here, alone and in combination, to perturbations both within and out with central carbon metabolism.

Table 3-1: Key metabolites with altered abundance in inflammatory macrophages according to one-way ANOVA or GLM. Shown here are the metabolites, their key immune specific pathways, their ANOVA-corrected p value (Benjamini-Hochberg false discovery rate (FDR) <0.05) and relevant citation. Most metabolites passed the GLM test with an FDR threshold of 0.05, the exception being metabolites highlighted in red ((R)-lactate (p.adjust (FDR) = 0.057) and 2 deoxy D-ribose-5-phosphate (p. adjust = 0.07)).

Metabolite	Pathway	p.adjust (FDR)	Reference
L-Citrulline	iNOS	<0.001	(Jha *et al*. 2015)
(R)-Lactate	Glycolysis	<0.001	(Jha *et al*. 2015; Tannahill *et al*. 2013)
2-Oxoglutarate	TCA cycle	<0.001	(Rubic *et al*. 2008; Jha *et al*. 2015)
Succinate	TCA cycle	<0.001	(Ji *et al*. 2016; Tannahill *et al*. 2013)
(S)-Malate	TCA cycle	<0.001	(Tannahill *et al*. 2013)
2 deoxy D-ribose-5-phosphate	Pentose Phosphate pathway	<0.001	(Ikeda *et al*. 2013)
Ribose 5-Phosphate	Pentose Phosphate pathway	<0.001	(Jha *et al*. 2015; Haschemi *et al*. 2012)
3-Phospho-D-glycerate	Pentose Phosphate pathway	<0.001	(Haschemi *et al*. 2012)
ɣ-L-Glutamy-L-cysteine	Oxidative stress response	<0.001	(Qiao *et al*. 2007)
Gluthathione disulphide (GSSH)	Oxidative stress response	<0.05	(Qiao *et al*. 2007)
Cyclic-ADP-ribose	CD38+ signalling	<0.001	(Willmott *et al*. 1996)
Dihydrobiopterin	Folate biosynthesis	<0.001	(Duch & Smith 1991)
2-Amino-4-hydroxy-6-hydroxymethyl-7,8-dihydropteridine	Folate biosynthesis	<0.001	(Duch & Smith 1991)
Itaconate	Anti-bacterial	<0.001	(Jha *et al*. 2015)

3.2.2.2 A generalised linear model incorporating the contribution of IFNγ and LPS stimuli

For analysing this dataset a generalised linear model (GLM) as implemented in the R coding language (GLM) (**Supplementary File 3-5**) was used. GLM is a generalised instance of the linear model LM (e.g., ANOVA procedure) (McCullagh & Nelder 1989). Here the permutations are performed using a least squares regression approach to describe the statistical relationship between one or more predictors (in this case are the stimuli) and a continuous response variable (in this instance is a given metabolites intensity).

GLM does not assume that residuals (data-points) are independent and applies one of several exponential family functions (Gaussian in our case). A Gaussian (Normal) distribution is assumed here (the default setting in this model in R), is

a limitation that is common to all datasets with small number of samples. As there were four replicates in each condition, it would not be reliable to try and test if the data fits another distribution. While using the LM function in R yields identical results, the GLM script (**Supplementary File 3-5**) is more flexible, with more available parameters (i.e. choice of distributions).

We have incorporated an interaction term, which is used when two predictor variables affect the outcome variable in a way that is non-additive. In our case the example is whether one immune stimulus has an effect on the response of another. This is particularly appropriate for this experiment as it is widely accepted that the effect of IFNγ and LPS can be synergistic (e.g., **Figure 3.5a**). In general terms:

$$model = lm(Y \sim X1 + X2 + X1:X2)$$

In R this function regresses Y on X1 (IFNγ), X2 (LPS), and the X1-by-X2 (IFNγ-by-LPS) interaction term.

In **Figure 3-8,** not only are there stimuli specific signatures induced by IFNγ and/or LPS visible, it is denoted where the effects are additive, antagonistic or synergistic, and one can see where metabolites are increased or decreased when compared to the non-treated control (M0). An additive effect is where each stimulus on there own causes a change but there is no additional change caused by their interaction. If there was an interaction between stimuli, this change could be synergy (the result of two stimuli is greater than the sum of there parts). Antagonism would be where the change caused by one stimulus prevented by the presence of another stimulus. There is overlap of metabolites that are affected by IFNγ, LPS and the interaction of both as shown in the Venn diagram (**Figure 3-8**). An example of this is where both IFNγ and LPS perturb a metabolite on their own but the effect of them together is additive (in the Venn diagram this is the set with 16 metabolites).

Here it is not distinguished whether one stimulus causes a greater effect than another (i.e., by comparing adjusted p values). An example would be if the largest increase is caused by one stimuli, and this increase is lessened when the other stimuli is present. We do not denote where the slight inhibition is

sufficient or not to cancel any biological effect of the overall increase that is present even in the presence of both stimuli. The reasoning behind this is to avoid the assumption that it is known what the thresholds (if any) at which metabolites may function in immune-metabolism. Nevertheless, the information necessary to do this (i.e., adjusted p values) is available in **Supplementary File 3-4.** All of these metabolites are listed in **Table 3-2**.

IFNγ causes a clear depletion of purine and pyrimidine related metabolites such as xanthine and uridine, and in some cases this is enhanced by the presence of LPS (hypoxanthine). In the case of L-citrulline, its increase can only be explained by the interaction term and this agrees with the result of **Figure 3-5 A** where iNOS activity requires the presence of both stimuli (note that with the exception of 1000ng LPS there is low nitrite levels when only one stimuli is present).

It is notable that increases in many of the hallmark metabolites of immune-metabolism can be explained by only one stimulus or a slight additive effect. For example, metabolites involved in glycolysis (fructose 1,6-bisphosphate and 3-phospho D-glycerate), the TCA cycle (2-oxoglutarate), and the PPP (ribose 5-phosphate and erythrose 4-phosphate), are all primarily driven by LPS. As these changes are relatively well known, the focus was switched to metabolites that were subject to either an additive or interaction term (**Figure 3-9**). Nevertheless, the list of metabolites, the levels of which are modulated by IFNγ, LPS or both is important in itself and this information is listed in **Table 3-2**.

An important additional note is on the limitations of untargeted metabolomics. A major issue is confidence in identification of putative metabolites. To this end the Metabolomics Standards Initiative (MSI) has published a classification system driven by community-agreed reporting standards (Sumner *et al*. 2007). Level one identifications denote where a putatively identified metabolite matches an authentic standard in both accurate mass and retention time. Additionally, identifications can be obtained by fragmentation of mass spectral features and comparing to publically available databases (mZCLOUD). In **Table 3-2**, this information is listed. It is important to note that identifications without additional confirmation from authentic standards or fragmentation match, are putative.

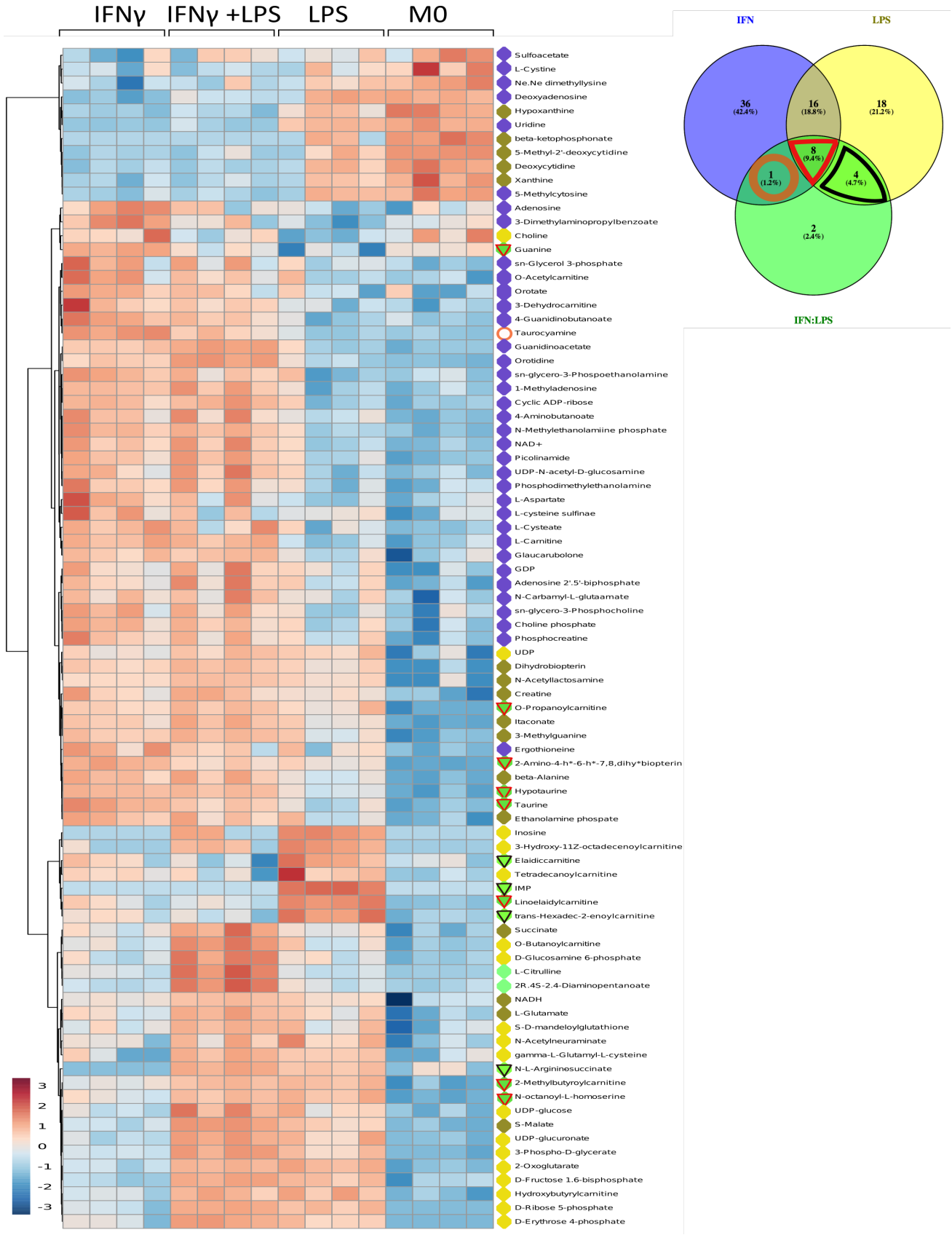

Figure 3-8: Metabolites with significantly (p.ajust (FDR) ≤ 0.05) altered levels. Colour code beside metabolite name corresponds to Venn diagram. IFN refers to metabolites that are perturbed by IFNγ, LPS refers to metabolites that are perturbed by LPS, and IFN:LPS refers to metabolites where the perturbation is caused by an interaction of the two stimuli. There is some overlap so coloured lines are used on the Venn diagram and heat-map key to denote this. The 85 metabolites shown here and additional information regarding confidence in identity can be found in **Table 3-2**. Andrew Pountain wrote the script used in this study.

Table 3-2: List of significantly altered metabolites from GLM. For metabolites denoted NoKegg, this indicates that these metabolites do not have a Kegg ID. Metabolites in brackets in the Isomers column are alternative identifications in the case of a fragment or alternative adduct. Note that elaidiccarnitine and linoelaidylcarnitine had similar retention times and thus one may be an adduct of the other. The same applies to Hypotaurine and taurine The 'Standard' column denotes whether an authentic standard was available and the 'Ms2' column denoted where there was a confirmatory match in the mZCLOUD database (described in more detail in materials and methods). The colour coding in the Set column is colour coded to match the Venn diagram in Figure 3-9 while Π denotes an intersect between any of the groups (circles) and IFN:LPS refers to the interaction group. In order to avoid division by zero, missing values were replaced with a value that is 25% of the intensity threshold (250). N/A denotes metabolites found in one condition only. Andrew Pountain wrote the script used in this study.

Kegg ID	Name	Standard	Isomers	MS^2	Set	Max FC
C00299	Uridine	Yes	3		IFN	10.2
NoKegg28	Orotidine	Yes	1		IFN	5.8
C00487	L-Carnitine	Yes	2	Yes	IFN	2.4
C00581	Guanidinoacetate		1		IFN	5.7
C01035	4-Guanidinobutanoate		3		IFN	1.6
C01210	N-Methylethanolamine phosphate		3		IFN	4.2
C01950	Picolinamide		4		IFN	2.7
C02376	5-Methylcytosine		4		IFN	2.3
C13050	Cyclic ADP-ribose		1		IFN	2.6
C02494	1-Methyladenosine		6		IFN	1.4
C00559	Deoxyadenosine	Yes	4		IFN	11.1
C05570	Ergothioneine		2		IFN	1.6
C05545	Ne,Ne dimethyllysine		1		IFN	2.0
C08764	Glaucarubolone		4		IFN	2.5
C00588	Choline phosphate	Yes	1		IFN	2.1
C02305	Phosphocreatine		1		IFN	1.9
C00003	NAD+		1		IFN	2.13
C00334	4-Aminobutanoate	Yes	15		IFN	2.0
C00506	L-Cysteate	Yes	1		IFN	1.7
C02636	3-Dehydrocarnitine		10		IFN	2.3
C01233	sn-glycero-3-Phosphoethanolamine		1		IFN	1.5
C02571	O-Acetylcarnitine	Yes	1		IFN	1.6
C00295	Orotate	Yes	2		IFN	4.5
C14168	3-(Dimethylamino)propyl benzoate		2		IFN	1.9
C00049	L-Aspartate	Yes	4		IFN	2.0
NoKegg34	L-cysteine sulfinate		2		IFN	1.6
C05829	N-Carbamyl-L-glutamate		5		IFN	1.6
C00043	UDP-N-acetyl-D-glucosamine		3		IFN	1.9
C00670	sn-glycero-3-Phosphocholine	Yes	1		IFN	1.6
C00212	Adenosine	Yes	3		IFN	1.8
C00491	L-Cystine	Yes	2		IFN	1.6
C00093	sn-Glycerol 3-phosphate	Yes	3		IFN	2.1
C13482	Phosphodimethylethanolamine		1		IFN	3.1
C03850	Adenosine 2',5'-bisphosphate	Yes	6 (choline phosphate)		IFN	2.2
C14179	Sulfoacetate		1		IFN	2.8
C00035	GDP	Yes	1		IFN	2.1
C00026	2-Oxoglutarate	Yes	7		LPS	4.6
C00117	D-Ribose 5-phosphate	Yes	16		LPS	N/A
C00354	D-Fructose 1,6-bisphosphate		14		LPS	10.6
NoKegg25	Hydroxybutyrylcarnitine		1		LPS	2.3

Kegg ID	Name	Standard	Isomer	Ms^2	Set	Max FC
C00197	3-Phospho-D-glycerate	Yes	3		LPS	7.3
C00167	UDP-glucuronate		3		LPS	3.9
C00294	Inosine	Yes	1		LPS	N/A
NoKegg7	3-Hydroxy-11Z-octadecenoylcarnitine		2		LPS	N/A
C00279	D-Erythrose 4-phosphate		4 (Orotidine)		LPS	N/A
C00015	UDP		1		LPS	6.9
C00270	N-Acetylneuraminate	Yes	3-phospho-D-glycerate)		LPS	1.5
C00029	UDP-glucose	Yes	3 (S-MALATE)		LPS	2.9
C00669	gamma-L-Glutamyl-L-cysteine	Yes	2		LPS	10.2
NoKegg6	Tetradecanoylcarnitine		2		LPS	1.9
C02862	O-Butanoylcarnitine		3		LPS	3.0
C00114	Choline	Yes	1		LPS	1.4
NoKegg22	S-D-mandeloylglutathione		1		LPS	3.9
C00352	D-Glucosamine 6-phosphate		8		LPS	2.1
C03943	(2R,4S)-2,4-Diaminopentanoate		6 (3-phospho-d		IFN:LPS	7.4
C00327	L-Citrulline	Yes	3	Yes	IFN:LPS	7.2
C00099	beta-Alanine	Yes	9		IFN Π LPS	2.8
C00262	Hypoxanthine	Yes	3	Yes	IFN Π LPS	7.6
C03592	5-Methyl-2'-deoxycytidine		1 (5-methyl-2'-		IFN Π LPS	2.4
C00881	Deoxycytidine		1		IFN Π LPS	3.8
NoKegg30	β-ketophosphonate		1		IFN Π LPS	N/A
C02230	3-Methylguanine		5		IFN Π LPS	12.0
C00611	N-Acetyllactosamine		8 (dihydrobiopterin)		IFN Π LPS	9.8
C00268	Dihydrobiopterin		4		IFN Π LPS	33.2
C00300	Creatine		2 (Glutamine)		IFN Π LPS	1.4
C00346	Ethanolamine phosphate	Yes	2 (Taurine)		IFN Π LPS	1.8
C00385	Xanthine	Yes	3	Yes	IFN Π LPS	2.8
C00490	Itaconate	Yes	7	Yes	IFN Π LPS	17.7
C00025	L-Glutamate	Yes	14	Yes	IFN Π LPS	2.0
C00149	(S)-Malate	Yes	4	Yes	IFN Π LPS	3.3
C00004	NADH	Yes	1 (Picolinamide)		IFN Π LPS	4.3
C00042	Succinate	Yes	7 (itaconate?)	Yes	IFN Π LPS	2.2
C00130	IMP	Yes	3		IFN:LPS Π	N/A
NoKegg4	trans-hexadec-2-enoylcarnitine		2		IFN:LPS Π	2.3
C03406	N-(L-Arginino)-Succinate		6		IFN:LPS Π	N/A
NoKegg2	Elaidiccarnitine		3		IFN:LPS Π	1.9
C01959	Taurocyamine		1		IFN:LPS Π	2.5
C00519	Hypotaurine		1 (Taurine)		ALL	2.8
C01300	2-Amino-4-hydroxy-6-hydroxymethyl-7, 8-		1		ALL	5.0
C00245	Taurine	Yes	1	Yes	ALL	1.8
NoKegg12	2-Methylbutyroylcarnitine		4		ALL	2.5
C00242	Guanine	Yes	3		ALL	10.9
C03017	O-Propanoylcarnitine		1		ALL	3.2
NoKegg19	N-(octanoyl)-L-homoserine		4		ALL	3.3
NoKegg3	Linoelaidylcarnitine		2 (elaidiccarnitine)		ALL	3.0

3.2.2.3 Interaction: additive, synergistic or antagonistic effects

In **Figure 3-9** the IFNγ depletion of purine and pyrimidine related metabolites and the synergistic production of citrulline is again apparent. Both LPS and IFNγ induce several classical inflammatory metabolites such as succinate, L-glutamate, (S)-malate and itaconate. While there is an additive effect from both stimuli, it is important that any strategy of inhibiting these metabolic pathways must account for the fact that unique to specific stimulus that may not be present in every disease.

What is striking is the appearance of carnitine related metabolites in this section. These are trans-hexadec-2-enoylcarnitine elaidiccarnitine and linoelaidylcarnitine. Note that elaidiccarnitine and linoelaidylcarnitine had similar retention times and thus one may be an adduct of the other L-carnitine, which is increased in the presence of IFNγ has also been reported to be increased in M2 macrophages (Jha *et al*. 2015). While some of the carnitine's production is maximised in the presence of IFNγ and LPS, there are 3 metabolites that the inducement by LPS is inhibited by the presence of IFNγ. Accumulation of acylcarnitines can result from incomplete ß-oxidation of fatty acids in mitochondria. Acylcarnitines can induce pro-inflammatory pathways so IFNγ may be acting to limit this.

Inosine monophosphate (IMP) also displays a similar trend to the acylcarnitines in that it was increased in LPS treatment samples but not in samples treated with both IFNγ and LPS. Alterations in levels of purines and pyrimidines have largely been attributed to the cost of engaging expansive transcriptional programmes. Alternative roles of these pathways as well as Taurine and ß-alanine metabolism are discussed further in section **3.2.3.2** where results of pathway analysis are presented.

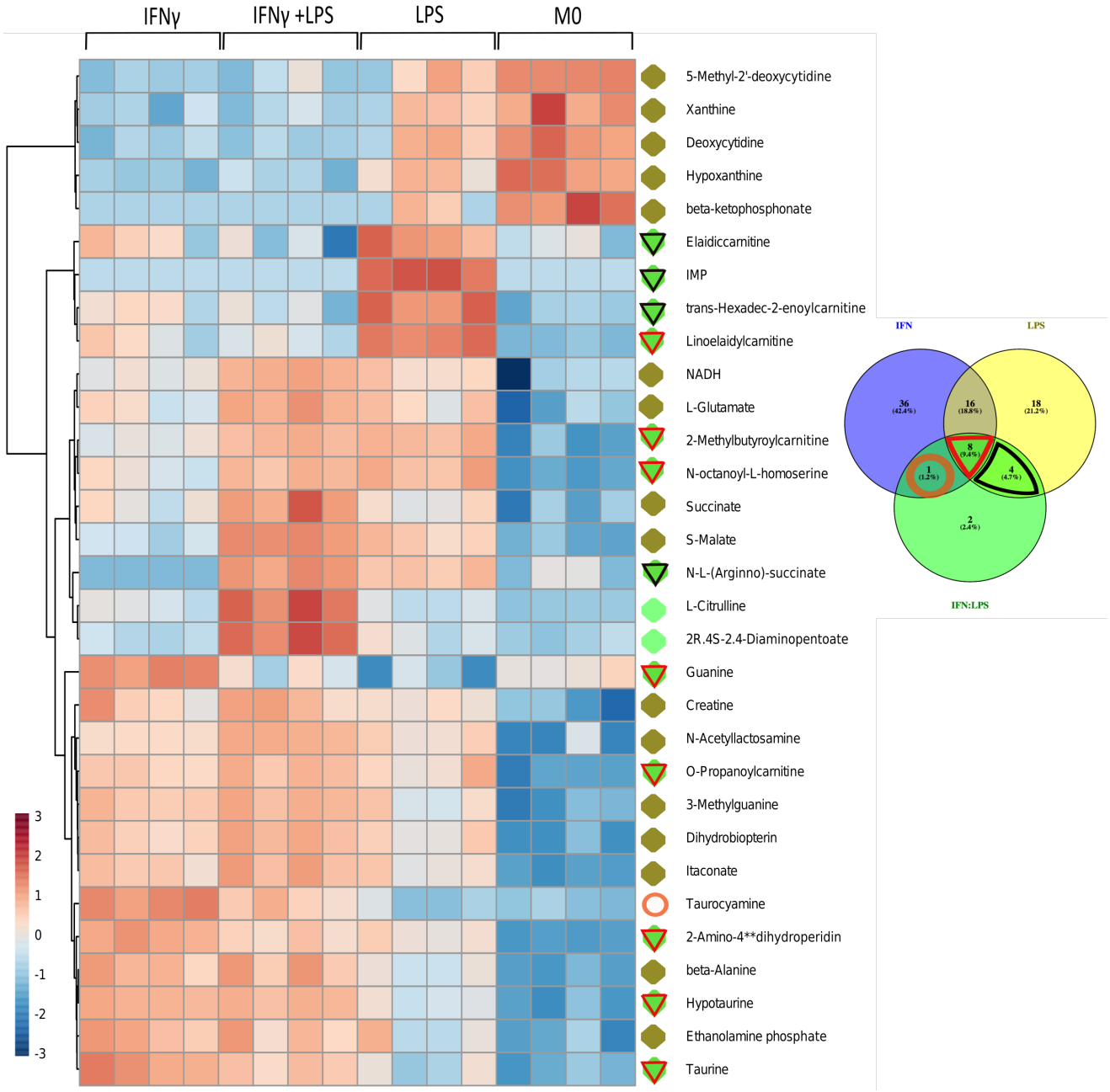

Figure 3-9: Heatmap of metabolites that display an additive or interaction effect. Colour key beside metabolite name corresponds to Venn diagram, which was made using Venny (Oliveros 2015).

3.2.2.4 Pathway analysis reveals immune-metabolic drivers

To formally categorise the contribution of LPS and IFNγ to biological pathways, pathway analysis was performed on log-transformed data using the pathway analysis module on MetaboAnalyst. A generalised logarithm transformation is used here. Generalized logarithm (glog) is a simple variation of ordinary log in order to deal with zero or negative values in the data set (where 'a' is a constant with a default value of 1).

$$glog_2 x = log_2 \frac{x + \sqrt{x^2 + a^2}}{2}$$

This allowed us to use the murine pathway library and upload a relevant background (all detected metabolites). The use of a background is important as it allows technical bias specific to the instrument used to be taken into account. Specifically, certain large pathways such as pyrimidine metabolite will not have every metabolite detected. If the metabolites with altered levels were subjected to enrichment analysis versus the entire pathway ignoring the fact that the status of many of these is unknown, this would not take into account the sampling bias that is present. Here a list of all detected metabolites was used as the background. The pathway enrichment analysis used here is based on the GlobalTest algorithm (Xia & Wishart 2010). Here the null hypothesis is that none of the covariates in the tested group is associated with the response. The alternative is that at least one of the covariates has such an association. To estimate node importance, the Relative-betweeness Centrality algorithm was selected. This measures number of shortest paths going through the node, focusing more on global network topology. Thus changes in metabolites at central nodes within or between pathways are given more importance than those at the extremities as they are more likely to modulate flux through the pathway (s).

First altered pathways either present exclusively in LPS or IFNγ affected subsets, the intersect/addition subset (LPSnIFN), or the set that contained any interaction effect was examined. Some of these pathways were exclusive to the following groups: LPS, IFNγ, the intersect of LPS and IFNγ sets, or interaction set. Some pathways were present in more than one of these groups i.e. there is

an impact of the interaction effect on arginine and proline metabolism but it is less than the additive effect (LPSnIFN). The results of this is summarised in **Table 3-3**. The entire list of significant hits from the GLM was also submitted to pathway analysis and used an impact score of ≥0.1 as a threshold to select a shortlist of pathways for further investigation.

We detect an exclusive role of IFNγ in nicotinate and nicotinamide metabolism, specifically, its increasing of NAD^+ levels. NAD^+ serves an oxidizing agent while NADH is a reducing agent and these have roles in multiple pathways. The additive effects of IFNγ and LPS cause increased NADH levels. Thus it appears IFNγ increases the oxidative potential of the macrophage, potentially to deal with increased glycolytic flux (Warburg shift). Other alternative uses of NAD^+ include Glyceraldehyde-3-phosphate dehydrogenase (GAPDH), which is a key glycolytic enzyme, IMP dehydrogenase (discussed below) and the generation of cyclic–ADP-ribose generated by CD38. Cyclic–ADP-ribose is a metabolite, the increase of which is driven by IFNγ in our experiment. Glutathione is an important anti-oxidant and while it or its reduced equivalent (GSSG), does not show large perturbations, LPS treatment caused a large increase in its precursor Y-L-Glutamyl-L-cysteine. Note that reliable detection of reduced versus oxidised metabolites such as these is a limitation of LCMS such as those used in this study.

LPS induced accumulation of inosine and inosine monophosphate (IMP) and an IFNγ mediated increased guanine were among the most significant changes detected in our study. Upon activation a macrophage needs to engage an inflammatory transcriptional profile and it would not be unexpected that this could affect nucleotide metabolism. Macrophages are end-differentiated cells, which are mainly non-proliferative so these metabolites are not required for DNA synthesis. There are, however, instances where changes in specific parts of these pathways have been shown to have important functions independent of RNA/DNA synthesis. In purine metabolism, xanthine oxidase (XO) catalyses the conversion of hypoxanthine into xanthine, producing H_2O_2 as a by-product. The free radicals produced here have been shown to activate the p38-MAPK-NFAT5 pathway and inhibiting XO via its inhibitor allopurinol limited inflammation in a

mouse model of arthritis (Kim *et al*. 2014c). Perturbations in the substrate and product of XO in stimulated cells were also observed.

Table 3-3: Pathway analysis of inflammatory macrophages. A background (all detected metabolites) was uploaded onto MetaboAnalyst and analysis carried out on metabolites unique to IFNγ, LPS or the interaction set. To avoid false positives from multiple comparisons, the entire list of significantly altered metabolites (according to the GLM) was analysis and this was used to set the 0.1 impact score threshold. The largest contributor (s) to pathway perturbation is indicated in the 'Causative' column and underlined values in the Impact summary denote the impact score obtained in the respective set.

	Entire		Pairwise		Causative	Impact Summary			
IFN exclusive	FDR	Impact	FDR	Impact		**IFN**	**LPS**	**IFNn LPS**	**Interact**
Nicotinate and nicotinamide metabolism	0.003	0.21	0.005	0.21	**IFN**	0.21			
LPS exclusive									
Glycolysis or Gluconeogenesis	0.001	0.1	0.001	0.1	**LPS**		0.1		
Pentose phosphate pathway	0.001	0.24	0.001	0.24	**LPS**		0.24		
Ascorbate and aldarate metabolism	0.001	0.4	0.001	0.4	**LPS**		0.4		
Pentose and glucuronate interconversions	0.001	0.47	0.001	0.47	**LPS**		0.47		
Starch and sucrose metabolism	0.001	0.25	0.001	0.25	**LPS**		0.25		
IFNnLPS									
Citrate cycle (TCA cycle)	0.001	0.14	0.001	0.07	**IFNnLPS = LPS**		0.07	0.07	
D-Glutamine and D-glutamate metabolism	0.001	1	0.001	1	**IFNnLPS**			1	
Glutathione metabolism	0.009	0.13	0.001	0.06	**LPS > IFNnLPS**		0.08	0.06	
Pyrimidine metabolism	0.001	0.13	0.001	0	**LPS**		0.07		
Glycerophospholipid metabolism	0.005	0.18	0.002	0	**IFN**	0.16	0.02		
beta-Alanine metabolism	0.001	0.44	0.001	0.44	**IFNnLPS**			0.44	
Interaction									
Purine metabolism	0.001	0.2	0.001	0.13	**Interaction**	0.02		0.04	0.13
Alanine, aspartate and glutamate metabolism	0.001	0.65	0.001	0.02	**IFN > IFNnLPS**	0.31	0.06	0.11	0.02
Arginine and proline metabolism	0.001	0.19	0.001	0.05	**IFNnLPS**	0.04		0.11	0.05
Taurine and hypotaurine metabolism	0.001	0.71	0.001	0.71	**Interaction**				0.71

Purine metabolism has previously been shown to be indispensable in the maturation of myeloid leukaemia cell lines (Knight *et al*. 1987). Knight *et al* observed that IMP was being diverted to guanine via increased IMP-dehydrogenase (IMPDH) activity. Inhibiting IMPDH drove cell maturation towards a neutrophil phenotype. An key immune-modulatory role for IMPDH has been

proposed in the case of the IC-21 murine macrophage cell line (Jonsson & Carlsten 2002). In this study the authors found that the IMPDH inhibitor mycophenolate mofetil suppressed production of pro-inflammatory cytokines, nitric oxide, and lactate dehydrogenase in macrophages. Additionally, the inhibition of these inflammatory mediators was abrogated by guanosine supplementation. An increase in both IMP and inosine was detected in LPS treated macrophages, an increase that was inhibited in the presence of IFNγ. Whether these pathways and key enzymes such as IMPDH are valid targets in an inflammatory setting remains to be determined.

Guanine levels have been shown to be required for the increase in cAMP induced by prostaglandin (PG) (Verghese & Snyderman 1983). PG are hormones, the levels of which are increased in activated macrophage. An increase in guanine was detected in this experiment but this was restricted to cells stimulated with IFNγ alone. While this may be a consequence of increased IMPDH activity (its catalysing the conversion of IMP to xanthosine monophosphate (XMP) is the first committed and rate-limiting step towards the *de novo* biosynthesis of guanine nucleotides), an increase in transcript abundance of the guanosine metabolising enzymes pnp and pnp2 has been detected in inflammatory macrophages (Jha *et al*. 2015). Pnp and pnp2 also catalyse inosine-hypoxanthine interconversions so it would be difficult to determine which, if any, of the multiple reactions are immune-modulatory. Nevertheless, it is apparent that the different stimulus are causing divergent perturbations to purine metabolism and it will be interesting to determine whether the metabolites have effector functions outwith nucleotide biosynthesis.

ß-alanine metabolism was significantly altered according to ANOVA, GLM and pathway analysis. It has been reported that the source of increased ß-alanine is a by-product of increased flux through arginine metabolism via carnosine synthase 1 (Carns1) in anti-inflammatory macrophages (Jha *et al*. 2015). Carns1 catalyses the conversion L-histidine and ß-alanine to Carnosine. An alternative source of ß-alanine is pyrimidine metabolism that was subject to stimuli specific perturbations. Furthermore, in the transcriptome data from *Jha et al*, there is an increase in transcript abundance of an enzyme (*dpys*) that carries out an

intermediate reaction in ß-alanine synthesis from pyrimidine metabolism (5,6-dihydrouracil to N-carbamoyl-ß-alanine).

There have also been some studies that have investigated the immune-modulating capability of ß-alanine (Prabha *et al*. 1988). Prabha *et al* reported that ß-alanine caused similar effects to taurine in heart and adipose tissue. In adipose tissue the addition of these metabolites was shown to result in down-regulation of lipoprotein lipase (LPL) activity and altered cholesterol metabolism. Harris *et al* found that IFNγ inhibits LPL at the level of transcription in macrophages (Harris *et al*. 2008). Interestingly, LPL has also been proposed to promote foam cell formation in macrophages (Babaev *et al*. 1999). As the increases presented here were present in all combinations of IFNγ treatment, it would be interesting to determine if ß-alanine has a role modulating LPL activity.

We also detected IFNγ-mediated increases in taurine and its related metabolites hypotaurine and taurocyamine. As previously mentioned, these metabolites have been shown to modulate cholesterol metabolism and LPL activity. Kim *et al* demonstrated that taurine inhibits nitric oxide induced apoptosis in murine RAW264.7 macrophages (Kim *et al*. 2009d). While taurine and taurine metabolites were increased in an IFNγ–dependent manner, whether this is a general protective process or if endogenous taurine production is sufficient to do the same remains to be determined.

3.3 Discussion

Development of a robust, high coverage metabolite extraction of macrophages has been established. In **Chapter 1** phenomenon of immune-metabolism was introduced as well as some of the hallmarks of inflammatory macrophage metabolism. In **Figure 3-10** the results of this chapter are shown in this context. Not only were well-known markers detected, it was possible to determine the relative contribution of each stimulus to these markers. Furthermore, there is a high-resolution readout of several perturbed modules the importance of which has not been interrogated in the context of immune-metabolism.

3.3.1 Classical markers: new insight

Previous studies examining immune metabolism in inflammatory macrophages have used either LPS or IFNγ and LPS in combination (Tannahill *et al*. 2013; Jha *et al*. 2015). This is to our knowledge, the first study, which has examined the contribution and interaction of each of these factors in a systematic fashion. This is especially relevant physiologically as *in vivo*, prior encounter of a naïve immune cell with a pathogen can be simulated by LPS, pre-adaptation of immune cells caused by Th_1 signalling by IFNγ, and interaction of a primed immune cell with a pathogen by the combination of both. In the context of disease, diagnosis often occurs after an immune response has been initiated, so any attempt to treat disease by modulating cell metabolism must take into account what these stimuli do in isolation and in combination.

3.3.1.1 Glycolysis, PPP and TCA cycle:

The detection of the Warburg effect was a key discovery in establishing the immune-metabolism field (Tannahill *et al*. 2013; Jha *et al*. 2015; Lampropoulou *et al*. 2016). Macrophages rapidly upregulate glucose uptake and several enzymes in glycolysis such as hexokinase and the highly active phosphofructokinase-1 isoform, u-PFK2 (Fukuzumi *et al*. 1996; Rodríguez-Prados *et al*. 2010). The Warburg effect offers cancer cells a means to utilise glucose for ATP production in the absence of oxygen. This is also the case for macrophages in hypoxic conditions. Increased glycolysis in the presence or reduced level of oxygen is also essential to generate NADPH (oxidative stress protection) and ribonucleotide precursors (possibly required for M1 transcriptional programme) via the PPP. In order to sustain high glycolytic flux NAD+ must be increased NAD^+ levels that are driven by IFNγ while increased fructose 1,6-bisphosphate and 3-phospho D-glycerate levels are induced by LPS. Lactate levels are increased but only in combination treatment so the source of increased NAD^+ levels in IFNγ treated samples remains to be determined. Nevertheless, perturbations in these pathways is in agreement with previous studies (Tannahill *et al*. 2013; Jha *et al*. 2015)

In the PPP, ribose 5 phosphate and erythrose 4-phosphate are increased in an LPS dependent manner indicating that a pathogen stimulus is critical for

increased production of NADPH and ribonucleotide precursors (Haschemi *et al*. 2012). Recently reported perturbations of the TCA cycle are also observed in our data such as increases in both itaconate production and succinate accumulation (Tannahill *et al*. 2013; Lampropoulou *et al*. 2016). As expected the arginino-succinate shunt requires synergistic activity from IFNγ and LPS to produce citrulline via *iNOS*. The effector metabolite of *iNOS*, $NO^{\bullet}$, while not detectable using LC-MS, was measured using the Griess assay.

3.3.1.2 Taurine, ß-alanine and Carnitine related metabolites

As mentioned in the results taurine and ß-alanine have previously been shown to prevent apoptosis and modulate lipid metabolism and in some instances this involves signalling pathways modulated by IFNγ (Prabha *et al*. 1988; Harris *et al*. 2008; Kim *et al*. 2009d). Lipid metabolism has previously been identified as important for M2 macrophages (Huang *et al*. 2014). A pro-inflammatory role has been suggested for incomplete lipid metabolism, which is a feature of incomplete ß-oxidation of fatty acids in mitochondria in increased acylcarnitines and has been observed in insulin resistance and type 2 diabetes mellitus (Rutkowsky *et al*. 2014). Rutkowsky *et al* reported that acylcarnitines induced cyclooxygenase-2 (Cox-2) in a chain length-dependent manner but this study exclusively used cell lines such as RAW 264.7 cells. On the other hand, a previous study has examined *in vivo* the role of fatty acid oxidation and auto-immune inflammation in the CNS in a murine multiple sclerosis (MS) model and found that fatty acid oxidation (FAO) was essential for disease progression. Furthermore, the authors found that FAO was essential for inflammatory T cell function and consequently disease progression (Shriver & Manchester 2011).

A recent study using carnitine palmitoyltransferase 2 (*Cpt2*) deficient macrophages found that while the cells could not undergo FAO, this was not required for M2 polarisation (Nomura *et al*. 2016). Etomoxir inhibits another key enzyme in lipid metabolism, carnitine palmitoyltransferase 1A (*Cpt1a*). This is a mitochondrial enzyme that is responsible for the formation of acyl carnitines by catalysing the transfer of the acyl group of a long-chain fatty acyl-CoA from coenzyme A to l-carnitine. However, Etomoxir (200 μM), inhibited IL-4 target genes in $Cpt2^{-/-}$ macrophages, suggesting either an off-target effect or an

unknown additional function for Cpt1a and the authors proposed that localised deletion of Cpt1a will be require to elucidate possible functions outwith FOA.

We observe perturbation of carnitine related metabolites, many of which were acylcarnitines. If these are pro-inflammatory effectors or a pro-inflammatory signature, it is possible that by reducing this, IFNγ has an important role regulating oxidation of ß –fatty acids. Regulation of lipid metabolism will require further investigation in the context of inflammatory macrophages, taking into account the type-(s) of stimulus/stimuli used.

3.3.1.3 Pyridines and purines

The engagement of a transcriptional profile is expected to require increased nucleotide synthesis and consumption. Changes in these pathways were detected but it is noticeable that these changes are not unidirectional and stimulus specific increases are not uniform. Guanine and inosine have been shown to modulate cell function so it will be interesting to determine if they have a similar role in inflammation. Finally, there were two modified nucleotide analogues that had altered levels; 5'-methyl-2'deoxycytidine (marker of *de-novo* DNA methylation: decreased by all stimuli) and 3-methyguanine (altered in leukaemia, tumours and immunodeficiency: increased by all stimuli). Whether these metabolites are indicative of essential epigenetic modifications is currently unknown. Methylation in the context of inflammatory genes and/in disease has been reported but has not been detected at a global level (Bayarsaihan 2016). Interestingly, Adenosine, which is known to down-regulate classical macrophage activation via the A2A G-protein–coupled cell membrane receptor (Hasko & Pacher 2012), is increased in an IFNγ-dependent manner. Whether this is indicative of a regulatory mechanism remains to be determined

3.3.2 Untargeted metabolomics: Strengths and weakness

This study has given unparalleled coverage of the metabolome of inflammatory cells. Our choice of protocol and platform has allowed us to look within and outwith central carbon metabolism. This coverage comes at a cost. While confidence in metabolite identifications can be strengthened by use of authentic standard and fragmentation, many metabolites are solely identified by accurate

mass and predicted retention time and thus are only **putatively identified**. Further targeted analysis (IE isotope labelling studies) and validation studies (medium deprivation and inhibitors) will be required to verify these results and any biological importance. Nevertheless, a robust method has been established that performed admirably well here. Furthermore, this method further enabled meeting the aim of **Chapter 4**: to obtain the *Leishmania*-infected macrophage metabolome.

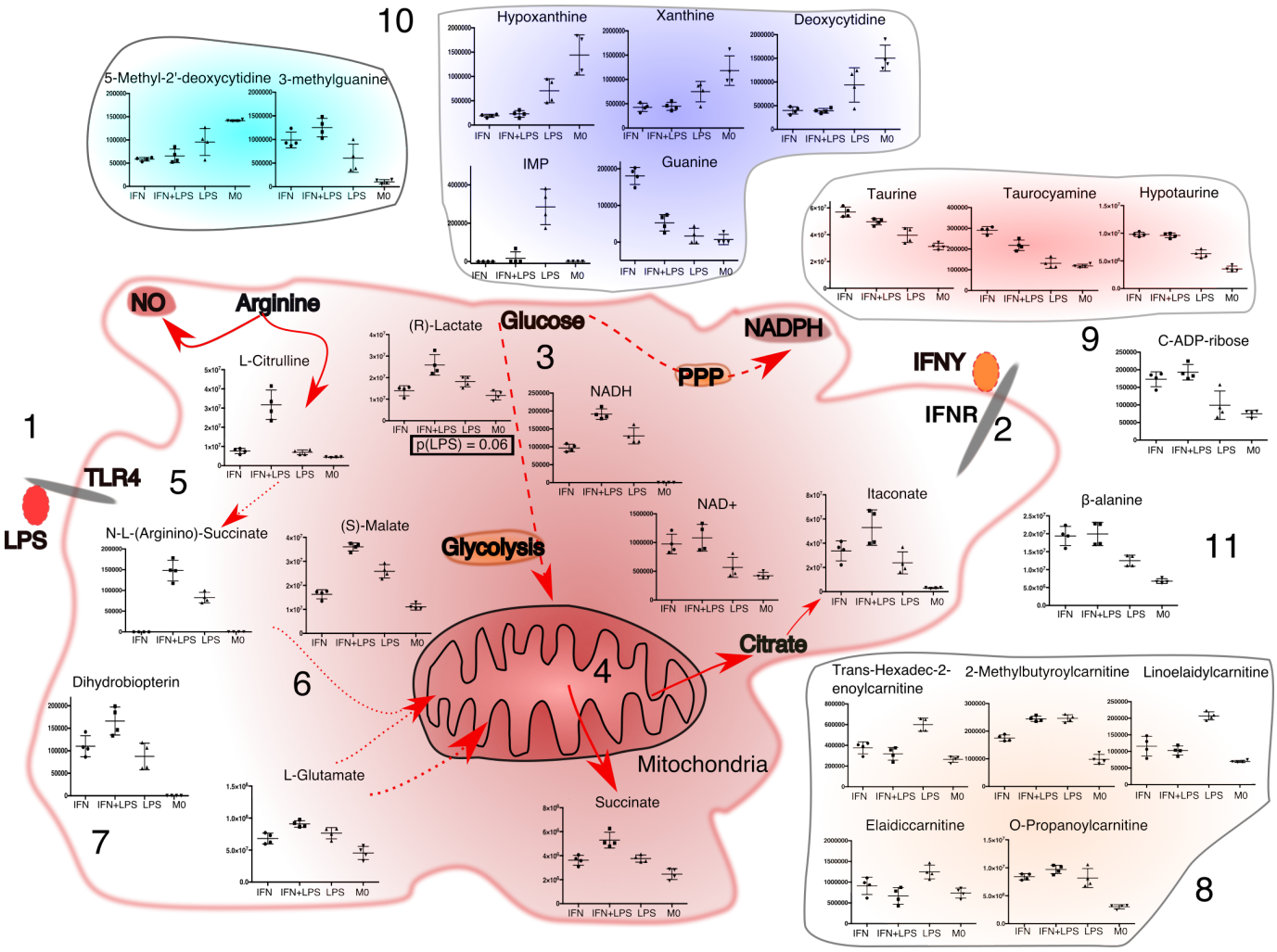

Figure 3-10: Our results in the context of macrophage immune-metabolism. Note that location of metabolites does not refer to cellular location. 1: & 2: Some macrophages were primed with IFNγ overnight and then some were stimulated with LPS for four hours. 3: This causes increase in metabolites in glycolysis ((R))-Lactate) and the PPP (Ribose-5-Phosphate, not shown). 4: Previously reported perturbations in the TCA cycle are indicated including Itaconate production and Succinate accumulation. 5: L-Arginine is metabolised to L-Citrulline and effector molecule NO*. 6: Arginine and Glutamate metabolism are connected with N-L- (Arginino)-Succinate and Aspartate (from Glutamate) allow for replenishment of the TCA cycle at the point of Fumarate. 7: Dihydrobiopterin is used to form the iNOS cofactor tetrahydrobiopterin by Dihydrobiopterin reductase. 8: Levels of select carnitine related metabolites are modulated by LPS and/or IFNγ. 9: Taurine metabolism is modulated by IFNγ. 10: Purine and pyrimidine metabolism displays as stimuli specific profile as did some modified analogues. 11: Levels of ß-alanine, which can originate from arginine, pyrimidine fatty acid or glutamate metabolism, were increased in M1 macrophages.

4 A complementary metabolome and transcriptome of the infected macrophage

4.1 Introduction

Macrophages are a key part of the innate immune system and possess a wide range of potent effector functions such as the generation of reactive oxygen and nitrogen species. Furthermore, they can produce a plethora of chemokines and cytokines that can cause the recruitment and activation of other immune cells. Using classical techniques from molecular biology and immunology has revealed a great deal about how the *Leishmania* parasite can avoid, supress, and/or survive these responses.

In **Chapter 1** there an introduction to studies that showed how *Leishmania* species recruit macrophages and drive a M2 polarisation by secreting promastigote secretory gel (PSG) (Rogers *et al*. 2009), and how different parasite species activate different complement mediated opsonisation and uptake pathways (Mosser *et al*. 1986; Domínguez *et al*. 2003). Not all of these studies used the same parasite species/strains, and this, in combination with variation caused by differences in hosts (i.e. mouse strain), or host cell type used makes it difficult to have a single and unified overview of how specific parasite species modulate the host cell. Instead, a patchwork-like model of parasite-host interactions and modulation emerges that contains processes that may not apply to all *Leishmania* species.

High throughput techniques such as transcriptomics and metabolomics are becoming increasingly important in this regard as they allow the systematic profiling of multiple biologically important processes simultaneously. These methods can be applied to multiple species and/or when multiple time-points are used, unprecedented insight into both pathogen and host biology can be obtained (Dillon *et al*. 2015; Fiebig *et al*. 2015; Fernandes *et al*. 2016).

Metabolomics has already revealed important changes in parasite metabolism as they differentiate between life cycle stages. Saunders *et al* used targeted MS based metabolomics on a model of the *L. mexicana* intracellular parasite and found that there is a switch to a stringent profile where parasites consume fewer

substrates but also produce fewer partly oxidised products of metabolism (Saunders *et al*. 2014). Lamour *et al* used NMR to profile the *L. major* infected macrophage (Lamour *et al*. 2012). While several changes were detected, the coverage of NMR is much less than that of LC-MS. Furthermore, as an antigen or phagocytic control was not used in their study, it is not possible to differentiate between general responses associated with consumption of particulate matter and live parasite induced perturbations.

Recently it was reported that *L. infantum* infected macrophages undergo a temporary shift to glycolysis (~6 hours post infection) before reverting to oxidative phosphorylation (~18 hours post infection) (Moreira *et al*. 2015). The focus of this study was, however, restricted to central carbon metabolism. Nevertheless, the findings were of interest hence the aim was to use as similar as possible time-points for the metabolic and transcriptomics profiling of *L. mexicana*-infected macrophages (**Figure 4-1**). Furthermore, flow-cytometry cell sorting was used to enrich for infected macrophages. The benefits of this are two-fold. Firstly, bystander cells are removed and secondly, intracellular parasites are synchronised.

Integration of 'Omics' is a new and challenging area of research. This approach has the power to reveal emergent properties not obvious in the individual datasets (Jha *et al*. 2015). This will be increasingly useful in utilising metabolomics datasets by linking a specific transcriptional pathway to metabolites that can occur in multiple pathways and *vice versa*. Furthermore, while transcriptomics offers unparalleled coverage, not all transcripts are translated and post-translational modifications to proteins can affect cell function. As alterations in metabolite abundance occur downstream of such effects (i.e. changes in enzyme expression influence metabolism), metabolomics offers a readout that is closer to actual phenotype, in that it is the metabolite building blocks that are ultimately polymerised into the molecular structures defining cellular architecture.

An antigen (or poly-antigen) control is commonly used in host-pathogen experiments. This control allows the detection of general responses that the live parasite may induce or supress as well as changes that only the live parasite may cause. The latter class of changes can include alterations caused by increased or

decreased levels of certain metabolites that are produced or consumed by the live parasite. In this chapter such a control was developed and utilised in both the transcriptomics and untargeted metabolomics profiling of *L. mexicana*-infected macrophages.

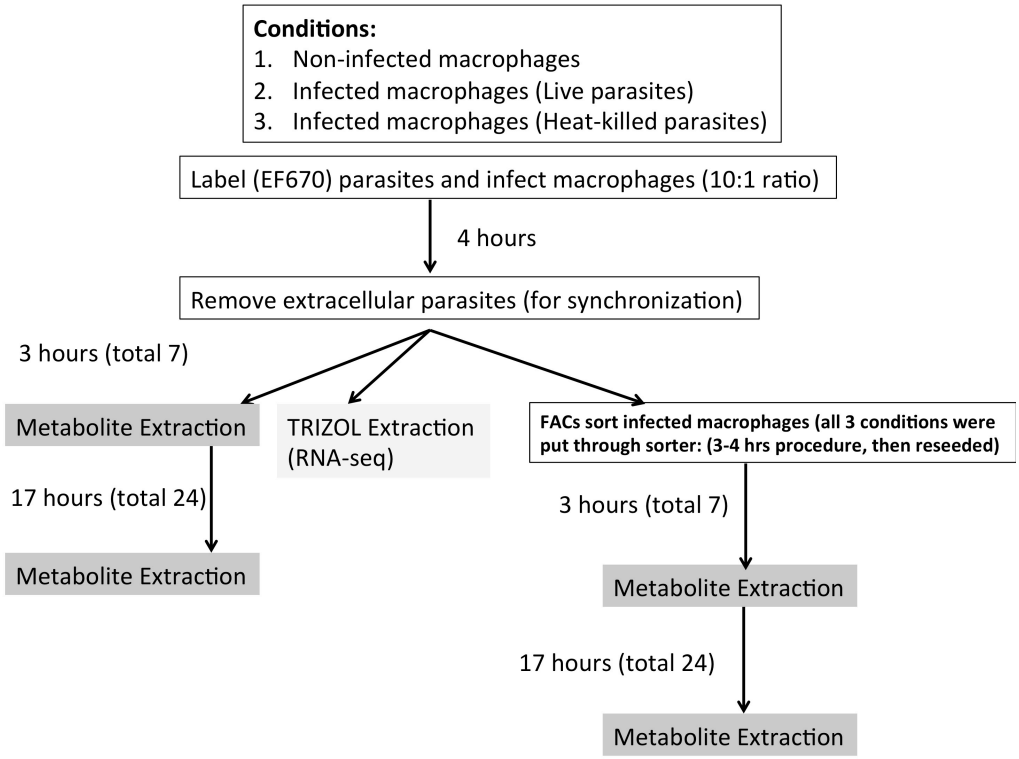

Figure 4-1: Experimental outline of Omics experiments in Chapter 4. Note that for the metabolomic experiments that did not involve FACs, there were M1 and M2 controls for each time-point.

4.2 Results

4.2.1 Establishing a heat-killed control and enrichment strategy

4.2.1.1 Heat-killed control

Several studies have used heat-killed parasites as an antigen control with heat-killing conditions ranging from 56ºC for 5 minutes to kill *L. amazonensis* to 65ºC to 45 minutes heat-killing of *L. donovani* (Morehead *et al*. 2002; Marr *et al*. 2014). The lowest temperature that reproducibly yielded non-live parasites in our hands was 48ºC for 12 minutes as characterised by growth curves (**Figure 4-2**) (see **2.6.4**). While different parasite strains have different sensitivities to heat (i.e. cutaneous stains die at 37ºC), and higher temperature could be used with the aim of denaturing enzymes, our objective was to heat-kill the parasite using the least harsh treatment possible in a controlled and reproducible manner. While Moreira *et al* used gamma-irradiated parasites

(Moreira *et al*. 2015), our X-ray source would have taken several hours to deliver an equivalent dose, which was unsuitable for our experimental design.

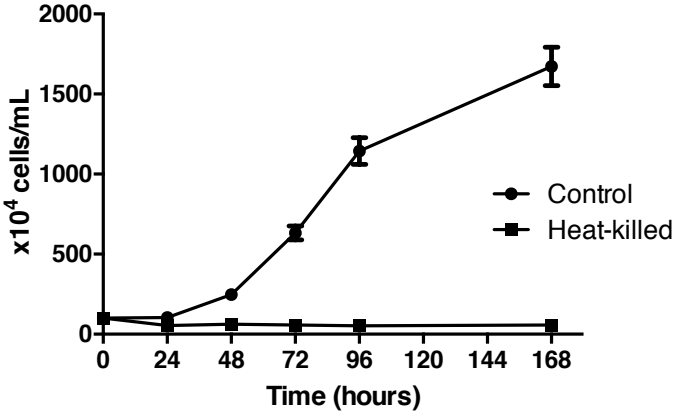

Figure 4-2: Growth curves comparing heat-killed parasites with control. Metacyclic promastigotes were heated to 48ºC for 12 minutes in a water bath then seeded at a density of 10^6 cells/mL in cRPMI, and growth at 32ºC, 5% CO_2 monitored. Results are representative of three independent experiments.

4.2.1.2 Flow cytometry enrichment of infected cells

To enrich for infected cells, metacyclic promastigotes (5 day old culture) were first labelled with EF670 (eBioscience) similarly to Moreira *et al*. 2015 (see **2.7.2**). This was done prior to heat killing to avoid subjecting the heat-killed parasites to multiple centrifugation steps. Infection was allowed to proceed for four hours before proceeding to the FACS protocol. After the protocol, cells were re-plated and subsequently processed samples at 7 hours (3 hours post infection end) and 24 hours (18 hours post infection end) after starting initial infection. 7 (3) hours and 24 (18) hours were chosen as previous studies have reported that important changes to metabolite and transcript levels occur at or near these time-points (Moreira *et al*. 2015; Dillon *et al*. 2015; Fernandes *et al*. 2016).

Additionally, our lab has observed a dramatic reduction in cells present in the non-treated groups (quantified by Clément Regnault, unpublished data, using the post-extraction protein measurement protocol described in **Chapter 3**) at later time-points (48hrs or later) severely reducing its suitability as a comparable control.

In **Figure 4.3**, the gating strategy is shown. Briefly cells were first gated based on size vs. granularity (forward scatter (FSC)-area vs side scatter (SSC)-area)

then singlets were selected (SSC-Area VS SSC-Height). Finally, the EF670^{+} population was selected (final row of panels, right two panels, second peak). In the second row of panels, the small particles positive for EF670 may correspond to extracellular parasites or debris of parasites or infected cells. Note that the Aria I (BD bioscience) was used to sort sample D while samples A and C on the Aria III (BD bioscience) in order to obtain sufficient cells. Identical samples were used for setting gates, and identical flow rate (cells/min) were used for each machine. Furthermore, after the procedure, all sample counts were verified using a haemocytometer (Greiner) and cell viability confirmed to be >95% using Trypan blue (Sigma). While this does not completely exclude that the different instruments are contributing to changes seen in a metabolite's level, given the similarity of results in sorted and non-sorted experiments, this is assumed to be minimal.

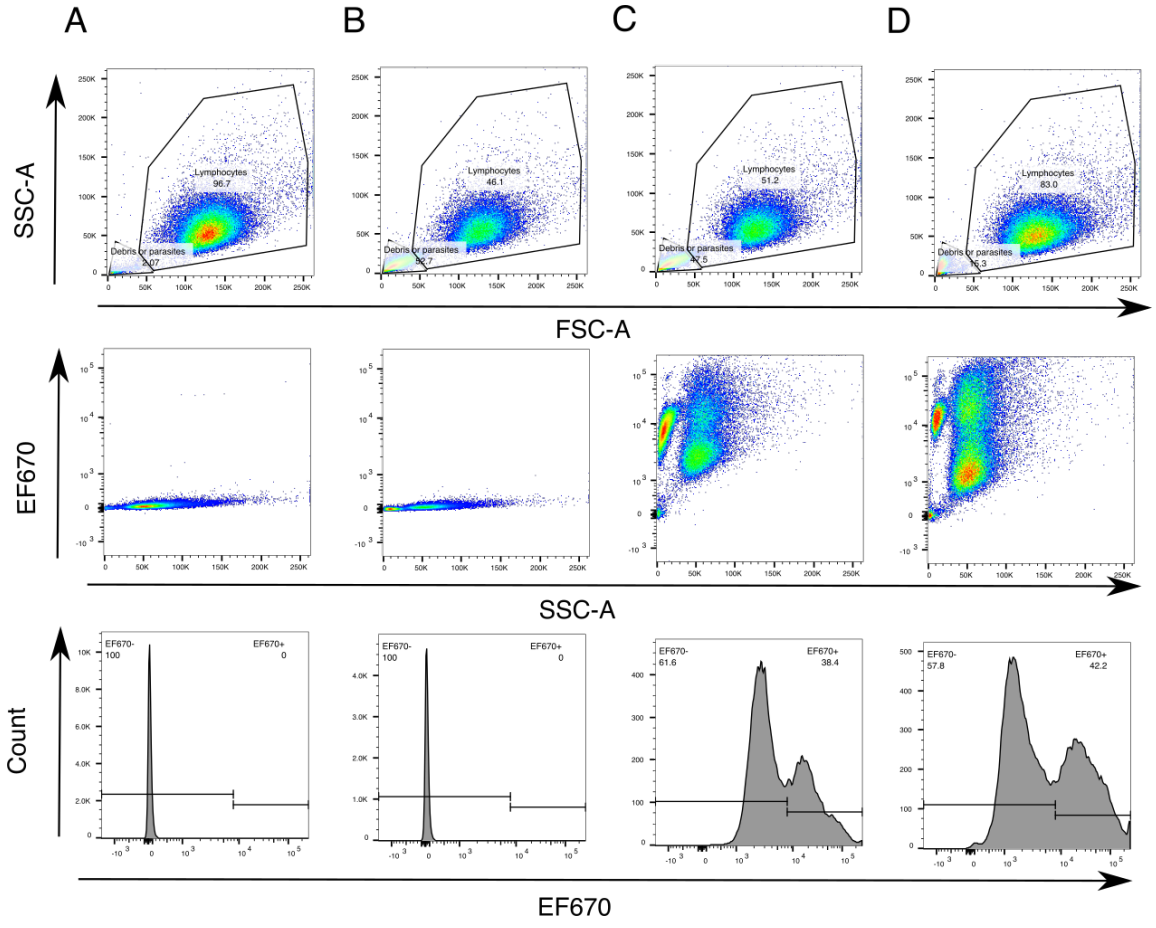

Figure 4-3: FACs enrichment strategy. The gates were set as denoted. Note that in **Chapter 3**, the 'lymphocyte' population was shown consistently to comprise of Cd11b and F4/80 positive cells (macrophages). The samples shown were as follows- A: Non-infected, B: Infected with non-labelled parasites, C: Infected with live parasites, D: Infected with heat-killed infected. These are the results of the Aria-III sort on which samples A and C were collected. The same samples were run on the Aria-I and similar results obtained (**Supplementary Figure 4-1**). Sample D was collected on the Aria-I. The second row of panels shows populations corresponding to infected and non-infected macrophages while the top left population comes from the debris/extracellular

parasite gate. The bottom row of panels shows the final gating used on the "Lymphocyte' (Macrophage) population shown in the first row.

4.2.2 The metabolome of the infected macrophages

We used a 46-minute protocol for our LC step to differentiate between L-citrulline and L-argininic acid, similar to that described in a recent publication (Westrop *et al*. 2015). L-citrulline and L-argininic acid are discussed in more detail in **Chapter 5**.

4.2.2.1 Validation of method; M1 immune metabolism

The experiment was executed as described in **3.1**. This section pertains to results obtained from samples not subjected to FACs sorting. Due to the limited number of cells obtained from FACs enrichment, 200,000 cells/replicate were used while 250,000 cells/replicate were used in non-sorted samples. In order to ensure that profiling method performed with less cells, M1 (IFNγ and LPS) and M2 (Il-4) controls were included. This allowed the testing of the reproducibility of some of the previous chapter's findings (IFNγ and LPS vs. M0) as well. Additionally, this allowed the interrogation of whether macrophages infected with live or heat-killed parasites were polarised in a similar manner to classical M1 or M2 models. The latter is discussed in the following section as well as the justification for conducting statistical analysis on each time-point separately.

Data filtering was conducted as in **3.2.2.1** but with the addition of an Xcalibur method to distinguish between L-argininic acid and L-citrulline. The result of this filtering in IDEOM and the Xcalibur method was a list of 280 metabolites. The identity of 76 of these was confirmed using authentic standards (MSI level 1). For statistical analysis one-way ANOVA was carried out a (using MetaboAnalyst) for both time-points independently with Fisher's least significant difference method (Fisher's LSD) being used for *post hoc* analysis as implemented in MetaboAnalyst. Note that the parasite specific samples were included in this analysis.

Naive samples for the first time-point were omitted, as there were only two replicates. Note that the input and output of this analysis are available in **Supplementary Files 4-(2-3) (Kegg IDs are shown, metabolite name is in Supplementary File 4-1).**

In **Table 4.1**, a summary of metabolites that had altered levels caused by M1 or M2 stimuli is presented. There were more metabolites with significantly altered levels (30 with FDR <0.05 and 4 with FDR <0.1) at the earlier time-point despite the lack of a naive control. At the later time-point there were 4 metabolites with an FDR <0.05 and 4 with a FDR <0.1. Most changes were M1 driven. The fact that the M1 stimulus used is quite strong/enriched is a possible explanation for this. Additionally, IL-4 treated macrophages are primed to have an anti-inflammatory response to pathogens (LPS). Thus there may be a more divergent phenotype if they were co-treated with LPS to be effector M2 cells. A similar approach taken in **Chapter 3** could also be used to dissect the immune and pathogen driven anti-inflammatory phenotypes.

We compared these results with those presented in **Chapter 3**. The time-point of choice was 7 hours as it is nearer to the 4 hours used in the M1 macrophage study in the previous chapter. A total of 24 metabolites were in common in both experiments (in bold in **Table 4-1**) with only 2 of these outside the FDR <0.5 cut-off. For all of these metabolites, the direction of change (vs. M0) was identical. Additionally, other metabolites such as UTP and uracil have a FDR <0.5 in **Chapter 3** when using an ANOVA instead of a GLM. Thus some discrepancies may be due to the different statistical method used.

Finally, three metabolites (D-fructose 6-phosphate, D-glyceraldehyde 3-phosphate, 4-methylene-L-glutamine) from the dataset presented in this chapter were found on the rejected list within the Ideom data processing pipeline (**2.12**). Differences in the identification process here may have been caused by increased separation during a long LC protocol used in this chapter. Another example of a limitation of data processing that is not unique to Ideom is that it can be difficult to differentiate between metabolites of which there are multiple isomers e.g. glyceraldehyde 3-phosphate and dihydroxyacetone phosphate. These limitations could potentially overcome by using authentic standards for the metabolites of question in combination with a different LC method that would separate them better.

Nevertheless, our protocol preforms well even with 12 fold fewer cells, and shows good concordance with some of the key findings of **Chapter 3.** Increased noise at the later time-point in conjunction with the lower number of replicates

(n=3 vs. n=4) limits the chances of determining if earlier perturbations are sustained. However, O-acetylcarnitine, which was increased in M1 macrophages at 7 hours, is higher in M2 macrophages at 24 hours. A detailed understanding of the role/regulation of carnitine metabolism will be required to interpret the biological relevance of these metabolites in M1 and M2 macrophages.

Table 4-1: Metabolites, the levels of which are altered in the presence of immune stimuli. Significance was determined by one-way ANOVA for each time-point with Fisher's LSD used for post-hoc analysis. Samples were analysed alongside infected samples. As KEGG IDs are less ambiguous, the equivalent KEGG IDs are in column 1. As certain metabolites are not in KEGG, arbitrary IDs are used for these. Metabolites whose alterations match those seen in Chapter 3 have names in bold. For the 24 hour time-point there were sufficient samples to include the M0 sample for analysis. In the 'Change' column, the altered condition is indicated and unless otherwise stated, the change is an increase. A match with an authentic standard, number of alternative isomers, match with mZCLOUD fragmentation database and maximum fold change (FC) are indicated in the last four columns. Maximum FC refers to the largest FC between any condition at denoted time-point. In order to avoid division by zero, missing values were replaced with a value that is 25% of the intensity threshold (250).

7 hrs ANOVA	Name	FDR	Change	Std	Iso	MS^2	Max FC
C00490	**Itaconate**	6.44E-09	M1	Yes	7	Yes	73.1
NoKegg30	**Hydroxybutyrylcarnitine**	2.72E-06	M1		1		4.8
C05933	N-(omega)-Hydroxyarginine	2.72E-06	M1		2		172.5
C02305	**Phosphocreatine**	3.89E-06	M1		1		2.5
C03017	**O-Propanoylcarnitine**	3.89E-06	M1		1		4.6
C00149	**(S)-Malate**	3.88E-05	M1	Yes	4		2.8
C00085	D-Fructose 6-phosphate	4.18E-05	M1	Yes	46		188.5
C02230	**3-Methylguanine**	5.22E-05	M1		5		1133.0
C01300	**2-Amino-4-hydroxy-6-hydroxymethyl-7,8-dihydropteridine**	7.62E-05	M1		1		691.0
C00669	**gamma-L-Glutamyl-L-cysteine**	7.62E-05	M1	Yes	2		391.2
C00581	**Guanidinoacetate**	7.97E-05	M1		1		4.8
C00118	D-Glyceraldehyde 3-phosphate	0.0002	M1		7		24.6
C00099	**B-Alanine**	0.0005	M1	Yes	1		3.4
C00670	**sn-glycero-3-Phosphocholine**	0.0005	M1	Yes	1		3.4
C00519	**Hypotaurine**	0.0006	M1		1		3.3
C00327	**L-Citrulline**	0.0008	M1	Yes	1		7.3
C02862	**O-Butanoylcarnitine**	0.001	M1		3		2.8
NoKegg32	**Orotidine**	0.0012	M1	Yes	1		2.3
C01109	4-Methylene-L-glutamine	0.0014	M1		2		7.5
C00019	S-Adenosyl-L-methionine	0.0014	M1		1		5.5
C00093	**sn-Glycerol 3-phosphate**	0.0018	M1	Yes	3		2.4
C01233	**sn-glycero-3-Phosphoethanolamine**	0.0018	M1		1		2.2
C00075	UTP	0.0031	M1		1		3.1
C00026	**2-Oxoglutarate**	0.0043	M1	Yes	7		3.3
C00042	**Succinate**	0.0056	M1	Yes	7		2.6
C00588	**Choline phosphate**	0.0056	M1	Yes	1		2.5
C00051	Glutathione	0.0078	M1	Yes	3		3.0
C00346	**Ethanolamine phosphate**	0.021	M1	Yes	2		1.8
C02571	**O-Acetylcarnitine**	0.033	M1	Yes	1		1.5
C00002	ATP	0.04	M1/2		4		2.1
C00036	Oxaloacetate	0.068	M2		3		1.5
NoKegg34	DL-2-Aminooctanoicacid	0.07	M1		4		1.6
C00245	**Taurine**	0.079	M1	Yes	1		1.5
C02990	[FA] O-Palmitoyl-R-carnitine	0.09	M2		1		1.6
C00299	**Uridine**	0.12	M1	Yes	3		1.8
C00106	Uracil	0.12	M1	Yes	2		2.0
24 hrs ANOVA	Name	FDR	Change	Std	Iso	MS^2	Max FC
C00669	gamma-L-Glutamyl-L-cysteine	0.015	M1	Yes	2		303.4
C01109	4-Methylene-L-glutamine	0.029	M1		2		28.9
C00085	D-Fructose 6-phosphate	0.038	M1	Yes	46		563.8
C00149	(S)-Malate	0.047	M1	Yes	4		3.2
C00327	L-Citrulline	0.058	M1	Yes	1	Yes	29.9
C02571	O-Acetylcarnitine	0.061	M2	Yes	1		3.3
C02427	L-Homocitrulline	0.076	M1		1		1284.7
C02230	3-Methylguanine	0.076	M1		5		1825.7
C00118	D-Glyceraldehyde 3-phosphate	0.081	M1		7		717.1
C03771	2 keto arginine	0.081	M2		1		3.1
C05933	N-(omega)-Hydroxyarginine	0.084	M1		2		1256.2

4.2.2.2 PCA and clustering analysis

It was immediately obvious that time of extraction had a large impact on metabolite levels as time accounted for the majority of the most significantly changed metabolites, with the magnitude of changes of these metabolites being greater between time-points when compared to those between the different conditions at each time-point. Firstly metabolites of each replicate were normalised to the median of that metabolite in the naïve macrophage for the relevant time-point (M0-normalised). While the median and mean should be the same in a normal distribution, the median is more accurate than the mean. Furthermore, with three-four replicates, it is not possible to see if a metabolite fits a normal distribution. The overall aim of this approach was to see if infecting the macrophages with either live or heat killed *Leishmania* skewed polarisation towards an M1 or M2 phenotype. Principal components analysis was conducted using MetaboAnalyst as it facilitates 3-D rotations. This was particularly useful as the first 2 components only explained a combined 43% of variation **(Figure 4-4a).**

It is apparent that replicates from the same sample groups at the earlier time-point cluster more tightly together with a larger spread obvious for some samples at the 24-hour time-point. Additionally, three of the 24-hour conditions (M1, M2 and Infected) used only three replicates. Rotating to view the third component shows that M1 macrophages are the most divergent with M2 and Infected (Live or heat-killed) showing minor separation (**Figure 4-4b**).

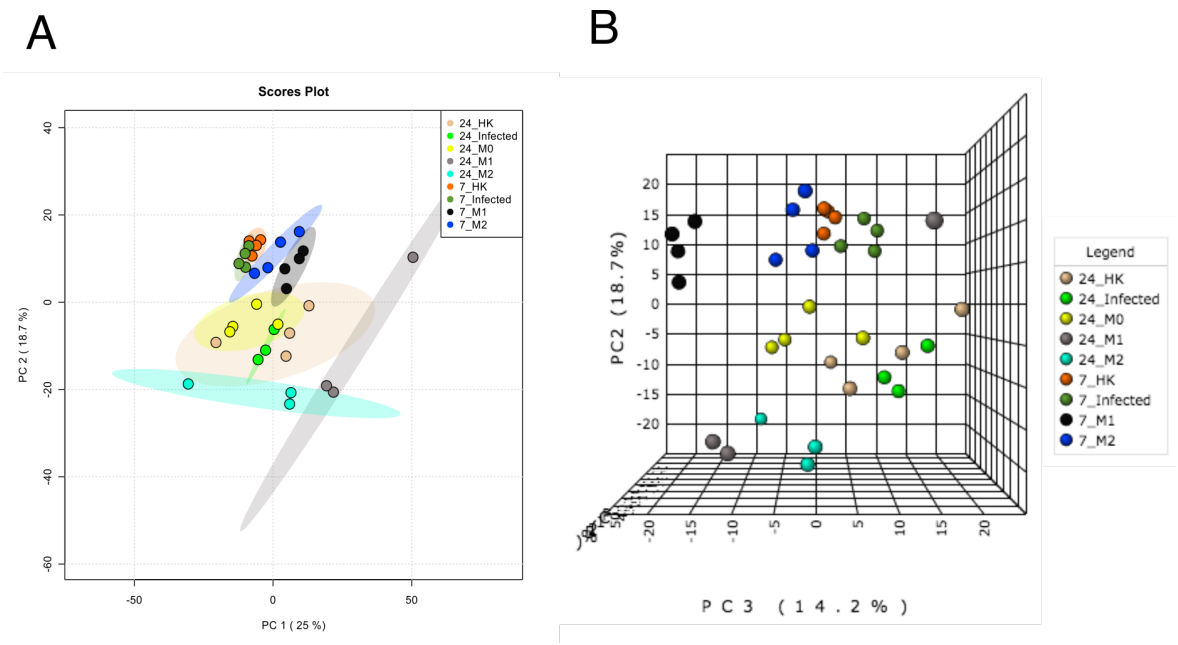

Figure 4-4: Principal components analysis (PCA) of naive, live or heat-killed parasite-infected macrophages, M1 and M2 macrophages. These results are for the experiment where samples **were not** subjected to FACS protocol. Values are M0-normalised (median) for the respective time-point. Note that M0 samples for the first time point was not included in constructing the graphs, as there was only two replicates. A: 2-D view. 95% confidence intervals are highlighted by the respective background colour. B: rotated 3D-PCA (of A) showing third component.

We next decided to conduct clustering analysis on these samples using the MetaboAnalyst clustering module to see how they separated. For this Euclidian distance measure and the Ward clustering algorithm (clustering to minimize the sum of squares of any two clusters) were used. A major factor driving clustering is time of extraction with a clear separation between time-points. For the seven-hour time-point the infected (live and heat-killed) macrophages were separate from both M1 and M2 groups. The second time-point was more variable with macrophages infected with heat-killed parasites, M2 and naive macrophages showing some overlap. While macrophages infected with live parasites seem to cluster near to the M1 samples, the variance in these groups and small number of replicates may be responsible.

As the effect of time of extraction was not removed from the data even after normalising each time-point to its respective naive control statistical analysis was conducted on each time-point separately. While time in culture is expected to have some effects, possibly due to cell death or increased cell size, alternative explanations include different efficiency of extraction at each time-point or minor variations in execution of protocol. Finally, while there are currently available resources for time-course analysis that take advantage of

linear model functions with a time factor incorporated, these require more than 2 time-points (Xia *et al*. 2015).

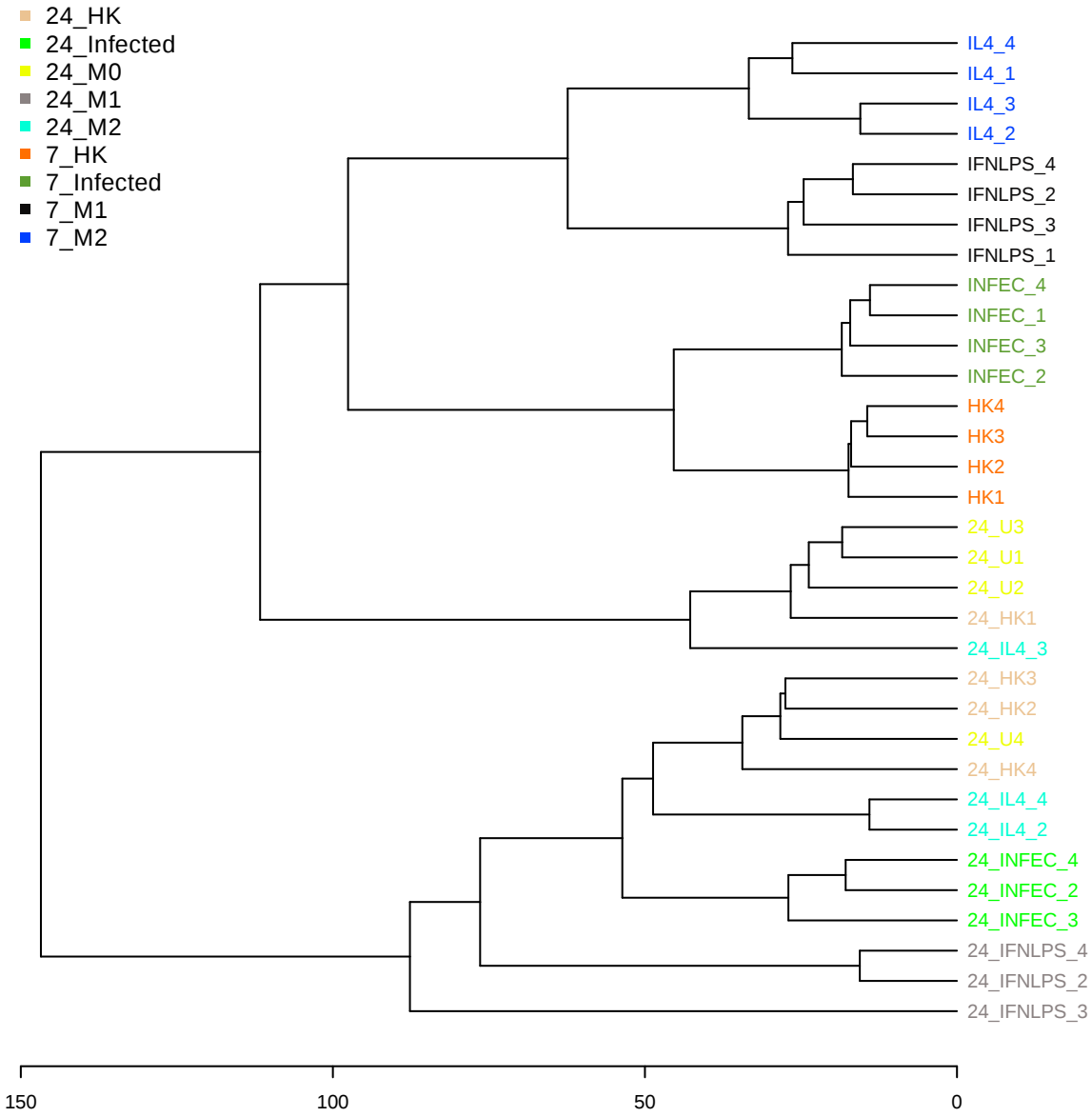

Figure 4-5: Clustering analysis of time resolved metabolome of infected, M1 and M2 macrophages. These results are for the experiment where samples **were not** subjected to FACS protocol. Values for each metabolite were normalised to the median of the M0 sample of the relevant time-point. For this analysis the two M0 samples from the 7 hours time-point are removed. The default MetaboAnalyst settings; Euclidian distance measure and Ward clustering algorithm were used. 24 hours time-point samples are as indicated, otherwise they are 7 hours.

4.2.2.3 Parasite driven changes

In agreement with PCA and clustering analysis, there were fewer significantly altered metabolites due to infection vs. M1 stimuli according to ANOVA. Some of these metabolites were only found in the infected macrophage and may be

unique to parasites **Table 4.2**; indeed several clearly were. While more changes were detected at the early time-point, this may be due to the increased variance present in the later time-point as well as there being only three replicates in the live-infection group. The magnitude of changes here was less than that detected in M1 macrophages with a maximum (of all pairwise comparisons) fold change range of 1.3-3.8 (metabolites where this is the case are indicated in column M1/2 in **Table 4.2**). Note that this is part of the analysis was presented in **Table 4-1**, but only parasite-perturbed metabolites are shown here. Thus it seems that there are fewer metabolic perturbations induced in the macrophage by parasites when compared to classical M1 stimuli. This is perhaps expected when considering the M1 stimulus used here is essentially an enriched and highly potent immunogenic component. This should be considered when investigating if the major increases and breaks in metabolic flux observed in classical model systems apply to models of infectious diseases. It is important to note that there were several MS features with no i.d. assigned that were not detected in non-infected macrophages. These could be further interrogated to see if they are novel parasite metabolites

Table 4-2: Metabolome of the infected macrophage. These results are for the experiment where samples were not subjected to FACS protocol. Significance was determined by one-way ANOVA for each time-point with Fishers LSD used for post-hoc analysis. Samples were analysed alongside M0 (for 24 hour samples only), M1 and M2 samples. As KEGG IDS are less ambiguous, the equivalent KEGG ID are in column 1. As certain metabolites are not in KEGG, arbitrary IDs are used for these. If a metabolite was altered by M1 or M2 stimuli, this is indicated in the 'M?' column. In the 'Change' column, other than parasite specific metabolites, the altered condition is indicated. Unless otherwise stated, the change is an increase. A match with an authentic standard, number of alternative isomers, match with mZCLOUD fragmentation database and maximum fold change are indicated in the last four columns. Maximum FC refers to the largest FC between any condition at the denoted time-point. In order to avoid division by zero, missing values were replaced with a value that is 25% of the intensity threshold (250). * Imidazole lactic acid: see text (4.3.2.1).

7 hrs anova	Name	FDR	M?	Change	Std	Iso	MS^n	Max FC
NoKegg41	Argininic acid	3.6E-16		Parasite	Yes	1	Yes	N/A
C03680	4-Imidazolone-5-propanoate*	4.6E-11		Parasite		4		N/A
C00408	L-Pipecolate	4.6E-11		Parasite		9		N/A
C03170	Trypanothione disulphide	6.1E-09		Parasite		1		N/A
NoKegg37	1-deoxyxylonojirimycin	1.6E-07		INF>HK		4		4.2
C00380	Cytosine	2.4E-07		INF>HK	Yes	1		4.3
NoKegg36	Ovothiol A	8.4E-05		Parasite		1		N/A
C00670	sn-glycero-3-Phosphocholine	0.00054	M1	HK>INF	Yes	1		1.5
C03771	2 keto-arginine	0.00057				1		1.9
C02728	N6-Methyl-L-lysine	0.0014		HK>INF		6		1.8
C00093	sn-Glycerol 3-phosphate	0.0018	M1	HK>INF	Yes	3		1.8
C01233	sn-glycero-3-Phosphoethanolamine	0.0018	M1	HK>INF		1		1.5
C01181	4-Trimethylammoniobutanoate	0.0043		HK>INF	Yes	4		1.3
C00588	Choline phosphate	0.0056	M1	INF>HK	Yes	1		1.9
C03916	1-Oleoylglycerophosphocholine	0.112		HK>INF		12		1.5
24 hrs anova	Name	FDR	M?	Change	Std	Iso	MS^n	Max FC
C03170	Trypanothione disulphide	0.00028		Parasite		1		N/A
NoKegg41	Argininic acid	0.0018		Parasite	Yes	1	Yes	N/A
C00408	L-Pipecolate	0.012		Parasite		9		N/A
NoKegg36	Ovothiol A	0.081		Parasite		1		N/A
C03680	4-Imidazolone-5-propanoate	0.098		Parasite		4		N/A
C00588	Choline phosphate	0.098	M2	INF>HK	Yes	1		3.8

4.2.3 Enriching the metabolic signal

In **4.2.1.2** the strategy for enriching for infected cells is outlined. According to FACs, roughly 40-45% of macrophages were infected in the experiment presented here. The presence of non-infected cells could dilute any parasite-induced alterations. Thus parasites were labelled so non-infected cells could be removed. The data presented here is not expected to be free from FACs-derived artefacts due to the prolonged time in PBS, multiple centrifugations and cell straining, and the FACs itself. To reduce this non-infected cells, as well as cells infected with live or heat-killed parasites were subjected to the same procedure.

4.2.3.1 PCA and clustering analysis

Clustering analysis and PCA was performed as described above. Again, time was a major factor in driving separation despite normalising metabolites in each replicate to the median of the M0 group for the respective time-point. Macrophages infected with either live or heat-killed parasites clustered together

with overlap for both time-points with the exception being the 24-hour time-point for macrophages infected with heat-killed parasites. Some parasite specific metabolites were present in the live or heat-killed groups at the earlier time-point but were near or below the detection limit in the heat-killed group for the 24-hour time-point. This can be explained when examining the loading plots for the PCA which shows L-argininic acid, L-pipecolic acid, 4-imidazolone-5-propanoate and ovothiol A were in the top 12 contributors to variance (data not shown). Note that an isomer of imidazolone-5-propanoate, imidazole lactic acid has been found in *Leishmania* species, and confirmed by authentic standard (Emily Armitage: *L. donovani*, personal communication) and fragmentation (MS^2 : *L. donovani, L. major* and *L. mexicana*) (Westrop *et al*. 2015) and thus may be a more likely identification. However these do not seem to be solely driving the clustering results. When these metabolites were omitted, the only major change in clustering analysis was that 24_SOR_INF (Live-infected, 24 hours) and SOR_UN_1 (M0, 7 hours) switched clades.

A

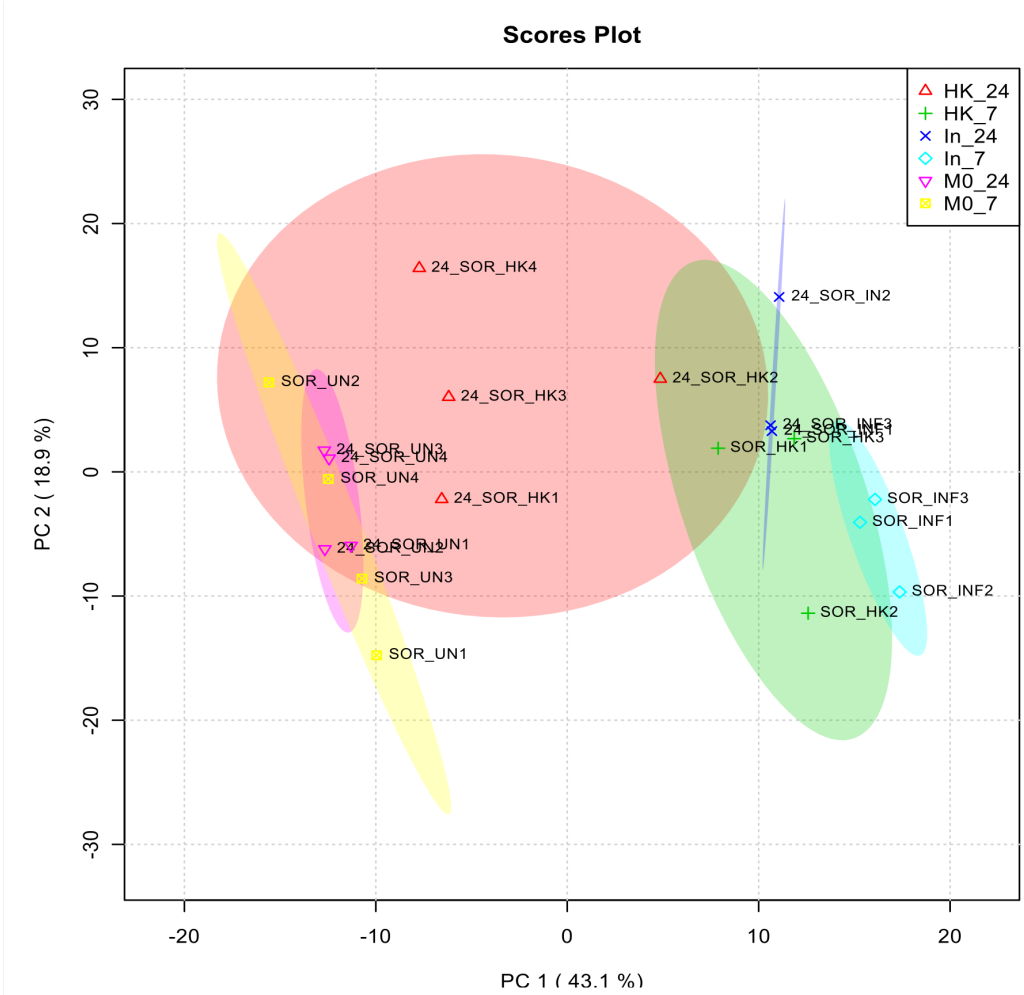
Scores Plot
HK_24
HK_7
In_24
In_7
M0_24
M0_7
24_SOR_HK4
24_SOR_IN2
SOR_UN2
24_SOR_HK2
24_SOR_HK3
24_SOR_IN3
24_SOR_IN1
SOR_HK3
SOR_HK1
24_SOR_UN3
24_SOR_UN4
SOR_UN4
SOR_INF3
24_SOR_HK1
SOR_INF1
24_SOR_UN1
24_SOR_UN2
SOR_UN3
SOR_INF2
SOR_HK2
SOR_UN1
PC 2 (18.9 %)
PC 1 (43.1 %)
30
20
10
0
-10
-20
-30
-20
-10
0
10
20

B

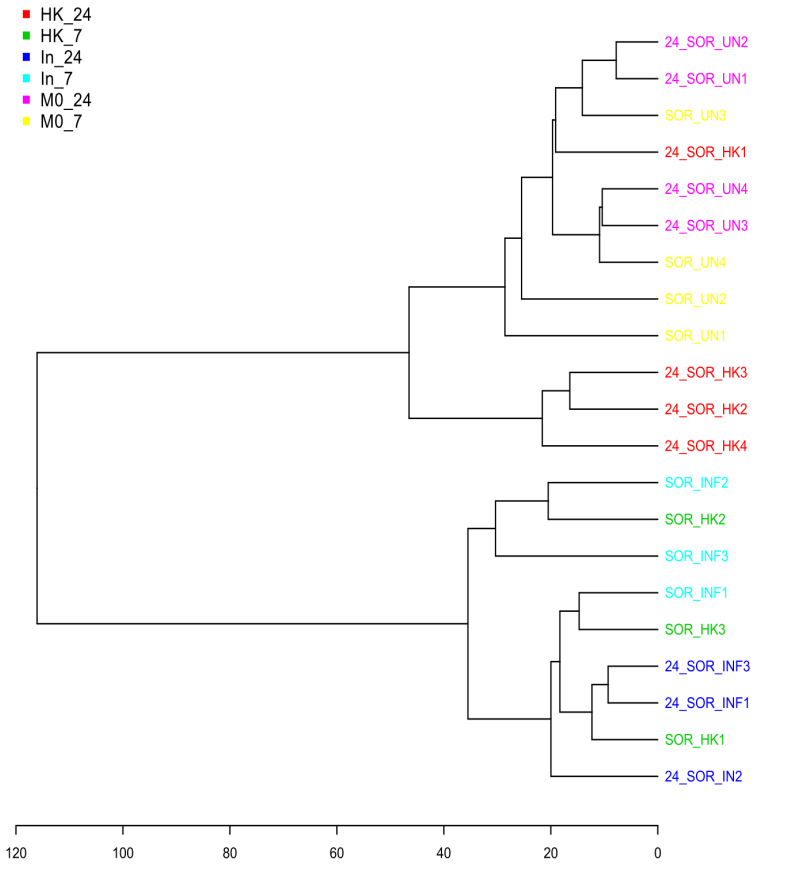
HK_24
HK_7
In_24
In_7
M0_24
M0_7
24_SOR_UN2
24_SOR_UN1
SOR_UN3
24_SOR_HK1
24_SOR_UN4
24_SOR_UN3
SOR_UN4
SOR_UN2
SOR_UN1
24_SOR_HK3
24_SOR_HK2
24_SOR_HK4
SOR_INF2
SOR_HK2
SOR_INF3
SOR_INF1
SOR_HK3
24_SOR_INF3
24_SOR_INF1
SOR_HK1
24_SOR_IN2
120
100
80
60
40
20
0

Figure 4-6: A: Principal components analysis (PCA) of naive, live or heat-killed parasite-infected macrophages that were put through our FACs protocol to enrich for infection. Values for each metabolite were normalised to the median of the M0 sample of the relevant time-point. 95% confidence intervals are highlighted by the respective background colour. B: Clustering analysis of time resolved metabolome of macrophages that were enriched for infection. The default MetaboAnalyst settings; Euclidian distance measure and Ward clustering algorithm were used here.

4.2.3.2 Data filtering and ANOVA

Data filtering was conducted as in **4.2.2.1**. The result of this filtering in IDEOM and the Xcalibur method was a list of 252 metabolites. The identity of 83 of these was confirmed using authentic standards (MSI level 1).

As above, ANOVA was performed on each time-point separately. Note that the input files for additional analysis are in **Supplementary Files 4-(5-6) (Kegg IDs are shown, metabolite name is in Supplementary File 4-4).** There were more metabolites with altered levels at both time points when compared to the non-sorted experiment. Again, some of these were only found in the infected macrophage only and may be unique to parasites (**Table 4.3).** While there are no M1 or M2 samples that were put through the FACs procedure, the M1/2 column has been added for reference (for changes also caused by M1 or M2 in **Table 4-1**). Notable for the 7-hour time-point itaconate and 4-aminobutanoate were increased in the heat-killed groups, but not with live parasites but this pattern was reversed at the second time-point.

Itaconate as mentioned previously, is a key metabolite associated with inflammation, and inhibits the glycoxylate shunt in certain bacteria as well as inhibiting the TCA cycle at the point of succinate dehydrogenase (Michelucci *et al*. 2013; Lampropoulou *et al*. 2016). 4-aminobutanoate, which is better known as GABA, is present in multiple pathways but is role in the GABA shunt has been shown to be essential for inflammatory macrophages (Tannahill *et al*. 2013). While GABA was not detected in the non-sorted samples, these samples were part of a different LC-MS run, and additionally, GABA found to be increased by IFNγ in **Chapter 3**.

In summary, these perturbations may be indicative of live parasites suppressing/failing to induce an M1 response, which, by contrast, is triggered when cells encounter heat-killed parasites. While this control has not been used in the context of metabolomics, this is in line with several previous studies

(Buchmüller-Rouiller & Mauël 1987; Banerjee *et al*. 2016). These studies found that heat-killed parasites, in contrast to the live parasites induce the respiratory burst and an inflammatory cytokine profile.

At the 24 hour time-point the macrophages infected with heat-killed parasites have increased levels of D-glyceraldehyde 3-phosphate and (S)-malate. Interestingly, (R)-2-hydroxyglutarate, which can be an incidental by-product of malate dehydrogenase activity is also increased; further supporting the presence of a perturbation in the TCA, perhaps in response to itaconate. The use of stable-isotope labelling of glucose will be required to get a better idea of what the live or heat-killed parasite does to flux through central carbon metabolism.

We next compared the results of both sorted and non-sorted experiments in order to obtain a list the most reproducible findings. A summary of this is presented in **Table 4-4**. For both time-points, and for two experimental groups that were extracted and run on the LC-MS platform at both times, parasite specific metabolites were reproducibly detected only in samples containing parasites.

It is possible that these metabolites might be present in serum samples of non-infected individuals either originating from different cell types or from the micro-biome. It will however, be interesting to see if these metabolites could potentially be used as novel biomarkers of infection. This will be explored further in **Chapter 5**. Furthermore, for other metabolites detected in both experiments, the direction/pattern of change was identical.

Table 4-3: Metabolome of the macrophage enriched for infection. Significance was determined by one-way ANOVA for each time-point with Fisher's LSD used for post-hoc analysis. As KEGG IDS are less ambiguous. The equivalent KEGG IDs are in column 1. As certain metabolites are not in KEGG, arbitrary IDs are used for these. Changes that pass the 0.05 FDR cut off have their FDR in bold. If a metabolite was altered by M1 or M2 stimuli, this is indicated in the M? column (Note that this refers to the results of a separate experiment that is summarised in Table 4-1). In the Change column, other than parasite specific metabolites, the altered condition is indicated. Unless otherwise stated, the change is an increase. A match with an authentic standard, number of alternative isomers, match with mZCLOUD fragmentation database and maximum fold change are indicated in the last four columns. Maximum FC refers to the largest FC between any condition at the denoted time-point. In order to avoid division by zero, missing values were replaced with a value that is 25% of the intensity threshold (250). * Imidazole lactic acid: see text (4.3.2.1). * means that this metabolite may be an incidental product of malate dehydrogenase activity.

7 hr	Name	FDR	M?	Change	STD	MS^2	Isomers	Max FC
Nokegg23	Argininic acid	**2.0E-11**		Parasite	Yes	Yes	1	N/A
Nokegg15	Ovothiol A	**2.0E-10**		Parasite			1	N/A
C03170	Trypanothione disulphide	**6.7E-10**		Parasite	Yes		1	N/A
C00408	L-Pipecolate	**2.1E-05**		Parasite			9	N/A
C03680	4-Imidazolone-5-propanoate*	**0.0002**		Parasite			4	N/A
C00490	Itaconate	**0.0005**	M1	HK	Yes	Yes	7	2.92
C00669	gamma-L-Glutamyl-L-cysteine	**0.0016**	M1	HK>INF>M0	Yes		2	2.69
C01233	sn-glycero-3-Phosphoethanolamine	**0.0016**	M1	HK>INF>M0			1	1.94
C00418	[FA methyl, hydroxy (5:0)] 3R-methyl-3,5-dihydroxy-pentanoic acid	**0.0024**		INF>HK>M0			14	6.08
C03274	Glycerophosphoglycerol	**0.0042**		INF>HK>M0			3	2.35
C02291	L-Cystathionine	**0.0042**		INF>HK>M0	Yes		4	N/A
C00559	Deoxyadenosine	**0.0049**		HK (lower)	Yes		4	2.03
C00334	4-Aminobutanoate	0.0076		HK	Yes		15	1.39
C00093	sn-Glycerol 3-phosphate	0.061	M1	HK	Yes		3	1.68
C01077	O-Acetyl-L-homoserine	0.062		INF and HK			10	1.53
C00670	sn-glycero-3-Phosphocholine	0.067	M1	HK	Yes		1	1.68
C00354	D-Fructose 1,6-bisphosphate	0.12	M1	HK	Yes		14	1.74
C03771	2-Keto-Arginine	0.12		HK			1	2.75
C00588	Choline phosphate	0.12	M1	INF	Yes		1	1.37

24 hr	Name	FDR	M?	Fisher's LSD	STD	MS^2	Isomers	Max FC
C03680	4-Imidazolone-5-propanoate*	**2.5E-06**		Parasite			4	N/A
C03170	Trypanothione disulphide	**2.5E-06**		Parasite	Yes		1	N/A
Nokegg23	Argininic acid	**9.1E-06**		Parasite	Yes	Yes	1	N/A
C00408	L-Pipecolate	**0.0002**		Parasite			9	N/A
C13482	Phosphodimethylethanolamine	**0.0002**		M0>INF>HK			1	1.72
C00118	D-Glyceraldehyde 3-phosphate	**0.0009**	M1	HK>M0>INF			7	1.27
C02291	L-Cystathionine	**0.0016**		INF>HK>M0	Yes		4	N/A
C00149	(S)-Malate	**0.0023**	M1	HK>M0>INF	Yes		4	1.39
C01233	sn-glycero-3-Phosphoethanolamine	**0.0023**		HK (lower)			1	1.58
C01087	(R)-2-Hydroxyglutarate	**0.0028**		HK>M0>INF	Yes		1 *	1.21
Nokegg15	Ovothiol A	**0.0048**		Parasite			1	N/A
C00093	sn-Glycerol 3-phosphate	**0.0072**		INF	Yes		3	1.63
C00900	2-Acetolactate	**0.016**		INF			16	1.23
Nokegg19	[FA dioxo(8:0)] 4,7-dioxo-octanoic acid	**0.03**		INF			4	1.44
C01210	N-Methylethanolamine phosphate	**0.03**		INF>M0>HK			3	1.64
C10660	Dictamnine	**0.03**		HK			2	1.18
C00270	N-Acetylneuraminate	**0.037**		HK (lower)	Yes		5	1.41
C06455	Hydroxymethylphosphonate	**0.045**		HK			2	1.15
C00212	Adenosine	**0.047**		HK	Yes	Yes	3	1.18
C01181	4-Trimethylammoniobutanoate	0.053		INF	Yes		6	1.43
C00670	sn-glycero-3-Phosphocholine	0.053		INF	Yes		1	1.53
C00334	4-Aminobutanoate	0.063		INF>M0>HK	Yes		15	1.43
Nokegg22	HEPES	0.063		HK (lower)	Yes		1	1.09
C03894	Propane-1,2-diol 1-phosphate	0.082		HK			2	2.44
C02728	N6-Methyl-L-lysine	0.082		INF and HK			6	1.07
C01042	N-Acetyl-L-aspartate	0.082		INF		Yes	4	1.28
C02928	2-Dehydro-D-xylonate	0.13		INF (lower)			2	1.32

Table 4-4: Summary of metabolites that were significantly altered in both sorted and non-sorted experiments. Parasite specific metabolites are underlined while glycerophospholipid metabolites perturbed in both sets are in bold. These samples were extracted separately and analyses on independent LC-MS runs. * Imidazole lactic acid: see text (4.3.2.1).

Non-sort 7h	7h common	Sort 7h	Non-sort 24h	24h common	Sort 24h
1-deoxyxylonojirimycin	Argininic acid	Itaconate	Choline phosphate	Argininic acid	D-Glyceraldehyde 3-phosphate
Cytosine	4-Imidazolone-5-propanoate*	gamma-L-Glutamyl-L-cysteine		4-Imidazolone-5-propanoate*	(S)-Malate
N6-Methyl-L-lysine	L-Pipecolate	[FA ***pentanoic acid		L-Pipecolate	(R)-2-Hydroxyglutarate*
4-Trimethyl-ammoniobutanoate	Trypanothione disulphide	Glycerophospho-glycerol		Trypanothione disulphide	2-Acetolactate
1-Oleoylglycero-phosphocholine	Ovothiol A	L-Cystathionine		Ovothiol A	L-Cystathionine
	2 Keto-Arginine	4-Aminobutanoate			4-Aminobutanoate
	sn-glycero-3-Phosphocholine	Deoxyadenosine			**sn-glycero-3-Phosphocholine**
	sn-Glycerol 3-phosphate	O-Acetyl-L-homoserine			**sn-Glycerol 3-phosphate**
	sn-glycero-3-Phosphoethanolamine	D-Fructose 1,6-bisphosphate			**sn-glycero-3-Phosphoethanolamine**
	Choline phosphate				[FA dioxo (8:0)] 4,7-dioxo-octanoic acid
					N-Methylethanolamine phosphate
					Dictamnine
					N-Acetylneuraminate
					Phosphodimethyl-ethanolamine
					Hydroxymethylphosphonate
					Adenosine
					4-Trimethyl-ammoniobutanoate
					HEPES
					Propane-1,2-diol 1-phosphate
					N6-Methyl-L-lysine
					N-Acetyl-L-aspartate
					2-Dehydro-D-xylonate

Other than parasite specific metabolites, glycerophospholipid metabolites made up the majority of significantly altered metabolites that were present in both experiments. Interestingly, these metabolites were also increased (albeit much more) in M1 macrophages. While these are not large changes (FC<2.0) it is notable that their patterns are nearly identical in both sorted and non-sorted data sets at the 7-hour time-point (**Figure 4-7**). At the 24-hour time-point, except for choline phosphate, these metabolites were slightly higher but only in

the sorted samples. Both sn-glycero-3-phosphocholine and choline phosphate have previously been reported to be increased in *L. major* infected macrophages (Lamour *et al*. 2012). Lipid metabolism will be discussed further in **4.2.5**.

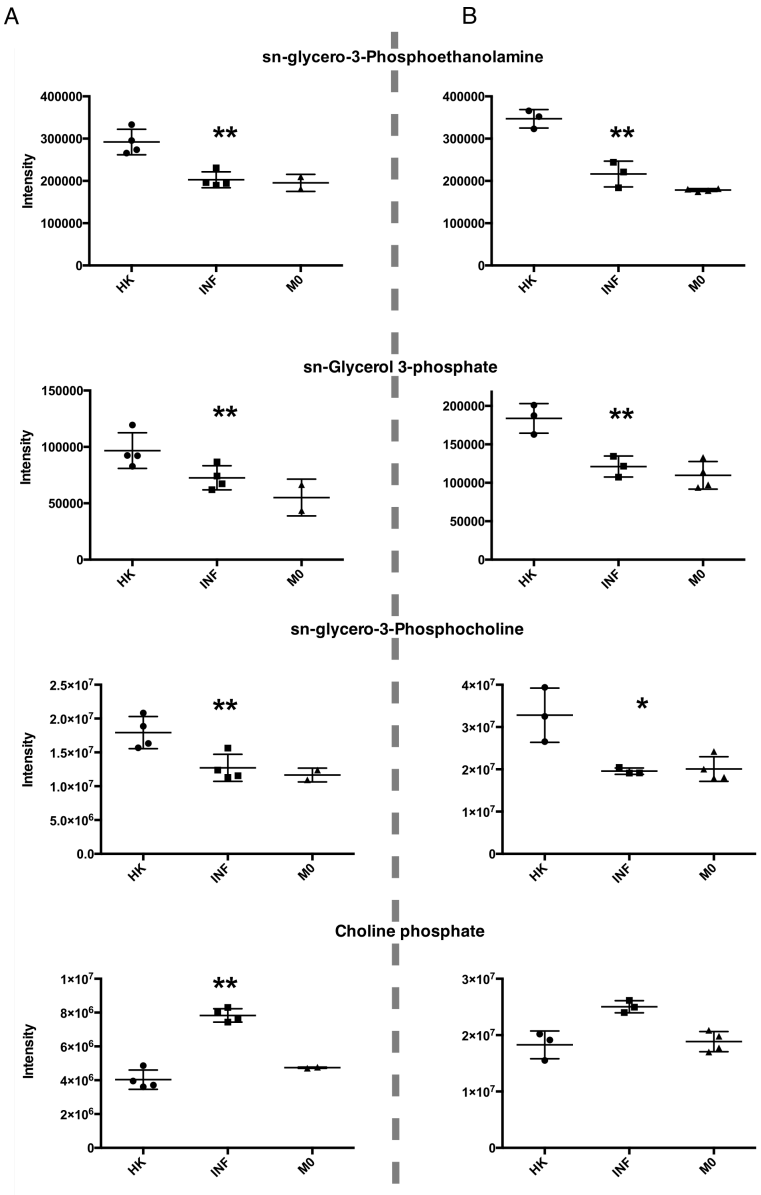

Figure 4-7: Metabolites involved in glycerophospholipid metabolism at the 7-hours time-point from A: samples not subjected to FACs protocol or B: cells subjected to FACs protocol. ** and * denotes metabolites that met the 0.05 and 0.01 FDR cut-offs respectively. Note that samples in A and B were made separately and run on independent LC-MS runs.

4.2.4 Transcriptome of infected macrophage

For differential expression analysis of transcriptomics data the DESeq2 package was used in conjunction with tool available on the Galaxy server that is hosted by Glasgow Polyomics (**2.13**). Briefly quality reports were generated on the forward and reverse fastq files by FASTQC (Andrews 2010) while alignment to the Ensemble mm10 version of the mouse genome (Aken *et al*. 2016) was carried out using HISAT2 (Kim *et al*. 2015b). The HTSeq-count Python package was used to generate raw count files (Anders *et al*. 2015). Once all these steps were completed on Galaxy (Afgan *et al*. 2016; Blankenberg *et al*. 2014), the count files were downloaded and differential analysis carried out on a local instance of DESeq2 (Love *et al*. 2014). Within DESeq2, the results function automatically performs independent filtering based on the mean of normalized counts for each gene. The idea of this is to avoid submitting genes with little or no chance of being called differentially expressed (DE) and thus set a more suitable FDR cut-off. Venny was used to classify overlap between pairwise comparisons and likelihood ratio model (LRT) (Oliveros 2015). A LRT inspects two models for the counts, a full model with a particular number of terms and a reduced model, in which some of the terms of the full model are removed. This is similar to the general linear model (GLM) used in Chapter 3 with the main difference being that a GLM uses calculation in linear regression, while the LRT implements a Negative Binomial GLM, which utilises analysis of deviance (ANODEV), where the deviance captures the difference in likelihood between a full and a reduced model.

We subsequently utilised principal components analysis (PCA) and Euclidean distance heatmap analysis to visualize the relationship between experimental datasets (**Figure 4.8**). The PCA plots demonstrated that samples from the same experimental condition grouped together demonstrating a high level of reproducibility between replicates. The main contributor to variation is infection status while the viability of the parasite contributes only 12%. The dendrograms associated with the Euclidean distance heatmaps further showed this point, with like samples clustering most closely with one another, the exception being one heat-killed infected sample.

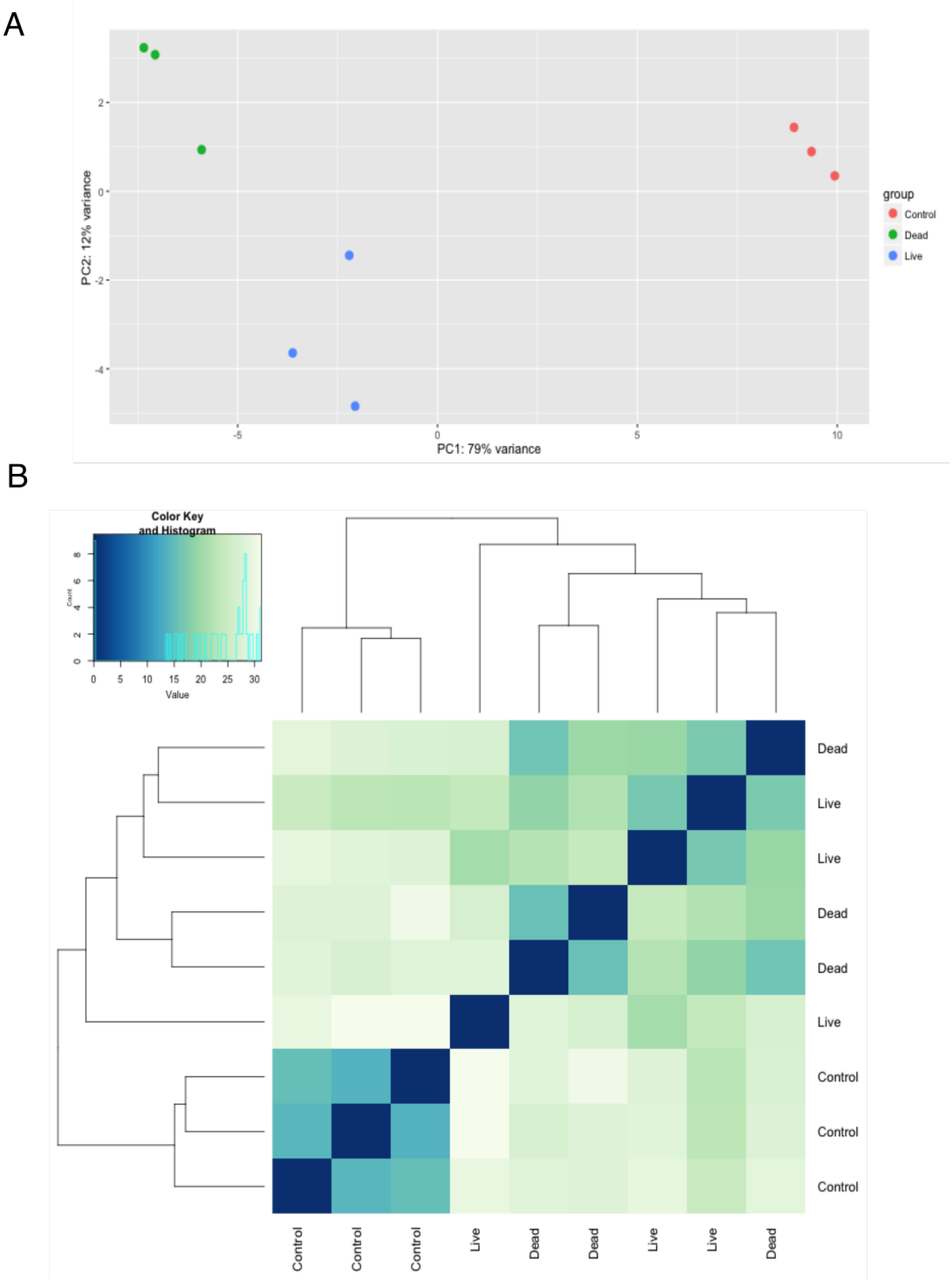

Figure 4-8: Global gene expression profiles of murine macrophages that are non-infected, infected with live or dead (heat-killed) parasites. Principal components analysis (PCA) plots (A) and heatmaps (B) of hierarchical clustering analyses on rLog transformed counts using Euclidean distance are shown. The analyses were performed using all annotated protein-coding genes following filtering for low counts. In the PCA plots, the first two principal components are shown on the X and Y-axes, respectively, with the percentage of total variance associated to that PC indicated.

Pairwise comparisons were carried out using the contrast function with a FDR cut-off of 0.05. Here a Wald test is used whereby the estimated standard error of a $\log_2$ fold change was used to test if it was equal to zero. The results of this

are summarised in **Figure 4-9:A-C**. Here the output of Plot-MA demonstrates that, within the DESeq2 pipeline, only genes with a large average normalized count contain sufficient information to be called as significant. Additionally, it supports the results of the PCA, as the majority of changes occur between the naive macrophage group and either infection group while relatively few genes are differentially expressed between the INF and HK group. To avoid false positives caused by multiple comparisons, results from the pairwise comparisons were intersected with the results for LRT (FDR cut-off of 0.05).

There were 26 genes unique to the LRT (**Supplementary Table 4-1)** so these were excluded from further analysis yielding the final groups shown in **Figure 4.9.** This resulted in a list of 4183 DE genes, which is ~87% of found DE using the various pairwise comparisons. In **Supplementary Table 4-1** these genes, the Venn subset information, Log_2 fold change, normalised counts and gene description are available.

Use of an antigen control (killed parasites) allows investigating responses that the live parasite actively suppresses or induces. For example, the subset of 365 genes in **Figure 4-9 (D-E)** could potentially be normal responses seen in response to killed parasites that are suppressed by the live parasite. Likewise the subset of 1343 could be considered to be antigen specific responses as the viability of the parasite is not important.

The subset containing 254 genes is particularly challenging as it affected by both antigen presence and parasite viability. Here the author does not attempt to differentiate between the relative contributions of each by the size of the adjusted pairwise p-values, as this would be oversimplifying cases where there is almost equal contribution. Furthermore, it would ignore the possibility that for certain pathways, there are thresholds for activation. A hypothetical example of this could be where a pathway requires a 2-fold increase of a particular enzyme for activation. If the heat-killed parasite activated a pathway by causing a 2.5 fold increase in an enzyme but the live parasite suppressed this to a 1.5-fold increase, using a binary cut-off described above would not capture this.

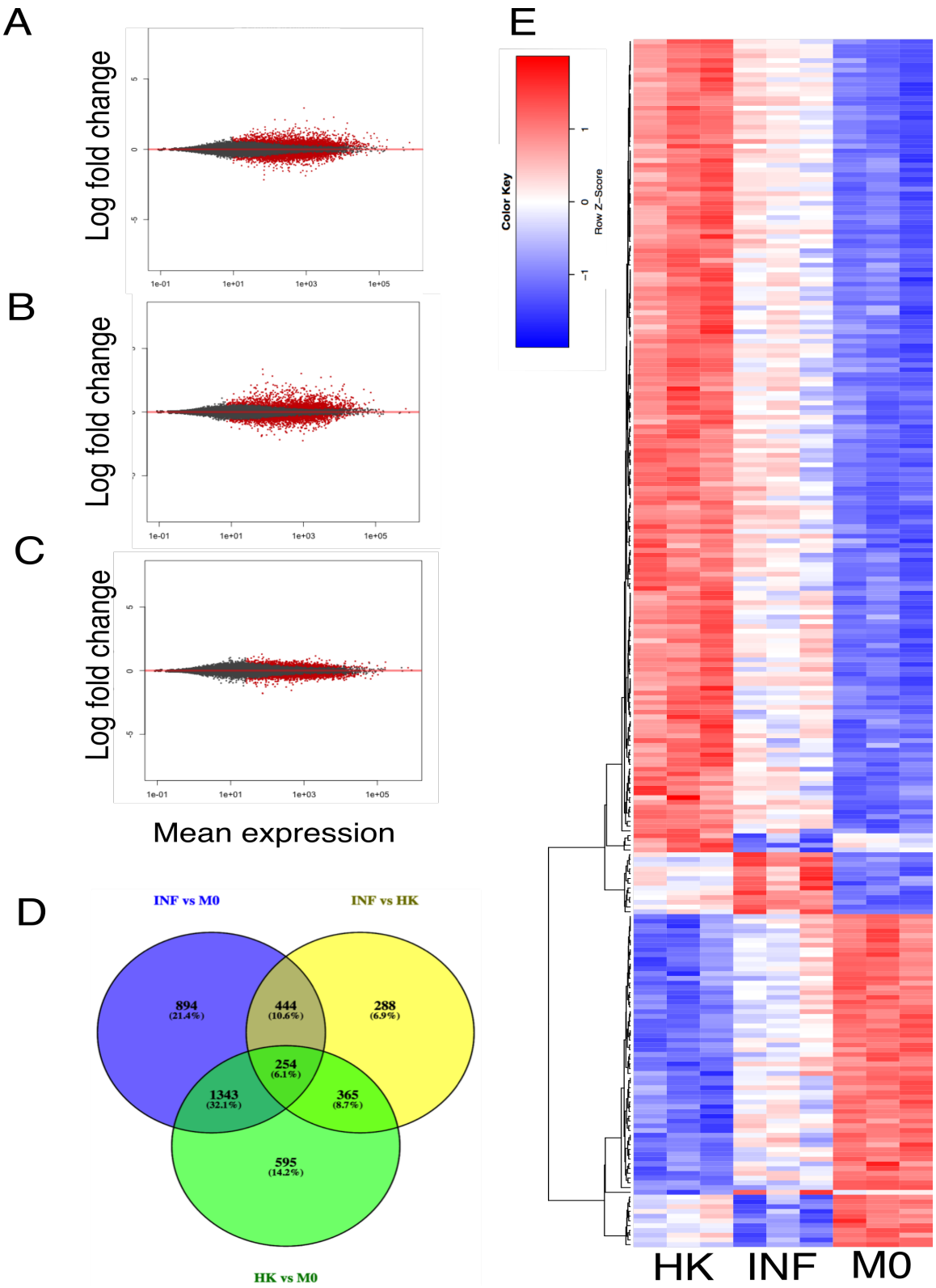

Figure 4-9: MA-Plots generated from the pairwise comparisons of A: Live infection (INF) vs M0, (B) Heat killed infection (HK) vs M0 and C: INF vs HK. These plots show the log2 fold changes from the treatment over the mean of normalized counts, i.e. the average of counts normalized by size factors. Here the points that are coloured red have an adjusted p value of less than 0.1. D: Intersect of differentially expressed genes obtained from pairwise comparisons (contrasts) that were contained in LRT Note that the 26 genes were unique to the LRT were excluded from further analysis. The Venn diagram was made with Venny (Oliveros 2015). E: Heatmap of 254 genes (normalized counts subjected to DESEQ2'S variance stabilising transformation) that are DE between all three conditions. The Heatmap was generated using Heatmap2 with hierarchal clustering method set to "average", Spearman distances and scaling used. Only rows were clustered.

In **Table 4-5** a list of genes that are DE (FC >2.15) between macrophages infected with live parasites (INF) versus macrophages infected with heat-killed parasites (HK). As some of this subset (254, 444, 365: **Figure 4-9)** were DE between INF or/and HK and Control (M0), this is denoted by the '±.' Symbol. In section **4.2.4.1** the results of this study are compared with those of (Fernandes *et al*. 2016). Genes in our study that have identical expression profiles with human orthologs in the previous study are marked by the '**§**' symbol in the $\log_2$ FC (M0) column. The human study was chosen as the authors subtracted the effect of phagocytosis by using latex beads.

Notable in the INF vs M0 subset are *Il-4*, which is upregulated by live parasites relative to the antigen control, and *Cxcl3*, the upregulation of which is inhibited by the live parasite. Other immunity related genes not shown in **Table 4-5** (these are not within fold-change cut-off selected here) include the Il-7 receptor (*Il-7r*) and *Ccrl2*, which were found to be similarly upregulated by Fernandes *et al*. While *Ccrl2* was upregulated by both *L. amazonensis* and *L. major*, only the latter upregulated *Il-7r*.

Genes related to peroxisome proliferator-activated receptors (PPAR) signalling were also strongly up regulated (*Fabp4* and *Angptl3*) with other members of the pathway down regulated (*Angptl4* and *Olr1*). PPARs are a group of nuclear receptor proteins that function as transcription factors regulating the expression of genes. They have essential roles in regulating of cellular processes such as differentiation, and metabolism (Feige *et al*. 2006).

While Fernandes *et al* found no perturbation in PPAR signalling pathway in *L. major* or *L. amazonensis* infected human macrophages either before or after subtracting the effect of phagocytosis, Dillon *et al* reported identical results for *Fabp4* and *Angptl4* in *L. major* infected murine macrophages and this difference was restricted to the 4 hour time-point (Dillon *et al*. 2015). Fernandes *et al* did observe an increase in Angptl4 at the four hours time-point in both species in contrast to the decrease seen here.

Possible explanations include the host cell type used (peritoneal versus monocyte derived) or host-species specific responses (human versus mouse). Nevertheless, *Angptl4* has previously been shown to inhibit fatty acid uptake

into mesenteric lymph node macrophages (Lichtenstein *et al*. 2010). It is interesting that the live parasite decreases the transcript of this inhibitor of fatty acid uptake relative to the heat-killed parasite as this makes sense for the intracellular stage of the parasite, which is dependent on lipid metabolism (Saunders *et al*. 2014).

Ppargc1b, which is a key member of PPAR signalling, is downregulated by the heat-killed parasite (-1.84 FC) but not by the live parasite (**Supplementary Table 4-2).** Interestingly Moreira *et al* found that live *L. infantum* increase *Ppargc1a* (albeit after 14 hours infection) but not *Ppargc1b* relative to their irradiated control. While the current study does not have later time-points, Dillon *et al* did not detect perturbations to *Ppargc1a* at any time-point. This may be due to differences between parasite species. Nevertheless, PPAR signalling and downstream, related pathways were found perturbed in our pathway analysis (**4.2.4.2**). These perturbations and how they might be linked with the alterations that were detected in glycerolipid and glycerophospholipid metabolisms are discussed in more detail later in this chapter.

Table 4-5: Top DE genes that are antigen-independent. The FC threshold is >2.15. The FC presented are expression levels from live parasites infected macrophages (INF) either relative to heat-killed infected cells (Log_2 FC (HK)) or to non-infected cells (Log_2 FC (M0)). The adjusted p value (p.adjust) is from the LRT If INF or HK was DE from M0, this is also indicated by "±" in the 'Other FC'. Genes displaying the same expression pattern as reported in Fernandes *et al* is denoted by ** (see 4.2.4.1).

ENSEMBLE ID	Description	Name	log_2 FC (HK)	padj	log_2 FC (M0)	Other FC
ENSMUSG00000022469	Rap guanine nucleotide exchange factor (GEF) 3	*Rapgef3*	1.86	5.4E-06	1.12	±
ENSMUSG00000000869	interleukin 4	*Il4*	1.62	1.9E-04	0.39	
ENSMUSG00000019845	epsilon-tubulin 1	*Tube1*	1.55	6.7E-03	0.21	
ENSMUSG00000062470	F-box and leucine-rich repeat protein 12, opposite strand	*Fbxl12os*	1.51	4.3E-03	0.95	
ENSMUSG00000028496	myeloid/lymphoid or mixed-lineage leukemia; translocated to 3	*Mllt3*	1.43	3.1E-04	0.49	
ENSMUSG00000089665	Foxo1 corepressor	*Fcor*	1.33	4.7E-02	0.23	
ENSMUSG00000062515	fatty acid binding protein 4, adipocyte	*Fabp4*	1.21	3.1E-41	1.57	±
ENSMUSG00000028553	angiopoietin-like 3	*Angptl3*	1.12	1.1E-02	0.89	±
ENSMUSG00000032014	out at first homolog	*Oaf*	-1.18	2.8E-17	0.45	HK>Inf>M0
ENSMUSG00000048537	pleckstrin homology like domain, family B, member 1	*Phldb1*	-1.21	6.9E-35	0.92 §	HK>Inf>M0*
ENSMUSG00000026475	regulator of G-protein signalling 16	*Rgs16*	-1.23	1.5E-06	0.29	HK up
ENSMUSG00000027962	vascular cell adhesion molecule 1	*Vcam1*	-1.24	8.4E-08	0.83	HK up
ENSMUSG00000054675	transmembrane protein 119	*Tmem119*	-1.26	3.9E-07	-0.68	±
ENSMUSG00000032420	5' nucleotidase, ecto	*Nt5e*	-1.27	2.4E-02	-0.40	
ENSMUSG00000029379	chemokine (C-X-C motif) ligand 3	*Cxcl3*	-1.29	1.3E-12	1.57 §	HK>Inf>M0±
ENSMUSG00000002289	angiopoietin-like 4	*Angptl4*	-1.30	3.6E-03	-0.56	
ENSMUSG00000060639	histone cluster 1, H4i	*Hist1h4i*	-1.31	1.4E-15	0.88	HK up±
ENSMUSG00000029287	transforming growth factor, beta receptor III	*Tgfbr3*	-1.36	2.0E-02	-0.68	
ENSMUSG00000024912	fos-like antigen 1	*Fosl1*	-1.39	4.1E-23	1.67 §	HK>Inf>M0±
ENSMUSG00000032724	ankyrin repeat and BTB (POZ) domain containing 2	*Abtb2*	-1.42	1.5E-14	0.97 §	HK>Inf>M0±
ENSMUSG00000021806	nidogen 2	*Nid2*	-1.43	7.6E-03	-0.32	
ENSMUSG00000030162	oxidized low density lipoprotein (lectin-like) receptor 1	*Olr1*	-1.48	1.5E-31	1.17 §	HK>Inf>M0±
ENSMUSG00000090877	heat shock protein 1B	*Hspa1b*	-1.49	4.8E-09	0.69	HK up
ENSMUSG00000091971	heat shock protein 1A	*Hspa1a*	-1.50	3.1E-26	1.31	HK>Inf>M0±
ENSMUSG00000003545	FBJ osteosarcoma oncogene B	*Fosb*	-1.50	3.3E-22	1.07 §	HK>Inf>M0±
ENSMUSG00000003070	ephrin A2	*Efna2*	-1.71	2.4E-15	1.56	HK>Inf>M0±
ENSMUSG00000038418	early growth response 1	*Egr1*	-1.74	2.0E-23	-0.29	
ENSMUSG00000041481	serine (or cysteine) peptidase inhibitor, clade A, member 3G	*Serpina3g*	-1.96	2.1E-03	-0.42	
ENSMUSG00000032487	prostaglandin-endoperoxide synthase 2	*Ptgs2*	-2.28	3.3E-34	2.07 §	HK>Inf>M0±
ENSMUSG00000022602	activity regulated cytoskeletal-associated protein	*Arc***	-2.30	8.0E-40	3.73 §	HK>Inf>M0±

In **Table 4-6** genes that are DE between macrophages infected with either live (INF) vs. heat-killed parasites (HK) or INF vs. M0 with a FC >3.2 are presented. As in **Table 4-5,** genes in our study that have similar expression profiles with human orthologs in the previous study are marked by a § in the $\log_2$ FC (M0) column. This set is specific to effects of infection that are independent to parasite viability. The *Slc7a11* transporter was one of the most upregulated genes in this study. *Slc7a11* is a cystine-glutamate antiporter that couples the uptake of one molecule of cystine with the release of one molecule of glutamate. Related to this, GABA was increased in samples infected with heat-killed parasites, but was higher in the samples containing live parasites at the later time-point. The increase of this transcript has been reported to be essential for T-cell proliferation (Levring *et al*. 2012), but has not been investigated in the context of macrophage activation or infection.

Interestingly, the anti-inflammatory interleukin 1 receptor antagonist *Il1rn* is upregulated. Both of these results are in agreement with the results from *Dillon et al* where this change was restricted to an early time-point (Dillon *et al*. 2015). This was also found to be the case in *L. amazonensis* and L. *major* infected human macrophages (Fernandes *et al*. 2016). Reports on the role for IL-1 in leishmaniasis have pointed to a negative contribution by this inflammatory cytokine. In the murine model (susceptible model: Balb/C) of *L. major* infection, IL-1 (α or ß) caused earlier disease progression, while a negative association for IL-1ß with disease severity caused by *L. mexicana* has also been reported (Voronov *et al*. 2010; Fernández-Figueroa *et al*. 2012). The mechanisms of how *Leishmania* eventually supresses Il1rn, remains to be determined.

Inflammatory chemokines such as *Ccl3*, *4* and *5*, *Cxcl1* and *16* were among other notable upregulated immunomodulatory mediators that are typical of a general inflammatory response while *IL-4* and *IL-6* receptors, *IL-16*, chemokines *Ccl7* and chemokine receptor *Cxcr3* were down regulated (these are not within fold-change cut-off selected here). Arginase (*Arg2*) was upregulated in infected macrophages. Of all these *Cxcl1* and *Il-6* showed similar expression profiles in infected human macrophages.

Table 4-6: Top DE genes that are antigen-dependent. The FC threshold is >3.2. The FC presented are expression levels from live parasites infected macrophages (INF) relative to non-infected cells (Log2 FC (M0)). The adjusted p value (p.adjust) is from the LRT. Genes displaying the same expression pattern as reported in Fernandes *et al* is denoted by "§" in the 'Log2 FC (M0)' column (see 4.2.4.1).

ENSEMBLE ID	Description	Name	padj	log_2 FC M0
ENSMUSG00000019817	pleiomorphic adenoma gene-like 1	*Plagl1*	1.0E-05	3.98 §
ENSMUSG00000027737	solute carrier family 7 (cationic amino acid transporter, y+ system), member 11	*Slc7a11*	3.2E-94	3.23 §
ENSMUSG00000048329	major facilitator superfamily domain containing 6-like	*Mfsd6l*	8.5E-04	2.83 §
ENSMUSG00000109864	EP300 interacting inhibitor of differentiation 3	*Eid3*	2.1E-12	2.45 §
ENSMUSG00000028517	phospholipid phosphatase 3	*Plpp3*	3.6E-37	2.40
ENSMUSG00000034472	RASD family, member 2	*Rasd2*	2.4E-05	2.40
ENSMUSG00000038508	growth differentiation factor 15	*Gdf15*	2.0E-33	2.29
ENSMUSG00000048108	transmembrane protein 72	*Tmem72*	1.1E-07	2.26
ENSMUSG00000021997	leucine rich repeat containing 63	*Lrrc63*	1.3E-02	2.20
ENSMUSG00000027313	ChaC, cation transport regulator 1	*Chac1*	2.8E-04	2.06
ENSMUSG00000002100	myosin binding protein C, cardiac	*Mybpc3*	1.4E-03	2.04
ENSMUSG00000026981	interleukin 1 receptor antagonist	*Il1rn*	3.1E-29	2.04 §
ENSMUSG00000030142	C-type lectin domain family 4, member e	*Clec4e*	9.6E-47	2.03
ENSMUSG00000037887	dual specificity phosphatase 8	*Dusp8*	2.8E-10	1.95 §
ENSMUSG00000020178	adenosine A2a receptor	*Adora2a*	2.0E-03	1.94
ENSMUSG00000074647	family with sequence similarity 83, member C	*Fam83c*	7.9E-08	1.93
ENSMUSG00000102037	B cell leukemia/lymphoma 2 related protein A1a	*Bcl2a1a*	2.0E-09	1.90
ENSMUSG00000040329	interleukin 7	*Il7*	2.6E-03	1.90 §
ENSMUSG00000024334	histocompatibility 2, O region alpha locus	*H2-Oa*	2.2E-03	1.89
ENSMUSG00000026873	PHD finger protein 19	*Phf19*	4.7E-03	1.86
ENSMUSG00000039646	vasorin	*Vasn*	1.4E-04	1.85
ENSMUSG00000024486	heparin-binding EGF-like growth factor	*Hbegf*	4.3E-07	1.78 §
ENSMUSG00000024014	proviral integration site 1	*Pim1*	1.4E-25	1.78 §
ENSMUSG00000028214	GTP binding protein (gene overexpressed in skeletal muscle)	*Gem*	2.5E-10	1.75 §
ENSMUSG00000000730	DNA (cytosine-5-)-methyltransferase 3-like	*Dnmt3l*	1.1E-04	1.75
ENSMUSG00000022534	Mediterranean fever	*Mefv*	5.2E-18	1.72
ENSMUSG00000034842	ADP-ribosyltransferase 3	*Art3*	2.0E-02	1.68
ENSMUSG00000051043	G protein-coupled receptor, family C, group 5, member C	*Gprc5c*	1.3E-23	-1.71
ENSMUSG00000055782	ATP-binding cassette, sub-family D (ALD), member 2	*Abcd2*	2.8E-36	-1.72
ENSMUSG00000020669	Sh3 domain YSC-like 1	*Sh3yl1*	3.6E-02	-1.83
ENSMUSG00000067199	frequently rearranged in advanced T cell lymphomas	*Frat1*	1.3E-16	-1.90 §
ENSMUSG00000056476	mediator complex subunit 12-like	*Med12l*	3.3E-06	-2.22
ENSMUSG00000054850	small integral membrane protein 10 like 2A	*Smim10l2*	1.8E-02	-2.27
ENSMUSG00000039783	kynurenine 3-monooxygenase (kynurenine 3-hydroxylase)	*Kmo*	1.8E-05	-2.57

4.2.4.1 Comparison with previous studies

Two recent studies carried out RNAseq of *Leishmania* infected macrophages at a similar time-point to us (Dillon *et al*. 2015; Fernandes *et al*. 2016). In the first study, *L. major* infection of murine macrophages was tracked over several time-points. In the second study, *L. major* and *L. amazonensis* infected human

macrophages as well as an additional phagocytic control were traced. Additionally, the authors composed a list of human genes that were DE after subtracting the phagocytosis effect and had a corresponding DE mouse orthologs. This list is comprised of ~50% of total murine DE genes. The list of all DE genes from the LRT were compared with DE genes that Fernandes *et al* subtracted the effect of phagocytosis from.

To this end, our list of DE genes was converted to human orthologs on Biomart (Durinck *et al*. 2009), obtaining 3613 hits that compared with DE genes from Fernandes *et al*. (**Figure 4-10, Supplementary Table 4-3**). 32% of our DE genes overlapped with either *L. amazonensis* or *L. major* DE genes or 20% to *L. amazonensis*. Note that **Figure 4-10 does not** state that these genes are DE between species IE while the 945 genes and 233 genes unique to *L. major* and *L. amazonensis* are DE relative to the naïve macrophage; they are not DE to each other. Fernandes *et al* conducted separate analysis between *L. major* and *L. amazonensis* and found only four genes to be DE (4hours post infection only). Interestingly 8 of the 30 genes most DE due to the live parasite and 10 of the 34 genes most DE due to infection, were among this set, having an identical FC directionality.

Next a Hypergeometric distribution test was used to check if overlap in **Figure 4-10** was random. This distribution is typically associated with urn models, i.e. there are n balls in an urn, y are painted red, and m balls are drawn from the urn. Then if X is the number of balls in sample of m that are red, X has a hyper-geometric distribution. Essentially n_A, denote DE genes from this study (*L. mexicana*), n_B denote DE genes from Fernandes *et al* (*L. major* or *L. amazonensis*), n_C denote the total number of genes (24850 genes in the *mm10* Ensemble genome), and n_{AB} denotes the overlap between AA and B. Then

$$n_{AB} \sim HG(n_A, n_C, n_B)$$

This was implemented in R using the following code:

```
n_Mex = 3613;n_Major = 3118; n_Transcriptome = 24850; n_Mex_Major = 1062
phyper(n_Mex_Major - 1, n_Mex, n_Transcriptome-n_Mex, n_Major, lower.tail = FALSE)
n_Mex = 3613;n_Amaz = 2057; n_Transcriptome = 24850; n_Mex_Amaz = 713
phyper(n_Mex_Amaz - 1, n_Mex, n_Transcriptome-n_Amaz, n_Amaz, lower.tail = FALSE)
```

For *L. mexicana vs. L. major* or *L. mexican*a vs. *L. amazonensis* the p values were 5.4e-195 and 3.4e-142 respectively, which is highly significant.

Furthermore, when repeating the above using 14402 as the 'transcriptome' that contains orthologs mapping one to one between mouse and human, the results were still significant. (1.97e-37; vs. *L. major*, 5.6e-41; vs. *L. amazonensis*).

Note that Fernandes *et al* accounted for phagocytosis, by contrasting infected samples to both bead-containing macrophages and uninfected control cells. Subsequently, for each gene, the authors selected the maximum p-value from these two contrasts for input into the BH multiple-testing adjustment. This selection process does not allow the prediction of appropriate responses that the parasite might suppress to some extent. Additionally, these differences may be due to the fact a different species of parasite was used (we used *L. mexicana*) or that their control was phagocytic while ours was antigenic).

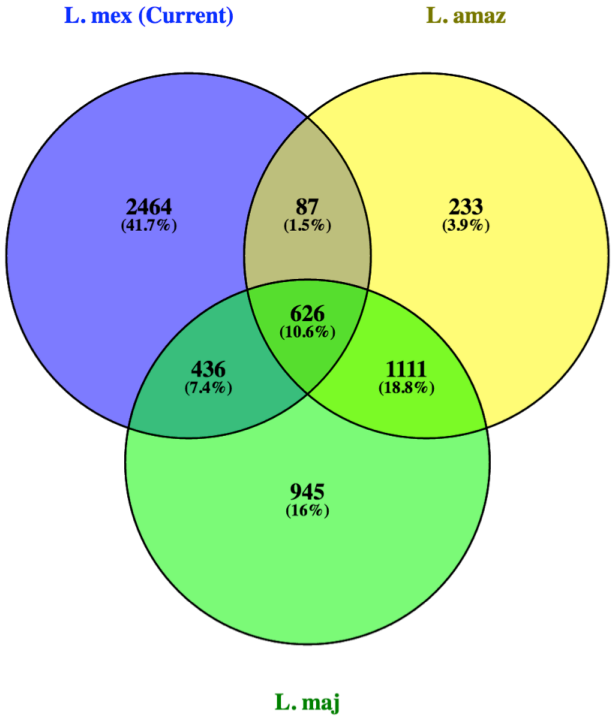

Figure 4-10: Comparison of DE genes from current study compared to DE genes (after accounting for phagocytosis) from Fernandes *et al*. The time-point in question from the latter study was 4 hours post infection. Note that Figure 4-9 does not state that these genes are DE between species IE while the 945 genes and 233 genes unique to *L. major* and *L. amazonensis* are DE relative to the naïve macrophage; they are not DE to each other. Venny was used to make diagram (Oliveros 2015).

4.2.4.2 Pathway analysis

For pathway analysis the aim was to differentiate between general immune responses to antigen and those induced by the live parasite. To this end DE genes from the three pairwise comparisons were analysed (**Figure 4-9**). Some of the resulting DE genes were pseudo/predicted, had no gene description, coded

for micro, small nucleolar or mitochondrial RNAs. While these are potentially interesting, they were filtered out prior to further analysis. Additionally, the library prep used was not designed to target these classes (there are custom library preparation for them), so coverage or bias could be an issue. Furthermore, this was necessary as many pathway analyses tools convert input to ENTREZ gene formatting. The conversion of ENSEMBLE (used here) to ENTREZ is not straightforward with each type having unique hits as well as some genes mapping to multiple loci, thus preventing one to one conversions. Pathway analyses tools do not accept datasets with a high percentage of non-ENTREZ mapping genes. Thus our filtering allowed us to lower non-mapping to a level permissible by analysis tools. This led to a reduction of DE genes from 4209 to 3729. Pathway analysis was carried out using Graphite using the *Mus musculus*, species and KEGG pathways (Sales *et al*. 2013).

Graphite Web also allows incorporation of Log_2 fold change values as well as allowing the user to supply a background (all genes detected by the platform) and a list of DE genes. This is particularly important when one considers that different types of mammalian cell have different expression profiles, with certain genes unique to a single cell type. In this instance the background was a list of genes that had at least one condition that contained two samples with a non-zero number of reads. When considering the coverage of RNAseq, it is reasonable to assume that this background is well representative of the subset of the transcriptome that is utilised by macrophages. As described above, entries that were pseudo/predicted, had no gene description, coded for micro, small nucleolar or mitochondrial RNAs were filtered as above. Note that an arbitrary LFC threshold was not set as this tended to lead to a bias towards genes with low read counts.

There are several options available in Graphite that allows the user to supply a list of pre-calculated DE genes alongside a platform background. These are the Hypergeometric test (used in **4.2.4.1**), and Signalling Pathway Impact Analysis (SPIA). Here the Hypergeometric test (used above) generates an estimate of the chance probability of observing a given number of genes from a pathway among the pre-selected differentially expressed genes. SPIA encapsulates key aspects of the data combining the fold change of the DE genes, the pathway enrichment and the topology of pathways (Tarca *et al*. 2009). Specifically, SPIA first

computes the Hypergeometric enrichment p-values (pND). As well as this, SPIA computes a perturbation factor as a linear function of the perturbation factors of all genes in a given pathway, whose significance is calculated through a bootstrap approach, pPERT. The combination of the two independent p-values (pNDE and pPERT) yields pG. Finally, pGs are then adjusted for multiple testing using either the false discovery rate (FDR) algorithm (pGFdr).

Our method of choice was SPIA as it takes into account all supplied information and not only lists effected pathways, but also predicts the nature of the impact, i.e. is it activation or inhibition? The database options available were the KEGG and Reactome databases. These databases contain pathway information that is bases on experimental work. For example, the Leishmaniasis KEGG pathway highlights genes and interactions (and relevant citations) that are associated with various species of *Leishmania*, some of which are mentioned in the introduction (i.e. gp63 protease). The results of this are presented in **Table 4-7** (detailed results is available in **Supplementary Table 4-4)**. Here the results contain hits with a minimum (pGFdr<0.1). The first column (INF) shows what happens in macrophages infected with live parasite in comparison to naïve macrophages. The second column (HK) shows what happens in macrophages infected with heat-killed parasites in comparison to naïve macrophages. The third column (LIVE) shows what happens in macrophages infected with live parasites in comparison to macrophages infected with heat-killed parasites.

It is important to state that while the live parasite might either increase or decrease pathway activation or inhibition relative to the heat killed parasite, this does not mean that it is sufficient to cancel out or reverse its affect (see KEGG: NF-kappa B signalling pathway for such an example).

Table 4-7: SPIA analysis of *L. mexicana* infected macrophages. INF refers to DE genes in the pairwise comparison of macrophages infected with live parasites versus non-infected macrophages. HK refers to DE genes from pairwise comparison of macrophages infected with heat-killed parasites versus non-infected macrophages. LIVE refers to DE genes from pairwise comparison of macrophages infected with live parasites versus heat killed parasites macrophages. The colour key is red for inhibition, green for activation and grey for either not detected at false discovery rate (FDR) algorithm (pGFdr)<0.1. Note that R-HSA-163200 (Respiratory electron transport, ATP synthesis by chemiosmotic coupling, and heat production by uncoupling proteins), R-HSA-174178 (APC/C:Cdh1 mediated degradation of Cdc20 and other APC/C:Cdh1 targeted proteins in late mitosis/early G1) and R-HSA-72662 (Activation of the mRNA upon binding of the cap-binding complex and eIFs, and subsequent binding to 43S) are stable REACTOME IDS used for the sake of abbreviation.


KEGG
INF
HK
LIVE
Insulin signaling pathway
Neurotrophin signaling pathway
p53 signaling pathway
Viral myocarditis
Jak-STAT signaling pathway
Transcriptional misregulation in cancer
Antigen processing and presentation
Alzheimer's disease
NOD-like receptor signaling pathway
Prostate cancer
Type II diabetes mellitus
T cell receptor signaling pathway
Notch signaling pathway
GnRH signaling pathway
Vascular smooth muscle contraction
PPAR signaling pathway
Measles
B cell receptor signaling pathway
Chagas disease (American trypanosomiasis)
Leishmaniasis
NF-kappa B signaling pathway
Toll-like receptor signaling pathway
Epstein-Barr virus infection
Osteoclast differentiation
Toxoplasmosis
Adipocytokine signaling pathway
Herpes simplex infection
Hepatitis B
Cell adhesion molecules (CAMs)
Apoptosis
Legionellosis
HIF-1 signaling pathway
Influenza A
Small cell lung cancer
Glioma
Hepatitis C
Melanoma
Chronic myeloid leukemia
Cell cycle
Bacterial invasion of epithelial cells
Colorectal cancer
Leukocyte transendothelial migration
Cholinergic synapse
Salmonella infection
REACTOME
INF
HK
LIVE
R-HSA-163200
Respiratory electron transport
M/G1 Transition
DNA Replication Pre-Initiation
SCF(Skp2)-mediated degradation of p27/p21
Regulation of activated PAK-2p34 by proteasome mediated degradation
Ubiquitin-dependent degradation of Cyclin D
Ubiquitin-dependent degradation of Cyclin D1
Signaling by Wnt
CDK-mediated phosphorylation and removal of Cdc6
p53-Dependent G1/S DNA damage checkpoint
Regulation of ornithine decarboxylase (ODC)
SCF-beta-TrCP mediated degradation of Emi1
Stabilization of p53
Degradation of beta-catenin by the destruction complex
Autodegradation of the E3 ubiquitin ligase COP1
p53-Dependent G1 DNA Damage Response
Autodegradation of Cdh1 by Cdh1:APC/C
CDT1 association with the CDC6:ORC:origin complex
APC/C:Cdc20 mediated degradation of Securin
APC/C:Cdc20 mediated degradation of mitotic proteins
Assembly of the pre-replicative complex
Destabilization of mRNA by AUF1 (hnRNP D0)
Activation of APC/C and APC/C:Cdc20 mediated degradation of mitotic proteins
p53-Independent DNA Damage Response
p53-Independent G1/S DNA damage checkpoint
Ubiquitin Mediated Degradation of Phosphorylated Cdc25A
R-HSA-174178
Cdc20:Phospho-APC/C mediated degradation of Cyclin A
Regulation of APC/C activators between G1/S and early anaphase
S Phase
APC/C-mediated degradation of cell cycle proteins
Regulation of mitotic cell cycle
Mitotic G1-G1/S phases
G1/S Transition
Cyclin D associated events in G1
G1 Phase
Eukaryotic Translation Elongation
Peptide chain elongation
GTP hydrolysis and joining of the 60S ribosomal subunit
Nonsense-Mediated Decay
Nonsense Mediated Decay Enhanced by the Exon Junction Complex
Cap-dependent Translation Initiation
Eukaryotic Translation Initiation
The citric acid (TCA) cycle and respiratory electron transport
R-HSA-72662
Meiosis
Interferon Signaling
Meiotic Recombination
Interferon gamma signaling
Interleukin-1 signaling
RNA Polymerase I Transcription
RNA Polymerase I Promoter Opening
RNA Polymerase I, RNA Polymerase III, and Mitochondrial Transcription
RNA Polymerase I Promoter Clearance
Telomere Maintenance
MAP kinase activation in TLR cascade
Signaling by Robo receptor
MAPK targets/ Nuclear events mediated by MAP kinases
Nuclear Events (kinase and transcription factor activation)
Glucose metabolism
PPARA Activates Gene Expression

Note that as there was varying numbers of DE genes in each set (2935 in INF, 2557 in HK and in 1351 LIVE) and this will have some consequence as well. Fernandes *et al* used a Hypergeometric test separately on genes either upregulated or down regulated by the parasite (and independent of phagocytosis) (Fernandes *et al*. 2016). This approach was not taken as it would not connect cases where down-regulation of inhibitors of pathways with the upregulation of activators. Fernandes *et al* restricted their pathway analysis to genes that were DE due to *L. major* infection and had mouse orthologs. Nevertheless, as reported by Fernandes *et al*, there is upregulation/activation of NF-kappa B signalling pathway, and Toll-like receptor signalling pathways. Interestingly, while induced by both the live and heat-killed parasite, the former does this to a significantly lesser extent. There were no down-regulated pathways in our study in common with Fernandes *et al*.

Inflammatory macrophages are reported to upregulate glycolysis and down regulate mitochondrial respiration. When taking this into consideration, it is notable in the Reactome section that the live parasites activate the TCA cycle and within it the respiratory electron response while heat killed parasites upregulate glucose metabolism. This would suggest that even at an early time-point the live parasite, unlike its “antigen” equivalent, polarises macrophages away from an inflammatory phenotype. As immune-metabolism is a relatively new field and as such is absent from databases, this was explored in more detail (**Figure 4-11**). The inset image in **Figure 4-11 (a)** shows the Reactome map of TCA related pathways. The example highlighted is cytochrome complex somatic (*cycs*) that is upregulated by the parasite. As *cycs* is an essential part the electron transport chain it is assigned a high impact score.

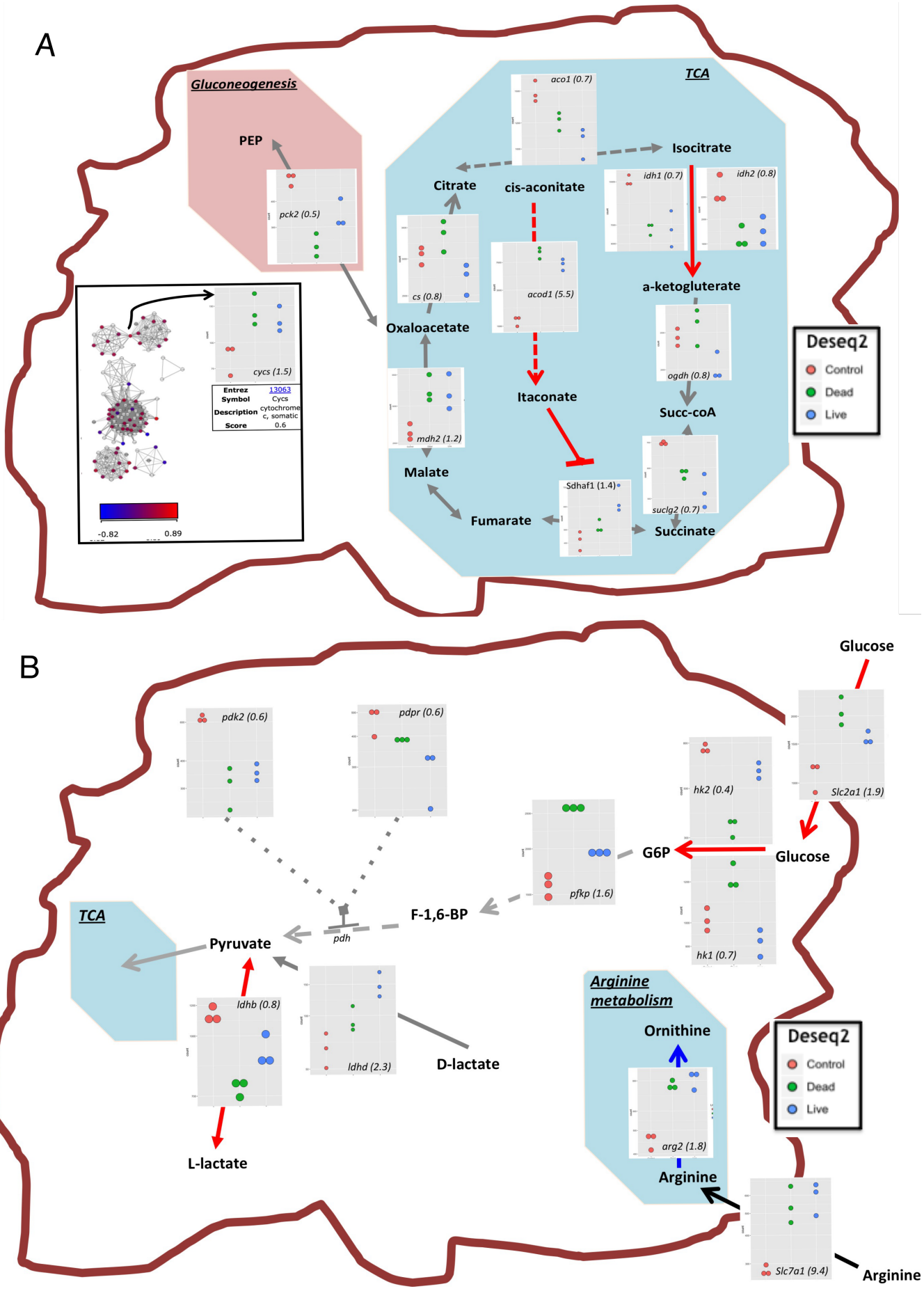
A
Gluconeogenesis
PEP
pck2 (0.5)
TCA
aco1 (0.7)
Isocitrate
Citrate
cis-aconitate
idh1 (0.7)
idh2 (0.8)
cs (0.8)
acod1 (5.5)
a-ketogluterate
Oxaloacetate
ogdh (0.8)
Itaconate
Succ-coA
mdh2 (1.2)
Malate
Sdhaf1 (1.4)
suclg2 (0.7)
Fumarate
Succinate
cycs (1.5)
Entrez 13063
Symbol Cycs
Description cytochrome c, somatic
Score 0.6
-0.82
0.89
Deseq2
Control
Dead
Live
B
Glucose
pdk2 (0.6)
pdpr (0.6)
hk2 (0.4)
Slc2a1 (1.9)
G6P
Glucose
pfkp (1.6)
F-1,6-BP
pdh
TCA
Pyruvate
hk1 (0.7)
ldhb (0.8)
ldhd (2.3)
D-lactate
Arginine metabolism
Ornithine
arg2 (1.8)
Arginine
L-lactate
Slc7a1 (9.4)
Arginine
Deseq2
Control
Dead
Live

Figure 4-11: Overview of immune-metabolic related pathways perturbed in infected macrophages. A :Inset shows Cytoscape TCA Reactome network produced by Graphite. As an example cytochrome S is highlighted and the normalised counts from Deseq2 shown. In light blue is the TCA cycle and an enzyme from Gluconeogenesis in pink. Reaction direction or reaction inhibition is as indicated and, multistep reactions are shown as dashed lines. Gene names and maximum fold change (in brackets) are shown in count plots In red arrows are reactions that have been shown to be critical for M1 macrophages. Specifically, Itaconate production by *Acod1* (I*rg1*) and down-regulation of *Idh* expression have been reported to be essential for M1 macrophages. B: Glycolysis is shown in detail. Reaction direction or reaction inhibition is as indicated, and multistep reactions are shown as dashed lines. Gene names and maximum fold change (in brackets) are shown in count plots In red arrows are reactions that have been shown to be critical for M1 macrophages while in blue arrows denote those to be essential in M2 macrophages. Arginine and glucose transporters are shown on cell periphery. TCA and arginine metabolism are highlight in light blue shading

Within the TCA cycle, there are several enzymes, of which the up- or –down regulation of which is essential for the M1 polarisation of macrophages (Jha *et al*. 2015). In M1 macrophages *idh1* expression is down-regulated leading to citrate accumulation. In M1 macrophages itaconate production from citrate is massively upregulated via *irg1 (acod1*). In our dataset, both live and killed parasite cause slight down-regulation of both *idh* isoforms and a ~5 fold increase in the transcript of *acod1*. In our metabolomics data while there was a slight increase in itaconate in cells infected with killed parasites, this was only in the FACS group. In non-sorted samples, M1 macrophages massively upregulated Itaconate levels. While this TCA signature seems present in infected cells, it is not as potently induced as when LPS is used to trigger a response. Thus it remains to be determined if this feature is functionally important or if the live parasite has to suppress it. Other enzymes in the TCA cycle had slightly altered levels, but a complete understanding of the effects of this will require stably labelled isotope experiments (e.g.. ^{13}C-glucose).

Another characteristic of inflammatory macrophages is increased uptake of glucose by up-regulating expression of transporters. There is some evidence of this with an infection driven 1.9-fold increase (heat-killed caused slightly larger increase than live parasite) of the glucose transporter *Slc2a1* in our dataset. Furthermore, live and heat-killed parasites have divergent affects on hexokinase isoforms. HK1 exclusively promotes glycolysis, whereas HK2 has a more multifaceted role, driving glycolysis when bound to mitochondria and glycogen synthesis when located in the cytosol (John *et al*. 2011). The upregulation of *hk1* and *pfkp* in cells infected with killed parasites points towards a higher glycolytic rate.

Arginine metabolism is key to both M1 and M2 macrophages. In murine cells, it can be taken up via transporters SLC7A1-3. SLC7A1 is constitutively expressed while SLC7A2 is cytokine inducible and is important for both M1 and M2 macrophages (Yeramian *et al*. 2006). Surprisingly there is an up-regulation of SLC7A1 only. In the Fernandes *et al* study, SLC7A1 was increased at all time-points for both parasite species but the increase was only larger than that induced by latex beads for *L. major* at 4 hours post infection (Fernandes *et al*. 2016). Both live and heat-killed parasites cause up-regulation or Arginase 2 (*Arg2*), which did not occur in the study by Fernandes *et al*. The role of *Arg2* in macrophages, which is localised in the mitochondria is less well known than its cytosolic equivalent and classical M2 marker, Arg1 (Yang & Ming 2014) and interestingly, in Chapter 3, if anything, it is upregulated in M1 macrophages (after 24 hours). A microarray based study on *L. amazonensis* amastigote infected BMDM (24 hour infection Balb/c) reported an increase in *Arg2* and confirmed this using qPCR (Osorio y Fortea *et al*. 2009). It will be interesting to see if these alterations in host arginine metabolism are important in the context of *L. mexicana*.

Not shown in Figure **4-11** is the down-regulation of *Deptor* by live (0.62 FC) and killed (0.48 FC) parasites. Deptor inhibits both mTORC1 and 2. This is interesting as *Leishmania* release the gp63 protease, which cleaves it (Halle *et al*. 2009). Deptor has been shown to upregulate glycolytic metabolism by preventing mTORC1 blocking the PI3K-Akt pathway signal transduction pathway (Meng *et al*. 2013). While this is an example of a gene being DE between all three conditions, whether there is a functional consequence caused by the live parasite down-regulating the Deptor to a significantly lesser extent than its antigen control remains to be determined.

4.2.5 Integration of Metabolomics and Transcriptomics Datasets

Integration of omics is a new and challenging area of research. While transcriptomics offers unmatched coverage, the fact that a gene is DE does not necessarily mean higher protein levels. Furthermore, as metabolites can occur in multiple pathways, transcriptomics can help elucidate the responsible enzymes. The integration module of MetaboAnalyst, which uses a Hypergeometric test for enrichment analysis and Betweeness Centrality topology analysis was used (Xia

et al. 2015). This was the method of choice here as this module accepts not only ENSEMBLE and KEGG IDs, but their fold change as well, outputting interactive images of maps that show metabolites, transcripts and whether they are up or down regulated. As there weren't sufficient cells to conduct RNAseq on cells subjected to the FACs protocol, integration of the transcriptomics data is restricted here to its non-sorted samples. Here the live versus heat-killed infection comparison was used due to insufficient replicates of non-infected samples in the metabolomics set. Excluding obvious parasite specific metabolites argininic acid, ovothiol A and trypanothione disulphide, this led to a list of 9 metabolites versus 1197 DE genes that had equivalent *Mus musculus* KEGG and Entrez hit.

Table 4-8: Significantly altered pathways containing both metabolites and transcripts from integration analysis. Total refers to sum of genes and metabolites present in pathway while expected refers to number of hits expected by chance.

Pathway	Total hits	Expecte	Metabolite name	Kegg ID	P.Value	Topology
Glycerolipid metabolism	72	2.9	sn-glycerol 3-phosphate	C00098	0.02	1.6
Glycerophospholipid metabolism	119	4.8	sn-glycerol 3-phosphate	C00098	0.1	0.6
			sn-glycero-3-Phosphocholine	C00670		
			sn-glycero-3-Phosphoethanolamine	C01233		
			Choline phosphate	C0588		

In **Table 4-8** the results of this analysis are presented. Glycerolipid and glycerophospholipid metabolism were the top pathways but this is expected as the majority of metabolites with altered abundance were from these pathways. Nonetheless, the related PPAR and Adipocytokine signalling pathways were perturbed in transcriptome pathway analysis so this was examined in more detail. In **Figure 4-12** the KEGG maps are presented alongside the transcriptional profile. Metabolite nodes are simply coloured red (increased) or green (decreased), comparing the live infected with heat-killed infected samples.

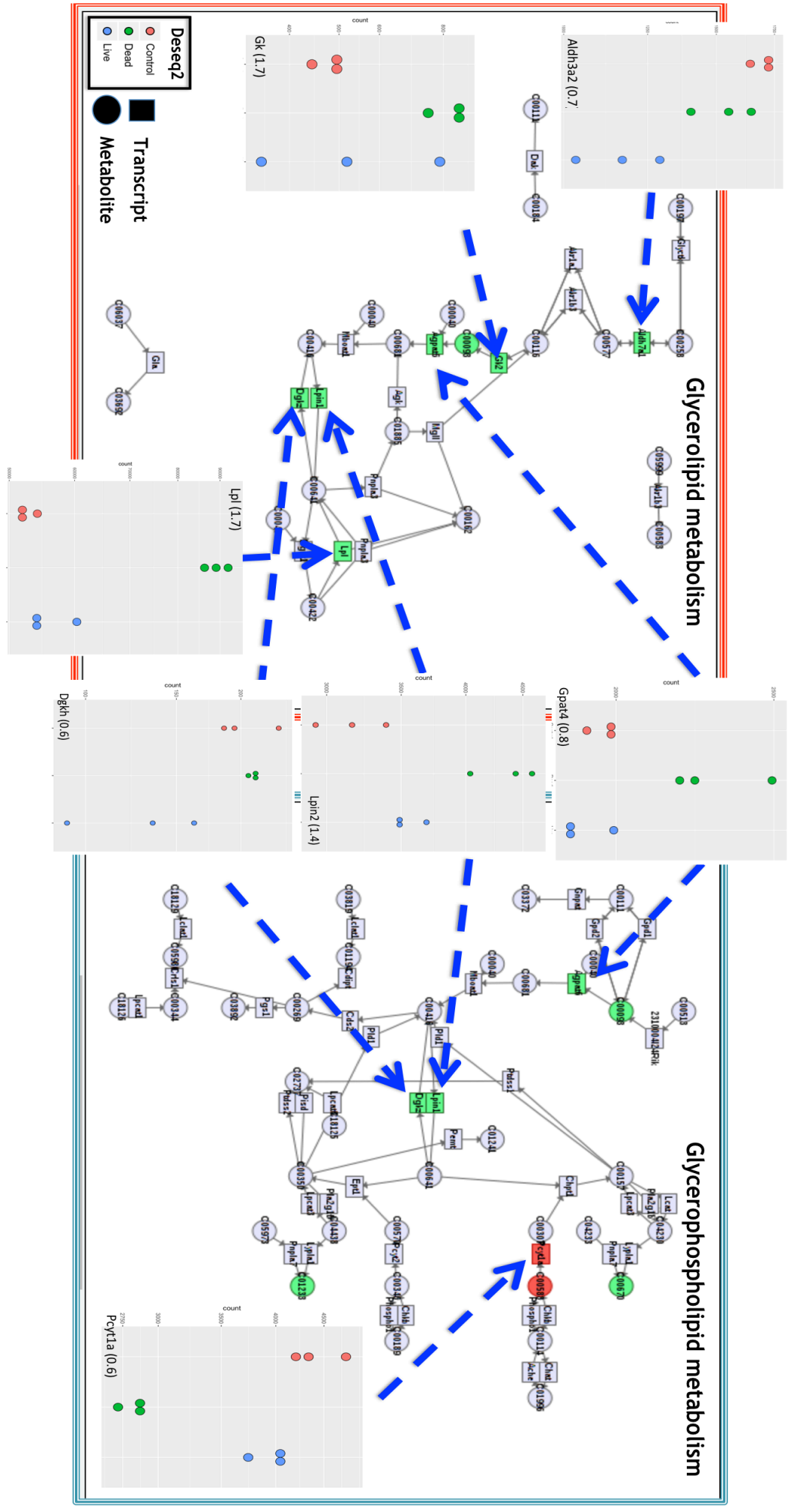
Glycerolipid metabolism
Glycerophospholipid metabolism
Deseq2
Control
Dead
Live
Transcript
Metabolite
Aldh3a2 (0.7)
Gk (1.7)
Lpl (1.7)
Dgkh (0.6)
Lpin2 (1.4)
Gpat4 (0.8)
Pcyt1a (0.6)
count

Figure 4-12: Overlay of KEGG metabolite and transcripts that are altered in infected macrophages. Metabolites are represented by round nodes and enzymes/transcripts by square nodes. Transcripts and their fold change are shown. Colour of metabolites refers to comparison of macrophages infected with live parasites versus macrophages infected with heat-killed parasites; red referring to metabolites or transcripts increased in Live-infected cells, green refers to metabolites or transcripts decreased in Live-infected cells.

Notable among the altered transcripts are lipoprotein lipase (*Lpl*). *Lpl* has been demonstrated to have a role in atherosclerosis and foam cell formation in macrophages, a processes that is associated with inflammation (Takahashi *et al*. 2013). Here the live parasite does not display the marked increase in transcript induced by the heat-killed parasite. As previously mentioned, the live parasites suppress the decrease in *Ppargc1b* caused by the heat-killed parasite. Ppargc1b has previously demonstrated to be required for oxidative fatty acid metabolism, which is associated with M2 metabolism (Vats *et al*. 2006). In this study Lpl and carnitine palmitoyltransferase 1A (Cpt1a) were associated with anti-inflammatory processes. Cpt1 is a key enzyme in lipid metabolism, catalysing formation of acyl carnitines. As mentioned in **Chapter 2**, the association of fatty acid oxidation (FAO) with M2 macrophage function is not fully understood, and Cpt1a may have additional immunomodulatory functions (Nomura *et al*. 2016). The transcript level of *Cpt1a* was decreased ~1.8 fold by the live parasite only in our data. Further work should be done on fully determining the extent to which parasite's modulate macrophage lipid metabolism and which of these are immunomodulatory and which are needed to meet the parasites requirement for lipids.

4.3 Discussion

This is to our knowledge, the first application of integrative omics approaches to *Leishmania* infection. Here the high coverage of transcriptomics is combined with a robust metabolomics protocol and an heat-killed antigen control to gain a detailed insight into host-pathogen interactions. At a metabolite level, potential parasite specific metabolites stood out while glycerolipid and glycerophospholipid metabolism displayed a highly reproducible profile. These perturbations, in combination with transcriptome alterations in the same pathways as well as PPAR signalling can be used to inform further experiments of the key targets and processes to target.

4.3.1 Building on and expanding from previous omics studies

4.3.1.1 Parasite specific metabolites: potential biomarkers

Among the most significantly altered metabolites were, unsurprisingly, parasite specific metabolites. However, this is the first instance of *Leishmania*-macrophage samples being subjected to untargeted metabolomics. L-argininic acid has previously been reported to be produced by multiple parasites species (Westrop *et al*. 2015). Not only is this finding confirmed in the current study but it is shown that it also takes place within the macrophage and that the naive macrophage or polarised (M1 or M2) macrophages do not make it. Similar results were found for L-pipecolic acid, ovothiol A, 4-imidazolone-5-propanoate (Imidazole lactic acid: see text (**4.3.2.1**)) and trypanothione disulphide. Further *in vivo* studies will be required to confirm if these are parasite specific as it is not possible to rule out of other cell types or components of the micro-biome might produce them.

4.3.1.2 Comparison with the literature: Transcriptomics

This study is the first example of a matched metabolomic and transcriptomics approaches. In comparison to previous transcriptomics studies, there are some similarities, but difference in library preparation and sequencing platforms, data processing pipelines, time-points, parasite or host species, or host cell type are compounding factors that will limit overlap. Previous studies have used heat-killed controls. For instance Rabhi *et al* conducted a time-course analysis of *L. major* infected murine BMDM (Balb/c) (Rabhi *et al*. 2012). A detailed comparison with this study was not possible as only a select list of 97 DE genes was published. While of 40 of the 47 genes that were detected as DE were in agreement with FC (**Supplementary Table 4-3)**, the microarray technology used in this study does not offer the resolution of RNAseq. Furthermore, a description of the heat-killing protocol was not available.

For this reason the results of this study were compared with those of Fernandes *et al* to not only compare overlap but to potentially have a shortlist of genes that are DE in human and mice specific model-*in vitro* systems (Fernandes *et al*. 2016). Additionally, this publication had a comprehensive supplement containing all DE genes before and after subtracting phagocytosis for both species. The

combination of these studies will allow differentiating between perturbations induced by the parasite metabolism and antigenic repertoire as well as its phagocytosis. The author of the current study is of the opinion that antigenic and phagocytic events should not simply be discounted as artefacts and subtracted, as it is likely that it is the combination of these alongside the live parasites metabolism that dictates macrophages responses.

4.3.1.3 Comparison with the literature: Immune-metabolism

A key study in integrating metabolomics and transcriptomics (Jha *et al*. 2015) used activated macrophages as their model system. This was used as a basis on which to examine our data to see if there were any similarities. Based on the Reactome pathway analysis, it seems that the live parasite activates the TCA cycle while the heat-killed parasite up-regulates glucose metabolism. Itaconate is a metabolite whose importance in the context of immune-metabolism is only recently being appreciated. It is produced by M1 macrophages causing succinate accumulation that ultimately results in the production of the inflammatory cytokine IL-1ß. Additionally, it has an important role in inhibiting ROS produced by increased flux through succinate dehydrogenase and has been proposed to impose a limit on inflammation (Lampropoulou *et al*. 2016; Chouchani *et al*. 2014).

Both live and killed parasites caused an increase in *Acod1 (Irg1*), which is the enzyme that produces itaconate. While there was an increase in itaconate at the early time-point, this was only in FACs enriched samples. Whether the live parasite suppresses itaconate, and thus succinate accumulation, remains to be determined. Nevertheless, the increase in *Acod1* transcript in conjunction with the increase in the glucose transporter is more in line with an M1 macrophage. On the other-hand, the increase in *Arg2* could potentially benefit the parasite. A possible explanation for these somewhat conflicting results is that the parasites engage multiple receptors on the macrophage surface, as well as differences between using parasites and supraphysiological dose (s) of immune stimulus (i). Studies using macrophages from *Irg1*/*Acod1* deficient mice for *Leishmania* infections could help shed some light on these the role of these perturbations.

4.3.1.4 Lipid metabolism and host-parasite interactions.

As *L. mexicana* parasites enter into a stringent metabolic state, up-regulating the uptake of fatty acids, (Saunders *et al*. 2014), it is interesting that perturbed lipid metabolism was a consistent result across both 'Omics' experiments. In the context of the *L. major*-infected macrophages, alterations in glycerophospholipids have been reported but these studies did not have the coverage seen here (Lamour *et al*. 2012). Lipid metabolism in the context of fatty acid oxidation has been associated with M2 macrophages but recent studies using macrophages deficient in key enzymes have shown that FAO and macrophage polarisation may be more complex than previously thought (Nomura *et al*. 2016).

Using both unbiased and comprehensive pathway analysis utilising KEGG and Reactome databases, PPAR signalling was perturbed in both. Furthermore, when examining genes with the largest FC values, members of this pathway including fatty acid binging proteins were present. There are readily available inhibitors for some of these such as FABP4 inhibitor CAS 300657-03-8 (Merck), which will facilitate further interrogation of the importance of these pathways.

4.3.2 Limitations and benefits of integrated Omics

A limitation of the integration approach here is the limited coverage that afflicts even untargeted metabolomics in comparison to transcriptomics. This is compounded by the uncertainty in metabolite identity. In comparison to models of macrophage M1 activation, parasites induce a much smaller repertoire of perturbed metabolites and the magnitude of these changes is of orders less. Furthermore, further studies based on the transcriptomics data presented here and elsewhere will first require validation such as time- course resolved qPCR, which is considered the gold standard with respect to confirming transcript changes. Nevertheless, as can metabolites can occur in multiple pathways, the ability to link a perturbed metabolite to a perturbed transcriptional network is invaluable.

An important role for lipid metabolism has previously been implicated in both the activated macrophage and intracellular parasite. Both 'Omics' approaches

here show perturbations in these and related pathways. Further targeted validation of these pathways will be required. For instance, the role of Cpt1a, and PPAR related enzymes reported here should be investigated in the context of *L. mexicana*. The novel parasite metabolites observed here in an infected host setting are promising and their potential as biomarkers must be investigated. While LC-MS is not a practical diagnostic tool, simple and cheap assay can be developed.

5 Arginine metabolism in *Leishmania mexicana*

5.1 Introduction

Arginine and arginine metabolism sits at the interface of *Leishmania* – macrophage interactions. Parasites of the *Leishmania* species are unable to synthesise the essential amino acid arginine (Vincendeau *et al*. 2003). Arginine is hydrolysed by the parasites arginase into L-ornithine and this is subsequently decarboxylated into putrescence by ornithine decarboxylase (ODC). Putrescine, together with an aminopropyl group from decarboxylated S-adenosyl-methionine, is converted by spermidine synthase to form the polyamine, spermidine. Spermidine is essential for growth and survival of *Leishmania* and other members of the trypanosomatid family. Additionally, spermidine along with glutathione is a substrate for trypanothione synthase, which synthesises the essential parasite-unique antioxidant, trypanothione. Trypanothione and trypanothione disulphide function similarly to the glutathione-glutathione disulphide redox system by neutralising the ROS produced by macrophages during infection (Fairlamb *et al*. 1985) and playing more general roles in cellular redox metabolism. While the parasite's arginase is essential to its viability, the growth defected observed in *Arginase*$^{-/-}$mutants can be rescued by supplementing with ornithine or polyamines (Gaur *et al*. 2007). Alternatively, *Leishmania* can scavenge polyamines from their environment using specific transporters (Naderer & McConville 2008).

It has been reported that for *L. mexicana,* while the polyamines generated by arginase are essential for *in vitro* growth, depletion of intracellular (macrophage) arginine levels is also necessary for infectivity and proliferation in its host cell (Gaur *et al*. 2007). In this study, the authors reported that arginase deficient parasites (*Arg-/-)* had lower infection rates and lower growth rates in murine bone marrow derived macrophages (BMDM). The authors found higher levels of nitric oxide in cells from lymph nodes of mice infected with *Arg*$^{-/-}$ parasites. This difference was abrogated in BMDM from mice deficient in iNOS implying that parasites use arginase to divert arginine away from NOS. A similar conclusion was reached from a study using *Arg*$^{-/-}$ *L.* major (Reguera *et al*. 2009). However a later study using the same mutant reported that while infectivity was slightly decreased, that infection development was delayed, and the parasites

were auxotrophic for polyamines, their requirement for polyamines seemed to be met by scavenging from the host (Muleme *et al*. 2009). These discrepancies may be due to a species-specific role for arginase or the use of the susceptible Balb/c mice in the last study versus the C57BL/6 used in the first two. A recent study reported that *Leishmania* parasites possess a sensor for extracellular L-arginine and can activate a specific arginine transporter (LdAAP3) in response or L-arginine deprivation, revealing a role for stage in the parasite life-cycle. (Goldman-Pinkovich *et al*. 2016).

It is well established that arginine has an essential role in host cell immunity. In inflammatory (M1) macrophages, arginine is utilised to generate $NO^{\bullet}$ via iNOS. This is an important effector molecule that is required for the controlling of pathogens, including Leishmania. On the other hand, anti-inflammatory (M2) macrophages upregulate arginase thereby diverting arginine to ornithine, ultimately resulting in increased levels of L-proline and polyamines. L-proline can be used in collagen formation while polyamines can help support cell proliferation, both of which are required for wound healing (Yang & Ming 2014).

Preliminary time course LC-MS data from our group suggested that *L. mexicana* procyclic promastigotes were producing and secreting a metabolite of the same mass and retention time of L-citrulline (Julie Kovářová, unpublished data). As this phenomenon was not present in *Trypanosoma brucei brucei,* this inferred that this latter parasite would lack a candidate enzyme capable of metabolising citrulline. Sources from L-citrulline include various nitric oxide synthases (NOS), the urea cycle, arginine deiminase (ADI) and dimethylarginase (DDAH).

ADI is a hydrolase that catalyses conversion of L-arginine to L-citrulline while DDAH positively regulates NOS by degrading its endogenous inhibitor, asymmetric dimethylarginine (ADMA). The presence of an ADI has been reported in several bacteria and parasite species such as *Mycoplasma arginini* and *Giardia intestinalis* (Takaku *et al*. 1992; Knodler 1998). In the case of the *M. arginini*, enzyme, its activity has been proposed to have anti-tumour properties (Takaku *et al*. 1992). While mammals use DDAH to regulate NOS, this enzyme has been found to be present in the bacteria *Pseudomonas aeruginosa* and a crystal structure obtained (Murray-Rust *et al*. 2001).

Interestingly, a previous study reported the existence of NOS in *Trypanosoma cruzi*, which served to protect the parasite from apoptosis-induced DNA damage (Piacenza *et al*. 2001) while a more recent paper reported this NOS was down-regulated upon attachment to the host extracellular matrix (Pereira *et al*. 2015). Certain bacteria have been shown to have endogenous NOS activity, with the responsible gene being identified (Gusarov *et al*. 2009). Ablating expression of the enzyme in bacteria revealed that these bacteria use NOS to protect against oxidative stress by inducing superoxide dismutase and to detoxify antibiotics either produced by other microorganisms or used as a treatment. Several studies have reported measuring NOS activity in *L. donovani* and *L. mexicana* extracts and using affinity chromatography to purify an enzyme with NOS activity (Basu *et al*. 1997; Genestra *et al*. 2006). However, these studies failed to identify a gene encoding NOS and several groups have subsequently failed to corroborate its presence (Steve Beverley, personal communication). *Leishmania* do not have an intact urea cycle as they lack an ornithine transcarbamoylase (OTC) and arginosuccinate lysase (ASL) (Camargo *et al*. 1978).

Although a compound of the mass of L-citrulline was clearly identified in Leishmania, it is noteworthy that other compounds, for example, L-argininic acid, have the same formula and thus exactly the same mass. As this work was proceeding, a study utilising metabolic profiling of various *Leishmania* species reported the presence of L-citrulline and L-argininic acid (Westrop *et al*. 2015). It has previously been suggested that this metabolite is made from L-arginine via 2 keto-arginine. Specifically, Westrop *et al* proposed that 2-keto arginine is formed via a transaminase reaction and in turn, converted by dehydrogenase enzymes to L-argininic acid. The authors further proposed that this was analogous to the mechanism in which tryptophan is degraded to indole 3-lactate. Finally, the authors reported that some L-citrulline was produced that was utilised to synthesise L-arginosuccinate via arginosuccinate synthase (ASS).

Lakhal-Naouar *et al* used a *L. donovani* cell line that overexpressed a dominant-negative mutant ASS to demonstrate that the enzyme is important for virulence (Lakhal-Naouar *et al*. 2012). The authors reported that L-citrulline and L-aspartate were not sufficient to replace L-arginine in cell medium, which is consistent with the absence of an ASL in the *Leishmania* genome. The authors

were, however, unable to generate a knock out due to a combination of apparent genomic instability and they're being three copies of the gene. Sardar *et al* managed to generate a mutant parasite with two of these copies deleted, which resulted in ASS protein levels being reduced below the detection limit of a western blot (Sardar *et al*. 2016). The authors reported that free thiol levels in this mutant cell line were decreased and that in L-arginine depleted medium the viability of the mutant cell line was attenuated on exposure to oxidative stress. This combined with the fact that the mutant parasite was less able to infect mice led the authors to propose that ASS has a role in the parasites anti-oxidant defence.

As arginine is essential to both the parasite and appropriate macrophage immune responses, it was hypothesised that by diverting arginine towards L-citrulline, the parasite might deprive the host NOS of its substrate. Bioinformatic analysis revealed a potential candidate protein for L-citrulline synthesis. As this gene is absent from *T. brucei brucei*, and quite divergent from other orthologs, it may also a candidate for an L-argininic synthesis. Concurrently stable –labelled isotope metabolomics were employed to trace the fate of arginine in *in vitro* models of both procyclic promastigotes and the intracellular amastigotes.

5.2 Results

5.2.1 A putative "Dimethylarginase" and arginine metabolism

To search for possible *Leishmania* orthologs of NOS, ADI and DDAH, The BLASTP function in Tritrypdb was used to search for hits of protein sequences with confirmed functions (Aslett *et al*. 2009). While no hit obtained for NOS, a match was obtained for a putatively identified DDAH. This gene, *Lmxm.08.1225* is annotated as a DDAH in Tritrypdb. However as DDAH and ADI are quite similar proteins and the *Leishmania* sequence is quite divergent from each, it is not possible to rule out either one, and a robust annotation based on the sequence alone is not feasible

5.2.1.1 Phylogenetic and structural analysis

An alignment was built using Clustal Omega (Sievers *et al*. 2011) taking the protein sequence of *Lmxm.08.1225* and known candidate genes for either ADI

and DDAH from BRENDA (Schomburg *et al*. 2004) (**2.14**). The alignment was manually corrected by me using CLC genomics (Qiagen) to ensure that experimentally confirmed catalytic and binding residues aligned and were annotated (**Figure 5-1A**). While *Lmxm.08.1225* (241 amino acids (aa) was shorter than most of the DDAH sequences (289-342 aa) other than the canine DDAH (185aa), it was much shorter than the ADIs (419-593aa). In **Figure 5-1** the analysis pertaining to DDAH is presented while that for ADI is available in **Supplementary Figure 5-1.**

Phylogenetic trees were made on Clustal Omega using the above groups with one example from the opposite group as an out-group. Nexml files were imported into Dendroscope (Huson & Scornavacca 2012) to give the final tree shown in **Figure 5-1 C**. Structural analysis was conducted using Phyre^2 (Kelley *et al*. 2015).

Phyre^2 a web based suite of tools that uses homology detection methods to take advantage of protein structure databases to predict and analyse protein structure. The top 10 results of this analysis are presented in **Table 5-1** (Full results are in **Supplementary File 5-1**) and the top hit shown in **Figure 5-1B**. The top hits of this analysis are as expected, DDAH and ADI though the percentage identity is slightly higher for DDAH. This is probably due to ADI being longer and thus will have lesser proportion covered by the alignment.

Table 5-1: Results of Phyre[2]. The first column refers to PDB id for structure that was used as template. The next column is 'Confidence'. This represents the probability (from 0 to 100) that the match between input sequence and a given template is a true homology. It does not represent the expected accuracy of the model - although the two are intimately related. The percentage identity between a input sequence and the matching template is in the %id column and relevant functional PDB information is in the final column.

Template (PDB)	Confidence	% i.d.	Template information	Species
d1h70a	100	33	**Fold:** Pentein, beta/alpha-propeller **Superfamily:** Pentein **Family:** Dimethylarginine dimethylaminohydrolase DDAH	***Pseudomonas aeruginosa***
c3i4aA	100	33	**PDB header:** hydrolase **Chain:** A: **PDB Molecule:** n(g),n(g)-dimethylarginine dimethylaminohydrolase 1 **PDB Title:** crystal structure of dimethylarginine dimethylaminohydrolase-1 (ddah-2 1) in complex with n5-(1- iminopropyl)-l-ornithine	***Human***
c2ci6A	100	31	**PDB header:** hydrolase **Chain:** A: **PDB Molecule:** n(g),n(g)-dimethylarginine dimethylaminohydrolase 1; **PDB Title:** crystal structure of dimethylarginine2 dimethylaminohydrolase i bound with zinc low ph	***Cow***
d1s9ra	100	20	**Fold:** Pentein, beta/alpha-propeller 20 **Superfamily:** Pentein **Family:** Arginine deiminase	***Mycoplasma arginini***
c4e4jJ	100	21	**PDB header**: hydrolase **Chain:** J: **PDB** Molecule: Arginine deiminase; **PDB Title**: crystal structure of arginine deiminase from *mycoplasma penetrans*	***Mycoplasma penetrans***
d1rxxa	100	24	**Fold:** Pentein, beta/alpha-propeller **Superfamily:** Pentein **Family:** Arginine deiminase	***Pseudomonas aeruginosa***
d1bwda	100	16	**Fold:** Pentein, beta/alpha-propeller **Superfamily**: Pentein **Family:** Amidinotransferase (Inosamine-phosphate amidinotransferase)	***Streptomyces griseus***
c4bofA	100	17	**PDB header:** hydrolase **Chain:** A: **PDB Molecule:** Arginine deiminase; **PDB Title:** crystal structure of arginine deiminase from group a *streptococcus*	***Streptococcus pyogenes***
c8jdwA	100	16	**PDB header:** transferase **Chain:** A: **PDB Molecule:** protein (l-arginine: glycine amidinotransferase); **PDB Title:** crystal structure of human l-arginine: glycine amidinotransferase in complex with l-alanine	***Human***
c1jdwA	100	17	**PDB header:** transferase **Chain:** A: **PDB Molecule:** l-arginine: glycine amidinotransferase; **PDB Title:** crystal structure and mechanism of l-arginine: glycine2 amidinotransferase: a mitochondrial enzyme involved in3 creatine biosynthesis	***Human***

The best match according to Phyre[2] is the *P. aeruginosa* DDAH followed by human, then cow. Interestingly glycine amidino-transferases (AGAT) had some homology. AGAT catalyses the transfer of an amidino group from L-arginine to glycine producing products L-ornithine and guanidinoacetate, the immediate precursor of creatine. This analysis largely matches the phylogenetic analysis and *P. aeruginosa* and other DDAH enzymes cluster together even when all ADIs are included with human NOS2 as an out-group (**Supplementary Figure 5-2).** While a DDAH seems slightly more likely than an ADI, *Lmxm.08.1225* is quite divergent limiting the conclusions that can be drawn from this analysis. Nevertheless, an arginine metabolising enzyme is a likely function.

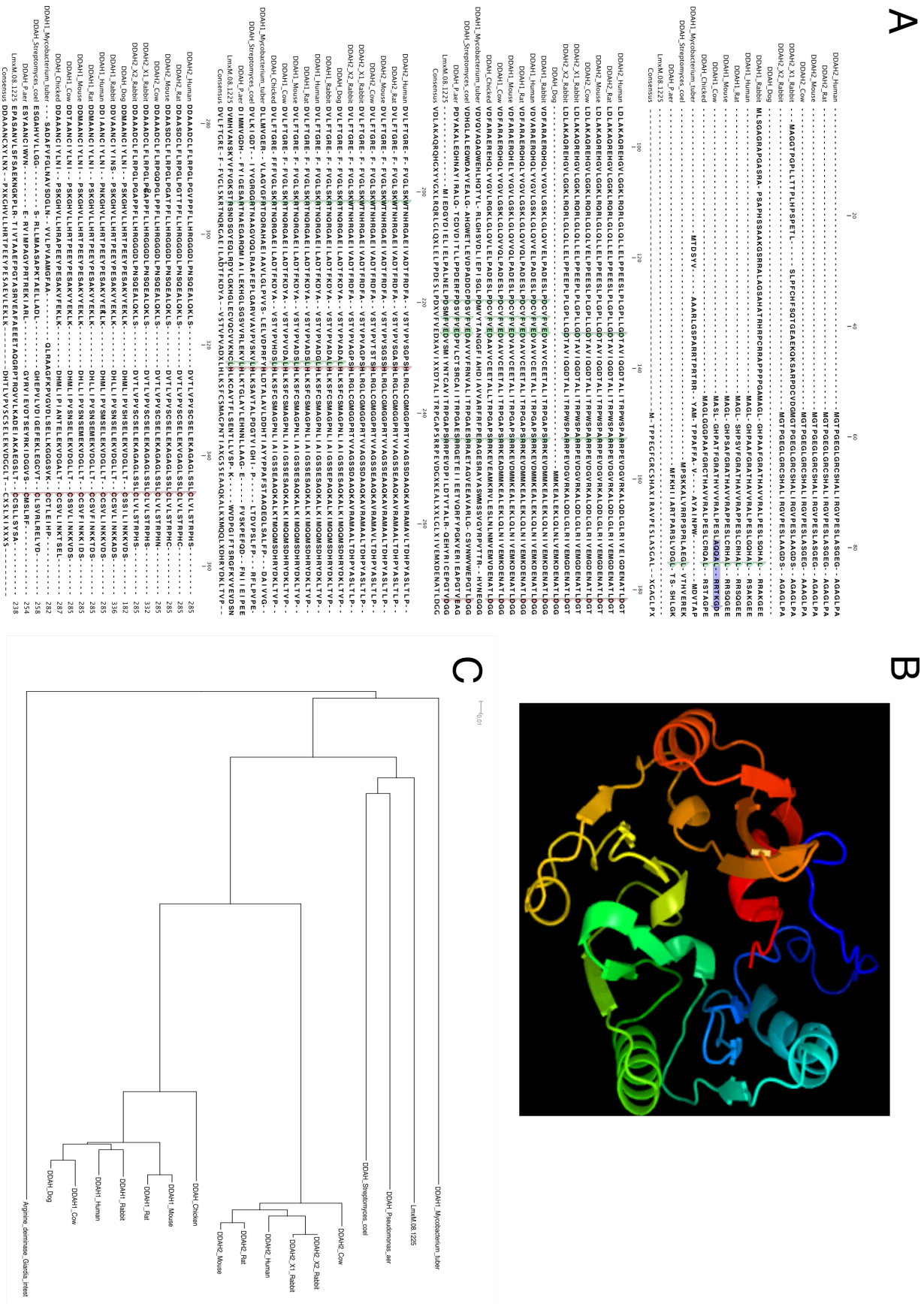

Figure 5-1: Clustering, structural and phylogenetic analysis of *Lmxm.08.1225*.
A: Alignment was generated using Clustal Omega and minimally edited to ensure experimentally validated active (red) and substrate (green) binding sites are aligned. Blue denotes the lid region present in bovine DDAH. B: Top hit (*P. aer* ddah) generated from Phyre[2] using *Lmxm.08.1225* as a template C: Phylogenetic tree was generated in Clustal Omega, and out-group set as *Giardia intestinalis* ADI in Dendroscope. Scale bar represents nucleotide substitutions per site. In **Supplementary Figure 5-2**, some ADI sequences are included with the above sequences, with human *iNOS* set as the out-group.

5.2.1.2 Assaying dimethylarginine and arginine utilising proteins

As the two top candidates were DDAH and ADI, the activity of these enzymes was assayed for (**2.9**). As a positive control for ADI commercially available enzyme was used. As there was no commercially available DDAH, the *P. aeruginosa* DDAH was cloned and overexpressed it in *E. coli* as carried out by (Wang *et al*. 2009b) (**Figure 5-2A**). Next enzyme was purified using nickel affinity chromatography (**Figure 5-2B**). The same approach was attempted with *Lmxm.08.1225* but was unsuccessful. As the Rosetta strain (DE3), which contains a plasmid coding for rare codons was used, it is unlikely that this is due to the use of these by the *L. mexicana* gene.

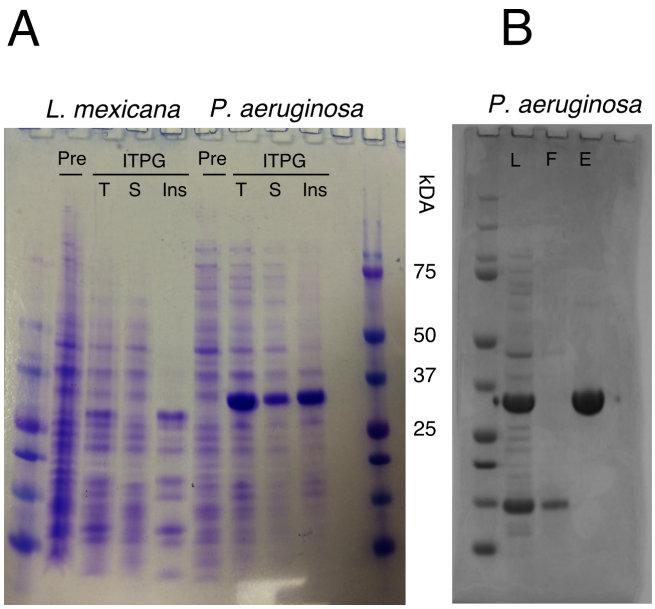

Figure 5-2: Overexpression in *E. coli* of DDAH from *P. aeruginosa* and putative DDAH/ADI from *L. mexicana*. A: Genes from *L. mexicana* (Lmxm.08.1225) and *P. aeruginosa* were cloned into the pET28a (+) vector as described in material and methods. IPTG (1mM) was used to induce overexpression at 37°C for 4 hours with shaking once cultures reached an OD600 of 0.4-0.5. Pre indicates pre-induction, T indicates total culture post induction, S indicates soluble fraction and Ins indicates insoluble fraction. B: Nickel-affinity chromatography of *P. aeruginosa* DDAH. L indicates sample that was loaded into column, F indicates the flow through and E indicates the fraction that was eluted in imidazole.

The commercial ADI and purified DDAH were then assayed alongside *Leishmania* cell extract using relevant substrates L-arginine (ADI) or asymmetric N^G,N^G-dimethylarginine (ADMA) and urease (Sigma) to remove urea (**Figure 5-3 A-C**). The assay used here relies on diacetyl monoxime (DAMO) derivatization of the ureido group in L-citrulline to form a coloured product. This assay is limited by the fact that it is discontinuous and relies on hazardous strong acids for colour development (Prescott & Jones 1969). An additional limitation is a lack of

absolute specificity as other ureido containing compounds such as urea and carbamyl asparte will be detected. While it was possible to control for the interference of urea by use of a urease, it is not possible to preclude the presence and interference of carbamyl aspartate. No detectable activity was observed in *Leishmania* extract even though protease inhibitors were used and commercial ADI was active within cell extract (we have not tested the same for *P. aeruginosa* DDAH).

With regards to the possibility of a *Leishmania* NOS, nitrite was not detectable using the Griess assay in spent medium from *Leishmania* cultures. Finally, we were unable to reproduce results that were obtained using affinity (2'5' ADP agarose) chromatography purification (**Supplementary Figure 5-3**) in two previous studies (Basu *et al*. 1997; Genestra *et al*. 2006). While ideally there would have been more replicates of these experiments, the results seen here, and in **5.2.1-3** do not support the presence of a L-citrulline producing enzyme.

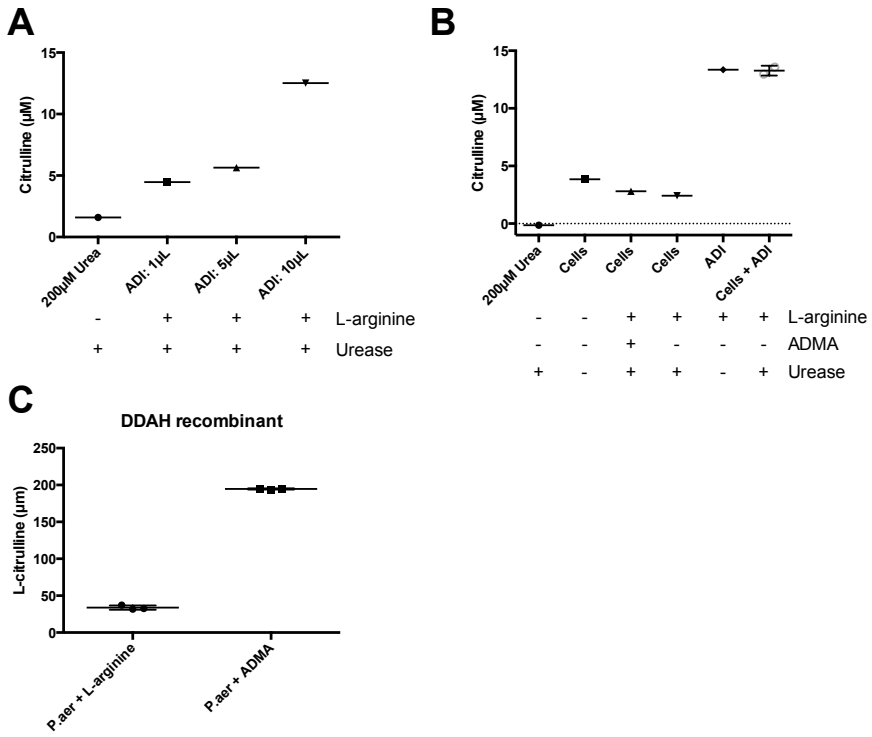

Figure 5-3: Results from colorimetric assay that is specific for L-citrulline. Note that A and B were carried out in 1mL cuvettes while C was carried out in 96 well format. See material and methods for further information on differences in protocol. The ADI protein functioned in two independent experiments with different conditions but this exact experiment was executed only once so results are indicative of one replicate A: Increasing amounts of ADI lead to increasing amounts of L-citrulline production. B ADI produces L-citrulline in dialysed cell extract. C: Recombinant DDAH from *P. aeruginosa* produces L-citrulline. Both readings in C were normalised to substrate control and measurements were carried out in triplicate.

5.2.1.3 Pilot Overexpression in OPPF

As overexpression work shown above, as well as with the use of a maltose binding protein solubilising tag and attempts of refold the protein using various combinations of L-arginine and NaCl was unsuccessful, an application as made to work at the Oxford Protein Production Facility-UK (OPPF-UK, Research Complex at Harwell, University of Oxford). This is a high-throughput protein over-expression screening facility based at the Harwell research complex. Briefly 12 plasmids (pOPINEneo, pOPINE-3C-HALO7, pOPINF, pOPINS3C, pOPINHALO7, pOPINMSYB , pOPINTRX, pOPINH , pOPINGM, pOPINP ,pOPINTolB and pOPING) were used in combination with native *Leishmania* sequence, or gene blocks (synthesised sequences) that were codon optimised for *E. coli*, HEK293 cell line or baculovirus / *Drosophila melanogaster* system.

All of the resulting 48 plasmids were used in *E. coli*, the HEK293 cell line or baculovirus / *Drosophila melanogaster* systems. The *E. coli* or the baculovirus / *Drosophila melanogaster* system failed to yield soluble protein. The HEK293 system did yield soluble protein, while one (6) was secreted (**Figure 5-4**). As the stable isotope labelled data did not support the presence of an L-citrulline producing enzyme, and creating stable over-expressing HEK293 clones is a time-consuming process, no further work was done with these plasmids. Note that the author was supervised and assisted by Dr. Louise Bird (Strategy, primer and gene

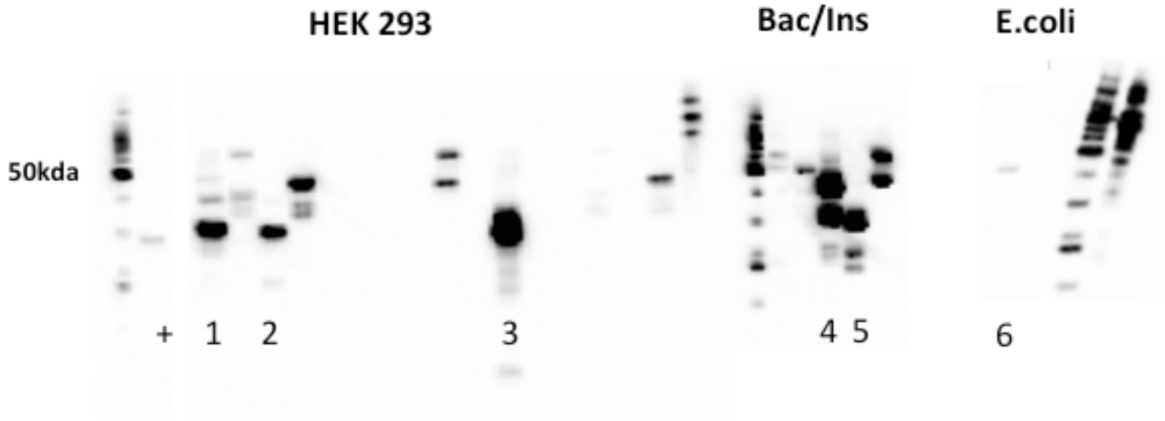

Figure 5-4: Results of overexpression of *Lmxm.08.1225* carried out that the OPPF-UK.
The results shown here are from the HEK293 system after a 3-day transient transfection. HEK 293, Bac/Ins, and E.coli refer to the codon-optimized sequence used. 1 = C terminal His, 2 = N terminal His, 3= Tol-B SS, 4= Sumo, 5 = SS-N terminal His, 6 = SS-N-HIS-3C-POI, + = GFP positive control. +, 1 - 5 are soluble intracellular proteins and 6 is secreted.

block design, plasmid generation and *E. coli* screening), Dr. Joanne Nettleship (HEK293 system), Prof. Ray Owens (Strategy). Additionally, the facility carried out the *Drosophila melanogaster* system after the authors two-week visit.

5.2.1.4 Overexpression in *Leishmania* and metabolic profiling

In parallel to the above experiments, overexpression in *L. mexicana* was conducted using an episomal overexpressing plasmid with either no tag or a 3' terminal his tag (pGL1002 Prof. Jeremy Mottram, originally pXG; Prof. Steve Beverly's lab) (Ha *et al.* 1996). A control using wild type parasites cultured in parallel was also used. In order to detect overexpression, RT-qPCR was used and this showed a large increase in transcript (**Figure 5-5a**). However attempts to detect an increase or presence of the 3'-tagged protein using either Coomassie blue or immuno-blotting (anti- his-tag) were unsuccessful.

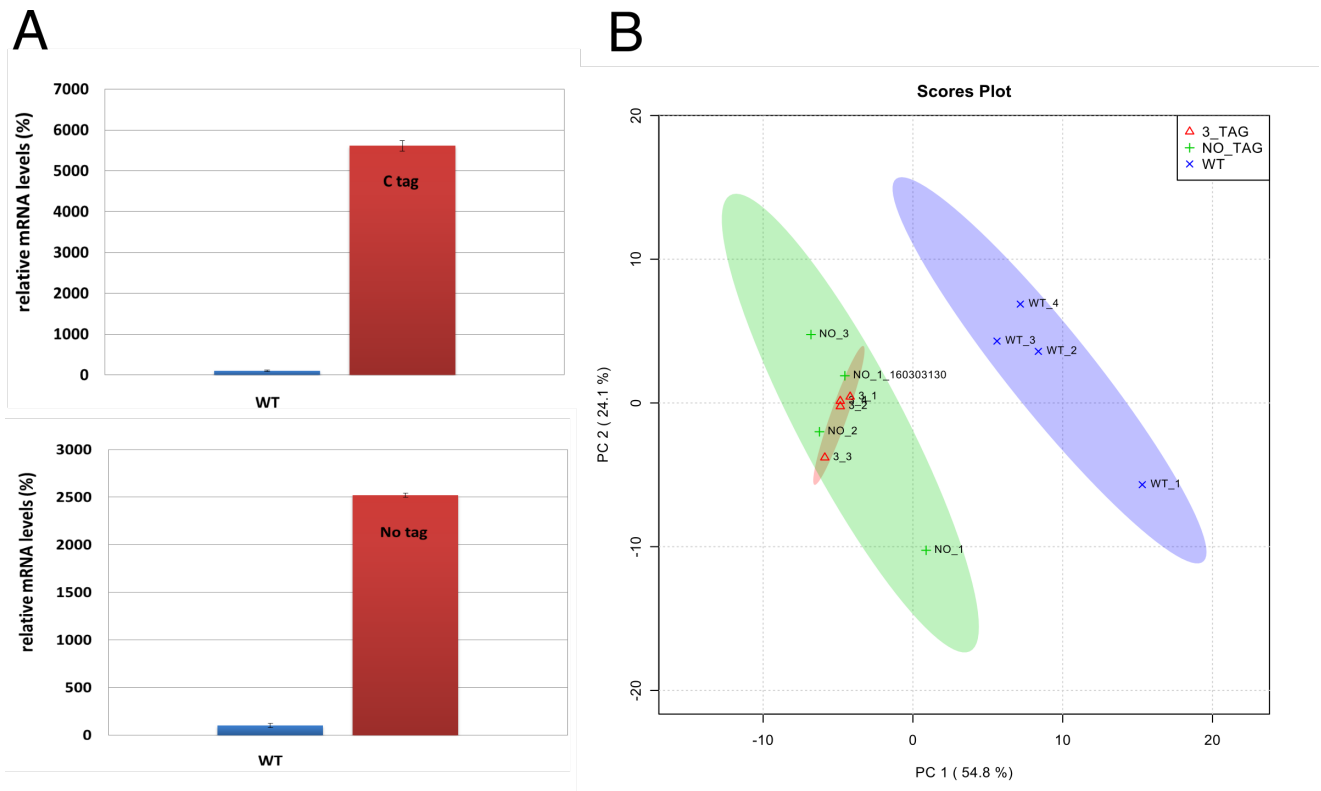

Figure 5-5: RT-qPCR of episomal over-expressors and PCA of metabolomics data. A: RT-qPCR was conducted on episomal over-expressors. The D-Delta method was used, normalising to *LmxmGPI8*. Data is representative of three biological replicates. **B:** PCA analysis was conducted on log transformed using MetaboAnalyst 95% confidence intervals are highlighted by the respective background colour.

Untargeted metabolomic profiling was carried out to investigate if there was a perturbation at the metabolic level. Data filtering was conducted as in **4.2.2.1**. The result of this filtering in IDEOM and the Xcalibur method was a list of 231 metabolites. The identity of 91 of these was confirmed using authentic standards (MSI level 1).

There was marked separation according to PCA between both over-expressor cell lines and wild-type control (**Figure 5-5b**). A one-way ANOVA was used to test for significance. In **Table 5-2** significantly altered metabolites (FDR <0.05) as well as 2 other arginine metabolism-related metabolites (FDR <0.1) are presented. The initial hypothesis tested here was that over-expression might lead to increased L-citrulline (or isomer L-argininic acid) production but levels of this metabolite (s) were not markedly altered.

Table 5-2: Metabolic alterations in parasites overexpressing *Lmxm.08.1225*. Significance was determined by one-way ANOVA for each time-point with Fishers LSD used for post-hoc analysis. As KEGG IDS are less ambiguous, the equivalent KEGG ID is in column 1. As certain metabolites are not in KEGG, arbitrary IDs are used for these. In the 'Change' column, the direction change of either one or both of the over-expressors to wild-type control is indicated. A match with an authentic standard, number of alternative isomers, match with mZCLOUD fragmentation database and maximum fold change are indicated in the last four columns. There were 3 peaks with the mass of L-homocitrulline, one of which was rejected by the Ideom pipeline due to its proximity to L-homocitrulline (first one). All three of these peaks were increased in terms of area in the episomal over-expressors.

Name	KEGG ID	FDR	Std	Isomer	M^{SG}	FC	Change
5-Methyl-2'-deoxycytidine	C03592	4.4E-05		1		8.5	Up
Deoxycytidine	C00881	5.0E-04	Yes	1		5.0	Up
Fagomine	C10144	7.3E-03		2		5.5	Down
1-Oleoylglycerophosphocholine	C03916	7.3E-03		12		7.5	Up
L-4-Hydroxyglutamate semialdehyde	C05938	7.3E-03		14		2.0	Down
(S)-Carnitine	C15025	7.3E-03		2		5.1	Down
L-Threonine	C00188	9.7E-03	Yes	11		3.5	Down
L-Homocitrulline.1	C02427	9.7E-03		1		28.4	Up
sn-Glycerol 3-phosphate	C00093	9.7E-03	Yes	1		6.2	Up
L-Phenylalanine	C00079	1.1E-02	Yes	7	Yes	2.6	Up
PC(16:0/5:0(COOH))	NoKegg24	1.1E-02		1		6.0	Up
(R)-2,3-Dihydroxy-3-methylbutanoate	C04272	1.3E-02		8		1.7	Down
Pantothenol	C05944	1.3E-02		1		3.8	Down
phosphinomethylmalate	NoKegg17	1.3E-02		3		3.3	Up
7-chloro-L-tryptophan	NoKegg11	1.3E-02		2		2.7	Down
Diethanolamine	C06772	1.3E-02		2		2.3	Up
Cytosine	C00380	1.3E-02	Yes	1		3.1	Up
Maltose	C00208	1.5E-02	Yes	42		2.9	Down
L-Valine	C00183	1.5E-02	Yes	17	Yes	1.8	Up
L-Arginine	C00062	1.6E-02	Yes	2	Yes	1.7	Up
Stachydrine	C10172	1.6E-02		2		2.7	Down
Phosphodimethylethanolamine	C13482	1.9E-02		1		2.5	Up
N-Methylethanolamine phosphate	C01210	1.9E-02		3		1.8	Up
L-Proline	C00148	1.9E-02	Yes	4	Yes	1.5	Up
3-(4-Hydroxyphenyl)lactate	C03672	1.9E-02		13		2.2	Up
N-α-acetyl-DL-norvaline	NoKegg2	1.9E-02		10		3.0	Down
D-Ribulose 1,5-bisphosphate	C01182	1.9E-02		3		3.6	Up
Maltotriose	C01835	2.4E-02		22		3.1	Down
Caffeic aldehyde	C10945	2.5E-02		12		3.9	Up
L-Homocitrulline	C02427	2.6E-02		1		5.2	Up
1-5-diazabicyclononane	NoKegg21	2.7E-02		2		2.5	Down
4-Guanidinobutanoate	C01035	2.8E-02		3		2.1	Up
N-Acetyl-L-leucine	C02710	2.8E-02		5		2.9	Up
Daminozide	C10996	2.9E-02		4		5.4	Up
sn-glycero-3-Phosphocholine	C00670	2.9E-02	Yes	1		2.2	Up
L-Glutamine	C00064	2.9E-02	Yes	6	Yes	1.5	Down
beta-Alanyl-L-arginine	C05340	2.9E-02		2		1.7	Down
L-Ornithine	C00077	3.0E-02	Yes	6	Yes	1.7	Up
L-Tyrosine	C00082	3.1E-02		11		2.4	Up
Acetyl-maltose	C02130	3.1E-02		1		2.7	Down
D-Glucose	C00221	3.1E-02		57		1.5	Up
Succinyl proline	C11711	3.1E-02		1		2.7	Up
S-Methyl-L-methionine	C03172	3.1E-02		6		2.1	Up
p-Coumaroyl quinic acid	C12208	3.2E-02		4		1.6	Up
Xanthine	C00385	3.4E-02	Yes	3		2.1	Up
2-Dehydro-3-deoxy-L-rhamnonate	C03979	3.4E-02		24		1.4	Up
L-Pipecolate	C00408	3.4E-02		9	Yes	1.6	Up
Carnosine	C00386	3.4E-02		3		2.2	Up
Choline phosphate	C00588	3.7E-02	Yes	1		1.2	Up
Iminodiacetate	NoKegg23	3.9E-02		4		2.0	Up
N-dimethylethanolamine	NoKegg25	3.9E-02		1		2.3	Up
2 keto-arginine	C03771	7.4E-02		1		1.7	Up
L-Argininic acid	NoKegg26	9.4E-02	Yes	1	Yes	1.5	Up

Note that the input files for additional analysis are in **Supplementary Files 5-(3-4) (Kegg IDs are shown, metabolite name is in Supplementary File 5-2)**.

L-citrulline levels were very low in all samples, and in fact its peak resembled a slight shoulder beside the L-argininic acid peak. The data is presented in heatmap format in **Figure 5-6**. While there are decreases and increases in several general pathways, 5 of these belong to arginine metabolism. Ideally an empty vector control would have been used to subtract the effect of growing the episomal over-expressors in antibiotic which influence cannot be ruled out.

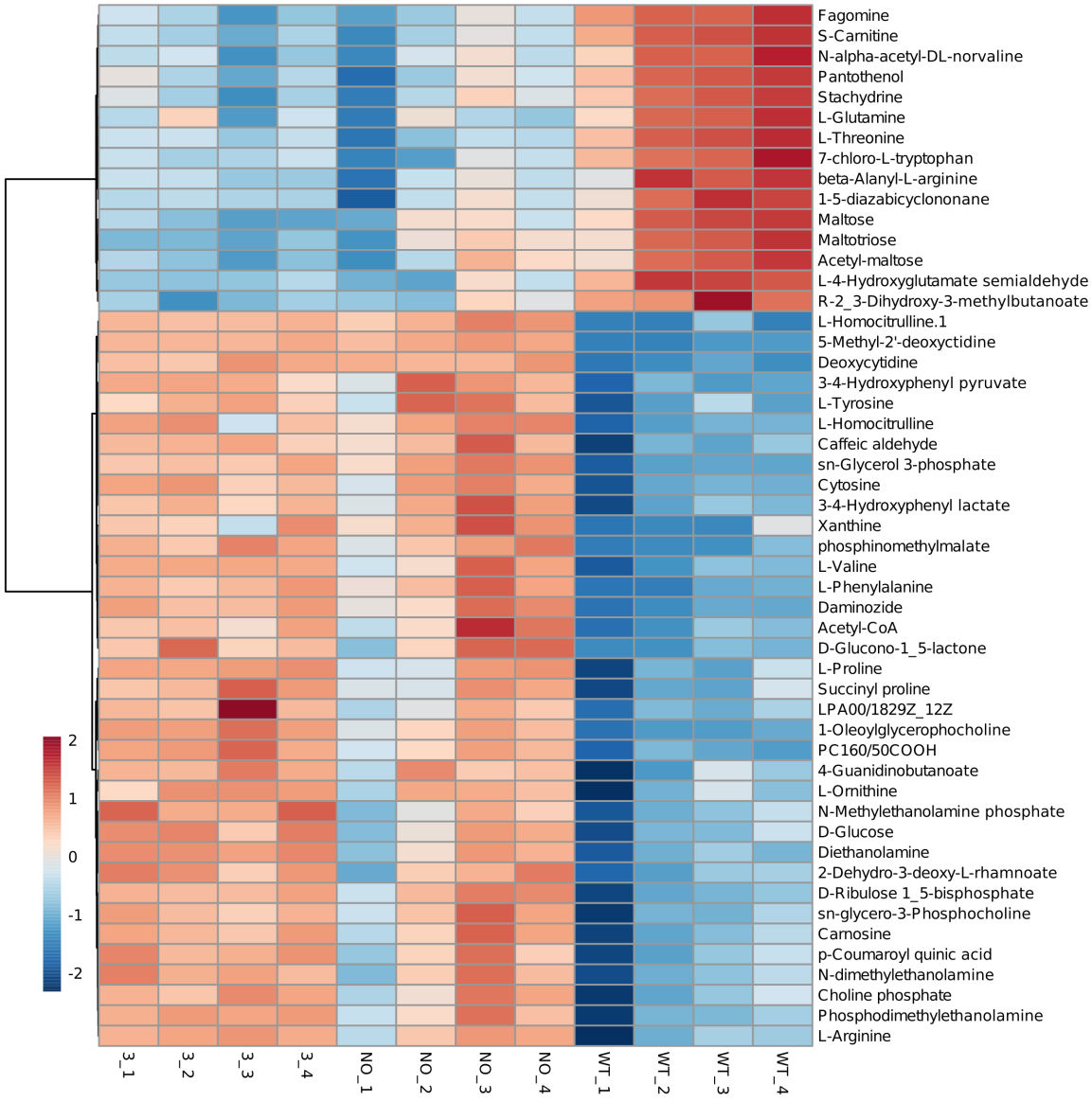

Figure 5-6: Heatmap analysis of significantly altered metabolites present in parasites overexpressing *Lmxm.08.1225*

While by its name, L-Homocitrulline would seem to be part of L-arginine metabolism, it instead is formed by a carbamoyl-phosphate: L-lysine carbamoyl-transferase in an orphan reaction. This reversible reaction is as follows:

Carbamoyl phosphate + L-Lysine <=> Orthophosphate + L-Homocitrulline.

A metabolite of this mass was detected by a previous publication (Westrop *et al*. 2015). A dataset of *L. mexicana* grown in $U^{13}C$-Lysine (Snezhana Akpunarlieva, unpublished data) was examined and there was no evidence of a labelled version of L-Homocitrulline. A peak of this mass was not present in infected, M1 or M2 macrophages. Additionally, there was no labelled version of the L-homocitrulline formula in $U^{13}C$-Arginine labelled samples. If *Lmxm.08.1225* is responsible for the increases in these peaks, it is independent of these two amino acids (L-lysine and L-arginine). Additionally it is possible that this is an adduct of the G418 antibiotic that the over-expressing parasites are maintained in.

(S)-carnitine was markedly decreased in our data. Checking the retention time of the authentic (R)-carnitine confirmed that this was a separate metabolite. There were no other identified metabolites (or masses) that had both a similar trend and retention time so unlikely this peak is an adduct. Note that (R)-carnitine, was detected and it matched the authentic standard in retention time and a MS^2 Spectra in mZCLOUD. The identity of '(S)-carnitine' could be investigated by obtaining and running an authentic (S)-carnitine with some of the samples mentioned here. Finally, while other metabolites with marked perturbations, such as deoxycytidine and 5-methyl-2'-deoxycytidine, there immediate relationship to *Lmxm.08.1225* is not immediately obvious.

For some of the metabolites presented here, especially L-argininic acid, the intensity was extremely high so dilutions of the QC were run to find a dilution factor that would get samples in the linear range. While these samples were run on the Fusion MS (Thermo), and the previous run were on the qExactive (Thermo), the results for arginine related metabolites are comparable. L-arginine, L-ornithine and 2 keto-arginine were increased in both over-expressor lines (**Figure 5-7**). Dimethyl-arginine was unchanged and while L-argininic acid was slightly higher, this trend did not reach statistical significance. Thus it seems that while *Lmxm.08.1225* may have some role in

L-arginine metabolism, it is not clear from the current data what this role might be. Given the diversity in sequence in this gene with other ADI and DDAH sequences from other species, this enzyme may have an alternative role. The role of this enzyme in infection of could be investigated by using the cell lines generated in this study (alongside an empty vector control) to infect BMDM. Additionally, the enzyme could be investigated further by generating a knockout cell line. This was attempted by using both a traditional homologous recombination replacement strategy and inducible Di-Cre system (Duncan *et al*. 2016) but were unsuccessful due to limited time. Further attempts using this approach or similar methods may be successful.

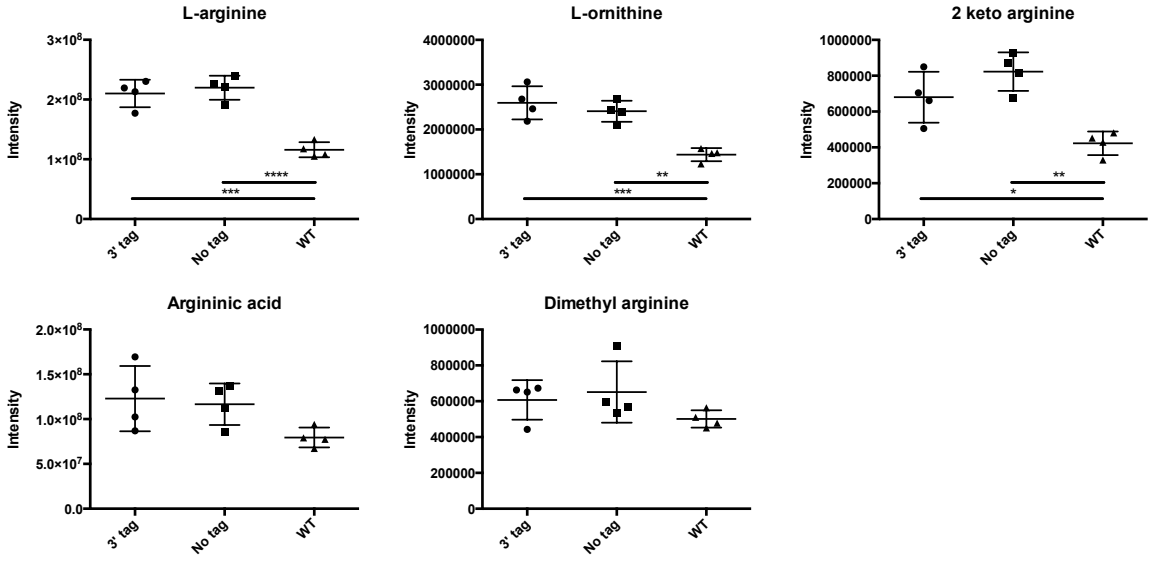

Figure 5-7: Arginine metabolism in cell lines over-expressing *Lmxm.08.1225*. One in ten dilutions were made of samples which were run on the Fusion (Thermo) MS. A method was written in Xcalibur (Thermo) In order to ensure that argininic acid was correctly chosen. Statistical significance was determined in Prism 6 (Graphpad) using a one-way ANOVA with Tukeys correction for multiple comparisons.

5.2.2 Arginine metabolism in procyclic promastigotes

While the essentiality of L-arginine to *Leishmania* species is well known, how the parasite utilises this amino acid is not fully understood. As a recent publication reported the synthesis of L-argininic acid and L-citrulline by multiple *Leishmania* species (Westrop *et al*. 2015), this was investigated further using stable isotope labelled-metabolomics. This approach was first applied in the procyclic promastigote form of the fly. Briefly, procyclic promastigotes were grown in medium containing 50% $U^{13}C$-L-arginine (Cambridge isotope laboratories,

enrichment 99%, cat: CLM-2265-H-0.1) until they reached mid-log stage (48 hours) at which point samples were made for LC-MS (See materials and methods). The key reasoning behind this approach that the same metabolite with various proportions of a labelled amino acid will have the same retention time but different masses.

Data analysis (for all stable isotope experiments) was conducted in conjunction with Fiona Achcar using mzMatch-ISO (Chokkathukalam *et al*. 2013). In this experiment a 26-minute LC protocol was used, which is unable to differentiate between L-argininic acid and L-citrulline. As the stable isotope labelled here is expected to give 6-^{13}C-labelled L-argininic acid and L-citrulline, these are treated as one in this section.

As *Leishmania* are confirmed to have an arginase, and the reaction from L-arginine to L-ornithine involves the loss of one carbon, it would be expected expect that L-ornithine would be 5-^{13}C-labelled and that is what happens (**Figure 5-8**). An OTC catalyses the conversion of from L-ornithine to L-citrulline and this reaction involves the incorporation of a carbon (non-labelled in this experiment) in the form of carbamoyl aspartate. If there is an OTC present in *Leishmania*, and this was responsible for L-citrulline formation, it would be expected that some L-citrulline to be 5-^{13}C-labelled and this is not the case (**Figure 5-8**). Thus it is obvious that this metabolite be it L-argininic acid or L-citrulline is formed by the reaction that acts on L-arginine without exchanging any carbons. Based on these results, ADMA could still be a substrate for an L-citrulline-forming DDAH as it 6-^{13}C-labelled. In positive mode, 2 keto-arginine was 6-^{13}C-labelled so it potentially could be converted to L-argininic acid.

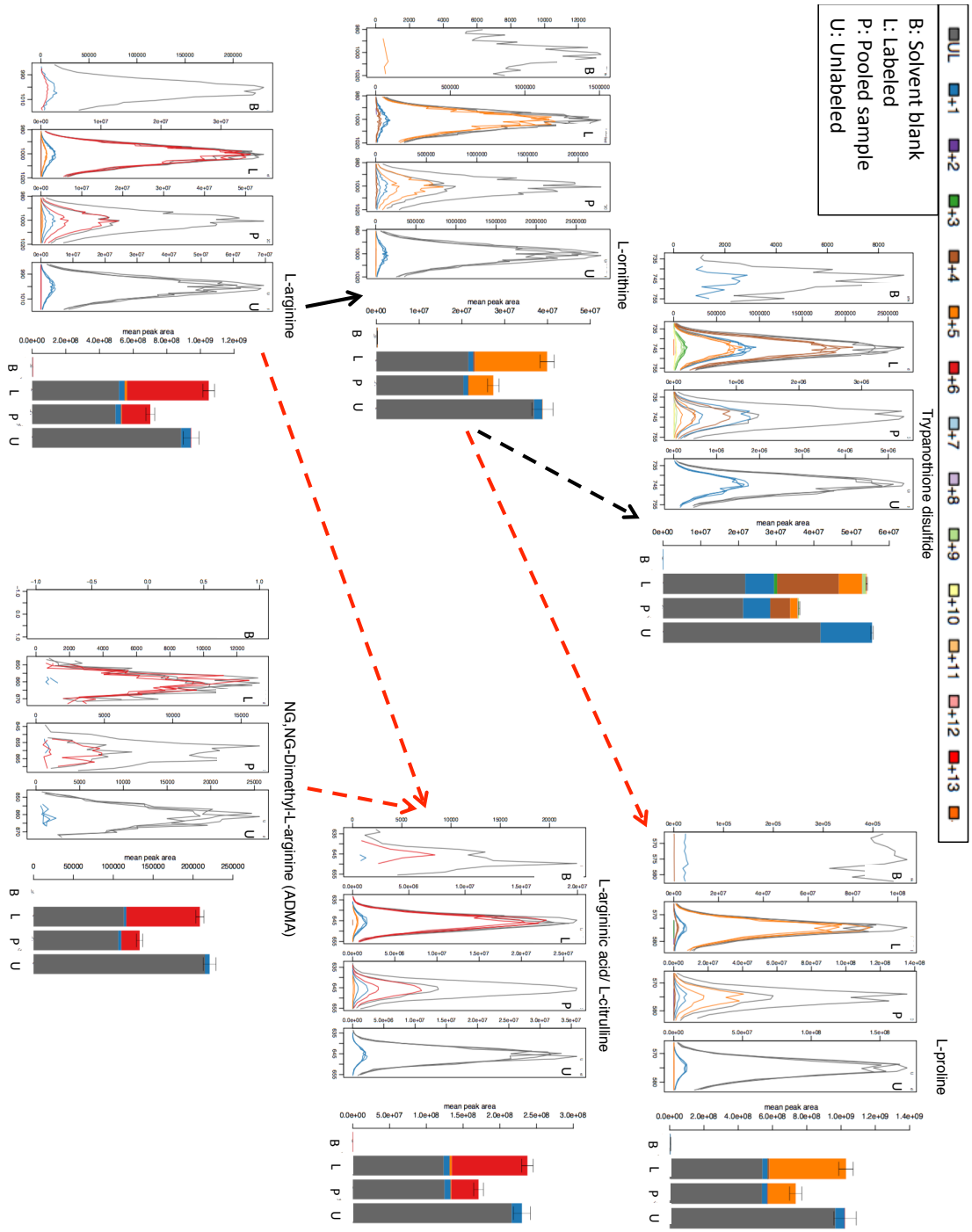

Figure 5-8: Stable isotope labelling of U-^{13}C-arginine metabolism in *L. mexicana* promastigotes. Data is from negative mode and panel on right represents the peak that has the denoted number of labelled carbons. These samples are from the procyclic promastigote (48 hours). As it was not possible to differentiate between L-argininic acid and L-citrulline in this experiment, the two names have been assigned to the same peak. Note that is not possible to differentiate between symmetric and asymmetric dimethylarginine on our LC-MS platform.

5.2.2.1 Origin of intracellular proline

A previous study has reported that *L. donovani* parasites preferentially import L-proline to use as an intracellular energy reservoir (Mazareb *et al*. 1999). This is thought to be necessary in promastigotes as L-proline is reported to be more

abundant in the fly, which uses it for flight (Mazareb *et al*. 1999). However, evidence for abundance of L-proline has only been reported in Tsetse fly (Bursell 1966). In our data, however it is apparent that the majority of L-proline originates from L-arginine. Previous studies used Earl's balanced salt solution in contrast to the rich medium (HOMEM) used here, which might explain some differences. Additionally, if the ratio of L-arginine to L-proline were different i.e. as reported in the fly, this might be expected to change the uptake of each. Nevertheless, when both amino acids are present, L-arginine is the consumed amino acid for *Leishmania* promastigotes.

5.2.3 Arginine metabolism in axenic amastigotes

In order to determine if arginine metabolism was similar in intracellular amastigotes as in promastigotes the above approach was applied to axenic amastigotes. Briefly parasites were transformed and cultured according to a well-established protocol (Bates *et al*. 1992) (**2.6.3**). Axenic amastigotes were grown for 72 hours in medium containing 50% $U^{13}C$-L-arginine. In addition to this, medium samples as well as fresh medium samples were analysed by LC-MS. The latter samples allowed us to confirm previous findings as well as demonstrate that the activity responsible for generating L-argininic acid is not present in serum though there is a small fraction of this mass present in labelled fresh media.

An example of such a reaction can be seen in **Figure 5-9** where arginase activity present in the serum is responsible for the generation of 5-($U^{13}C$)-labelled L-ornithine. In the case of axenic amastigotes, less L-proline is derived from L-arginine when compared to promastigotes. Whether this reflects increased L-proline uptake or the axenic amastigotes generally less profligate metabolic state remains to be determined. Finally fresh and spent media samples from the **5.2.2** were re-run using the longer LC protocol to determine if the parasites do or do not make L-citrulline and no difference were detected (**Supplementary Figure 5-4**).

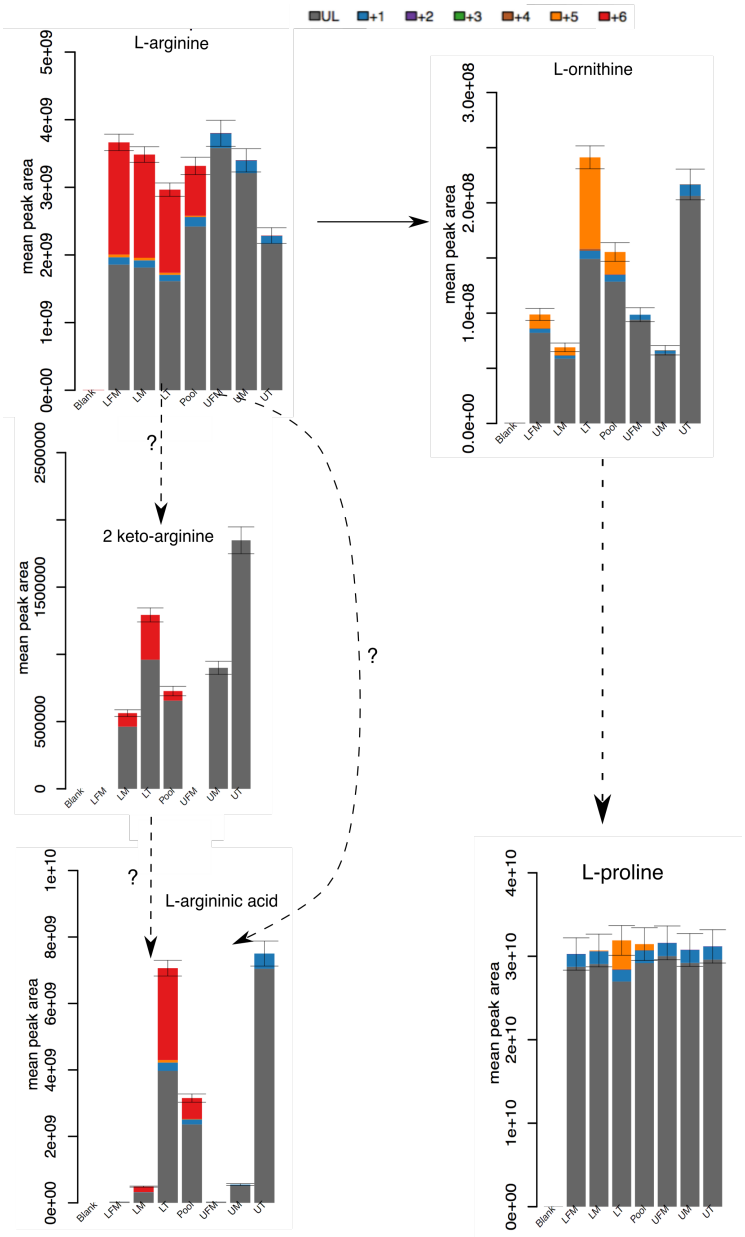

Figure 5-9: Arginine metabolism in axenic amastigotes. L-argininic acid is generated from L-arginine in this life stage and is not explained by serum activity. Less L-proline is labelled when compared to promastigotes. Dashed lines represent hypothetical (?) or multi-step reactions. The abbreviations used are as follows; Solvent blank = Blank, Labelled fresh medium = LFM, Labelled spent medium = LM, Labelled intracellular content = LT, Pool sample= Pool, Un-labelled fresh medium = UFM Un-labelled intracellular content = UT, Un-labelled spent medium = UM, and Un-labelled intracellular content = UT. Cells were cultured for 72 hours.

5.2.4 A stable labelled metabolomics separates isomers

While it was possible to separate L-argininic acid and L-citrulline using a longer LC method, and confirm this using authentic standards, the L-argininic acid was ordered as a one off custom synthesis and thus not widely applicable. To address this, (guanido$^{15}N_2$)-L-arginine (Cambridge Isotope Laboratory, Inc, enrichment 98%, cat: NLM-395-0.5), which is commonly used as a tracer of iNOS activity, was

purchased. The reasoning behind this is that if L-arginine were converted to L-argininic acid, oxygen exchange would occur at the opposite end of the amino acid, thus the product would retain two-labelled nitrogens. On the other hand, the conversion of L-arginine to L-citrulline occurs at the guanido-end of L-arginine and thus L-citrulline should be single nitrogen labelled. The net result of this is that the two metabolites can be separated by mass. Mid-log procyclic promastigotes were grown in 50% labelled medium in combination the long LC method here to see if naturally abundant 1-^{15}N-labelled-L-argininic acid masked 1-^{15}N-labelled-L-citrulline or *vice versa*.

Approximately 50% of L-argininic acid was not labelled which reflects roughly the expected 50% labelling (**Figure 5-10**). As mentioned above in **5.2.2**, some L-citrulline may be formed by serum. It is likely that a protein such as NOS, that is present in the heat-inactivated serum, retains enough activity to do this. It is important to state that the different peak height observed for L-argininic acid was much larger and L-citrulline either is at a low intensity or hidden by the much larger L-argininic acid peak. Therefore is seems that the vast majority of L-arginine is metabolised to L-argininic acid. Note, however, that though when examining the authentic standards for both (100 μM each), the peak for L-argininic acid is much larger than that of L-citrulline (**Supplementary Figure 5-5)** so differences in peaks need not necessarily correspond to differences in concentrations but reflecting differential ionisation. Nevertheless, as mentioned above, L-citrulline production is not different between fresh and spent medium (**Supplementary Figure 5-4**) so it seems unlikely the parasites produce any.

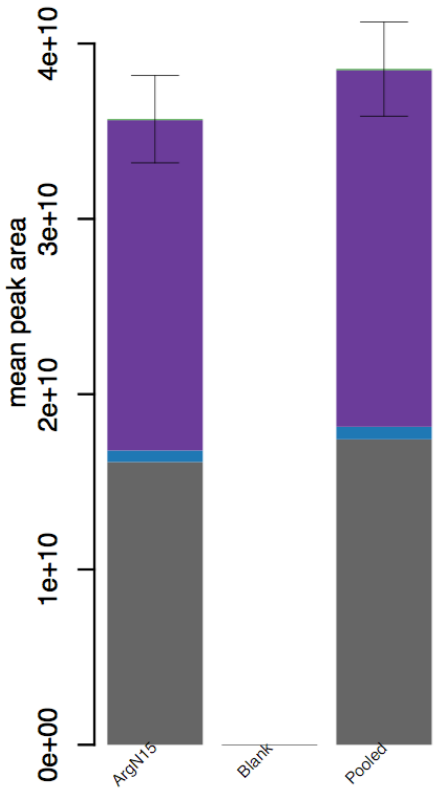

Figure 5-10: 5-11: 50%-(guanido$^{15}N_2$)-L-arginine LC-MS profiling of *L. mexicana* procyclic promastigotes. Averages from three biological replicates are shown. Purple is 2 x ^{15}N-labelled, Blue is 2 x ^{15}N-labelled and grey is non-labelled metabolite matching the L-argininic acid in retention time. Graph was made using mzMATCH-ISO (from Fiona Achcar).

5.2.5 Fragmentation analysis of *Leishmania* infected macrophages with authentic L-citrulline and L-argininic acid standards

L-argininic acid was purchased (American Custom Chemical Corporation) and rerun with labelled samples and with the samples described in **Chapter 4**. Authentic standard mixes are routinely run as part of Glasgow Polyomics services and L-citrulline is one of these. Fragmentation (MS_2) was carried out on the standards and pooled samples. The result of this analysis on infected macrophage (FACS enriched) samples is shown in **Figure 5-11.** This sample is chosen as L-citrulline from the macrophage and L-argininic acid from the parasite is present. The fragmentation spectrum for these peaks is shown and expected fragments are indicated. In the case of the blue coloured formula, it points to the first fragment while the red coloured formula is a subsequent fragment of this.

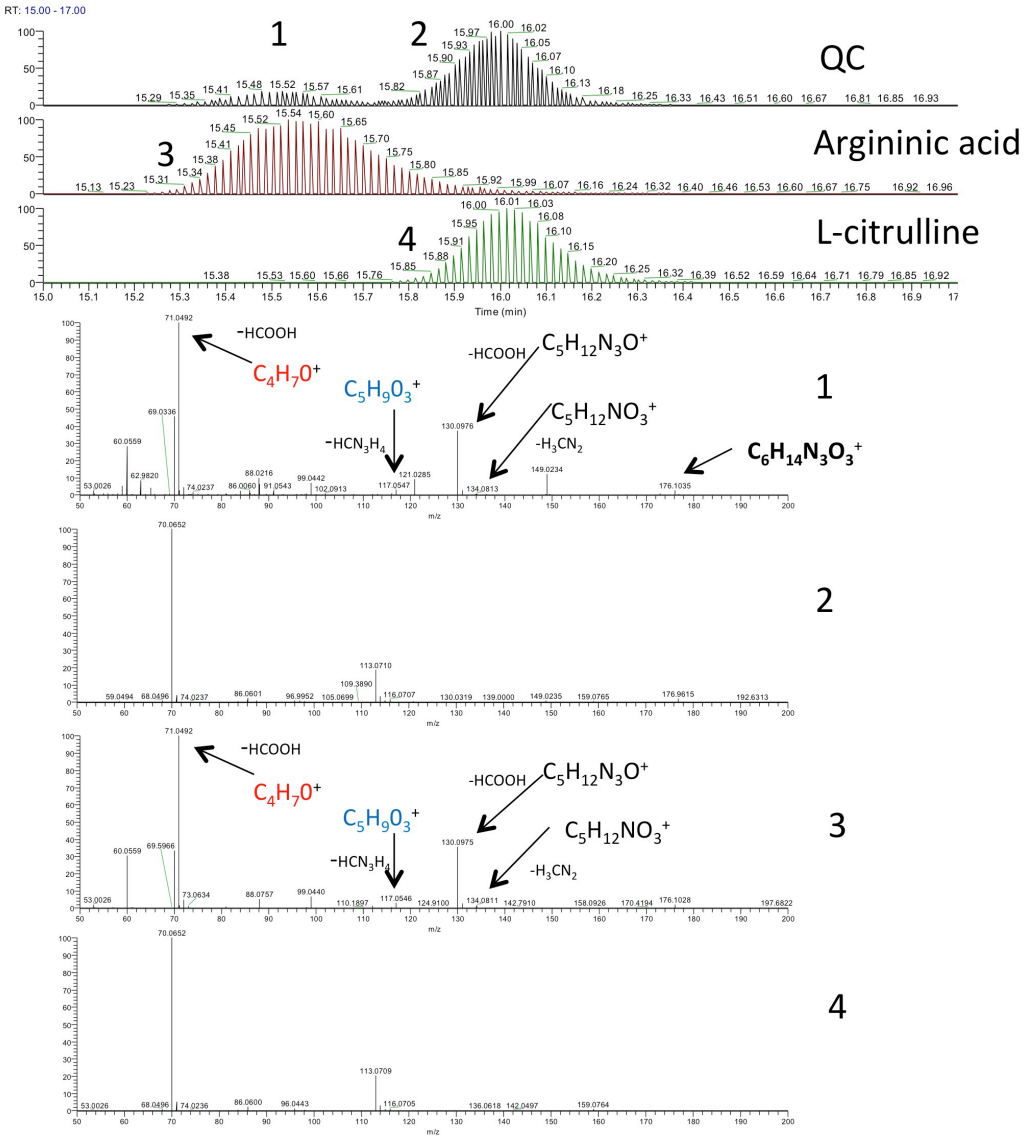

Figure 5-12: MS_2 analysis of L-argininic acid and L-citrulline present in pooled sample from FACs enriched infected macrophages experiment (Chapter 4). Samples and authentic standards are as indicated (note that L-citrulline is part of a standard mix routinely run by Glasgow Polyomics). MS_2 spectra are shown for the parent mass (bold) from the indicated peaks. The formula in blue coloured font is an instance where a fragment was subsequently fragmented to yield the formula in red coloured font.

5.2.6 Multiplex cytokine profiling of L-argininic acid treated M1 macrophages

One hypothesis about a function for L-argininic acid is that its synthesis results in the depletion of the substrate of *iNOS*, L-arginine. Given the importance of arginine metabolism for M1 macrophages it is possible that a metabolite that is produced by the degradation of L-arginine could interfere with general M1 effector functions. It is also of interest whether the product of L-lysine degradation that were found in macrophages infected with parasites only, L-pipecolic acid might also be immunomodulatory. In order to test these

hypotheses, the Luminex murine multiplex assay (Invitrogen) was used to see if either pre- or simultaneous incubation of BMDM with L-argininic acid or L-pipecolic acid could inhibit the LPS mediated increase of pro-inflammatory cytokines (**2.8.2**). Some of the M0, M1 and M2 controls in this assay were presented in **Chapter 4**. Note that an MTT assay (**2.8.4**) was first used to ensure that compounds were not toxic at levels tested (**Supplementary Figure 5-6).** As 4 biological replicates were used, a repeated measure one-way ANOVA with Dunnett's multiple comparisons test was used in Prism6 (Graphpad). No such inhibition was observed. Unexpectedly an increase was seen in the case of monocyte chemoattractant protein 1 (MCP-1 (CCL2), denotes $P \leq 0.01$, FC = ~1.7) (**Figure 5-12**). In the introduction it was mentioned how certain pathogenic strains of *Leishmania* (including *L. mexicana*) release the gp63 protease which causes an NF-κB cleavage resulting in a novel heterodimer that translocate to the nucleus, driving expression of pro-inflammatory cytokines such as CXCL2, CCL2, CCL3 and CCL4 (Gregory *et al*. 2008). A potential explanation would be that the parasites use L-argininic acid to recruit further macrophages to infect. However, further work will need to be done such as seeing if L-argininic acid on its own can increase CCL2 levels. Whether L-argininic acid can efficiently (if at all) traverse the macrophage membrane remains to be determined. Unfortunately at the concentrations used here, L-argininic acid is detected in the Griess assay (possibly due to contaminating L-arginine in commercial sample) while no effect was seen at lower concentrations.

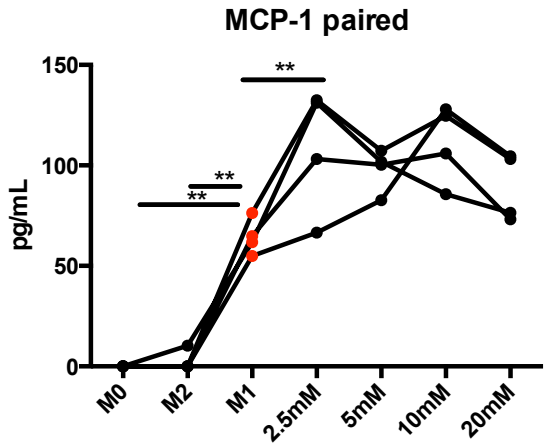

Figure 5-13: Luminex profile of MCP-1. Matching paired values from 4 biological replicates are shown. BMDM were incubated overnight with the indicated amount of L-argininic acid prior to 6 hour stimulation with LPS (100 ng/mL) Significance was determined using a repeated measure one-way ANOVA with Dunnett's multiple comparisons test was used in Prism6 (Graphpad). ** denotes $P \leq 0.01$.

5.3 Synthesis of 2 keto-arginine

As it was not possible to purchase 2 keto-arginine, it was synthesised in order to confirm the identity of the metabolite in our LCMS data. This metabolite has quite low intensity so identification by MS_2 is not suitable. Furthermore, this compound may be useful if it is an intermediate in L-argininic acid synthesis, and a candidate enzyme is isolated, it will be required as a substrate. Synthesis was carried out based on a method described by (Wellner & Meister 1960) (**2.9.1**). Briefly; dried snake venom (Sigma) from the *Crotalus adamanteus* (Eastern diamondback rattlesnake) was used as a source of L-amino oxidase alongside its cofactor FAD. Catalase (Sigma) was used to prevent 2 keto-arginine being attacked by the reactions by-product, hydrogen peroxide. L-amino oxidase catalyses the following reaction:

$$\text{L-amino acid} + H_2O + O_2 \text{ <-> A 2 oxo-acid} + NH_3 + H_2O_2$$

In **Figure 5-13,** the LC-MS analysis of the product of this reaction is shown as well as an enzyme-only and solvent blank controls. The mass spectrum on the bottom panel shows masses present in the indicated retention time in the enzyme plus substrate sample. There is only one peak with this mass and it is apparent in the total ion chromatograph (TIC) for positive mode that this mass is the most abundant mass in the sample. The naturally present 1-C_{13} secondary peak is also visible in the spectrum (mass = 174.0872 + 1.00335 = 175.08055). Additionally, this peak is 6.56% as abundant as the parent peak which matches well with the expected abundance (1.109% [C_{13} abundance] x 6 = 6.65%). When run alongside *Leishmania* samples the synthesised 2 keto-arginine was shown to co-elute with a peak of the same mass indicating that indeed this molecule is present in *Leishmania* (Clement Regnault: *L. mexicana* and Emily Armitage: *L. donovani*, personal communication).

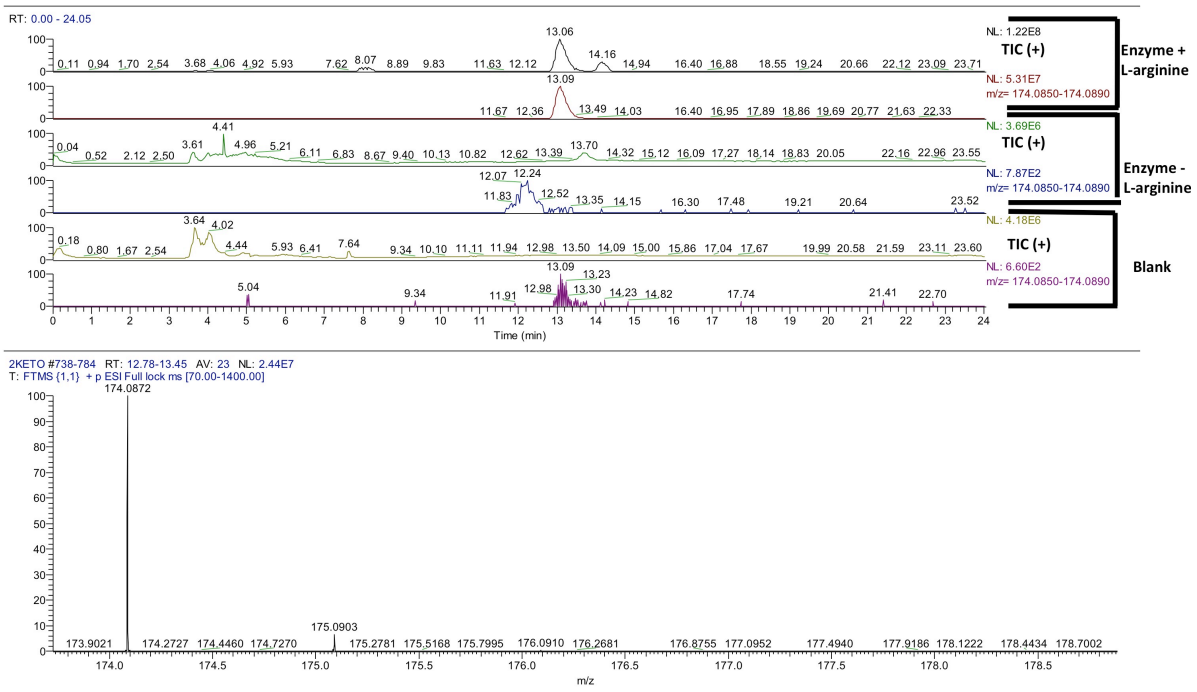

Figure 5-14: LC-MS analysis of synthesised 2 keto-arginine. Samples are as indicated and the total ion chromatograph (TIC), mass ranges, and mass spectrum are all positive mode. Figure was made using Xcalibur (Thermo). The peak at retention time 13.06-13.09 (minutes) is 2 keto-arginine. L-arginine (not shown) had a retention time of 21.3 (minutes).

5.4 Discussion

While it well established that L-arginine is both essential to *Leishmania* parasites and is indispensible to the pro-inflammatory M1 macrophage, its fate in the parasite is not fully understood. The reporting of L-argininic acid synthesis by multiple Leishmania species by Westrop *et al* and the work here shows that there is much more research needed on this subject. While previous studies have reported NOS activity in Leishmania (Basu *et al*. 1997; Genestra *et al*. 2006), the use of stable isotope labelling here strongly indicate that detected L-citrulline is an incidental artefact of bovine NOS present in serum.

Amino acids can be used in energy metabolism and it has been reported that *L. mexicana* promastigotes have several amino acid transporters that preferentially import L-proline to use it as an intracellular energy reservoir (Mazareb *et al*. 1999). It is shown here that L-arginine is preferentially taken up by *L. mexicana* promastigotes and that it is the main source of L-proline in our culture conditions. This does not occur to the same extent in axenic amastigotes but whether is due to increased L-proline uptake or the amastigotes lipid-dependent and generally less profligate metabolic state (Saunders *et al*. 2014) is

not clear. It is important to mention that L-proline use was previously thought to be more relevant to promastigotes due to supposed L-proline abundance in the tsetse fly (Bursell 1966). Whether the same for the sandfly remains to be tested. Based on the experiments presented in this chapter the current model of arginine metabolism in *Leishmania* has been expanded (**Figure 5-15).** Some new pathways are shown in **Figure 5-15** involve enzymes that should be studied further to determine their importance and possible therapeutic targeting.

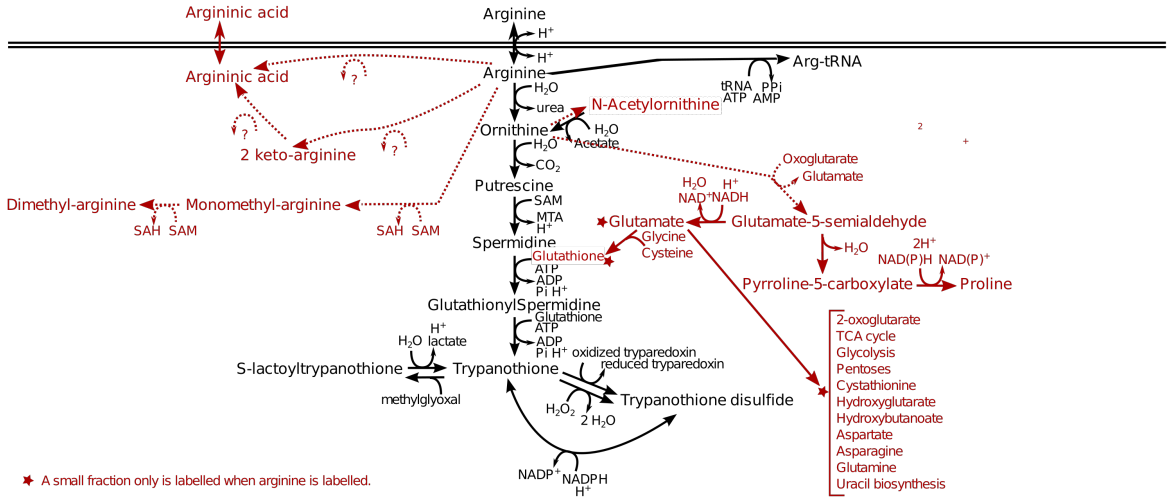

Figure 5-15: Summary of utilisation of L-argininic acid by *L. mexicana*. In black are previously experimentally validated pathways. In red are pathways that have been validated by the stable-labelled isotope experiments described in the current chapter. Dashed lines indicate multistep or hypothetical (?) reactions.

5.4.1 Argininic acid, waste, effector or biomarker

Argininic acid has most commonly being referred to in the context of human disease where there are defects in known arginine-metabolism related enzymes (C. G. da Silva *et al*. 1999; Livesay *et al*. 2008). These defects are arginase deficiency and have been confirmed using arginase knockout mice. These studies proposed that a transamination reaction produces 2 keto-arginine from L-arginine and that the 2 keto-arginine is subsequently hydrogenated to L-argininic acid. However, the enzymes that are responsible for these reactions are unknown. While argininic acid may be an incidental product of L-arginine degradation, it has been reported that L-argininic acid can inhibit iNOS activity (IC_{50} 388.0 ± 46.5 μM) (Grant *et al*. 1998). It will be interesting to know whether L-argininic acid produced by *Leishmania* parasites can reach these levels and if its synthesis, in combination with host and parasite arginase activity, lowers

L-arginine levels enough to affect iNOS efficiency. The detection of this metabolite in a previous study (Westrop *et al*. 2015) and detailed and robust analysis presented here show that it exists in the context of pathogenic infections. Finally, as it is shown here that, host cells do not produce this metabolite; the possibility of its use as a biomarker should be explored further.

5.4.2 Future directions

Given that so little is known about L-argininic acid, it will require substantial work to elucidate the enzyme responsible for its synthesis. Additionally, there is no evidence that 2 keto-arginine is an intermediate in its synthesis. While it would be possible to add 2 keto-arginine to cell extract, it is quite possible that the transaminase reaction that makes it is reversible. Thus 2 keto-arginine would be converted back to L-arginine and if another enzyme was responsible, it would convert it to L-argininic acid. Interestingly 2 keto-arginine and other keto-acids have been reported to be able to scavenge reactive oxygen species (Nath *et al*. 1995) and this itself warrants further work. The current study is limited by the fact that the only way of detecting L-argininic acid is by LC-MS, which is time-consuming and expensive, so ideally a cheap and quick colorimetric assay would aid future work. If L-argininic acid has potential to be used biomarker, pilot studies using murine infection models should be carried out.

6 General discussion

6.1.1 The Omics, future applications

The advent of Omics techniques has seen an exponential growth in the amount of biological data at a systems level. This includes genomics, transcriptomics, proteomics and metabolomics. Additionally, there is a myriad of '-Omics' terms used to describe the different levels of regulation of the above such as the methylome and epigenome. These approaches offer unprecedented ability to capture detailed information across the different levels that make up complex biological systems.

The application of these techniques has moved beyond examining single species (i.e. DNA sequencing of different species) to complex disease scenarios such as host-pathogen interactions in isolated cellular systems or even whole organisms. Examples of this include studies searching for single nucleotide polymorphisms (SNPS) that are associated with disease or disease susceptibility, or studies searching for metabolites that can serve as biomarkers/ risk factors of disease. An even more complex application is the use of the Omics to detect/model the mechanisms of disease. These diseases range from infectious disease such as *Leishmaniasis* to autoimmune diseases such as rheumatoid arthritis. The starting point for such studies is simple *in vitro* systems that use limited and well-defined inputs and outputs. The overarching aim of this protect was to apply Omics techniques to a classical systems (the M1 macrophage), building on previous studies in order to use the established techniques to detect/model the mechanisms of *Leishmania* manipulation of its host cell, the macrophage.

6.1.2 Metabolic profiling of classical M1 macrophages: new insight

In this project a robust protocol for the extraction of macrophages that offers high coverage of the macrophage metabolome was developed. In **Chapter 1** the phenomenon of immune-metabolism was introduced alongside some of the hallmarks of inflammatory macrophage metabolism. While it can be argued that using a single inflammatory stimulus reduces biological noise, several studies have used the single stimulus (LPS) (Tannahill *et al*. 2013) or a combination of stimuli (IFNγ and LPS) (Jha *et al*. 2015; Lampropoulou *et al*. 2016) to obtain a

phenotype to profile. These studies have not examined what each stimulus does nor how they interact.

This is, to our knowledge, the first study to examine the contribution of each factor and how each stimulus can enhance or inhibit the other. The linear model used here will also be applicable to other systems of where combinations of inputs used. An example of this is combinatorial medical treatments or models of infection of host with multiple species.

In the context of the inflammatory macrophage, well-established metabolic features include the presence of the Warburg shift in conjunction with rapidly upregulated glucose uptake and flux through glycolysis. Increased flux through the pentose phosphate pathway for the purpose of generating NADPH and ribonucleotide precursors is another key feature (Haschemi *et al*. 2012). Finally, perturbations of the TCA cycle such as increases in both itaconate production and succinate have been shown to be essential for M1 macrophage functions (Lampropoulou *et al*. 2016).

The protocol used in this project consistently showed perturbations in these key pathways showing that our methodology can and does detect biologically relevant processes. At this point the author would like to stress that while confidence in metabolite identifications can be strengthened by use of authentic standard and fragmentation, many metabolites are solely identified by accurate mass and predicted retention time and thus are only **putatively identified**. This is clearly denoted throughout this thesis.

No previous study has investigated if immune stimuli act synergistically, additively or antagonistically. An immediate and obvious test of this would be *iNOS* activity. The action of this enzyme requires synergistic activity from IFNγ and LPS. Additionally, the incidental product of this enzyme, L-citrulline, is a key part of the arginino-succinate shunt that replenishes the fragmented (anapleurotic) TCA cycle. Our LM correctly calls L-citrulline as being exclusively dependent on the interaction of IFNγ and LPS. Next, pathways that have not been examined in detail in the context of immune-metabolism were interrogated.

Two metabolites/pathways that were strongly modulated by IFNγ were taurine and ß-alanine. Interestingly both of these have previously been shown to prevent apoptosis and modulate lipid metabolism and in some instances this involves signalling pathways modulated by IFNγ (Prabha *et al*. 1988; Harris *et al*. 2008; Kim *et al*. 2009d). Lipid metabolism has previously been identified as important for M2 macrophages (Huang *et al*. 2014). However a recent study using macrophages deficient in a key enzyme in this pathway, carnitine palmitoyltransferase 2 (Cpt2), found that while the cells could not undergo fatty acid oxidation (FAO), this was not required for M2 polarisation (Nomura *et al*. 2016). LPS driven perturbation of carnitine related metabolites were detected, some of which were repressed by IFNγ. Given the uncertainty about the role of FAO in macrophage polarisation, further work will be needed to elucidate the biological relevance of this.

The engagement of a transcriptional profile is expected to require increased nucleotide synthesis and consumption. Changes in the pathways of purine and pyrimidine metabolism were also detected. Interestingly these changes are not consistent within pathways and stimulus-specific increases are not uniform. Guanine and inosine have been shown to modulate cell function so it will be interesting to determine if they have a similar role in inflammation (Verghese & Snyderman 1983; Jonsson & Carlsten 2002). Finally, there were two modified nucleotide analogues that had altered levels; 5'-methyl-2'deoxycytidine (marker of *de-novo* DNA methylation: decreased by all stimuli) and 3-methyguanine (altered in leukaemia, tumours and immunodeficiency: increased by all stimuli). Whether these changes potentially are new examples of metabolites having roles outwith their biosynthetic pathway remains to be determined.

6.1.3 The *Leishmania* infected macrophage

Once a robust protocol was established, the next stem was to move from simple models of inflammation to a model of *Leishmania* infection of host cells. It is reasonable to expect this to be more representative of disease as pathogens engage multiple receptors on the host cell (Mosser *et al*. 1986). Furthermore, different host responses are engaged depending on the dose of stimulus used or the cell type. For instance in the case of LPS stimulation, primary human immune cells are more sensitive than primary murine immune cells which in turn

are more sensitive than cultured cell lines (Copeland *et al*. 2005; Schroder *et al*. 2012). Furthermore, use of LPS at high concentrations (≥1μg/mL) can result in apoptosis (Haase *et al*. 2003).

This is to our knowledge, the first application of integrative omics approaches to a pathogenic disease, which in this study is *Leishmania* infection. Here the high coverage of transcriptomics, our robust metabolomics protocol and a heat-killed antigen control are combined to gain a detailed insight into host-pathogen interactions. At a metabolite level, potential parasite specific metabolites stood out while glycerolipid and glycerophospholipid metabolism displayed a highly reproducible profile. These perturbations, in combination with transcriptome alterations in the same pathways as well as PPAR signalling can be used to inform further experiments of the key targets and processes to target.

Among the most significantly altered metabolites were, unsurprisingly, parasite specific metabolites. However, this is the first instance of *Leishmania*-macrophage samples being subjected to untargeted metabolic profiling using LC-MS. L-argininic acid, L-pipecolic acid, ovothiol A, 4-imidazolone-5-propanoate (Imidazole lactic acid: see text (4.3.2.1)) and trypanothione disulphide have previously been reported to be produced by multiple parasite species (Westrop *et al*. 2015). In the current study the author has shown that the parasite synthesis these metabolites within the macrophage and that neither naive macrophages nor polarised (M1 or M2) macrophages make them. Further *in vivo* studies will be required to investigate if these metabolites might serve as biomarkers indicative of the presence of *Leishmania*. If so, a simple and cheap assay can be developed to aid quick, easy and large-scale diagnostic screening.

On its own, the list of DE genes obtained from analysis of our transcriptomics data matches well with a recent transcription profiling of *Leishmania* infected human macrophages (Fernandes *et al*. 2016). As this study subtracted the effect of phagocytosis, the combination of these two data sets can help distinguish between antigenic, phagocytic and live parasite induced host perturbations.

While in the first result chapter there is list of marked perturbed metabolites, many of which are key to macrophage function. By including these controls it is obvious that *Leishmania* infection causes much less drastic alterations.

Interestingly, some previously reported changes (Jha *et al*. 2015) at a metabolite and transcript level are present in our data. Based on the results of our pathway analysis, it seems that the live parasite activates the TCA cycle, which is more in line with M2 macrophages while the heat-killed parasite up-regulates glucose metabolism, which is more in line with M1 macrophages. While significant, many of the increases and decreases were not very large (<1.5 fold) so their biological significance is not immediately obvious and further work will be required. It is important to note that the magnitude of some of these changes are not much less that those reported to be important for M1 macrophage function (i.e. succinate, Tannahill et a, 2012).

On both a metabolite and transcript level, perturbations in lipid metabolism were observed. This is particularly interesting seeing that *L. mexicana* parasites have been reported to enter into a stringent metabolic state, up-regulating the uptake of fatty acids (Saunders *et al*. 2014) While lipid metabolism in the context of fatty acid oxidation has been associated with M2 macrophages, the role of this process may be more complex than previously thought, as mentioned above (Nomura *et al*. 2016). In our metabolomics data, the heat-killed parasites cause increases also caused by M1 stimuli. At a transcript level, the live and heat-killed parasites causes distinct changes, with some of the most marked differences being in PPAR pathway, a key network in regulating lipid metabolism. More work is needed to dissect the role of this pathway the context of *L. mexicana*.

6.1.4 L-arginine: at the interface of host-parasite interactions

At the crux of host-parasite interactions, L-arginine has essential roles in determining whether disease progresses or is resolved. The reporting of L-argininic acid synthesis by multiple *Leishmania* species by Westrop *et al* showed that there is much to learn about L-arginine metabolism in the parasite. While previous studies have reported NOS activity in *Leishmania* (Basu *et al*. 1997; Genestra *et al*. 2006), the use of stable isotope labelling here strongly indicate that detected L-citrulline is an incidental artefact of bovine NOS present in serum.

A previous study reported that *L. mexicana* promastigotes and amastigotes have unique amino acid transporters that preferentially import L-proline to use as an intracellular energy reservoir (Mazareb *et al*. 1999). In the current study the author has shown that L-arginine is preferentially taken up by *L. mexicana* promastigotes and that it is the main source of intercellular L-proline in our culture conditions. Whether the reported L-proline abundance in the tsetse fly (Bursell 1966) applies to the sandfly remains should be tested, but it seems that profound physiological differences exist between these dipteran insects.

Finally, the use of stable isotope labelling presented here gives strong confirmation of the synthesis of L-argininic acid by *Leishmania* parasites. While its presence has been reported in the context of human disease where there are defects in known arginine-metabolism related enzymes (C. G. da Silva *et al*. 1999; Livesay *et al*. 2008). These studies proposed that 2 keto-arginine was formed from the transamination of L-arginine and that the 2 keto-arginine is subsequently hydrogenated to L-argininic acid. However, the enzymes that are responsible for these reactions are unknown. Furthermore, there is no evidence to preclude the possibility of a direct conversion of L-arginine to L-argininic acid, and our data is consistent with both routes.

One previous study reported that L-argininic acid can inhibit iNOS activity (IC_{50} 388.0 ± 46.5 μM) (Grant *et al*. 1998). While the concentrations of L-argininic acid within the macrophage have not quantified in the current study, further work should be done to determine if it reaches these levels within the host cell and if its synthesis, in combination with host and parasite arginase activity, lowers L-arginine levels enough to effects iNOS activity.

Appendices

Supplementary File 2-1: MS^2 settings used in current study.

Supplementary File 2-2: Contains r code, Deseq2 session info (versions) used in this study as well as the final (including SPIA pathway analysis) and intermediate files.

Supplementary File 3-1: Kegg IDs and their equivalent metabolite name. Note that for metabolites without existing Kegg IDs, an arbitrary name was chosen (i.e., Nokegg1).

Supplementary File 3-2: Input file as used for analysis of MetaboAnalyst (ANOVA and PCA).

Supplementary File 3-3: Input file used for GLM analysis.

Supplementary File 3-4: Results of GLM, ANOVA and there overlap is shown. Metabolites where significance was reported for only one method are coloured in red. For significantly altered metabolites in the GLM results (second tab), maximum fold change, and Venn class information is shown. In the Zero column, metabolites that were absent from one condition are indicated as a NA.

Supplementary File 3-5: Script used to implement GLM. A text file with the samples in rows is required. The first column can have the header sample, the second row is IFN, third is LPS, and after this are the metabolites and their intensities. 0 and one denote presence or absence of these stimuli (Ex: M0 is 0, 0; IFN is 1, 0; LPS is 0, 1; and IFN_LPS is 1, 1).

Supplementary Figure 4-1: Results of FACS enrichment on Aria-I.

Supplementary File 4-1: Kegg IDs and their equivalent metabolite name. Note that for metabolites without existing Kegg IDs, an arbitrary name was chosen (i.e., Nokegg1). This is for non-FACS-sorted samples.

Supplementary File 4-2: Input file as used for analysis of MetaboAnalyst (ANOVA and PCA). This is for non-FACS-sorted samples.

Supplementary File 4-3: Results of ANOVA and multiple comparisons are shown. This is for non-FACS-sorted samples.

Supplementary File 4-4: Kegg IDs and their equivalent metabolite name. Note that for metabolites without existing Kegg IDs, an arbitrary name was chosen (i.e., Nokegg1). This is for FACS-sorted samples.

Supplementary File 4-5: Input file as used for analysis of MetaboAnalyst (ANOVA and PCA). This is for FACS-sorted samples.

Supplementary File 4-6: Results of ANOVA and multiple comparisons are shown. This is for FACS-sorted samples.

Supplementary Table 4-1: 26 genes unique to the LRT, DE (p adjusted (LRT) <0.5) genes, the Venn subset information, Log_2 fold change, normalised counts and gene description are available.

Supplementary Table 4-2: Same information as **Supplementary Table 4-1** but the Log_2 fold change revers to HV vs M0.

Supplementary Table 4-3: Overlap between current study and *Fernandes et al 2016* (**Figure 4-9**), Rabhi *et al* 2012.

Supplementary Table 4-4: Detailed results of SPIA analysis as conducted on Graphite.

Supplementary File 5-1: Full results of Phyre^2 analysis are presented in this file.

Supplementary File 5-2: Kegg IDs and their equivalent metabolite name. Note that for metabolites without existing Kegg IDs, an arbitrary name was chosen (i.e., Nokegg1).

Supplementary File 5-3: Input file as used for analysis of MetaboAnalyst (ANOVA and PCA).

Supplementary File 5-4: Results of ANOVA and multiple comparisons are shown.

Supplementary Figure 5-1: Alignment of ADI from *Mycoplasma arginini*, *Mycoplasma hominis*, *Clostridium perfringens*, *Pseudomonas aeruginosa* and *Pseudomonas putida* with *Lmxm.08.1225*. Purple represent key conserved sequence motifs among ADIs. Green are residues involved in binding of the substrate and/or catalysis.

Supplementary Figure 5-2: Phylogenetic analysis of all *Lmxm.08.1225* alongside ADI genes, all DDAH genes with human NOS2 set as an out-group.

Supplementary Figure 5-3: A and B are results of 2'5' ADP agarose) chromatography purification. A: Elutions are as described in methods. B: Results of subsequent anion exchange chromatography. Elutions are as described in methods. Most abundant proteins are highlighted.

Supplementary Figure 5-4: Comparison of the authentic standards for both L argininic acid and L-citrulline (100μM each).

Supplementary Figure 5-5: Comparison of the L-citrulline and L-argininic acid levels in fresh and spent medium samples.

Supplementary Figure 5-6: Results of MTT assay was first used to ensure that compounds (L-pipecolic acid and L-argininic acid) were not toxic at levels tested

List of References

Abramson, S. & Gallin, J., 1990. Il-4 Inhibits Superoxide Production by Human Mononuclear Phagocytes. *Journal of Immunology*, 144(2), pp.625–630.

Afgan, E. *et al.*, 2016. The Galaxy platform for accessible, reproducible and collaborative biomedical analyses: 2016 update. *Nucleic Acids Research*, 44(W1), pp.W3–W10.

Aga, E. *et al.*, 2002. Inhibition of the spontaneous apoptosis of neutrophil granulocytes by the intracellular parasite *Leishmania major*. *Journal of Immunology*, 169(2), pp.898–905.

Aken, B.L. *et al.*, 2016. The Ensembl gene annotation system. *Database*, 2016, p.baw093.

Alexander, J., Satoskar, A.R. & Russell, D.G., 1999. *Leishmania* species: models of intracellular parasitism. *Journal of Cell Science*, 112 Pt 18, pp.2993–3002.

Alvar, J. *et al.*, 2012. Leishmaniasis worldwide and global estimates of its incidence. *PLoS ONE*, 7(5), p.e35671.

Anders, S., Pyl, P.T. & Huber, W., 2015. HTSeq--a Python framework to work with high-throughput sequencing data. *Bioinformatics (Oxford, England)*, 31(2), pp.166–169.

Andrews, S., 2010. Babraham Bioinformatics - FastQC A Quality Control tool for High Throughput Sequence Data. *bioinformatics.babraham.ac.uk*. Available at: http://www.bioinformatics.babraham.ac.uk/projects/fastqc

Aslett, M. *et al.*, 2009. TriTrypDB: a functional genomic resource for the Trypanosomatidae. *Nucleic Acids Research*, 38(Database), pp.D457–D462.

Babaev, V.R. *et al.*, 1999. Macrophage lipoprotein lipase promotes foam cell formation and atherosclerosis in vivo. *Journal of Clinical Investigation*, 103(12), pp.1697–1705.

Bain, C.C. *et al.*, 2016. Long-lived self-renewing bone marrow-derived macrophages displace embryo-derived cells to inhabit adult serous cavities. *Nature communications*, 7, p.ncomms11852.

Banerjee, S. *et al.*, 2016. Attenuated *Leishmania* induce pro-inflammatory mediators and influence leishmanicidal activity by p38 MAPK dependent phagosome maturation in *Leishmania donovani* co-infected macrophages : Scientific Reports. *Scientific Reports*, 6(22335), pp.1–14.

Basu, N. *et al.*, 1997. Isolation of a nitric oxide synthase from the protozoan parasite, *Leishmania donovani*. *FEMS Micobiology Letters*, 156, pp.43–47.

Bates, P. *et al.*, 1992. Axenic cultivation and characterization of *Leishmania mexicana* amastigote-like forms. *Parasitology*, (105), pp.193–202.

Bayarsaihan, D., 2016. Epigenetic mechanisms involved in modulation of inflammatory diseases. *Current Opinion in Clinical Nutrition and Metabolic*

Care, 19(4), pp.263–269.

Belkaid, Y. *et al.*, 2000. A Natural Model of *Leishmania major* Infection Reveals a Prolonged "Silent" Phase of Parasite Amplification in the Skin Before the Onset of Lesion Formation and Immunity. *The Journal of Immunology*, 165(2), pp.969–977.

Berrow, N.S. *et al.*, 2007. A versatile ligation-independent cloning method suitable for high-throughput expression screening applications. *Nucleic Acids Research*, 35(6), p.e45.

Bern, C. et al., 2008. Complexities of Assessing the Disease Burden Attributable to Leishmaniasis. PLoS Nehlected Tropical Diseases, 2(10), pp. -e313

Bhandari, V. *et al.*, 2012. Drug Susceptibility in *Leishmania* Isolates Following Miltefosine Treatment in Cases of Visceral Leishmaniasis and Post Kala-Azar Dermal Leishmaniasis. *PLoS Neglected Tropical Diseases*, 6(5), pp.–e1657.

Bird, L.E., 2011. High throughput construction and small scale expression screening of multi-tag vectors in Escherichia coli. *Methods*, 55(1), pp.29–37.

Bird, L.E. *et al.*, 2013. Application of In-Fusion™ Cloning for the Parallel Construction of *E. coli* Expression Vectors. In *Methods in Molecular Biology*. Methods in Molecular Biology. Totowa, NJ: Humana Press, pp. 209–234.

Blankenberg, D. *et al.*, 2014. Dissemination of scientific software with Galaxy ToolShed. *Genome biology*, 15(2), p.403.

Brittingham, A. *et al.*, 1995. Role of the *Leishmania* surface protease gp63 in complement fixation, cell adhesion, and resistance to complement-mediated lysis. *Journal of Immunology*, 155(6), pp.3102–3111.

Buchmüller-Rouiller, Y. & Mauël, J., 1987. Impairment of the oxidative metabolism of mouse peritoneal macrophages by intracellular *Leishmania* spp. *Infection and Immunity*, 5(3), pp.587–593.

Bursell, E., 1966. Aspects of the flight metabolism of tsetse flies (*Glossina*). *Comparative Biochemistry and Physiology*, 19(4), pp.809–818.

Buxbaum, L.U., 2015. Interleukin-10 from T Cells, but Not Macrophages and Granulocytes, Is Required for Chronic Disease in *Leishmania mexicana* Infection J. A. Appleton, ed. *Infection and Immunity*, 83(4), pp.1366–1371.

Buxbaum, L.U. *et al.*, 2003. Cysteine protease B of *Leishmania mexicana* inhibits host Th1 responses and protective immunity. *Journal of Immunology*, 171(7), pp.3711–3717.

Camargo, E.P. *et al.*, 1978. *Trypanosoma* spp., *Leishmania* spp. and *Leptomonas* spp.: Enzymes of ornithine-arginine metabolism. *Experimental Parasitology*, 46(2), pp.141–144.

Cameron, P. *et al.*, 2004. Inhibition of lipopolysaccharide-induced macrophage IL-12 production by *Leishmania mexicana* amastigotes: The role of cysteine peptidases and the NF-kappa B signaling pathway. *Journal of Immunology*,

173(5), pp.3297–3304.

Carlsen, E.D. *et al.*, 2015. Interactions between Neutrophils and *Leishmania braziliensis* Amastigotes Facilitate Cell Activation and Parasite Clearance. *Journal of innate immunity*, 7(4), pp.354–363.

Carvalho, L.P. *et al.*, 2012. Lymph node hypertrophy following *Leishmania major* infection is dependent on TLR9. *The Journal of Immunology*, 188(3), pp.1394–1401.

Casgrain, P.-A. *et al.*, 2016. Cysteine Peptidase B Regulates *Leishmania mexicana* Virulence through the Modulation of GP63 Expression. *PLoS Pathogens*, 12(5), p.e1005658.

Charmoy, M., Auderset, F., *et al.*, 2010. The Prominent Role of Neutrophils during the Initial Phase of Infection by *Leishmania* Parasites. *Journal of Biomedicine and Biotechnology*, 2010(2), pp.1–8.

Charmoy, M., Brunner-Agten, S., *et al.*, 2010. Neutrophil-Derived CCL3 Is Essential for the Rapid Recruitment of Dendritic Cells to the Site of *Leishmania major* Inoculation in Resistant Mice. *PLoS Pathogens*, 6(2), pp.–e1000755.

Chokkathukalam, A. *et al.*, 2013. mzMatch–ISO: an R tool for the annotation and relative quantification of isotope-labelled mass spectrometry data. *Bioinformatics (Oxford, England)*, 29(2), p.281.

Chouchani, E.T. *et al.*, 2014. Ischaemic accumulation of succinate controls reperfusion injury through mitochondrial ROS. *Nature*, 515(7527), pp.431–435.

Conceição, J. *et al.*, 2016. Characterization of Neutrophil Function in Human Cutaneous Leishmaniasis Caused by *Leishmania braziliensis*. *PLoS Neglected Tropical Diseases*, 10(5), pp.e0004715–e0004715.

Copeland, S. *et al.*, 2005. Acute Inflammatory Response to Endotoxin in Mice and Humans. *Clinical and Vaccine Immunology*, 12(1), pp.60–67.

Cox, F.E.G., 2002. History of human parasitology. *Clinical microbiology reviews*, 15(4), pp.595–612.

Creek, D.J. *et al.*, 2012. IDEOM: an Excel interface for analysis of LC-MS-based metabolomics data. *Bioinformatics (Oxford, England)*, 28(7), pp.1048–1049.

Croft, S.L. & Olliaro, P., 2011. Leishmaniasis chemotherapy--challenges and opportunities. *Clinical microbiology and infection : the official publication of the European Society of Clinical Microbiology and Infectious Diseases*, 17(10), pp.1478–1483.

Cubbon, S. *et al.*, 2010. Metabolomic applications of HILIC-LC-MS. *Mass Spectrometry Reviews*, 29(5), pp.671–684.

da Silva, C.G. *et al.*, 1999. In vitro inhibition of Na+,K+-ATPase activity from rat cerebral cortex by guanidino compounds accumulating in hyperargininemia.

Brain Research, 838(1-2), pp.78–84.

da Silva, R. & Sacks, D.L., 1987. Metacyclogenesis is a major determinant of *Leishmania* promastigote virulence and attenuation. *Infection and Immunity*, 55(11), pp.2802–2806.

Di Palma, S. *et al.*, 2011. Zwitterionic hydrophilic interaction liquid chromatography (ZIC-HILIC and ZIC-cHILIC) provide high resolution separation and increase sensitivity in proteome analysis. *Analytical Chemistry*, 83(9), pp.3440–3447.

Dillon, L. *et al.*, 2015. Simultaneous transcriptional profiling of *Leishmania major* and its murine macrophage host cell reveals insights into host-pathogen interactions. *BMC genomics*, 16.

Domínguez, M. *et al.*, 2003. Early mechanisms of *Leishmania* infection in human blood. *Microbes and Infection*, 5(6), pp.507–513.

Donovan, C., 1903. The etiology of the heterogeneous fevers of India. *British medical journal*, 2(2239), p.1401.

Duch, D. & Smith, G., 1991. Biosynthesis and function of tetrahydrobiopterin. *The Journal of Nutritional Biochemistry*, 2(8), pp.411–423.

Duncan, S.M. *et al.*, 2016. Conditional gene deletion with DiCre demonstrates an essential role for CRK3 in *Leishmania mexicana* cell cycle regulation. *Molecular Microbiology*, 100(6), pp.931–944.

Dunn, W.B., 2008. Current trends and future requirements for the mass spectrometric investigation of microbial, mammalian and plant metabolomes. *Physical biology*, 5(1), p.011001.

Durinck, S. *et al.*, 2009. Mapping identifiers for the integration of genomic datasets with the R/Bioconductor package biomaRt. *Nature Protocols*, 4(8), pp.1184–1191.

Ehrchen, J.M. *et al.*, 2010. Keratinocytes Determine Th1 Immunity during Early Experimental Leishmaniasis. *PLoS Pathogens*, 6(4), p.e1000871.

Ehrchen, J.M. *et al.*, 2008. The absence of cutaneous lymph nodes results in a Th2 response and increased susceptibility to *Leishmania major* infection in mice. *Infection and Immunity*, 76(9), pp.4241–4250.

Fairlamb, A. *et al.*, 1985. Trypanothione: a novel bis(glutathionyl)spermidine cofactor for glutathione reductase in trypanosomatids. *Science*, 227(4693), pp.1485–1487.

Falcão, S.A.C. *et al.*, 2015. Exposure to *Leishmania braziliensis* triggers neutrophil activation and apoptosis. *PLoS Neglected Tropical Diseases*, 9(3), p.e0003601.

Feige, J.N. *et al.*, 2006. From molecular action to physiological outputs: Peroxisome proliferator-activated receptors are nuclear receptors at the crossroads of key cellular functions. *Progress in Lipid Research*, 45(2),

pp.120–159.

Fernandes, M.C. *et al.*, 2016. Dual Transcriptome Profiling of *Leishmania*-Infected Human Macrophages Reveals Distinct Reprogramming Signatures. *mbio.asm.org*.

Fernández-Figueroa, E. *et al.*, 2012. Disease Severity in Patients Infected with *Leishmania mexicana* Relates to IL-1ß. *PLoS Neglected Tropical Diseases*, 6(5).

Fiebig, M., Kelly, S. & Gluenz, E., 2015. Comparative Life Cycle Transcriptomics Revises *Leishmania mexicana* Genome Annotation and Links a Chromosome Duplication with Parasitism of Vertebrates. *PLoS Pathogens*, 11(10), p.e1005186.

Fiers, W. *et al.*, 2004. Complete nucleotide sequence of bacteriophage MS2 RNA: primary and secondary structure of the replicase gene. *Nature*, 260(5551), pp.500–507.

Fukuzumi, M. *et al.*, 1996. Endotoxin-induced enhancement of glucose influx into murine peritoneal macrophages via GLUT1. *Infection and Immunity*, 64(1), pp.108–112.

Gade, D.W., 1979. Inca and colonial settlement, coca cultivation and endemic disease in the tropical forest. *Journal of Historical Geography*, 5(3), pp.263–279.

Gantt, K.R. *et al.*, 2001. Oxidative responses of human and murine macrophages during phagocytosis of *Leishmania chagasi*. *Journal of Immunology*, 167(2), pp.893–901.

Gaur, U. *et al.*, 2007. An Effect of Parasite-Encoded Arginase on the Outcome of Murine Cutaneous Leishmaniasis. *The Journal of Immunology*, 179(12), pp.8446–8453.

Gautier, E.L. *et al.*, 2012. Gene-expression profiles and transcriptional regulatory pathways that underlie the identity and diversity of mouse tissue macrophages. *Nature Immunology*, 13(11), pp.1118–1128.

Genestra, M. *et al.*, 2006. Nitric oxide biosynthesis by *Leishmania amazonensis* promastigotes containing a high percentage of metacyclic forms. *Archives of Microbiology*, 185(5), pp.348–354.

Goldman-Pinkovich, A. *et al.*, 2016. An Arginine Deprivation Response Pathway Is Induced in *Leishmania* during Macrophage Invasion. *PLoS Pathogens*, 12(4), p.e1005494.

Goncalves, R. *et al.*, 2011. Platelet activation attracts a subpopulation of effector monocytes to sites of *Leishmania major* infection. *Journal of Experimental Medicine*, 208(6), pp.1253–1265.

Grant, S.K. *et al.*, 1998. Structural Requirements for Human Inducible Nitric Oxide Synthase Substrates and Substrate Analogue Inhibitors. *Biochemistry*, 37(12), pp.4174–4180.

Gregory, D.J. *et al.*, 2008. A novel form of NF-kappaB is induced by *Leishmania* infection: involvement in macrophage gene expression. *European Journal of Immunology*, 38(4), pp.1071–1081.

Gueirard, P. *et al.*, 2007. Trafficking of *Leishmania donovani* promastigotes in non-lytic compartments in neutrophils enables the subsequent transfer of parasites to macrophages. *Cellular Microbiology*, 0(0), pp.100–111.

Guimarães-Costa, A.B. *et al.*, 2009. *Leishmania amazonensis* promastigotes induce and are killed by neutrophil extracellular traps. *PNAS*, 106(16), pp.6748–6753.

Gusarov, I. *et al.*, 2009. Endogenous Nitric Oxide Protects Bacteria Against a Wide Spectrum of Antibiotics. *Science*, 325(5946), pp.1380–1384.

Ha, D.S. *et al.*, 1996. Use of the green fluorescent protein as a marker in transfected *Leishmania*. *Molecular and Biochemical Parasitology*, 77(1), pp.57–64.

Haase, R. *et al.*, 2003. A Dominant Role of Toll-Like Receptor 4 in the Signaling of Apoptosis in Bacteria-Faced Macrophages. *The Journal of Immunology*, 171(8), pp.4294–4303.

Halle, M. *et al.*, 2009. The *Leishmania* Surface Protease GP63 Cleaves Multiple Intracellular Proteins and Actively Participates in p38 Mitogen-activated Protein Kinase Inactivation. *Journal of Biological Chemistry*, 284(11), pp.6893–6908.

Harkins, K.M. *et al.*, 2016. Phylogenomic reconstruction supports supercontinent origins for *Leishmania*. *Infection Genetics and Evolution*, 38, pp.101–109.

Harris, S.M. *et al.*, 2008. The interferon-γ-mediated inhibition of lipoprotein lipase gene transcription in macrophages involves casein kinase 2- and phosphoinositide-3-kinase-mediated regulation of transcription factors Sp1 and Sp3. *Cellular Signalling*, 20(12), pp.2296–2301.

Haschemi, A. *et al.*, 2012. The Sedoheptulose Kinase CARKL Directs Macrophage Polarization through Control of Glucose Metabolism. *Cell Metabolism*, 15(6), pp.813–826.

Hasko, G. & Pacher, P., 2012. Regulation of Macrophage Function by Adenosine. *Arteriosclerosis, Thrombosis, and Vascular Biology*, 32(4), pp.865–869.

Haug, K. *et al.*, 2013. MetaboLights--an open-access general-purpose repository for metabolomics studies and associated meta-data. *Nucleic Acids Research*, 41(Database issue), pp.D781–D786.

Hayani, K., Dandashli, A. & Weisshaar, E., 2015. Cutaneous leishmaniasis in Syria: clinical features, current status and the effects of war. *Acta dermato-venereologica*, 95(1), pp.62–66.

Heinzel, F.P. *et al.*, 1989. Reciprocal expression of interferon gamma or interleukin 4 during the resolution or progression of murine leishmaniasis. Evidence for expansion of distinct helper T cell subsets. *Journal of*

Experimental Medicine, 169(1), pp.59–72.

Heinzel, F.P. *et al.*, 1993. Recombinant Interleukin-12 Cures Mice Infected with *Leishmania major*. *Journal of Experimental Medicine*, 177(5), pp.1505–1509.

Horning, E.C. & Horning, M.G., 1971. Metabolic Profiles: Gas-Phase Methods for Analysis of Metabolites. *Clinical Chemistry*, 17(8).

Howard, J.G., 1980. Immunological regulation of experimental cutaneous leishmaniasis. III. Nature and significance of specific suppression of cell-mediated immunity in mice highly susceptible to *Leishmania tropica*. *Journal of Experimental Medicine*, 152(3), pp.594–607.

Hsu, A.C. & Scott, P., 2007. *Leishmania mexicana* infection induces impaired lymph node expansion and Th1 cell differentiation despite normal T cell proliferation. *Journal of Immunology*, 179(12), pp.8200–8207.

Huang, S.C.-C. *et al.*, 2014. Cell-intrinsic lysosomal lipolysis is essential for alternative activation of macrophages. *Nature Immunology*, 15(9), pp.846–855.

Hurrell, B.P. *et al.*, 2015. Rapid Sequestration of *Leishmania mexicana* by Neutrophils Contributes to the Development of Chronic Lesion. *PLoS Pathogens*, 11(5), p.e1004929.

Hurrell, B.P., Regli, I.B. & Fabienne Tacchini-Cottier, 2016. Different *Leishmania* Species Drive Distinct Neutrophil Functions. *Trends in Parasitology*, 32, pp.392–401.

Huson, D.H. & Scornavacca, C., 2012. Dendroscope 3: an interactive tool for rooted phylogenetic trees and networks. *Systematic biology*, 61(6), pp.1061–1067.

Ikeda, R. *et al.*, 2013. Molecular basis for the regulation of hypoxia-inducible factor-1α levels by 2-deoxy-D-ribose. *Oncology reports*, 30(3), pp.1444–1448.

Jha, A.K. *et al.*, 2015. Network integration of parallel metabolic and transcriptional data reveals metabolic modules that regulate macrophage polarization. *Immunity*, 42(3), pp.419–430.

Ji, J. *et al.*, 2016. Microbial metabolite butyrate facilitates M2 macrophage polarization and function. *Scientific Reports*, 6, p.24838.

John, S., Weiss, J.N. & Ribalet, B., 2011. Subcellular Localization of Hexokinases I and II Directs the Metabolic Fate of Glucose. *PLoS ONE*, 6(3), p.e17674.

Jonsson, C.A. & Carlsten, H., 2002. Mycophenolic acid inhibits inosine 5′-monophosphate dehydrogenase and suppresses production of pro-inflammatory cytokines, nitric oxide, and LDH in macrophages. *Cellular Immunology*, 216(1-2), pp.93–101.

Kamhawi, S., 2006. Phlebotomine sand flies and *Leishmania* parasites: friends or foes? *Trends in Parasitology*, 22(9), pp.439–445.

Kamhawi, S. *et al.*, 2004. A Role for Insect Galectins in Parasite Survival. *Cell*,

119(3), pp.329–341.

Kelley, L.A. *et al.*, 2015. The Phyre2 web portal for protein modeling, prediction and analysis. *Nature Protocols*, 10(6), pp.845–858.

Kellina, O.I., 1973. Differences in the sensitivity of inbred mice of different lines to *Leishmania tropica major*. *Meditsinskaia parazitologiia i parazitarnye bolezni*, 42(3), pp.279–285.

Kelly, B. & O'Neill, L.A.J., 2015. Metabolic reprogramming in macrophages and dendritic cells in innate immunity. *Cell Research*, 25(7), pp.771–784.

Khamesipour, A. *et al.*, 2005. Leishmanization: Use of an old method for evaluation of candidate vaccines against leishmaniasis. *Vaccine*, 23(28), pp.3642–3648.

Kim, D.-H. *et al.*, 2015a. LC-MS-based absolute metabolite quantification: application to metabolic flux measurement in trypanosomes. *Metabolomics*, 11(6), pp.1721–1732.

Kim, D., Ben Langmead & Salzberg, S.L., 2015b. HISAT: a fast spliced aligner with low memory requirements : Nature Methods : Nature Research. *Nature Methods*, 12(4), pp.357–362.

Kim, N.-H. *et al.*, 2014c. The xanthine oxidase-NFAT5 pathway regulates macrophage activation and TLR-induced inflammatory arthritis. *European Journal of Immunology*, 44(9), pp.2721–2736.

Kim, S.Y., Park, T. & Kim, H.W., 2009d. Inhibition of Apoptosis by Taurine in Macrophages Treated with Sodium Nitroprusside. In C. 50, ed. *Advances in Experimental Medicine and Biology*. Advances in Experimental Medicine and Biology. New York, NY: Springer New York, pp. 481–489.

Kimblin, N. *et al.*, 2008. Quantification of the infectious dose of *Leishmania major* transmitted to the skin by single sand flies. *PNAS*, 105(29), pp.10125–10130.

Knight, R. *et al.*, 1987. Inosine monophosphate dehydrogenase and myeloid cell maturation. *bloodjournal.org*, 69(2), pp.634–639.

Knipp, M. & Vašák, M., 2000. A Colorimetric 96-Well Microtiter Plate Assay for the Determination of Enzymatically Formed Citrulline. *Analytical Biochemistry*, 286(2), pp.257–264.

Knodler, L.A., 1998. Cloning and Expression of a Prokaryotic Enzyme, Arginine Deiminase, from a Primitive Eukaryote *Giardia intestinalis*. *Journal of Biological Chemistry*, 273(8), pp.4470–4477.

Lainson, R., 2010. The Neotropical *Leishmania* species: a brief historical review of their discovery, ecology and taxonomy. *Revista Pan-Amazônica de Saúde*, 1(2), pp.13–32.

Lakhal-Naouar, I. *et al.*, 2012. *Leishmania donovani* Argininosuccinate Synthase Is an Active Enzyme Associated with Parasite Pathogenesis. *PLoS Neglected*

Tropical Diseases, 6(10), p.e1849.

Lamour, S.D. *et al.*, 2012. Metabolic characterization of *Leishmania major* infection in activated and nonactivated macrophages. *Journal of Proteome Research*, 11(8), pp.4211–4222.

Lampropoulou, V. *et al.*, 2016. Itaconate Links Inhibition of Succinate Dehydrogenase with Macrophage Metabolic Remodeling and Regulation of Inflammation. *Cell Metabolism*, 24(1), pp.158–166.

Leader, D.P. *et al.*, 2011. Pathos: A web facility that uses metabolic maps to display experimental changes in metabolites identified by mass spectrometry. *Rapid Communications in Mass Spectrometry*, 25(22), pp.3422–3426.

Leishman, W.B., 1903. *On the Possibility of the Occurrence of Trypanosomiasis in India*, The British medical Journal.

León, B., López-Bravo, M. & Ardavín, C., 2007. Monocyte-derived dendritic cells formed at the infection site control the induction of protective T helper 1 responses against *Leishmania*. *Immunity*, 26(4), pp.519–531.

Lessa, H.A. *et al.*, 2001. Successful treatment of refractory mucosal leishmaniasis with pentoxifylline plus antimony. *The American journal of tropical medicine and hygiene*, 65(2), pp.87–89.

Levings, M.K. & Schrader, J.W., 1999. IL-4 inhibits the production of TNF-alpha and IL-12 by STAT6-dependent and -independent mechanisms. *Journal of Immunology*, 162(9), pp.5224–5229.

Levring, T.B. *et al.*, 2012. Activated human CD4+ T cells express transporters for both cysteine and cystine. *Scientific Reports*, 2.

Lichtenstein, L. *et al.*, 2010. Angptl4 Protects against Severe Proinflammatory Effects of Saturated Fat by Inhibiting Fatty Acid Uptake into Mesenteric Lymph Node Macrophages. *Cell Metabolism*, 12(6), pp.580–592.

Livesay, J.C. *et al.*, 2008. Increased plasma and tissue guanidino compounds in a mouse model of hyperargininemia. *Molecular Genetics and Metabolism*, 93(2), pp.172–178.

Lodge, R., Diallo, T.O. & Descoteaux, A., 2006. *Leishmania donovani* lipophosphoglycan blocks NADPH oxidase assembly at the phagosome membrane. *Cellular Microbiology*, 8(12), pp.1922–1931.

Loeuillet, C., Bañuls, A.-L. & Hide, M., 2016. Study of *Leishmania* pathogenesis in mice: experimental considerations. *Parasites & Vectors*, 9(1), p.1.

Love, M.I., Huber, W. & Anders, S., 2014. Moderated estimation of fold change and dispersion for RNA-seq data with DESeq2. *Genome biology*, 15(12), p.550.

Marr, A.K. *et al.*, 2014. *Leishmania donovani* infection causes distinct epigenetic DNA methylation changes in host macrophages. *PLoS Pathogens*, 10(10),

pp.e1004419–e1004419.

Maugeri, D.A. *et al.*, 2003. Pentose phosphate metabolism in *Leishmania mexicana*. *Molecular and Biochemical Parasitology*, 130, pp.117–125.

Mazareb, S., Fu, Z.Y. & Zilberstein, D., 1999. Developmental Regulation of Proline Transport in *Leishmania donovani*. *Experimental Parasitology*, 91(4), pp.341–348.

McCullagh, P. & Nelder, J.A., 1989. *Generalized Linear Models, Second Edition*, CRC Press.

McGettrick, A. *et al.*, 2016. *Trypanosoma brucei* metabolite indolepyruvate decreases HIF-1α and glycolysis in macrophages as a mechanism of innate immune evasion. *PNAS*, published ahead of print, pp.1–10.

McGwire, B. & Satoskar, A., 2014. Leishmaniasis: clinical syndromes and treatment. *QJM*, 107(1), pp.7–14.

Meiser, J. *et al.*, 2016. Pro-inflammatory Macrophages Sustain Pyruvate Oxidation through Pyruvate Dehydrogenase for the Synthesis of Itaconate and to Enable Cytokine Expression. *Journal of Biological Chemistry*, 291(8), pp.3932–3946.

Meng, Z.-X. *et al.*, 2013. Baf60c drives glycolytic metabolism in the muscle and improves systemic glucose homeostasis through Deptor-mediated Akt activation. *Nature Medicine*, 19(5), pp.640–645.

Michelucci, A. *et al.*, 2013. Immune-responsive gene 1 protein links metabolism to immunity by catalyzing itaconic acid production. *Proceedings of the National Academy of Sciences of the United States of America*, 110(19), p.7820.

Miranda-Verastegui, C. *et al.*, 2009. First-line therapy for human cutaneous leishmaniasis in Peru using the TLR7 agonist imiquimod in combination with pentavalent antimony. *PLoS Neglected Tropical Diseases*, 3(7), p.e491.

Mondragon-Shem, K. *et al.*, 2015. Severity of old world cutaneous leishmaniasis is influenced by previous exposure to sandfly bites in Saudi Arabia. *PLoS Neglected Tropical Diseases*, 9(2), pp.e0003449–e0003449.

Moon, J.-S. *et al.*, 2015. mTORC1-Induced HK1-Dependent Glycolysis Regulates NLRP3 Inflammasome Activation. *Cell reports*, 12(1), pp.102–115.

Morehead, J., Coppens, I. & Andrews, N.W., 2002. Opsonization modulates Rac-1 activation during cell entry by *Leishmania amazonensis*. *Infection and Immunity*, 70(8), pp.4571–4580.

Moreira, D. *et al.*, 2015. *Leishmania infantum* Modulates Host Macrophage Mitochondrial Metabolism by Hijacking the SIRT1-AMPK Axis. *PLoS Pathogens*, 11(3), pp.e1004684–e1004684.

Mosser, D.M. *et al.*, 1986. *Leishmania* species: Mechanisms of complement activation by five strains of promastigotes. *Experimental Parasitology*, 62(3),

pp.394–404.

Mou, Z. *et al.*, 2015. Identification of broadly conserved cross-species protective *Leishmania* antigen and its responding CD4(+) T cells. *Science translational medicine*, 7(310), pp.–310ra167.

Muleme, H.M. *et al.*, 2009. Infection with Arginase-Deficient *Leishmania major* Reveals a Parasite Number-Dependent and Cytokine-Independent Regulation of Host Cellular Arginase Activity and Disease Pathogenesis. *The Journal of Immunology*, 183(12), pp.8068–8076.

Murray-Rust, J. *et al.*, 2001. Structural insights into the hydrolysis of cellular nitric oxide synthase inhibitors by dimethylarginine dimethylaminohydrolase. *Nature Structural Biology*, 8(8), pp.679–683.

Naderer, T. & McConville, M.J., 2008. The *Leishmania*-macrophage interaction: a metabolic perspective. *Cellular Microbiology*, 10(2), pp.301–308.

Nagle, A.S. *et al.*, 2014. Recent developments in drug discovery for leishmaniasis and human African trypanosomiasis. *Chemical Reviews*, 114(22), pp.11305–11347.

Nath, K.A. *et al.*, 1995. alpha-Ketoacids scavenge H_2O_2 in vitro and in vivo and reduce menadione-induced DNA injury and cytotoxicity. *American Journal of Physiology - Cell Physiology*, 268(1), pp.C227–C236.

Nettleship, J.E. *et al.*, 2015. Transient expression in HEK 293 cells: an alternative to *E. coli* for the production of secreted and intracellular mammalian proteins. *Methods in molecular biology (Clifton, N.J.)*, 1258, pp.209–222.

Nettleship, J.E., Rahman-Huq, N. & Owens, R.J., 2009. The production of glycoproteins by transient expression in Mammalian cells. *Methods in molecular biology (Clifton, N.J.)*, 498, pp.245–263.

Ng, L.G. *et al.*, 2008. Migratory Dermal Dendritic Cells Act as Rapid Sensors of Protozoan Parasites. *PLoS Pathogens*, 4(11), pp.–e1000222.

Nomura, M. *et al.*, 2016. Fatty acid oxidation in macrophage polarization. *Nature Immunology*, 17(3), pp.216–217.

O'Neill, L.A.J. & Pearce, E.J., 2016. Immunometabolism governs dendritic cell and macrophage function. *The Journal of experimental medicine*, 213(1), pp.15–23.

Olekhnovitch, R. *et al.*, 2014. Collective nitric oxide production provides tissue-wide immunity during *Leishmania* infection. *Journal of Clinical Investigation*, 124(4), pp.1711–1722.

Oliveira, F. *et al.*, 2015. A sand fly salivary protein vaccine shows efficacy against vector-transmitted cutaneous leishmaniasis in nonhuman primates. *Science translational medicine*, 7(290), p.290ra90.

Oliver, S., 1998. Systematic functional analysis of the yeast genome. *Trends in*

Biotechnology, 16(9), pp.373–378.

Oliveros, J., 2015. Venny. An interactive tool for comparing lists with Venn's diagrams. *bioinfogp.cnb.csic.es*. Available at: http://bioinfogp.cnb.csic.es/tools/venny/index.html

Osorio y Fortea, J. *et al.*, 2009. Transcriptional signatures of BALB/c mouse macrophages housing multiplying Leishmania amazonensis amastigotes. *BMC genomics*, 10(1), p.119.

Pedrique, B. *et al.*, 2013. The drug and vaccine landscape for neglected diseases (2000–11): a systematic assessment. *The Lancet*, 1 (6), pp.e371-e379

Peitsch, M.C. & Tschopp, J., 1991. Assembly of macromolecular pores by immune defense systems. *Current Opinion in Cell Biology*, 3(4), pp.710–716.

Pelis, K., 2006. *Charles Nicolle, Pasteur's Imperial Missionary*, Boydell & Brewer.

Pereira, M. *et al.*, 2015. Down Regulation of NO Signaling in *Trypanosoma cruzi* upon Parasite-Extracellular Matrix Interaction: Changes in Protein Modification by Nitrosylation and Nitration. *PLoS Neglected Tropical Diseases*, 9(4), p.e0003683.

Peters, N. *et al.*, 2008a. In vivo Imaging reveals an Essential Role for Neutrophils in Leishmaniasis Transmitted by Sand Flies. *Science*, 322(5908), pp.1634a–1634a.

Peters, C. *et al.*, 1995b. The role of macrophage receptors in adhesion and uptake of *Leishmania mexicana* amastigotes. *Journal of Cell Science*, 108 (Pt 12), pp.3715–3724.

Petritus, P.M. *et al.*, 2012. *Leishmania mexicana* Induces Limited Recruitment and Activation of Monocytes and Monocyte-Derived Dendritic Cells Early during Infection. *PLoS Neglected Tropical Diseases*, 6(10), pp.–e1858.

Piacenza, L., Peluffo, G. & Radi, R., 2001. -Arginine-dependent suppression of apoptosis in *Trypanosoma cruzi*: Contribution of the nitricoxide and polyamine pathways. *PNAS*, 98(13), pp.7301–7306.

Pimenta, P.F. *et al.*, 1994. Evidence that the vectorial competence of phlebotomine sand flies for different species of *Leishmania* is controlled by structural polymorphisms in the surface lipophosphoglycan. *PNAS*, 91(19), pp.9155–9159.

Prabha, A.N.L., Leelamma, S. & Kurup, P.A., 1988. Similar effects of ß-alanine and taurine in cholesterol metabolism. *Journal of Biosciences*, 13(3), pp.263–268.

Prescott, L.M. & Jones, M.E., 1969. Modified methods for the determination of carbamyl aspartate. *Analytical Biochemistry*, 32(3), pp.408–419.

Proudfoot, L. *et al.*, 1996. Regulation of the expression of nitric oxide synthase and leishmanicidal activity by glycoconjugates of *Leishmania* lipophosphoglycan in murine macrophages. *PNAS*, 93(20), pp.10984–10989.

Puentes, S.M. *et al.*, 1990. Serum resistance of metacyclic stage *Leishmania major* promastigotes is due to release of C5b-9. *Journal of Immunology*, 145(12), pp.4311–4316.

Qiao, M. *et al.*, 2007. Increased Expression of Glutathione Reductase in Macrophages Decreases Atherosclerotic Lesion Formation in Low-Density Lipoprotein Receptor-Deficient Mice. *Arteriosclerosis, Thrombosis, and Vascular Biology*, 27(6), pp.1375–1382.

Rabhi, I. *et al.*, 2012. PLOS Neglected Tropical Diseases: Transcriptomic Signature of *Leishmania* Infected Mice Macrophages: A Metabolic Point of View. *PLoS Neglected Tropical Diseases*, 6(8).

Raes, G. *et al.*, 2005. Macrophage galactose-type C-type lectins as novel markers for alternatively activated macrophages elicited by parasitic infections and allergic airway inflammation. *Journal of leukocyte biology*, 77(3), pp.321–327.

Ramdas, S., 2012. Cruel disease, cruel medicine: self-treatment of cutaneous leishmaniasis with harmful chemical substances in Suriname. *Social Science & Medicine*, 75(6), pp.1097–1105.

Reguera, R.M. *et al.*, 2009. *Leishmania major* lacking arginase (ARG) are auxotrophic for polyamines but retain infectivity to susceptible BALB/c mice. *Molecular and Biochemical Parasitology*, 165(1), pp.48–56.

Remer, K.A. *et al.*, 2010. Natural killer cells support the induction of protective immunity during dendritic cell-mediated vaccination against *Leishmania major*. *Immunology*, 131(4), pp.570–582.

Ribeiro-Gomes, F.L. *et al.*, 2012. Efficient capture of infected neutrophils by dendritic cells in the skin inhibits the early anti-*Leishmania* response. *PLoS Pathogens*, 8(2), pp.e1002536–e1002536.

Ritter, U. *et al.*, 2004. CD8α- and Langerin-negative dendritic cells, but not Langerhans cells, act as principal antigen-presenting cells in leishmaniasis. *European Journal of Immunology*, 34(6), pp.1542–1550.

Ritter, U., Frischknecht, F. & van Zandbergen, G., 2009. Are neutrophils important host cells for *Leishmania* parasites? *Trends in Parasitology*, 25(11), pp.505–510.

Rodríguez-Prados, J.-C. *et al.*, 2010. Substrate fate in activated macrophages: a comparison between innate, classic, and alternative activation. *Journal of Immunology*, 185(1), pp.605–614.

Rogers, M. *et al.*, 2009. Proteophosophoglycans regurgitated by *Leishmania*-infected sand flies target the L-arginine metabolism of host macrophages to promote parasite survival. *PLoS Pathogens*, 5(8), p.e1000555.

Rogers, M.E., 2012. The role of *Leishmania* proteophosphoglycans in sand fly transmission and infection of the mammalian host. *Frontiers in Microbiology*, 3.

Rogers, M.E. *et al.*, 2004. Transmission of cutaneous leishmaniasis by sand flies is enhanced by regurgitation of fPPG. *Nature*, 430(6998), pp.463–467.

Rogers, M.E., Chance, M.L. & Bates, P.A., 2002. The role of promastigote secretory gel in the origin and transmission of the infective stage of *Leishmania mexicana* by the sandfly *Lutzomyia longipalpis*. *Parasitology*, 124, pp.495–507.

Romano, A. *et al.*, 2014. Cross-species genetic exchange between visceral and cutaneous strains of *Leishmania* in the sand fly vector. *PNAS*, 111(47), pp.16808–16813.

Ross, R., 1903. Further notes on Leishman's bodies. *British medical journal*, 2(2239), p.1401.

Rubic, T. *et al.*, 2008. Triggering the succinate receptor GPR91 on dendritic cells enhances immunity. *Nature Immunology*, 9(11), pp.1261–1269.

Rutkowsky, J.M. *et al.*, 2014. Acylcarnitines activate proinflammatory signaling pathways. *American journal of physiology. Endocrinology and metabolism*, 306(12), pp.E1378–87.

Sacks, D. & Noben-Trauth, N., 2002. The immunology of susceptibility and resistance to *Leishmania major* in mice. *Nature Reviews Immunology*, 2(11), pp.845–858.

Sales, G. *et al.*, 2013. Graphite Web: web tool for gene set analysis exploiting pathway topology. *Nucleic Acids Research*, pp.1–9.

Sanabria, M.X.H. *et al.*, 2008. Role of Natural Killer Cells in Modulating Dendritic Cell Responses to *Leishmania amazonensis* Infection. *Infection and Immunity*, 76(11), pp.4793–4794.

Sanger, F., Nicklen, S. & Coulson, R., 1977. DNA sequencing with chain-terminating inhibitors. *Proceedings of the National Academy of Sciences of the United States of America*, 74(12), p.5463.

Sardar, A.H. *et al.*, 2016. Genetic Manipulation of *Leishmania donovani* to Explore the Involvement of Argininosuccinate Synthase in Oxidative Stress Management. *PLoS Neglected Tropical Diseases*, 10(3), p.e0004308.

Saunders, E.C. *et al.*, 2014. Induction of a Stringent Metabolic Response in Intracellular Stages of *Leishmania mexicana* Leads to Increased Dependence on Mitochondrial Metabolism. *PLoS Pathogens*, 10(1), p.e1003888.

Scheltema, R.A. *et al.*, 2008. Increasing the mass accuracy of high-resolution LC-MS data using background ions: a case study on the LTQ-Orbitrap. *Proteomics*, 8(22), pp.4647–4656.

Schlein, Y., Jacobson, R.L. & Shlomai, J., 1991. Chitinase secreted by *Leishmania* functions in the sandfly vector. *Proceedings. Biological sciences / The Royal Society*, 245(1313), pp.121–126.

Schomburg, I. *et al.*, 2004. BRENDA, the enzyme database: updates and major

new developments. *Nucleic Acids Research*, 32(Database issue), pp.D431–3.

Schonian, G. *et al.*, 2003. PCR diagnosis and characterization of *Leishmania* in local and imported clinical samples. *Diagnostic microbiology and infectious disease*, 47(1), pp.349–358.

Schroder, K. *et al.*, 2012. Conservation and divergence in Toll-like receptor 4-regulated gene expression in primary human versus mouse macrophages. *PNAS*, pp.955–953.

Scott, P. & Novais, F.O., 2016. Cutaneous leishmaniasis: immune responses in protection and pathogenesis. *Nature Reviews Immunology*.

Secundino, N. *et al.*, 2010. Proteophosphoglycan confers resistance of *Leishmania major* to midgut digestive enzymes induced by blood feeding in vector sand flies. *Cellular Microbiology*, 12(7), pp.906–918.

Sellick, C.A. *et al.*, 2010. Evaluation of extraction processes for intracellular metabolite profiling of mammalian cells: matching extraction approaches to cell type and metabolite targets. *Metabolomics*, 6(3), pp.427–438.

Shriver, L.P. & Manchester, M., 2011. Inhibition of fatty acid metabolism ameliorates disease activity in an animal model of multiple sclerosis. *Scientific Reports*, 1.

Shweash, M. *et al.*, 2011. *Leishmania mexicana* promastigotes inhibit macrophage IL-12 production via TLR-4 dependent COX-2, iNOS and arginase-1 expression. *Molecular Immunology*, 48(15-16), pp.1800–1808.

Sievers, F. *et al.*, 2011. Fast, scalable generation of high-quality protein multiple sequence alignments using Clustal Omega. *Molecular Systems Biology*, 7(1), pp.539–539.

Sousa, L.M.A. *et al.*, 2014. Neutrophils have a protective role during early stages of *Leishmania amazonensis* infection in BALB/c mice. *Parasite Immunology*, 36(1), pp.13–31.

Stacklies, W. *et al.*, 2007. pcaMethods a bioconductor package providing PCA methods for incomplete data. *Bioinformatics (Oxford, England)*, 23(9), pp.1164–1167.

Stierhof, Y.D. *et al.*, 1999. Filamentous proteophosphoglycan secreted by *Leishmania* promastigotes forms gel-like three-dimensional networks that obstruct the digestive tract of infected sandfly vectors. *European journal of cell biology*, 78(10), pp.675–689.

Sumner, L.W. *et al.*, 2007. Proposed minimum reporting standards for chemical analysis Chemical Analysis Working Group (CAWG) Metabolomics Standards Initiative (MSI). *Metabolomics*, 3(3), pp.211–221.

t'Kindt, R. *et al.*, 2010. Towards an unbiased metabolic profiling of protozoan parasites: optimisation of a *Leishmania* sampling protocol for HILIC-orbitrap analysis. *Analytical and bioanalytical chemistry*, 398(5), pp.2059–2069.

Tacchini-Cottier, F. *et al.*, 2000. An Immunomodulatory Function for Neutrophils During the Induction of a CD4+ Th2 Response in BALB/c Mice Infected with *Leishmania major*. *The Journal of Immunology*, 165(5), pp.2628–2636.

Takahashi, M. *et al.*, 2013. Macrophage lipoprotein lipase modulates the development of atherosclerosis but not adiposity. *The Journal of Lipid Research*, 54(4), pp.1124–1134.

Takaku, H. *et al.*, 1992. *In vivo* anti-tumor activity of arginine deiminase purified from *Mycoplasma arginini*. *International Journal of Cancer*, pp.244–249.

Tannahill, G.M. *et al.*, 2013. Succinate is an inflammatory signal that induces IL-1β through HIF-1α. *Nature*, 496(7444), pp.238–242.

Tarca, A.L. *et al.*, 2009. A novel signaling pathway impact analysis. *Bioinformatics (Oxford, England)*, 25(1), pp.75–82.

Teixeira, C.R. *et al.*, 2005. Saliva from *Lutzomyia longipalpis* induces CC chemokine ligand 2/monocyte chemoattractant protein-1 expression and macrophage recruitment. *Journal of Immunology*, 175(12), pp.8346–8353.

Trapnell, C. *et al.*, 2012. Differential gene and transcript expression analysis of RNA-seq experiments with TopHat and Cufflinks. *Nature Protocols*, 7(3), pp.562–578.

UtcNTDs, 2016. The Fourth Report: Reaching the unreached | Uniting to Combat NTDs. *unitingtocombatntds.org*. Available at: http://unitingtocombatntds.org/report/fourth-report-reaching-unreached

Uzonna, J.E., Joyce, K.L. & Scott, P., 2004. Low dose *Leishmania major* promotes a transient T helper cell type 2 response that is down-regulated by interferon gamma-producing CD8(+) T cells. *Journal of Experimental Medicine*, 199(11), pp.1559–1566.

Van Assche, T. *et al.*, 2011. *Leishmania*-macrophage interactions: insights into the redox biology. *Free Radical Biology and Medicine*, 51(2), pp.337–351.

van der Greef, J. & Smilde, A.K., 2005. Symbiosis of chemometrics and metabolomics: past, present, and future. *Journal of Chemometrics*, 19(5-7), pp.376–386.

van Zandbergen, G. *et al.*, 2004. Cutting edge: neutrophil granulocyte serves as a vector for *Leishmania* entry into macrophages. *Journal of Immunology*, 173(11), pp.6521–6525.

Vats, D. *et al.*, 2006. Oxidative metabolism and PGC-1β attenuate macrophage-mediated inflammation. *Cell Metabolism*, 4(1), pp.13–24.

Verghese, M.W. & Snyderman, R., 1983. Hormonal activation of adenylate cyclase in macrophage membranes is regulated by guanine nucleotides. *The Journal of Immunology*, 130(2), pp.869–873.

Vinaixa, M. *et al.*, 2016. Mass spectral databases for LC/MS- and GC/MS-based

metabolomics: State of the field and future prospects. *Trends in Analytical Chemistry*, (78).

Vincendeau, P. *et al.*, 2003. Arginases in parasitic diseases: Trends in Parasitology. *Trends in Parasitology*, 19(1), pp.9–12.

Vincent, I.M. *et al.*, 2010. A molecular mechanism for eflornithine resistance in African trypanosomes. *PLoS Pathogens*, 6(11), p.e1001204.

Vinet, A.F. *et al.*, 2009. The *Leishmania donovani* Lipophosphoglycan Excludes the Vesicular Proton-ATPase from Phagosomes by Impairing the Recruitment of Synaptotagmin V. *PLoS Pathogens*, 5(10), p.e1000628.

Voronov, E. *et al.*, 2010. IL-1-induced inflammation promotes development of leishmaniasis in susceptible BALB/c mice. *International Immunology*, 22(4), pp.NP–NP.

Wang, X. *et al.*, 2009a. Inducible nitric-oxide synthase expression is regulated by mitogen-activated protein kinase phosphatase-1. *Journal of Biological Chemistry*, 284(40), pp.27123–27134.

Wang, Y. *et al.*, 2009b. Developing dual and specific inhibitors of dimethylarginine dimethylaminohydrolase-1 and nitric oxide synthase: Toward a targeted polypharmacology to control nitric oxide. *Biochemistry*, 48(36), p.8624.

Watson, D.G., 2010. The potential of mass spectrometry for the global profiling of parasite metabolomes. *Parasitology*, 137(9), pp.1409–1423.

Weischenfeldt, J. & Porse, B., 2008. Bone Marrow-Derived Macrophages (BMM): Isolation and Applications. *CSH protocols*, 2008, p.pdb.prot5080.

Wellner, D. & Meister, A., 1960. Crystalline l-Amino Acid Oxidase of *Crotalus adamanteus*. *Journal of Biological Chemistry*, 235(7), pp.2013–2018.

Westrop, G.D. *et al.*, 2015. Metabolomic Analyses of *Leishmania* Reveal Multiple Species Differences and Large Differences in Amino Acid Metabolism. *PLoS ONE*, 10(9), p.e0136891.

WHO, 2010. Control of the leishmaniases. *WHO/Expert Committee on the Control of Leishmaniases*, pp.1–186.

WHO, 2012. London Declaration on Neglected Tropical Diseases. Available at: http://www.who.int/neglected_diseases/London_Declaration_NTDs.pdf

Willmott, N. *et al.*, 1996. Nitric Oxide-induced Mobilization of Intracellular Calcium via the Cyclic ADP-ribose Signaling Pathway. *Journal of Biological Chemistry*, 271(7), pp.3699–3705.

Wright, J.H., 1903. Protozoa in a Case of Tropical Ulcer (“Delhi Sore”). *The Journal of medical research*, 10(3), pp.472–477.

Xia, J. & Wishart, D.S., 2010. MetPA: a web-based metabolomics tool for pathway analysis and visualization. *Bioinformatics (Oxford, England)*, 26(18), pp.2342–2344.

Xia, J. *et al.*, 2015. MetaboAnalyst 3.0—making metabolomics more meaningful. *Nucleic Acids Research*, 43(W1), pp.W251–W257.

Xue, J. *et al.*, 2014. Transcriptome-Based Network Analysis Reveals a Spectrum Model of Human Macrophage Activation. *Immunity*, 40(2), pp.274–288.

Yadav, S.P., 2007. The wholeness in suffix -omics, -omes, and the word om. *Journal of biomolecular techniques : JBT*, 18(5), p.277.

Yang, Z. & Ming, X.-F., 2014. Functions of Arginase Isoforms in Macrophage Inflammatory Responses: Impact on Cardiovascular Diseases and Metabolic Disorders. *Frontiers in Immunology*, 5.

Yeramian, A.E. *et al.*, 2006. Arginine Transport via Cationic Amino Acid Transporter 2 Plays a Critical Regulatory Role in Classical or Alternative Activation of Macrophages. *The Journal of Immunology*, (176), pp.5918–5924.

Yuan, M. *et al.*, 2012. A positive/negative ion-switching, targeted mass spectrometry-based metabolomics platform for bodily fluids, cells, and fresh and fixed tissue. *Nature Protocols*, 7(5), pp.872–881.